TRANSACTIONS
OF THE ASME
Series B

Journal of ENGINEERING FOR INDUSTRY

February 1959

Divisions: AVIATION • MACHINE DESIGN • MANAGEMENT • PROCESS INDUSTRIES • MAINTENANCE AND PLANT ENGINEERING • RAILROAD • PRODUCTION ENGINEERING • MATERIALS HANDLING • RUBBER AND PLASTICS • PETROLEUM • SAFETY • TEXTILE • WOOD INDUSTRIES • Research Committees: METAL PROCESSING • FLOW OF BULK MATERIALS • ELEVATORS • MECHANICAL SPRINGS

Published Quarterly by
THE AMERICAN SOCIETY OF MECHANICAL ENGINEERS

TRANSACTIONS OF THE ASME
Series B

Journal of
ENGINEERING FOR INDUSTRY

VOLUME 81 • SERIES B • NUMBER 1
February 1959

CONTENTS

1 **Dynamic Loading of Spur Gear Teeth**
A. Y. Attia

10 **Analytical Design of an Ackermann Steering Linkage**
W. A. Wolfe

15 **Structural Error Analysis in Plane Kinematic Synthesis**
Ferdinand Freudenstein

23 **The Design of Linkages to Generate Functions of Two Variables**
C. W. Allen

30 **Helical Springs of Hollow Circular Cross Section**
C. W. Bert

37 **Design of Helical Springs for Minimum Weight, Volume, and Length**
R. T. Hinkle and I. E. Morse, Jr.

43 **Stress and Strain in Spinning Paraboloid Dishes**
M. J. Cohen

51 **Torispherical Shells—A Caution to Designers**
G. D. Galletly

67 **Drilling by Vibration**
R. Simon

77 **Vibrations of Vertical Pressure Vessels**
C. E. Freese

92 **Technical Briefs**
Revisions to Published Chart: Metals for High-Pressure Hydrogenation Plants
G. A. Nelson

EDITORIAL DEPARTMENT

Editor, J. J. JAKLITSCH, JR.
Editor Emeritus, GEORGE A. STETSON
Consulting Editor, LEO BLODGETT
Production, JEAN NORTH
Art Editor, HENRY BALFOUR

OFFICERS OF THE ASME

President, G. B. WARREN
Secretary, O. B. SCHIER, II
Treasurer, E. J. KATES
Assistant Treasurer, H. J. BAUER

PUBLICATIONS COMMITTEE

Chairman, JOHN de S. COUTINHO
B. G. A. SKROTZKI
HENDLEY N. BLACKMON
R. D. MINDLIN
MARTIN GOLAND

Junior Representatives
A. T. WUSKA
A. S. GOLDSTEIN

REGIONAL ADVISORY BOARD

Region I, ROY L. PARSELL
Region II, GLENN R. FRYLING
Region III, F. J. HEINZE
Region IV, FRANCIS C. SMITH
Region V, H. M. CATHER
Region VI, C. R. EARLE
Region VII, M. POPOVICH
Region VIII, LINN HELANDER

Published quarterly by The American Society of Mechanical Engineers. Publication office at 20th and Northampton Streets, Easton, Pa. The editorial department is located at the headquarters of the Society, 29 West Thirty-Ninth Street, New York 18, N. Y. Cable address, "Mechaneer," New York. Price $3.00 a copy, $10.00 annually; to members, $1.50 a copy, $5.00 annually. Add 50 cents for postage to all countries outside the United States, Canada, and Pan American Union. Changes of address must be received at Society headquarters seven weeks before they are to be effective on the mailing list. Please send old as well as new address.... By-Law: The Society shall not be responsible for statements or opinions advanced in papers or ... printed in its publications (B13, Par. 4).... Entered as second-class matter March 2, 1928, at the Post Office at Easton, Pa., under the Act of August 24, 1912... © Copyrighted, 1959, by The American Society of Mechanical Engineers. Reprints from this publication may be made on condition that full credit be given the Transactions of the ASME, Series B — Journal of Engineering for Industry, and the author, and that date of publication be stated.

TRANSACTIONS OF THE ASME
is indexed by the Engineering Index, Inc.

TRANSACTIONS OF THE ASME Series A

Journal of
ENGINEERING FOR POWER
Volume 81 • Series A • Number 1

CONTENTS FOR JANUARY, 1959

The January, 1959, issue of the Transactions of the ASME—Series A—*Journal of Engineering for Power* (available at $1.50 per copy to ASME members; $3.00 to nonmembers), contains the following papers:

Studies of Air Pollution Control by Southern California Edison Company, by A. J. Haagen-Smit. (57—SA-59), *Page 1*

Characteristics of Airborne Particles, by T. A. Rich. (57—SA-56), *Page 7*

Stage Performance and Radial Meeting of Axial Compressor Blade Rows, by Jeffrey Watkins. (58—SA-21), *Page 13*

The Measured and Visualized Behavior of Rotating Stall in an Axial-Flow Compressor and in a Two-Dimensional Cascade, by Gino Sovran. (58—SA-20), *Page 24*

Availability Balance of Steam Power Plants, by C. A. Meyer, G. J. Silvestri, and J. A. Martin. (58—SA-16), Page 35

Pulverized-Coal Transport Through Pipes, by R. C. Patterson. (58—SA-24), *Page 43*

Operating Results of an Experimental Supercritical Steam Generator, by E. Daman, H. Phillips, J. Vail, and S. Ling. (58—SA-17), Page 55

Some Notes on the Strength of the Enrico Fermi Reactor Vessel Structure, by F. R. Beyer. *Page 66*

Some Thoughts About the Development of Automotive Gas-Turbine Units, by A. T. Bowden and W. Hryniszak. (58—SA-26), *Page 73*

Electrostatic Shaft Voltage on Steam-Turbine Rotors, by J. M. Gruber and E. F. Hansen. (58—SA-5), *Page 97*

TRANSACTIONS OF THE ASME Series C

Journal of
HEAT TRANSFER
Vol. 81 • Series C • No. 1

CONTENTS FOR FEBRUARY, 1959

The February, 1959, issue of the Transactions of the ASME—Series C—*Journal of Heat Transfer* (available at $1.50 per copy to ASME members; $3.00 to nonmembers), contains the following papers:

Wave Theory of Heat Transfer in Film Boiling, by Yan Po Chang. (58—SA-19), *Page 1*

A Boundary-Layer Treatment of Laminar-Film Condensation, by E. M. Sparrow and J. L. Gregg. (58—SA-2), *Page 13*

Transient Response of Heated Air in an Enclosure With Heat Losses, by W. A. Wolfe. (58—SA-3), *Page 19*

Natural-Convection Heat Transfer in Liquids Confined by Two Horizontal Plates and Heated From Below, by Samuel Globe and David Dropkin, *Page 24*

Transient Heat Transfer for Laminar Forced Convection in the Thermal Entrance Region of Flat Ducts, by R. Siegel and E. M. Sparrow. (58—HT-3), *Page 29*

Generalized Correlation of Boiling Heat Transfer, by S. Levy. (58—HT-8), *Page 37*

Heat Transfer to a Boiling Liquid—Mechanism and Correlations, by Kurt Engelberg-Forster and R. Greif. (58—HT-11), *Page 43*

Transient Heat Conduction in Elliptical Plates and Cylinders, by E. T. Kirkpatrick and W. F. Stokey. (58—HT-10), *Page 54*

Calculation of Transients in a Cross-Flow Heat Exchanger, by G. M. Dusinberre. (58—HT-5), *Page 61*

Free Convection, Forced Convection, and Acoustic Vibrations in a Constant Temperature Vertical Tube, by T. W. Jackson, W. B. Harrison, and W. D. Boteler. (58—HT-6), *Page 68*

Summary—Selected References on Gas Turbines, Regenerative Cycles, Rotary Regenerators, and Associated Heat-Exchange and Pressure-Drop Information, by W. E. Hammond. *Page 75*

Investigation of Heat Transfer, Flow, and Heat Exchangers as Related to Turbine Cooling, by H. H. Ellerbrock, Jr., and J. N. B. Livingood. *Page 79*

Progress and Development of Gas-Turbine Regenerators, by Sven Holm and R. L. Lyerly. *Page 86*

Heat Transfer and Friction for Fluids Flowing Over Surfaces at High Temperatures and High Velocities, by R. G. Deissler and A. L. Loeffler, Jr. *Page 89*

A New Technique for Measuring the Spectral Emissivity of Solids at High Temperatures, by P. E. Glaser and H. H. Blau, Jr. (58—AV-29), *Page 92*

A. Y. ATTIA

Lecturer, Department of Mechanical Engineering, Ein Shams University, Abbassia, Cairo, Egypt

Dynamic Loading of Spur Gear Teeth

The paper presents results of strain gage investigations conducted on steel spur gears to measure the instantaneous load on the tooth under static and dynamic conditions.

Introduction

THE DYNAMIC LOADING on spur gear teeth is the maximum momentary load imposed on the gear teeth by the conditions of service including the influence of errors in the gear teeth. The extent and nature of the dynamic loading have long been open questions. Its magnitude is always assessed with considerable amount of guesswork aided with different empirical and theoretical formulas. The well-known formulas are those of Buckingham [1],[1] Tuplin [2, 3], and Reswick [4].

In this investigation the electric resistance strain gages have been used to record the deflections of the gear teeth and to measure the maximum instantaneous load on the tooth as it traverses the zone of contact at different speeds and under different loads.

The test gears are made of E.N. 39-4 1/4 per cent Ni-Cr case-hardened steel. They are of 5-in. mesh circle diameter and 20 teeth of the British Standard Involute form with 20-deg pressure angle and 4-diametral pitch.

The Measuring Apparatus

The machine used is 5-in. center gear testing machine shown in Fig. 1. It is of the power circulating type in which two pairs of gears having the same tooth ratio are joined by two shafts in which torque is applied to load one pair of gears against the other, the driving motor being required to supply only the rotation and the power losses.

The test gears are mounted on readily accessible splined shafts in one gear box which is fixed rigidly to the base of the machine and the power return gears (or slave gears), which are of greater face width, are mounted on similarly splined shafts in another gear box which is free to rotate in trunnions about the axis of the input drive shaft. The four gear shafts are joined by means of splined sleeves to two coupling shafts, one of which incorporated two Hooke's joints to accommodate the movement of the power return gear box in its trunnion. On the latter gear box is built a balanced loading lever by means of which, together with the 1000-lb spring balance and screw device, torque can be applied to the gear system while the gears are rotating.

The two test gear shafts were replaced by two longer shafts extending to the outside test gear box in order to carry the test gears in easily accessible positions. Each test gear is fastened to the flange of its shaft by ten pins.

The Strain Gage Arrangement

As shown in Fig. 2 a small rectangular piece of steel was soldered to the side of one of the teeth of the driven gear. A steel disk of the same diameter as that of the gear was fastened firmly to the body of the gear. The small soldered piece projected into a rectangular slot in the disk with about 0.05-in. clearance. The outer surface of the disk and the steel piece were ground together.

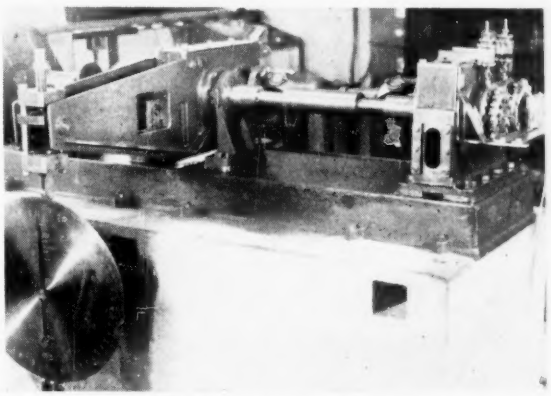

Fig. 1 Five-inch center gear testing machine

An electric resistance strain gage, of the Rotol wire-wound type of 10,000-ohms resistance and 1/2 × 3/8-in. size, was fixed to the steel disk and to the gear, so as to bridge the gap.

The strain gage in this case is used as extensometer to measure the deflection of the loaded tooth with respect to the unstrained disk.

A slip-ring arrangement, shown in Fig. 2, is used to transmit the electric signal from the strain gage fixed on the rotating gear to the stationary recording apparatus. It consists of nickel-plated copper disks mounted on a hollow spindle screwed to the machine shaft carrying the test gears. The copper disks are separated from one another by perspex washers. Short lengths of wire were taken through the spindle and out through radial holes and soldered on the copper disks. The copper disks dip in mercury inside cylindrical cavities of a perspex container which is fixed on a frame extended from the machine.

The Electric Circuit

The circuit diagram as shown in Fig. 3 is the general form of Wheatstone Bridge in which the strain gage is one of the arms. The calibration of the circuit is carried out by an accurate resistance in series with one of the arms. A Cambridge spot galvanometer was used for the static calibration of the strain gage. For the dynamic measurements a Furzhill Oscilloscope of the type 1684 N was used. The traces were recorded on 5-B 52 Ilford-35 mm film by a Cossor Camera of speed varying from 0.1 to 25 in. per second.

Experimental Procedure

Experiments were carried out to record the deflections of the point on the profile where the strain gage is fixed at different speeds and at different loads.

Traces were also recorded for the tooth deflections under different loads when the machine was slowing down to rest. These

[1] Numbers in brackets designate References at end of paper.

Contributed by the Machine Design Division and presented at the Semi-Annual Meeting, New York, N. Y., June 15–19, 1958, of THE AMERICAN SOCIETY OF MECHANICAL ENGINEERS.

NOTE: Statements and opinions advanced in papers are to be understood as individual expressions of their authors and not those of the Society. Manuscript received at ASME Headquarters, December 16, 1957. Paper No. 58—SA-32.

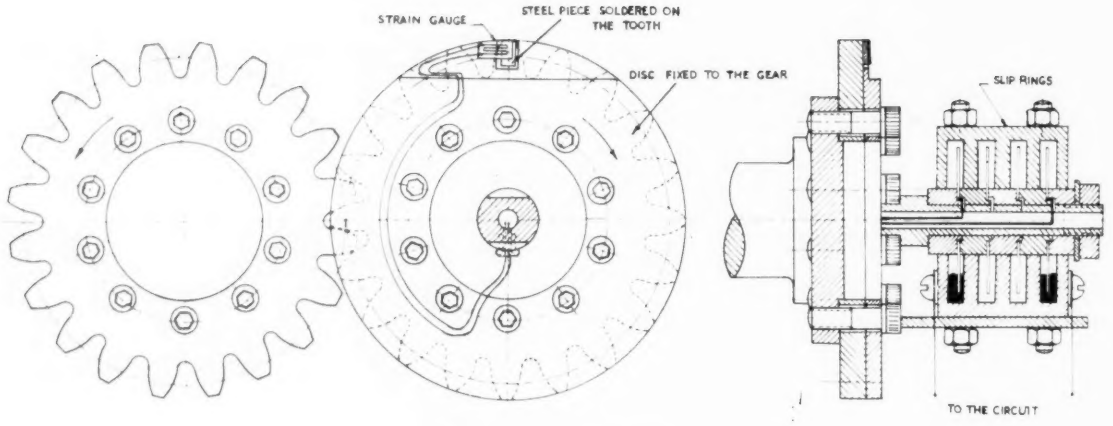

Fig. 2 Strain-gage arrangement

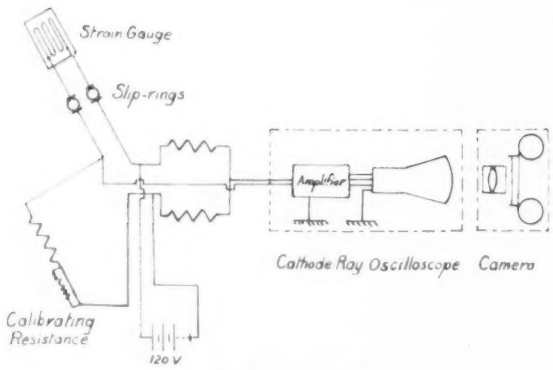

Fig. 3 Electric circuit

traces, if compared with the corresponding traces recorded at speed, will show the effect of speed on the tooth deflection and the position of the maximum dynamic loading. The mesh between the gears was changed by pushing the driven gear shaft out after releasing its coupling bolts and rotating it until any desired tooth of the driving gear came in mesh with the tooth carrying the strain gage. By changing the mesh between the gears the amount and distribution of the errors between the gears were also changed.

Dynamic and static records were taken for each mesh and compared with the corresponding static relative displacement diagrams.

Calibrations of the Strain Gage

1 The oscilloscope screen was calibrated just before and after each dynamic record.

2 Calibration curves of the tooth deflections under static loads were recorded at very low speed. From these curves, sets of curves could be drawn for the tooth deflection in terms of the change in resistance of the strain gage, when contact takes place at any point on the path of contact.

3 Static calibration curves of the strain gage, when the load is carried by only one pair of teeth along the whole path of contact, was carried out by inserting a steel shim of 0.003-in. thickness between the working faces of the mating teeth. The strain gage was then calibrated under different static loads at different points on the path of contact.

Measurement of the Resultant Errors Between the Gears

The static relative displacements between the gears at different meshes were measured by the sine bar method. By this method it is possible to measure the irregularity in motion between the gears over very small angular displacements. The apparatus, as shown in Fig. 4, is composed of two equal V arms fixed to the gears by steel teeth welded at the ends of the arms. Each arm is tightened to the gears by means of a tie bolt. Each arm carries between its two branches a flexible steel shim with half a steel ball soldered to its end.

Two dial indicators, one at each end, are fixed to the arms and could be adjusted vertically so that their styluses are centered on the balls. The two balls rest on two equal columns of slip gages set on a perfectly flat surface. The flexible strips were adjusted by a vernier so that the distances between the center of the ball and that of the gear are equal on both sides.

The two gears were set at the starting point of contact of the test tooth. The dial indicators were then set to read the same reading over the two piles of the slip gages. Equal slip gages were then taken off or added to the two piles and the gears were rotated until each ball touched the surface of its column. The difference between the readings of the dial indicators gives the difference in circumferential displacements measured at the ends of the measuring arms. By simple geometry the difference between the angular displacements of the gears can be determined.

Fifty readings were taken for each set of mesh between the gears. These readings cover the path of contact of the pair of teeth under test together with half the path of each of the neighboring pairs of teeth.

Experimental Results

The recorded traces represent the deflections of the strain-gage point under the applied load at different points on the tooth profile. They provide a clear picture of the tooth behavior as the result of the load conditions and the elastic properties of the material. They also show the effect of speed, irregularity in motion, and the applied load on the maximum momentary load on the tooth.

In the trace shown in Fig. 5 point k is the start of tooth contact and point t is its end. The rise in the trace before point k shows the strain on the tooth before it comes into contact. This strain is transmitted to the tooth from the preceding strained tooth through the body of the gear.

The steep rise kl shows the sudden sharing of load between the

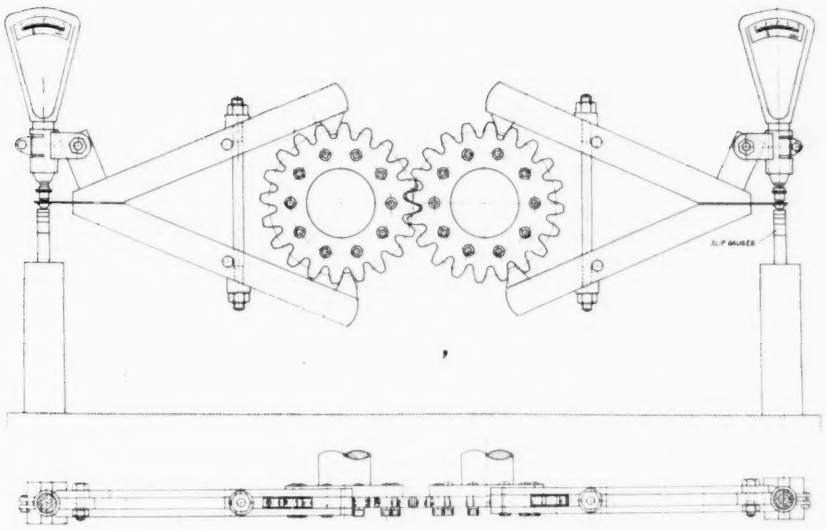

Fig. 4 Sine bar method for measuring resultant errors in gear teeth

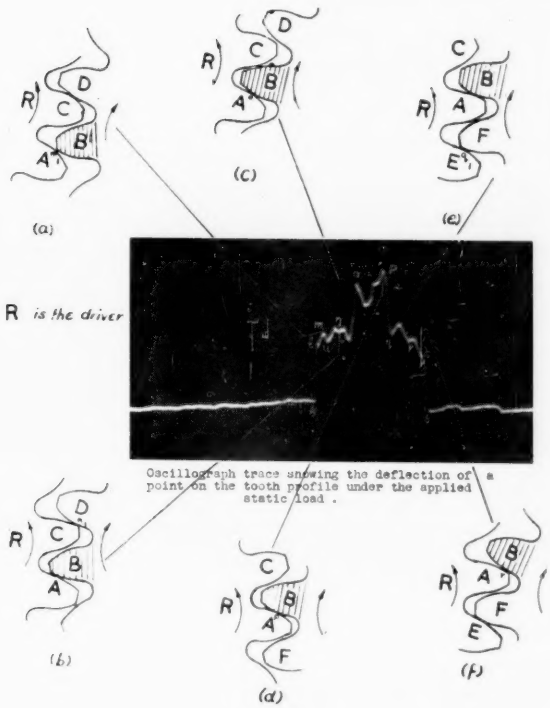

Fig. 5

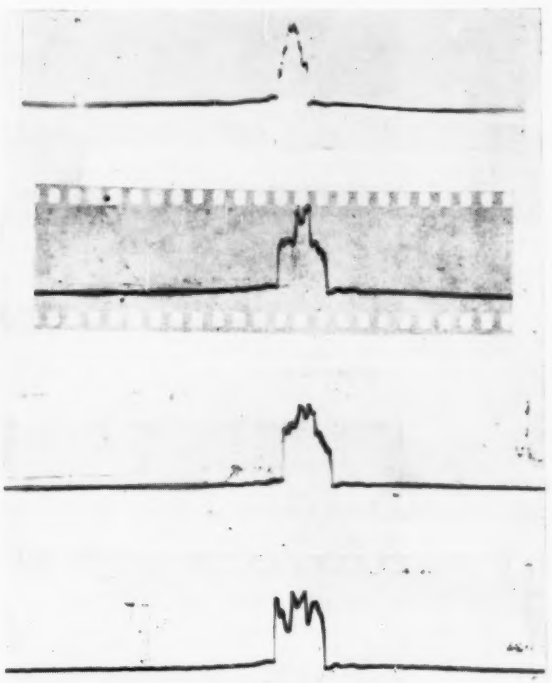

Fig. 6 Oscilloscope traces recorded for different teeth under transmitted load of 1570 lb/in. and at low speed of 10 rpm

tooth and its preceding one. The bump shown on the trace at point m is caused by the tip of the tooth B coming in action in its trochoidal path and interfering with the flank of the tooth at point m, Fig. 5(a).

At point n, Fig. 5(b), the teeth C and D leave contact causing a slight increase of load between teeth A and B. This is shown on the trace by a rise at point n followed by a drop at the start of zone of single contact.

The single zone contact starts after point n and ends at q when the teeth E and F, Fig. 5(e), come into contact.

The drop of load at point q is due to the interference between teeth E and F at point q, Fig. 5(e). This interference increases at the same time the load on tooth F. The bump at the point r is also due to the interference between the tip of the tooth A and tooth B on its way out, Fig. 5(f). A slight negative deflection is noticeable at the end of contact t. This happens as the result of the sudden drop of load and the instantaneous return of the tooth root after it has been lifted up by the applied load.

After point t and as soon as the tooth returns to its normal

position it comes back quickly under the influence of the strain in the body of the gear transmitted to the tooth from the following loaded tooth. This is shown by the stepped rise in the trace after point *t*.

Effect of the Combined Inaccuracy

Fig. 6 shows four traces recorded for the deflection of the tooth under test when it was in four different meshes with the driving gear. The load applied in each case was 1570 lb/in. of face width and the traces were recorded at speed of 10 rpm. The traces have the same characteristics which were explained before. A slight change in the shape of the bumps may be noticed and this may be due to the amount and nature of the interference between the tips of the teeth and their mating points on the profile. This interference depends also on how the tips of the teeth were worn off after a few rotations of the newly cut gears.

The changes in the load distribution between the same tooth and its mating teeth in different meshes are also noticeable by comparing the rises in the traces at the start and end of contact. This difference in the load distribution between any two pairs of teeth sharing the load depends upon the combined stiffness of each pair and upon the combined spacing inaccuracy.

Effect of the Transmitted Load

Fig. 7 shows four sets of oscilloscope traces recorded at very low speeds for the tooth under test in four different meshes. In each set, traces for three different tooth loads are shown. By comparing these traces, the effect of the transmitted tooth load on the tooth deflection may be studied.

Under very light loads the driven gear does not perfectly follow the driver but it is sometimes free, to a certain extent, to move ahead as far as the backlash between the gears permits. Any positive errors in spacing or interference at the first point of contact may speed up the driven gear and slow down the driver which may cause separation between the teeth and back-to-back contact if the backlash is not sufficient. This is shown by the traces recorded at light loads, Fig. 7, where the different zones of load distribution are not well defined as in the case of heavily loaded gears. This is because at light loads the loads are not heavy enough to oppose the effect of the errors.

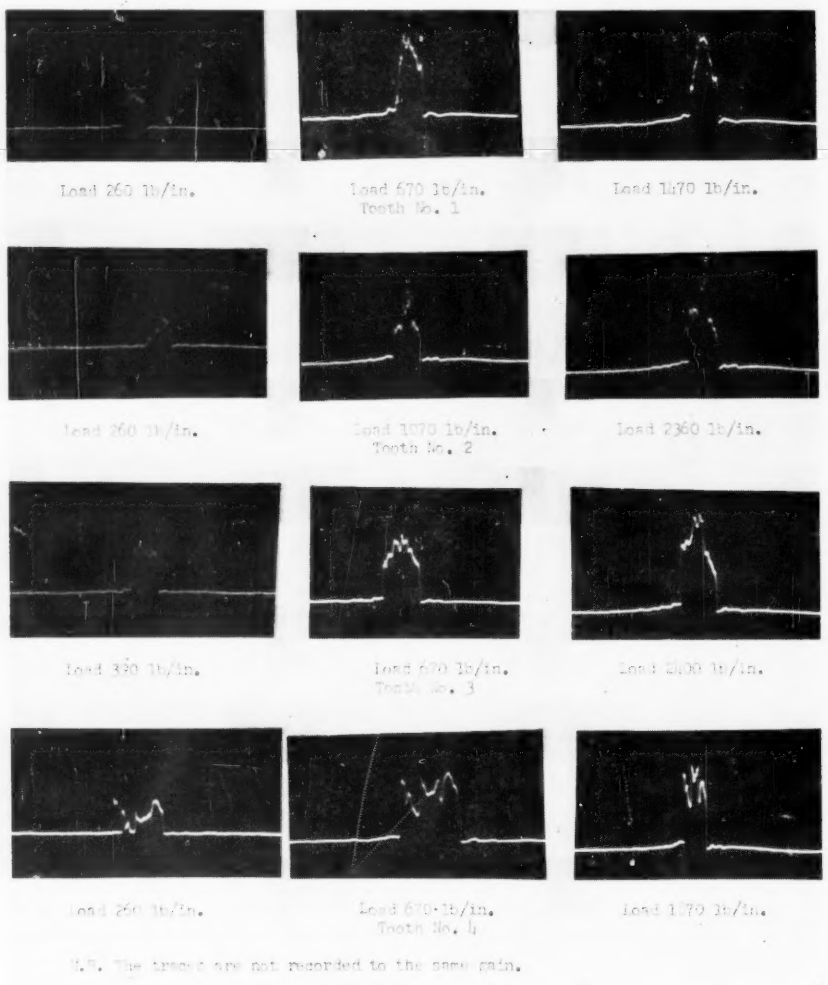

Fig. 7 Oscilloscope traces showing the change of the deflection curves of the tooth with the change of the static transmitted load

The deflection of the tooth and its increase with the increase of the applied load also changes the conditions of loading between the teeth sharing the load. This may cause excess interference, premature contact, or changes in the clearances and the gaps that may exist as a result of profile errors or base pitch errors. In the case of tooth No. 4, Fig. 7, the tooth load dropped to zero as a result of a gap between the teeth. With the increase of the applied load the gap gradually decreases by the tooth deflection and the teeth start sharing the load as shown on the traces recorded at heavier loads.

Dynamic Measurements

The dynamic effect of pitch errors on tooth loading was studied by comparing the traces recorded at different speeds with those recorded at very low speeds. The amount of dynamic increase at different points on the path of contact together with the magnitude and position of the maximum tooth load were also determined.

Fig. 8 shows the traces recorded for tooth deflections under no load at different speeds. These traces show the presence of double peak loading for every tooth contact. At the speed of 2100 rpm there is no time for the double peak to take place and the pattern has started to change.

The double-peak loading is due mainly to the introduction of the errors at the start of contact and the free motion of the unloaded teeth.

The dynamic effect on the teeth when they are loaded is different. The separation of the teeth due to impact is resisted by the transmitted load. Fig. 9 shows the oscilloscope traces recorded at different speeds and under static transmitted load of 852 lb/in. width. Up to a speed of 2100 rpm there was no noticeable change in the stress pattern for the tooth for the same mesh.

Fig. 10 shows the graphical representation of the change of the normal force on the tooth with the change of speed and transmitted load for different teeth in mesh with the measuring tooth.

Fig. 11 shows the dynamic and static tooth-load diagrams, derived from the recorded traces and the calibration curves, for certain mesh between the gears.

Fig. 12 shows the static relative displacement diagram for different angular positions. Fig. 13 shows the maximum dynamic increments and their changes with the speed of the gears and the static transmitted loads. The two dotted lines shown in Fig. 13

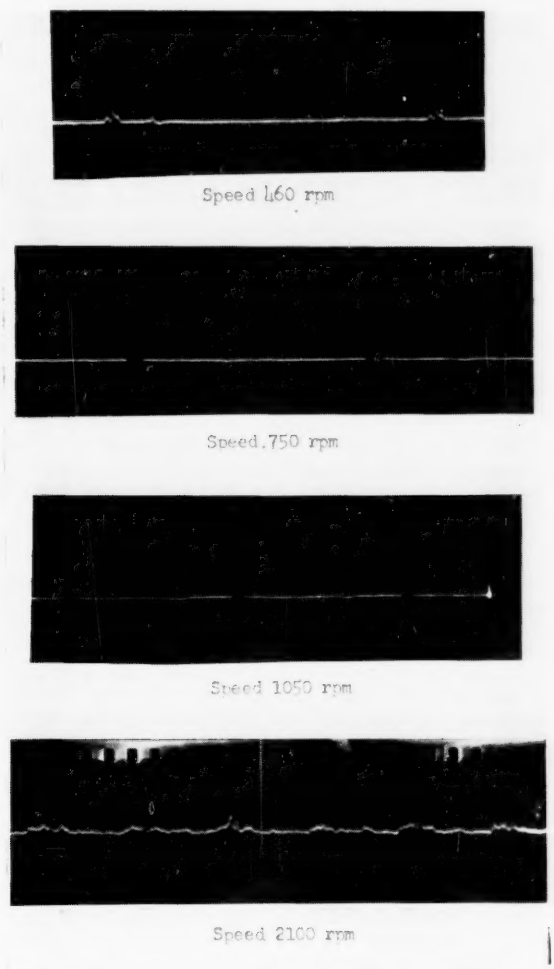

Fig. 8 Oscilloscope traces showing the dynamic effect at different speeds and no transmitted load

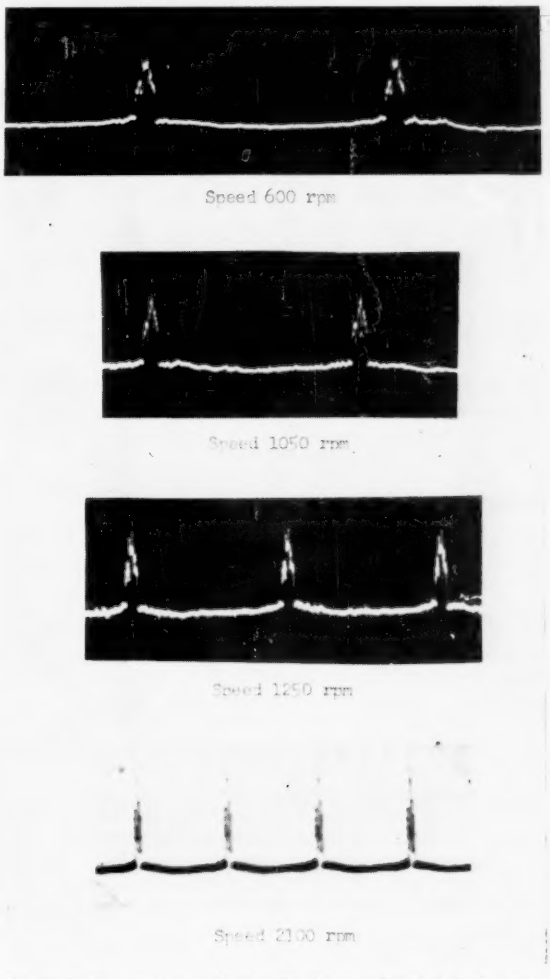

Fig. 9 Oscilloscope traces showing the changes of tooth deflection curve at different speeds and at constant static transmitted load of 852 lb/in. of face width

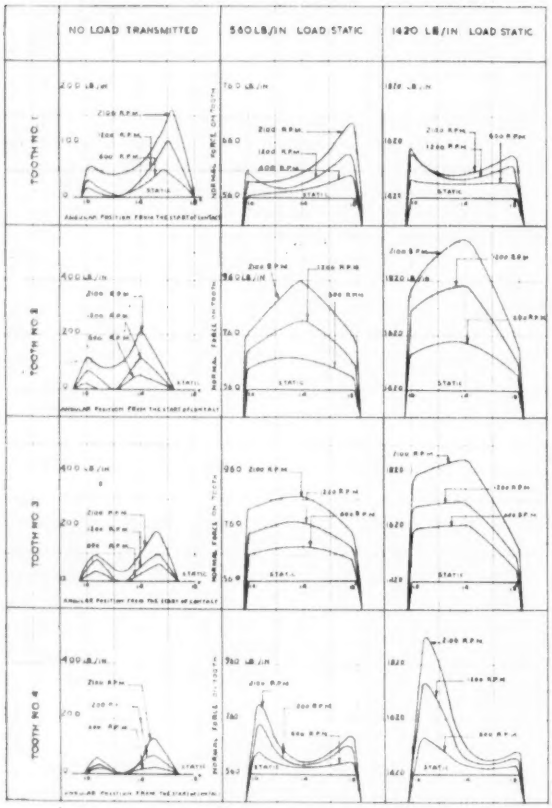

Fig. 10 Normal force on the tooth as it passes the single zone contact for four different gear meshes and different speeds and transmitted load

give the values of the dynamic increment loads as calculated by the formulas derived by Buckingham [1] and Tuplin [2]. Fig. 14 shows the maximum load on the tooth plotted against the transmitted loads for different speeds.

Discussion of Results

The dynamic records obtained from testing 10 different teeth showed that the position of the maximum dynamic loads on the tooth does not occur at any fixed phase of engagement. It could also be seen that the dynamic effect on the tooth is not so simple as that which might be expected to result from the simple engagement of smooth teeth with a simple pitch error. The traces showed that the tooth-load diagram is not a smooth one, but consists of bumps, sudden rises, and drops, and the pattern is not the same for all the teeth in the same gear. It was also observed that there is dynamic increment loading at the moments when the motion of the test tooth is interrupted by other teeth sharing the load with it, coming in mesh or leaving contact. To reach a precise evaluation of the maximum tooth load and its location, the motion of the gear tooth and its vibrations should be studied as a continuous motion interrupted by the initial interference between the teeth at the start of contact causing forced vibratory motion followed by a free motion. This free motion is interrupted by the irregularity in motion caused by the machining errors and the deflection of the tooth under the applied load. The motion then faces further interruption caused by the other teeth leaving contact. The motion then becomes more complicated when the teeth start to take over all the load as a result of

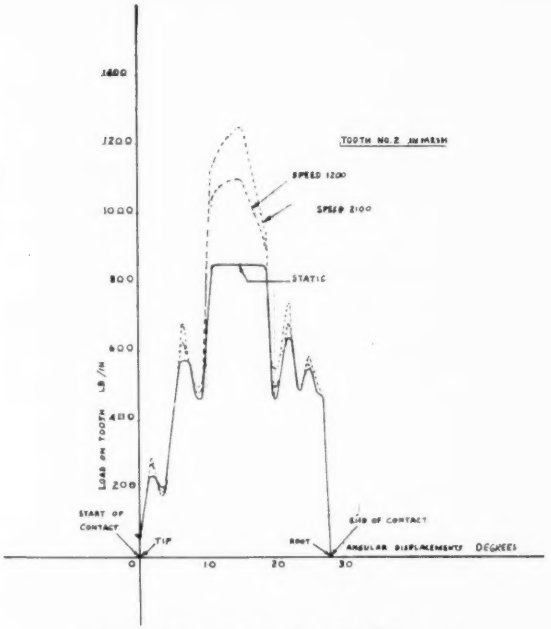

Fig. 11 Dynamic and static tooth load diagrams

which a complex vibratory motion takes place during the zone of single contact. The amount and position of the dynamic load depends upon the maximum amplitude of this motion.

In this investigation the results of tests carried out under normal operating loads show that Buckingham's equations give very high values of dynamic increments. Tuplin's equations, although they do not take the effect of the static transmitted load into consideration, give nearer values to the experimentally measured ones.

Conclusions

Electric resistance strain gages can be used as extensometers to measure the elongations over very short gage lengths. By this it means it is possible to study the deflections of the gear tooth under load and accordingly to investigate the static and dynamic loading on the tooth.

The strain in the body of the gear causes the tooth to deform before it comes in mesh. This deformation together with the existing base pitch errors between the teeth cause impacts, sudden rises, and drops in the load curves of the tooth with the result of the occurrence of dynamic increments of load when the gears run at speed.

For the case of the test gears, of contact ratio of 1.55, the maximum dynamic load occurs during the zone of single contact, but it does not occur at any fixed position of engagement.

Results also show that the load on any particular tooth at any particular speed varies as the transmitted load varies.

Further Investigations

Many more tests should be carried out in a high-speed gear testing machine to study the effect of the dynamic loading at very high speeds and heavier transmitted loads of gears of different numbers of teeth, pitches, and contact ratios. Some more points that come to mind include the following:

1 Effect of different lubricants on dynamic loading on gears.

2 Effect of surface finish and tooth-profile modification on dynamic loading.

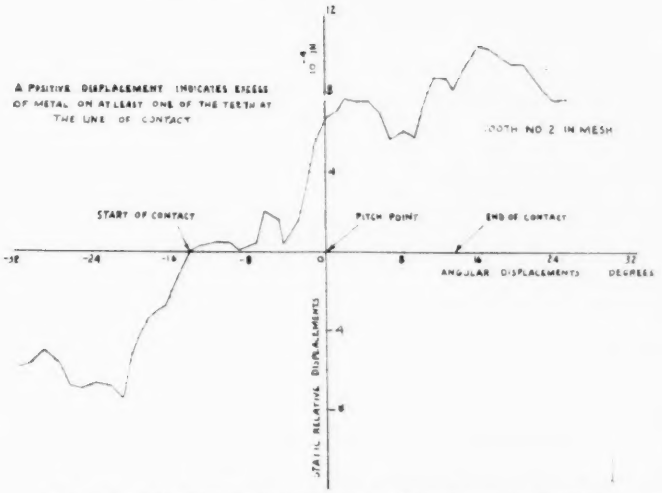
A POSITIVE DISPLACEMENT INDICATES EXCESS OF METAL ON AT LEAST ONE OF THE TEETH AT THE LINE OF CONTACT
TOOTH NO 2 IN MESH
START OF CONTACT
PITCH POINT
END OF CONTACT
ANGULAR DISPLACEMENTS DEGREES
TOTAL RELATIVE DISPLACEMENTS

Fig. 12 Static relative displacements at different angular positions

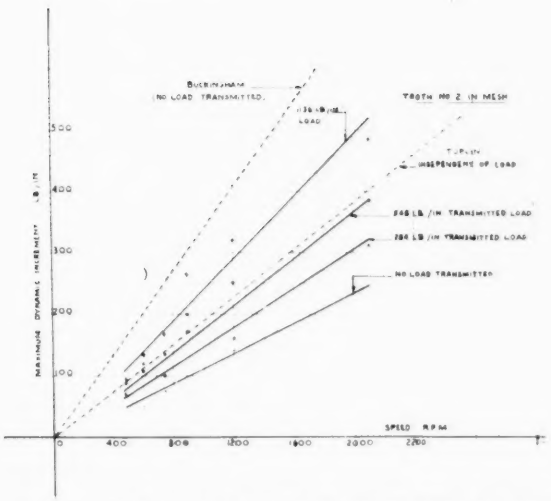

Fig. 13 Maximum dynamic increments at different speeds and static loads

3 Effect of torsional vibrations and dynamic unbalance on dynamic loading.

4 Effect of cyclic variation of the externally applied load on the dynamic loading.

Acknowledgment

Grateful acknowledgment is due to Prof. W. A. Tuplin, Professor of Applied Mechanics, The University of Sheffield, England, for his continuous help, encouragement, and valuable ideas during his supervision of this work.

References

1 E. Buckingham, "Analytical Mechanics of Gears," McGraw-Hill Book Company, Inc., New York, N. Y., 1949.

2 W. A. Tuplin, "Gear-Tooth Stresses at High Speed," *Proceedings of The Institution of Mechanical Engineers*, vol. 163, 1950, pp. 162–167.

3 W. A. Tuplin, "Dynamic Loads on Gear Teeth," *Machine Design*, vol. 25, no. 10, 1953, p. 203.

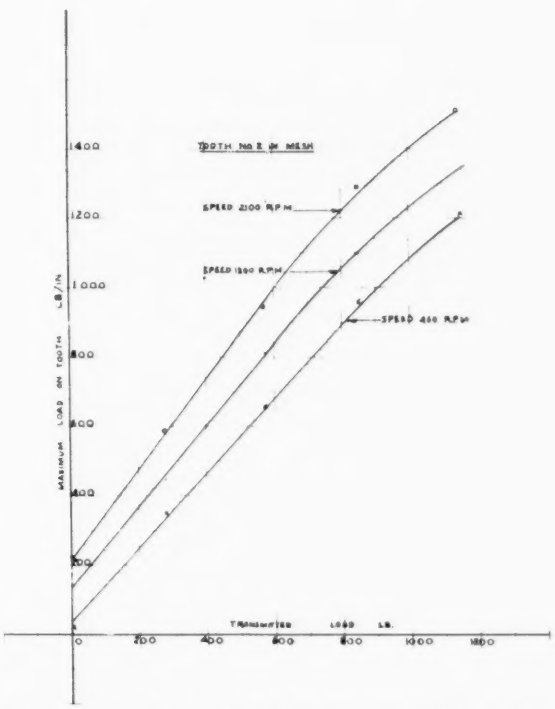

Fig. 14 Maximum load on tooth at different transmitted loads and speeds

4 J. B. Reswick, "Dynamic Loads on Spur and Helical-Gear Teeth," TRANS. ASME, vol. 77, 1955, pp. 635–644.

DISCUSSION

W. Coleman[2]

The writer is quite favorably impressed by the author's work. He should continue on this project to learn more about the effects of other variables as outlined in his concluding section. We

[2] Gear Engineering Department, Gleason Works, Rochester, N. Y.

should especially like to see work done with the effects of tip modification.

One of the problems with this sort of test is the determination of the magnitude of the errors under a given load. The tooth may start out with a conjugate tooth shape under no load, but will assume a nonconjugate tooth shape under load. Conversely, the tooth may start out with a nonconjugate shape under no load, but may assume a conjugate tooth shape under one specific load. Does the author have a means of checking conjugacy under load? Correlation between errors at no load and errors under a specific load deserve more study.

The author states that he measured the gear-tooth errors. Could he indicate the magnitude of the errors on the specific teeth on which tests were performed? These data would be helpful in making comparisons with other methods for calculating the dynamic loads.

The author deserves thanks in his efforts to further the understanding of gear-tooth behavior under load.

T. P. Goodman[3]

This pioneering experimental investigation is a welcome contribution toward the increased understanding of the nature of dynamic loading in gear teeth. Readers of the paper will also be interested in the parallel investigations of Niemann and Rettig[4,5] in Germany, and of Richardson[6] in the United States.

E. J. Wellauer[7]

The subject paper is an extremely valuable contribution to the complex problem of gear-tooth capacity and rather particularly as regards the measurement of dynamic loads. This subject has been in a confused situation mainly because the contributions of previous researchers had been made prior to the advent of modern measuring instruments of high accuracy. The paper indicates that much further work can be done on this subject and the writer is quite certain this start will encourage other research along this line.

Perhaps the most valuable evidence contributed by the paper is that the dynamic-load increment as suggested by Buckingham and Tuplin cannot be generalized. Modern gear-rating methods have recognized this factor and attempt to evaluate dynamic loading by more accurate means. The use of the transmitted load as a parameter in studying the dynamic increment is interesting, particularly since Fig. 14 of the paper shows that, for certain speeds and mesh conditions, the percentage of the dynamic increment reduces as the load increases. This has always been an accepted phenomenon and late research in the author's laboratory has tended to indicate that the flexibility of the gear teeth is very much involved with the quantitative aspect of this phenomenon.

The writer would be interested in knowing whether or not the author studied the comparison between the static relative displacements under various torque loadings. In addition, the physical dimensions and stiffness of shafts and supports, and errors in mounting would enable the data to be quantitatively analyzed more completely.

The author is to be congratulated on his fine work and it is hoped that he will contribute further information on this subject.

[3] Assistant Professor of Mechanical Engineering, Massachusetts Institute of Technology, Cambridge, Mass. Assoc. Mem. ASME.

[4] G. Niemann and H. Rettig, "Dynamische Zahnkräfte," *VDI Zeitschrift*, vol. 99, 1957, pp. 89, 131.

[5] H. Rettig, "Dynamische Zahnkraft," Dissertation, Technische Hochschule, Munich, Germany, 1957.

[6] H. H. Richardson, "Static and Dynamic Load, Stress, and Deflection Cycles in Spur Gearing," ScD thesis, Department of Mechanical Engineering, Massachusetts Institute of Technology, Cambridge, Mass., 1958.

[7] Assistant Chief Engineer, The Falk Corporation, Milwaukee, Wis. Mem. ASME.

Author's Closure

The author wishes to thank the discussers for their valuable comments. Mr. Coleman points out very correctly to the effect of the change of conjugacy under load on the maximum dynamic tooth load. The author believes that, for Ni-Cr, case-hardened

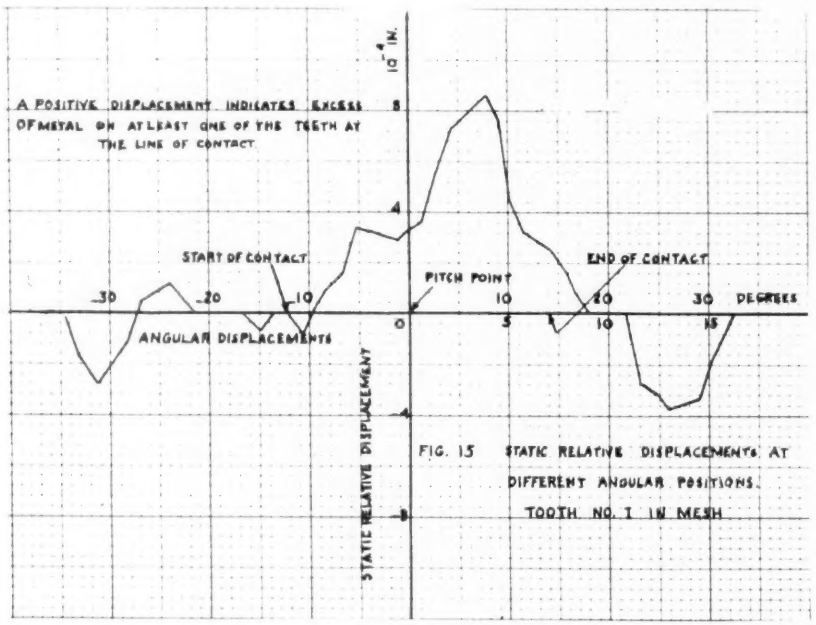

FIG. 15 STATIC RELATIVE DISPLACEMENTS AT DIFFERENT ANGULAR POSITIONS. TOOTH NO. 1 IN MESH

steel gears as the test gears, and under static transmitted loads as those at which the present results were obtained, such effect would be little compared to the effect of the combined resultant errors between the gears as they roll.

It is not only the magnitude of errors between two gears in mesh that counts in calculating the dynamic loading or in comparing between any two pairs of gears. There are many other factors such as the time of insertion of error at the moment when the maximum dynamic loading occurs, the shape and nature of the error itself, the shape of the cyclic change of error along the path of tooth contact, and many other factors. All or some of these factors change in nature and magnitude under load and at speed which makes the analysis of the problem very complicated if treated as a pure vibration problem.

Fig. 12 which shows the change of error of one tooth was given as a sample of results of tests carried out by the author[8] on the teeth of the test gears. For the sake of interest and comparison, Figs. 15, 16, and 17 together with Fig. 12 form the static relative displacement curves at different angular positions for the four specified teeth whose test results were given in Fig. 10, respectively.

[8] A. Y. Attia, "Dynamic Loads of Spur Gear Teeth," PhD thesis. Department of Applied Mechanics, The University of Sheffield, England, 1956.

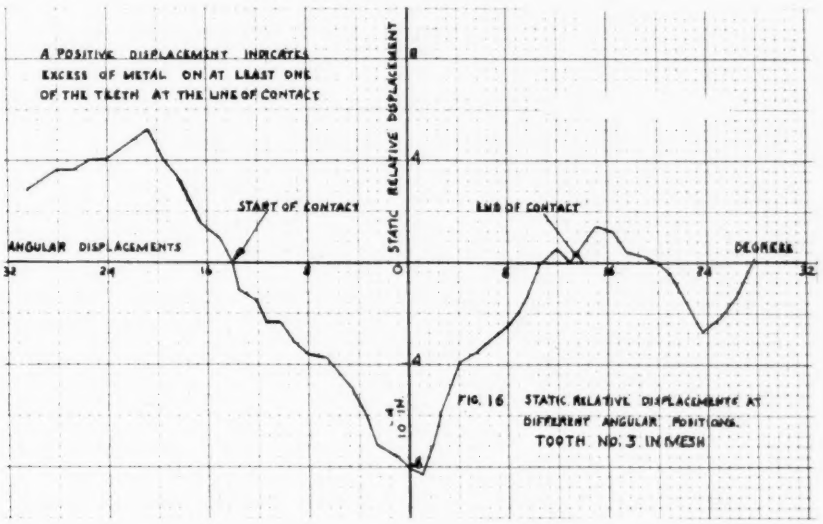

FIG. 16 STATIC RELATIVE DISPLACEMENTS AT DIFFERENT ANGULAR POSITIONS. TOOTH NO. 3 IN MESH

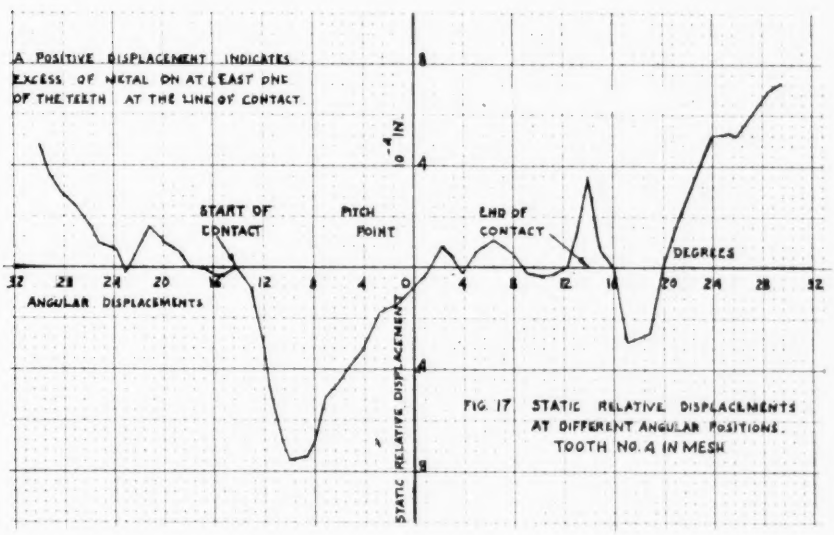

FIG. 17 STATIC RELATIVE DISPLACEMENTS AT DIFFERENT ANGULAR POSITIONS. TOOTH NO. 4 IN MESH

Analytical Design of an Ackermann Steering Linkage

W. A. WOLFE

Associate Professor of Mechanical Engineering, The University of British Columbia, Vancouver, British Columbia, Canada. Mem. ASME

A method is outlined whereby the dimensions of an Ackermann steering linkage may be determined analytically. The theoretical relation between the angles of rotation of the front wheels of a vehicle is derived and it is shown how this relation may be approximated by a symmetrical four-bar linkage.

The method is briefly as follows:

The basic relation between the angles of the four-bar linkage is derived and the theoretically correct relation between the angles is used to express the four-bar linkage equation as a function of one variable. If this derived equation can be made equal to zero for a suitable range of wheel-turning angle by proper adjustment of the coefficients, then the magnitudes of the coefficients will determine the physical dimensions of the linkage.

A direction solution as indicated does not seem possible so an approximate solution is developed by expressing the derived equation as a power series and adjusting the coefficients of this series so that the sum of the lower order terms deviates the least from zero.

Nomenclature

θ, ϕ = angles of rotation of the steering wheels
α = initial angle between levers of steering mechanism and fixed link, when wheels are in straight-ahead position
w = wheel-base of vehicle
d = distance between pivot centers of steering wheels (length of fixed link)
a = length of crank
b = length of coupler
ψ = angle between coupler and fixed link
$\gamma = \dfrac{d}{w}$ = ratio of pivot centers to wheel-base
$\beta = \dfrac{a}{d}$ = ratio of lever length to pivot center distance
$X = \cot \phi$
$Y = \cot \theta$
$t = \dfrac{1}{Y} = \tan \theta$
i = defined by relation $i^2 = -1$

As is well known, the independently pivoted front wheels of a vehicle should satisfy the relation

$$\cot \phi - \cot \theta = \frac{d}{w} = \gamma \qquad (1)$$

where the variables are as indicated in Fig. 1.

Although a mechanism can be designed for actuating the steering wheels which will reproduce this relation exactly, it has not found favor and is usually replaced by a four-bar linkage which reproduces the desired motion approximately. The author's purpose is to show how such a four-bar linkage can be designed analytically.

Consider the linkage sketched in Fig. 2. If the linkage is considered in its symmetrical position, then deviations from this position can be expressed in terms of the angles ϕ and θ, as follows:

$$ae^{i(\alpha+\phi)} + be^{i\psi} = d + ae^{i(\pi-\alpha+\theta)}$$

or

$$be^{i\psi} = d - ae^{i(\theta-\alpha)} - ae^{i(\phi+\alpha)} \qquad (2)$$

writing $-i$ for i

$$be^{-i\psi} = d - ae^{-i(\theta-\alpha)} - ae^{-i(\phi+\alpha)}$$

multiply

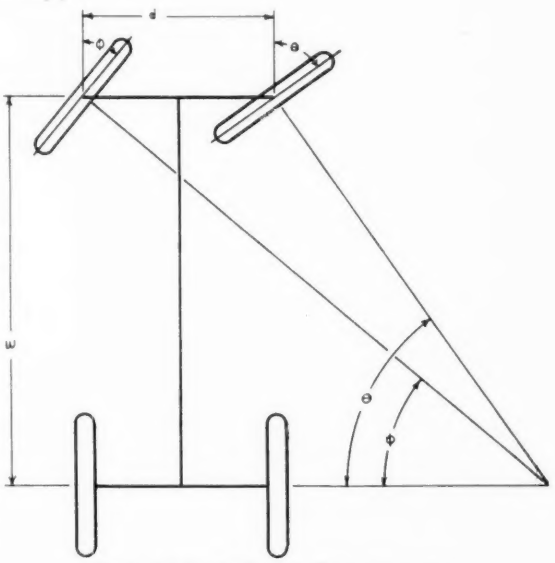

Fig. 1 Relation for theoretically correct steering

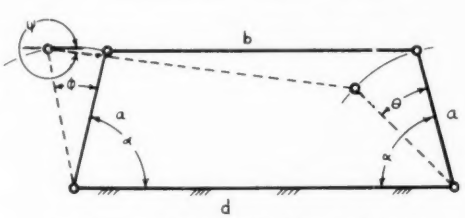

Fig. 2 Relation for symmetrical four-bar linkage

Contributed by the Machine Design Division and presented at the Semi-Annual Meeting, Detroit, Mich., June 15–19, 1958, of THE AMERICAN SOCIETY OF MECHANICAL ENGINEERS.

NOTE: Statements and opinions advanced in papers are to be understood as individual expressions of their authors and not those of the Society. Manuscript received at ASME Headquarters, December 17, 1957. Paper No. 58—SA-31.

$$b^2 = d^2 + 2a^2 - 2ad\cos(\theta - \alpha) - 2ad\cos(\phi + \alpha) + 2a^2\cos(\theta - \phi - 2\alpha) \quad (3)$$

A further relation may be obtained from (3) by observing that in the initial position ϕ and θ are each zero or

$$b^2 = d^2 - 4ad\cos\alpha + 2a^2(1 + \cos 2\alpha) \quad (4)$$

Now subtracting (4) from (3) gives

$$2a^2\cos 2\alpha - 4ad\cos\alpha = 2a^2\cos(\theta - \varphi - 2\alpha) - 2ad[\cos(\phi - \alpha) + \cos(\theta + d)] \quad (5)$$

Equation (5) is easily rewritten as

$$\frac{a^2}{d^2}\cos 2\alpha - \frac{2a}{d}\cos\alpha = \frac{a^2}{d^2}\cos(\theta - \phi - 2\alpha) - \frac{a}{d}[\cos(\phi - \alpha) + \cos(\theta + \alpha)] \quad (6)$$

For simplicity introduce the symbol $\beta = a/d$ and $R = \beta^2(\cos 2\alpha - 2\beta\cos\alpha)$

$$R = \beta^2\cos(\theta - \phi - 2\alpha) - \beta[\cos(\phi - \alpha) + \cos(\theta + \alpha)] \quad (7)$$

Now if one calls $\cot\phi = X$
and $\cot\theta = Y$

Then equation (1) may be written

$$X - Y = \frac{d}{w} = \gamma \quad (8)$$

and equation (7) as

$$R = \beta^2\left\{\frac{1 + XY}{[(1 + X^2)(1 + Y^2)]^{1/2}}\cos 2\alpha + \frac{X - Y}{[(1 + X^2)(1 + Y^2)]^{1/2}}\sin 2\alpha\right\} - \beta\left\{\left[\frac{X}{(1 + X^2)^{1/2}} - \frac{Y}{(1 + Y^2)^{1/2}}\right]\cos\alpha + \left[\frac{1}{(1 + Y^2)^{1/2}} - \frac{1}{(1 + X^2)^{1/2}}\right]\sin\alpha\right\} \quad (9)$$

Now equation (8) is the relation desired between X and Y for the proper steering of the vehicle and one wishes to approximate this relation by equation (9). One method of accomplishing this would be to substitute $X = Y + \gamma$ in (9) and to require that the resulting expression be satisfied for all values of Y. However, the last requirement cannot be met, therefore one seeks to adjust the coefficients of the derived equation so that it deviates least from zero. That is

$$f(Y) = R - \beta^2\left\{\frac{1 + Y(Y + \gamma)}{[(1 + Y^2)(1 + (Y + \gamma)^2)]^{1/2}}\cos 2\alpha + \frac{\gamma}{[(1 + Y^2)(1 + (Y + \gamma)^2)]^{1/2}}\sin 2\alpha\right\} + \beta\left\{\left(\frac{Y + \gamma}{[1 + (Y + \gamma)^2]^{1/2}} - \frac{Y}{(1 + Y^2)^{1/2}}\right)\cos\alpha + \left(\frac{1}{(1 + Y^2)^{1/2}} - \frac{1}{[1 + (Y + \gamma)^2]^{1/2}}\right)\sin\alpha\right\} \quad (10)$$

should exhibit the smallest deviation in absolute value from zero over the desired range of the variable Y. To accomplish this, one has at his disposal the parameters α and β.

Equation (10) in its present form seems to resist a direct attack, but it can be transformed into an infinite series by the substitution of $t = 1/Y$ and expanding in terms of t with the obvious restriction on the magnitude of t.[1]

A laborious but straightforward calculation gives the transformed equation as

$$f(t) = t^2(\gamma\beta^2\sin 2\alpha + \beta\cos\alpha - \beta\gamma\sin\alpha) + t^3(-\gamma^2\beta^2\sin 2\alpha - \beta\gamma\cos\alpha + \beta\gamma^2\sin\alpha) + t^4\left(-\frac{\gamma^2\beta^2}{2}\cos 2\alpha + \beta^2\gamma(\gamma^2 - 1)\sin 2\alpha - \beta\left[\frac{3}{4} - \frac{3}{2}\gamma^2\right]\cos\alpha - \beta\left[\gamma^3 - \frac{3}{2}\gamma\right]\sin\alpha\right) + t^5\left(\beta^2\left[\gamma^3 + \frac{15}{4}\gamma\right]\cos 2\alpha + \beta^2\gamma(2\gamma - \gamma^3)\sin 2\alpha - \beta\left[2\gamma^3 - \frac{3}{2}\gamma\right]\cos\alpha - \beta(3\gamma^2 - \gamma^4)\sin\alpha\right) \quad (11)$$

At this point some remarks on equation (11) seem pertinent. First there is a complete absence of terms not involving t, and second the coefficients of t^2 and t^3 are, with the exception of algebraic sign and a multiplying factor γ, the same. Hence by suitable selection of the parameters α and β one can make the coefficients of t^2 and t^3 zero simultaneously so that the variation of $f(t)$ from zero can be made to depend upon the fourth and higher powers of t. If a new phrase may be introduced one may say that the four-bar linkage is a well-conditioned linkage for this application. Further, the two parameters α and β are involved so that the designer may vary their values and obtain a linkage of suitable physical dimensions.

Table 1 shows the results of a calculation based on making the coefficients of t^2 and t^3 zero for one set of parameters. Here $\alpha = 65$ deg and β is computed as 0.0797, γ was arbitrarily taken as 0.5. The first column gives an arbitrary displacement θ, the second the theoretically correct corresponding angle ϕ, and the third the angle actually generated by the four-bar linkage. For the value of γ (0.5) selected, the series is valid for values of t up to approximately tan 30 deg. One notes that the linkage after 30 deg for θ begins to deviate more and more from the theoretically correct value.

The question naturally arises as to whether or not the accuracy of the mechanism can be improved by operations involving the coefficient of t^4. One could argue that the coefficients of t^2, t^3, and t^4 can all be made zero by suitable selection of the parameters. However, this procedure deprives the designer of all freedom in the selection of the dimensions of the linkage. For this reason another approach seems desirable.

The first three terms of the series may be written as

$$t^4 + \gamma Pt^3 - Pt^2 = f_1(t) \quad (12)$$

or

$$t^2[t^2 + \gamma Pt - P] = t^2 f_2(t) \quad (13)$$

where

[1] One expands expressions of the form $[1 + (2\gamma t + (1 + \gamma)^2 t^2]^{-1/2}$ whence $2\gamma t + (1 + \gamma)^2 t^2 < 1$ and t is of course $\tan\theta$.

$$P = \frac{\gamma \sin \alpha - \cos \alpha - \gamma\beta \sin 2\alpha}{\gamma\beta(\gamma^2 - 1)\sin 2\alpha - \frac{\gamma^2\beta}{2}\cos 2\alpha - \left(\frac{3}{4} - \frac{3}{2}\gamma^2\right)\cos \alpha + \left(\frac{3}{2}\gamma - \gamma^3\right)\sin \alpha} \quad (14)$$

One now has a choice of forcing $f_1(t)$ or $f_2(t)$ to deviate least in absolute value from zero for $0 \leqslant t \leqslant \tan 30$ deg.

The writer does not perceive any method of selecting the better expression from $f_1(t)$ and $f_2(t)$, and indeed, he first attempted to improve the accuracy of the linkage by forcing $f_1(t)$ to deviate least from zero. However, the results were disappointing because the accuracy was actually reduced. When $f_2(t)$ was selected, the accuracy of the linkage was improved. Hence in what follows, $f_2(t)$ will be used.

Here and hereafter the parameter γ is assumed to have the value 0.5. Referring to Fig. 3(a), one attempts to force $f_2(t)$ to lie between values of $\pm L$ for $0 \leqslant t \leqslant t_1$.[2] The magnitude of P is easily found as follows:

Considering Fig. 3, at $t = 0$, the expression $t^2 + \frac{P}{2}t - P$ assumes the value $-L$, that is

$$-P = -L \quad (15)$$

and at

$$t = t_1$$

one has

$$t_1^2 + \frac{P}{2}t_1 - P = L \quad (16)$$

adding (15) to (16) and solving for P gives

$$P = \frac{2t_1^2}{4 - t_1} \quad (17)$$

[2] The possibility indicated in Fig. 3(b) cannot be considered here because with γ fixed in advance the unknowns L, P, and t_0 must satisfy four independent equations simultaneously.

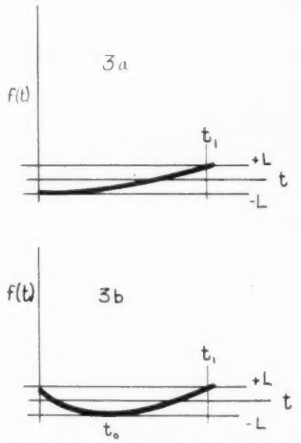

Fig. 3 Sketch showing possible variation in $F(t)$

Table 1 The comparison between the theoretically correct angle, Phi-True, and the actual angle generated by the linkage, Phi-Linkage

$\alpha = 65°$ $\beta = .0797$ $\gamma = 0.5$ $P = 0$

Theta°	Phi-True	Phi-Linkage
0	0.000	0.000
1	0.992	0.991
2	1.966	1.966
3	2.924	2.923
4	3.866	3.865
5	4.792	4.790
6	5.703	5.700
7	6.600	6.594
8	7.482	7.472
9	8.351	8.336
10	9.206	9.185
11	10.048	10.018
12	10.878	10.837
13	11.696	11.641
14	12.502	12.431
15	13.297	13.206
16	14.081	13.966
17	14.855	14.712
18	15.619	15.443
19	16.373	16.160
20	17.118	16.862
21	17.854	17.549
22	18.582	18.221
23	19.301	18.879
24	20.013	19.522
25	20.717	20.149
26	21.414	20.762
27	22.104	21.359
28	22.788	21.941
29	23.466	22.508
30	24.137	23.059
31	24.803	23.595
32	25.464	24.114

Table 2 The comparison between β for the unmodified and modified solutions

α	β, P = 0	β, P = .19478
65	.07972	-.14276
66	.13466	-.09433
67	.19330	-.04319
68	.25621	.01107
69	.32408	.06896
70	.39774	.13107
71	.47818	.19810
72	.56661	.27086

Table 3 Comparison between the angles generated by the unmodified and modified linkages. (Unmodified linkage: $P = 0$, $\alpha = 66$ deg, $\beta = 0.13466$. Modified linkage: $P = 0.19478$, $\alpha = 70$ deg, $\beta = 0.1310$.)

Theta	Phi-True	Phi-Linkage Unmodified	Error	Phi-Linkage Modified	Error
0	0.000	0.000	.000	0.000	.000
1	0.991	0.991	.000	0.993	.002
2	1.966	1.996	.000	1.973	.007
3	2.924	2.923	-.001	2.938	.014
4	3.865	3.865	.000	3.891	.026
5	4.791	4.790	-.001	4.831	.040
6	5.702	5.700	-.002	5.758	.056
7	6.599	6.594	-.005	6.671	.072
8	7.481	7.472	-.009	7.573	.092
9	8.349	8.336	-.013	8.461	.112
10	9.204	9.184	-.020	9.338	.134
11	10.046	10.018	-.028	10.201	.155
12	10.876	10.836	-.040	11.053	.177
13	11.694	11.640	-.054	11.891	.197
14	12.500	12.429	-.071	12.718	.218
15	13.295	13.203	-.092	13.532	.237
16	14.079	13.962	-.117	14.333	.254
17	14.853	14.707	-.146	15.122	.269
18	15.616	15.436	-.180	15.898	.282
19	16.370	16.151	-.219	16.661	.291
20	17.115	16.851	-.264	17.412	.297
21	17.851	17.536	-.315	18.149	.298
22	18.579	18.206	-.373	18.874	.295
23	19.298	18.861	-.437	19.585	.287
24	20.010	19.500	-.510	20.283	.273
25	20.714	20.124	-.590	20.968	.254
26	21.411	20.732	-.679	21.639	.228
27	22.101	21.325	-.776	22.296	.195
28	22.784	21.902	-.882	22.939	.155
29	23.462	22.463	-.999	23.569	.107
30	24.133	23.008	-1.125	24.183	.050
31	24.799	23.537	-1.262	24.783	-.016
32	25.460	24.049	-1.411	24.916	-.544
33	26.116	24.544	-1.572	24.131	-1.985
34	26.766	25.023	-1.743	23.375	-3.409

Inserting $\gamma = 0.5$ into equation (14) and solving for β in terms of α and P gives

$$\beta = \frac{(4 - 5P)\sin\alpha - (8 - 3P)\cos\alpha}{(4 - 3P)\sin 2\alpha - P\cos 2\alpha} \tag{18}$$

Equation (18) can now be solved for a range of values of α and the most suitable values of α and β selected for a particular application. If in equation (18) P is given the value zero, then (18) expresses the relation between α and β for the first approximation.

Table 2 shows the results of computations using equation (18) and gives values of β for $P = 0$ and $P = 0.19478$. Table 3 shows the results for the linkages with $P = 0$, $\alpha = 66$, $\beta = 0.13466$; and $P = 0.19478$, $\alpha = 70$, $\beta = 0.13107$.

Acknowledgment

The author wishes to thank the Computing Center at the University of British Columbia for the use of the ALWAC III E Digital Computing Machine on the computations for this paper.

DISCUSSION

T. P. Goodman[3]

By ingenious use of the properties of the four-bar linkage, the author has reduced the problem of designing a steering linkage to the classical problem of computing the dimensions of a four-bar linkage which approximately fulfills a desired relationship between the input angle and the output angle. The usefulness of the paper would be enhanced if the author would indicate how his method of solving this classical problem compares with other published methods, and how generally applicable his method is.

As a possible extension of the author's investigation, alternative steering linkages could be evaluated in terms of the total tire wear caused by their respective errors. Such an evaluation would involve measurements or estimates of the probability distribution of turning angles encountered during ordinary use of the vehicle, as well as measurements or estimates of the amount of tire wear caused by any given amount of error.

Author's Closure

The author wishes to thank Professor Goodman for his discussion, wherein he mentions the problem of tire wear as affected by the geometry of the steering linkage. The author agrees that this is an important problem but confesses that it is beyond his experience to relate turning angles to tire wear.

It was the author's purpose in writing the paper to stimulate interest in the attack on the design of linkages by analytical methods and in particular to indicate how the methods of Tscheybscheff can be applied.

In reply to Professor Goodman's comment on the applicability of the method the following simple example is offered.

Fig. 4 represents an inversion of the slider-crank chain with the length of the crank equal to the length of the fixed member. It is desired to determine the length b of the sliding member so that the point P traces an approximate straight line ($x = x_0$) for a range of $-\theta_0 \leqslant \theta \leqslant \theta_0$. Because of symmetry one may deal with the range $0 \leqslant \theta \leqslant \theta_0$.

One sees immediately that:

$$z = 2a\cos\phi \tag{19}$$

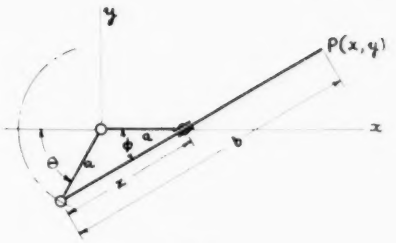

Fig. 4

$$\cos\phi = \frac{x - a}{b - z} \tag{20}$$

and

$$x = \frac{1}{2a}(-z^2 + bz + 2a^2) \tag{21}$$

upon eliminating $\cos\phi$ from equations (19) and (20).

Now one wishes $x - x_0 = \frac{1}{2a}(-z^2 + bz + 2a^2 - 2ax_0) = f(z)$ to deviate as little as possible from zero. Let the deviation be $\pm L$. For this example assume $\theta_0 = 60$ deg. Then if z_1 is the value of z at $\theta = 0$, and z_3 the value of z at $\theta = 60$ deg, one finds:

$$z_1 = 2a \tag{22}$$

$$z_3 = a\sqrt{3} \tag{23}$$

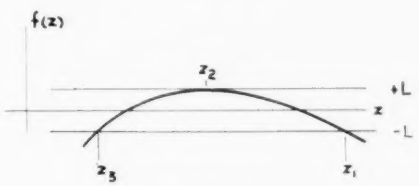

Fig. 5

Fig. 5 indicates the desired form of $f(z)$. That is, at z_1 and z_3, $f(z) = -L$ and at some as yet undetermined value of z_2, $(s) = +L$. Hence at points z_1 and z_3 one has:

$$z^2 - bz + 2ax_0 - 2a^2 - 2aL = 0 \tag{24}$$

and this equation must be of the form,

$$(z - z_1)(z - z_3) = 0 \tag{25}$$

whence

$$z_1 + z_3 = b \tag{26}$$

$$z_1 z_3 = 2ax_0 - 2a^2 - 2aL \tag{27}$$

A similar argument for the point z_2 gives,

$$z_2 = \frac{b}{2} \tag{28}$$

$$z_2^2 = 2ax_0 - 2a^2 + 2aL \tag{29}$$

[3] Assistant Professor of Mechanical Engineering, Massachusetts Institute of Technology, Cambridge, Mass. Assoc. Mem. ASME.

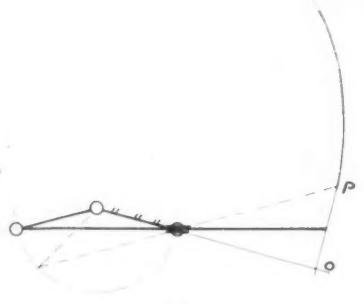

Fig. 6

From equations (4), (5), (8), (9), (10), and (11) one finds the following equalities for:

$$b = a(2 + \sqrt{3}) = 3.7321a \tag{30}$$

$$x_0 = \frac{a}{4}\left(1 + \frac{(2 + \sqrt{3})^2}{4} + 2\sqrt{3}\right) = 2.7366a \tag{31}$$

$$L = \frac{a}{4}\left(\frac{(2 + \sqrt{3})^2}{4} - 2\sqrt{3}\right) = 0.0045a \tag{32}$$

Fig. 6 shows the mechanism drawn for $a = 1$ in. OP is the half length of the desired straight line. The deviations from the straight line within the range are of the order of 0.005 in.

In conclusion the author feels that the success of this method depends upon the selection of a suitable parameter such as z, but that once this parameter is found it is a routine but perhaps tedious matter to determine the dimensions of a linkage.

FERDINAND FREUDENSTEIN

Associate Professor of Mechanical Engineering, Columbia University, New York, N. Y.
Assoc. Mem. ASME

Structural Error Analysis in Plane Kinematic Synthesis

Methods are developed for estimating and obtaining minimum structural error in the approximate synthesis of plane, function, or path-generating mechanisms. The application to a four-bar function generation mechanism is worked out with the aid of a large-scale digital computer used in the manner of a servo loop.

Introduction

In recent times a number of techniques for synthesizing mechanisms have been discussed in the literature. A basic requirement in applying these techniques is the attainment of motions which are sufficiently close approximations to the desired ones. As long as the number of adjustable mechanism proportions are finite, however, a difference will in general exist between the desired and generated motions and is called the structural error. This error exists in addition to those arising from manufacturing variations and elastic effects which are not considered here, but it can be minimized.

The development of design methods for advanced forms of mechanisms is beginning to lead to their greater utilization in the general machinery, instrumentation, and automation fields. The computations involved are lengthy, however, and require the use of large-scale computers to reduce them to a practical level. One such computer has been used for the automatic generation of "Five-Point Approximations" in this investigation. Previous work on error minimization [1][1] has dealt with the more simple forms of mechanism for which closed-form analytical solutions exist. The mathematics useful for the purpose belongs to that branch which is called the Theory of Approximation [2].

Nomenclature

Notation is similar to that used in [3] and is briefly repeated here: $y = f(x)$ is the ideal function, the function to be generated within the range $x_s \leq x \leq x_f$, by means of two analogous quantities, ϕ and ψ, called input and output terminals, respectively. In Fig. 1, for instance, these are represented as shaft rotations of a four-bar mechanism $ABCD$, in which $\phi = \angle XAB$ radians and $\psi = \angle ADC$ in radians. $y_s = f(x_s)$, $y_f = f(x_f)$ and the numbers x_s, y_s, x_f, y_f correspond to the angles ϕ_s, ψ_s, ϕ_f, ψ_f respectively, according to the equation:

$$\phi = \phi_s + r_\phi(x - x_s) \tag{1}$$

$$\psi = \psi_s + r_\psi(y - y_s) \tag{2}$$

$$r_\phi = \text{input scale factor} = \frac{\Delta\phi}{\Delta x}$$

where $\Delta\phi = \phi_f - \phi_s$; $\Delta x = x_f - x_s$

$$r_\psi = \text{output scale factor} = \frac{\Delta\psi}{\Delta y}$$

where $\Delta\psi = \psi_{max} - \psi_{min}$; $\Delta y = y_{max} - y_{min}$

x_i = precision point, point at which generated function coincides with ideal function. In an n-point approximation there are n such points (x_i, y_i) where $y_i = f(x_i)$. n is called the order number. The corresponding terminal values are (ϕ_i, ψ_i).

$g(x)$ = generated function

The General Questions of Approximate Synthesis

What is the minimum value of the structural error $|f(x) - g(x)|_{max}$ and how can it be attained?

Basic Theory

The following remarks, referring to function generation, can be applied with slight modification to path generation. From the theory of approximation first developed by Chebichev [4, 5] it can be shown that—expressed in nonrigorous terms—the ideal function deviates least from the generated function in an approximation in which the number of independently adjustable mechanism proportions is equal to the number n of precision points. Furthermore, the same numerical value of the maximum error must be attained with successive alteration in sign at least $(n + 1)$ times within the range of mechanization. If these conditions are satisfied, the maximum value of the structural error is minimized.

Error Between Precision Points—General

This error depends upon the function, the range, the mechanism, and the range of motion of the mechanism. Let the ideal function, $f(x)$, and the generated function, $g(x)$, be assumed continuous in the first n derivatives, where n is the order number, within the range (x_s, x_f). Consider the expression

$$R = f(x) - g(x) - L(x - x_1)(x - x_2)(x - x_3)\ldots(x - x_n) \tag{3}$$

where L is a constant so chosen that R vanishes at $(n + 1)$ points within the interval (x_s, x_f). Using Rolle's Theorem [6], the nth derivative of R with respect to x must vanish at some point, $x = \xi$, within the interval (x_s, x_f):

$$L = f^{(n)}(\xi) - g^{(n)}(\xi) \tag{4}$$

whence the error $\epsilon(x) = f(x) - g(x)$ is given by

$$\epsilon(x) = \frac{1}{n!}(x - x_1)(x - x_2)\ldots(x - x_n)\left[f^{(n)}(\xi) - g^{(n)}(\xi)\right] \tag{5}$$

where ξ is not in general equal to the value of x at which the error is sought, but is determined by Equation (4) and is therefore a function of x. According to Equations (1) and (2) the error $\epsilon(\phi) = \psi - \psi_A$ (where ψ is the ideal function and ψ_A the generated function) is given by:

$$\epsilon(\phi) = \frac{1}{n!}(\phi - \phi_1)(\phi - \phi_2)\ldots(\phi - \phi_n)\left[r_\psi\, y^{(n)}(\xi) - \frac{d^n\psi(\xi)}{d\phi^n}\right] \tag{6}$$

---

[1] Numbers in brackets designate References at end of paper.

Contributed by the Machine Design Division and presented at the Semi-Annual Meeting, Detroit, Mich., June 15–19, 1958, of The American Society of Mechanical Engineers.

Note: Statements and opinions advanced in papers are to be understood as individual expressions of their authors and not those of the Society. Manuscript received at ASME Headquarters, December 13, 1957. Paper No. 58—SA-12.

It is usually not possible to establish an upper limit to the structural error, because of the difficulty of estimating upper bounds for the higher derivatives in Equation (6).

Chebichev Spacing

The Chebichev polynomial $T_n(\phi)$ [7] (first chapter) is defined by the Equation $T_n(\phi) = \phi^n + p_{n-1}\phi^{n-1} + p_{n-2}\phi^{n-2} + \ldots + p_1\phi + p_o$, where the coefficients p_i are chosen so that in a given interval (ϕ_s, ϕ_f) the maximum value of $T_n(\phi)$ deviates least from zero—when compared to other polynomials of the same degree with leading coefficient unity.

These polynomials are well known. The maximum value of $T_n(\phi)$ is given by $(\phi_f - \phi_s)^n/(2^{2n-1})$. The spacing of the precision points ϕ_i, such that

$$\prod_{i=1}^{n} (\phi - \phi_i)$$

represents the Chebichev polynomial $T_n(\phi)$ within the interval (ϕ_s, ϕ_f), will be called "Chebichev spacing." The error function for this spacing is given by Equation (1–2) of Table 1. The precision points ϕ_i in an n-point Chebichev spacing are obtained [6] as the projections on the ϕ-axis of $(2n)$ equidistant points on the circumference of a circle, center $\phi = \phi_s + {}^1/_2\Delta\phi$, radius ${}^1/_2\Delta\phi$, and symmetrically disposed with respect to the ϕ-axis. Analytically, this leads to Equations (1–3) and (1–4) of Table 1. An intuitive way of considering this spacing is to note its relationship to trigonometric interpolation [6], and also to picture it as a spacing which constrains the function more closely at the ends than at the middle, since the behavior outside the interval (ϕ_s, ϕ_f) is not specified.

Small Ranges

Despite the absence of information concerning the nature of the mechanism or of the ideal function, certain generalizations concerning optimization can be made. In Equation (1–2), for instance, it can be seen that when the range of x and ϕ is sufficiently small so that the derivatives in that equation are essentially constant, Chebichev spacing is necessarily optimum. This is intuitively reasonable by observing that over small ranges all functions or curves look alike; i.e., at first observation like a straight line and to an nth approximation, like an $(n-1)$st degree polynomial.

Finite Ranges

If the generated function is a polynomial of the $(n-1)$st degree, Equation (5) for the error becomes

$$\epsilon(x) = \frac{1}{n!} \prod_{i=1}^{n} (x - x_i) f^n(\xi)$$

in which $f^{(n)}(\xi)$ can no longer be assumed constant, thereby shifting or distorting the Chebichev spacing in a manner not readily predicted. As the number of precision points become infinite, however, it can be shown by expanding the ideal function into a series of Chebichev polynomials [5], that Chebichev spacing becomes optimum in an asymptotic fashion provided the ideal function is analytic. Since mechanisms do not usually generate polynomials, this does not apply without modification to linkages. As a first trial-spacing, Chebichev spacing is valuable, however, even for finite ranges. A more refined estimate is obtained by considering not only the ideal function but also the mechanism, even though crudely.

Modified Chebichev Spacing

Any mechanism synthesizes the function $f(x)$ or the inverse function $f^{-1}(x)$ depending upon which terminal is considered the input terminal. Optimum spacing of precision points, $\psi = \psi_i$, of the output variable for $f(x)$ should become the optimum spacing of the precision points, $\phi = \phi_i$, of the input variable for $f^{-1}(x)$. This symmetry consideration, due to Skarksi [8], ought to be included in the choice of optimum spacing. For small intervals, however, the spacing ought to reduce to Chebichev spacing. Combining these two ideas we obtain the modified spacing given by Equations (1–5) to (1–8) of Table 1. This spacing takes somewhat longer to compute than Chebichev spacing, but is usually closer to optimum.

Table 1 Error equations and precision-point spacing in point approximations

$$\epsilon(\phi) = \frac{1}{n!}(\phi-\phi_1)(\phi-\phi_2)\ldots(\phi-\phi_n)\left[\frac{n!}{\beta^n}\frac{d^n y(\xi)}{dx^n} - \frac{d^n \psi(\xi)}{d\phi^n}\right] \quad [1\text{-}1]$$

WHERE $\phi_s \leq \phi \leq \phi_f$ AND $x_s \leq \xi \leq x_f$; ξ IS A FUNCTION OF x

FOR CHEBICHEV SPACING

$$\epsilon(\phi) \leq \frac{1}{n!}\frac{1}{2^{2n-1}}\left[\frac{(\Delta x)^n}{\Delta y}\frac{d^n y(\xi)}{dx^n} - \frac{(\Delta\phi)^n}{\Delta\psi}\frac{d^n\psi(\xi)}{d\phi^n}\right] \quad [1\text{-}2]$$

THE PRECISION POINTS, $\phi = \phi_i$, $i = 1,2,3,\ldots,n$, ARE GIVEN BY

$$\phi_i = \tfrac{1}{2}(\phi_s+\phi_f) - \tfrac{1}{2}(\phi_f-\phi_s)\cos\alpha_i \quad i = 1,2,3,4,5 \quad [1\text{-}3]$$

$$\alpha_i = (2i-1)\frac{\pi}{2n} \text{ RADIANS}, \quad \alpha_o = 0, \quad \alpha_{n+1} = 180^\circ \quad [1\text{-}4]$$

MODIFIED CHEBICHEV SPACING

$$\delta_{(i)(i+1)} = \phi_{i+1} - \phi_i = \tfrac{1}{2}\Delta\phi\,(\cos\alpha_i - \cos\alpha_{i+1}) \quad [1\text{-}5]$$

$$\delta_{(i)(i+1)} + |\psi_{(i)(i+1)}| = \lambda_{(i)(i+1)}(\Delta\phi + \Delta\psi) \quad [1\text{-}6]$$

WHERE $\lambda_{(i)(i+1)} = \tfrac{1}{2}(\cos\alpha_i - \cos\alpha_{i+1}) \quad i = 0,1,2,\ldots n \quad [1\text{-}7]$

$$= \sin\frac{\pi}{2n}\sin\frac{i\pi}{n}, \quad i = 1,2,\ldots,(n-1) \quad [1\text{-}8]$$

IN EQ. [1-5] – [1-8] AND GENERALLY IT IS ASSUMED THAT

$\phi_o = \phi_s$, $x_o = x_s$, $\phi_{n+1} = \phi_f$, $x_{n+1} = x_f$, $\psi(\phi_k) = \psi_k$

ESTIMATE OF LEAST MAXIMUM ERROR, ϵ_{min}

$$\epsilon^2_{min} = \frac{\sum_{i=0}^{n}\left[\epsilon^2_{(i)(i+1)}\dfrac{\chi_{(i)(i+1)}}{\delta_{(i)(i+1)}}\right]}{\sum_{i=0}^{n}\dfrac{\chi_{(i)(i+1)}}{\delta_{(i)(i+1)}}} \quad \text{(ALL } \epsilon\text{'S ARE } e(x)) \quad [1\text{-}9]$$

$\chi_{ij} = x_j - x_i$; $x_{n+1} = x_f$; $x_o = x_s$; i,j ARE PRECISION POINTS

$$\delta_{ij} = \frac{\sin^{-1}x_j - \sin^{-1}x_i}{x_j - x_i} \quad (\text{IF } x^2 < 1) \approx \frac{1}{x_{ij}}(\sin^{-1}x_j - \sin^{-1}x_i) \quad [1\text{-}10]$$

THE RANGE IS ASSUMED NORMALIZED TO $-1 \leq x \leq 1$. FOR CHEBICHEV SPACING, 5-POINT APPROXIMATION

$$\epsilon^2_{min}(\phi)(x) = .005(\epsilon^2_{01} + \epsilon^2_{56}) + .137(\epsilon^2_{12} + \epsilon^2_{45}) + .358(\epsilon^2_{23} + \epsilon^2_{34}) \quad [1\text{-}11]$$

Variation of Structural Error With Range

For small ranges, the maximum structural error in an n-point Chebichev spacing is proportional to the nth power of the range (x_s, x_f). For finite ranges this nth power law may be quite inaccurate. In general the rate of decrease of the maximum error with the range (x_s, x_f) depends on the derivative properties of $f(x)$, and is not readily predicted, although it appears to decrease more rapidly (if the range is reduced) if the higher derivatives are small. The variation with input range (ϕ_s, ϕ_f) is also difficult to determine, but appears much smaller than the variation with the range (x_s, x_f). It may be concluded that all generalizations are dangerous, especially in this field.

Variation of Structural Error With Order Number

The variation with the range Δx is generally large compared to the variation with order number. The variation again depends on the derivative properties of the ideal function—the smaller the nth derivatives, the more rapid the decrease with increasing n. If these derivatives have a known upper bound, more specific theorems can be adduced [2, 5]. By expansion into a series of

Chebichev polynomials it can be shown [5] that for analytic ideal functions, very small ranges, and very large order numbers, the asymptotic rate of decrease of the structural error for each additional precision point is given by $1/2(a_{n+2}/a_{n+1})$, where a_n is the coefficient of x^n in the Taylor series expansion of the ideal function $f(x)$.

For the Chebichev polynomial $T_n(\phi)$ the ideal function is ϕ^n which changes when n does. In the range $(-1, 1)$, however, as n approaches infinity, ϕ^n approaches zero, and one might consider this special case one in which the maximum error decreases by a factor of two for each additional precision point. This rate of decrease is not generally valid, however, as in the example $f(x) = 1/(x - a)$, $a > 1$, in the range $(-1, 1)$ considering approximations by nth-degree polynomials for which [2]

$$\epsilon_{\max} = \frac{1}{a^2 - 1}\,[a - (a^2 - 1)^{1/2}]^n$$

This error is reduced by the factor $1/[a - (a^2 - 1)^{1/2}]$ for each additional precision point. This factor approaches unity (no gain in accuracy) as a approaches unity and is infinite (maximum gain in accuracy) as a becomes infinite. In the former case, the derivatives of $f(x)$ become very large, in the latter case, very small. For monotonic functions the ratio of greatest to least values of the nth derivative of $f(x)$ may serve as a qualitative guide.

Estimation of Minimum Structural Error

Among the useful properties of the Chebichev polynomials $T_k(x)$ in the range $(-1, 1)$ are the following [9]:

$$\left.\begin{aligned} &\int_{-1}^{1} \frac{T_r(x)T_s(x)}{(1 - x^2)^{1/2}}\,dx = 0 \quad (r \neq s) \\ &I = \int_{-1}^{1} \frac{[f(x) - y_n(x)]^2}{(1 - x^2)^{1/2}}\,dx = \text{minimum}, \\ &\qquad \text{when } y_n(x) = \sum_{r=1}^{n} q_r T_r(x) \end{aligned}\right\} \quad (7)$$

The first integral expresses orthogonality with respect to the weight function $(1 - x^2)^{1/2}$; the second integral states that among all nth-degree polynomials which are to approximate $f(x)$ a least-square type of minimum error occurs when $y_n(x)$ consists of the first n terms of the expansion of $f(x)$ into a series of Chebichev polynomials. This suggests the thought that for small ranges and high order numbers $y_n(x) \rightarrow g(x)$, the generated function. If $\epsilon(x) = f(x) - y_n(x)$, then

$$I = \int_{x_s}^{x_f} \frac{\epsilon^2}{(1 - x^2)^{1/2}}\,dx = \text{minimum}$$

when $\epsilon_{\max}$ is minimized.

This fact can be used to estimate the minimum value of the error as follows: The error curve is approximated by a series of straight lines passing through the precision points and the points of extreme error, and the integral I is computed for each interval x_{ij} by assuming an average value of the weight function, as in Equation (1–10). Then for the interval (x_i, x_j), $j = (i + 1)$, the contribution I_{ij} to I is given by $I_{ij} = [\epsilon_{ij}(x)]^2(x_j - x_i)/(3\delta_{ij})$. In the optimum condition all the ϵ_{ij}'s are numerically equal, say, to $\epsilon_{\min}$. The integral I can be evaluated for the given error distribution and for the assumed optimum condition, and the two values equated. This is based on the assumption that, with respect to approximations not differing too much from the optimum, I is essentially constant.

This is similar in philosophy to Rayleigh's principle for calculating natural frequencies of a beam, say, the strain-energy of which is at a minimum for the actual deflection curve, but does not vary much with changes in the assumed shape of the deflection curve. Hence we can state that

$$I = \Sigma\left(\frac{\epsilon_{ij}{}^2 x_{ij}}{3\delta_{ij}}\right) = \epsilon_{\min}{}^2\,\Sigma\left(\frac{x_{ij}}{3\delta_{ij}}\right)$$

whence derives the estimate, Equation (1–9), Table 1. For Chebichev spacing in five-point approximations, this Equation becomes Equation (1–11) of Table 1.

For other spacings this equation retains the same general form, but the coefficients will be different. The various simplifying assumptions made in the derivation of Equation (1–11) mean that the value of $\epsilon_{\min}$ obtained therein is not exact. Theory states that the minimum error lies between the greatest and least values of ϵ_{ij}, but Equation (1–11) is somewhat more specific.

Error Minimization by Successive Approximation

1 Five-Point Function Generation With a Four-Bar Mechanism. In this special case, chosen to illustrate the general method, the ideal function $f(x)$ and the range (x_s, x_f) are given; the linkage proportions (a, b, c, d, ϕ_s, ψ_s), Fig. 1, are to be determined. The ranges $\Delta\phi$, $\Delta\psi$, can be selected according to the recommendations of reference [3]; generally equal ranges, less than 120 degrees are reasonable. A convenient program for a digital computer utilizes a symmetric manner of solving Equation (2), [3], relating angles ϕ and ψ in Fig. 1, using complex numbers. The latter have been used also, among others, by Blokh [10] and Sieker [11, 12]. In this way, Equation (2) [3], is transformed into Equation (2–5), Table 2, in which the solution is outlined. The computer input consists of four corresponding rotations ϕ_{ij}, ψ_{ij}, which are obtained from the five precision points (ϕ_i, ψ_i). Equation (2–5) and (2–7) constitute a symmetrical linear system of simultaneous equations in the unknowns X, Y, Z, X, Y, Z, defined in Table 2. These unknowns are linear functions of k, Equation (2–7), where k is a real number obtained from Equation (2–15) which possesses at least one real root. The linkage proportions are given by Equations (2–20) through (2–23). A number of logical decisions involving choice of multivalued functions such as arc tangent, for instance, are not included.

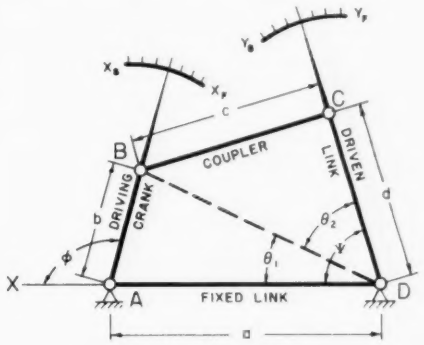

Fig. 1 Four-bar mechanism

2 Existence and Nature of Solutions. Equations (2–5) and (2–7) are solvable if the matrix of the coefficients is of the same rank as the augmented matrix. In particular it is sufficient if ∇ Equation (2–8) is nonzero. For nontrivial solutions, furthermore, k must be real and c^2 positive. The latter leads to Equation (2–21).

Folding linkages, i.e., linkages in which all links are in line, are to be avoided. Such linkages, and no others, occur when the precision points (ϕ_i, ψ_i) possess central asymmetry in the sense

Table 2 Computation of five-point approximation using four-bar mechanism as function generator

$$p_1 = \frac{ab}{a^2+b^2-c^2+d^2} \quad [2\text{-}1]$$

$$p_2 = \frac{ad}{a^2+b^2-c^2+d^2} \quad [2\text{-}2]$$

$$p_3 = \frac{bd}{a^2+b^2-c^2+d^2} \quad [2\text{-}3]$$

$$X = -p_1 e^{i\phi_1} \; ; \; Y = p_2 e^{i\psi_1} \; ; \; Z = p_3 e^{i(\phi_1-\psi_1)} \quad [2\text{-}4]$$

SELECT PRECISION POINTS ϕ_i, ψ_i $(i=1,2,\ldots 5)$ AND COMPUTE

$\phi_{1j} = \phi_j - \phi_1$; $\psi_{1j} = \psi_j - \psi_1$ $(j = 2,3,4,5)$

$\bar{X}, \bar{Y}, \bar{Z}$ = COMPLEX CONJUGATES OF X, Y, Z

$$e^{i\phi_{1j}}X + e^{i\phi_{1j}}\bar{X} + e^{i\psi_{1j}}Y + e^{i\psi_{1j}}\bar{Y} + e^{i(\phi_{1j}-\psi_{1j})}Z + e^{i(\phi_{1j}-\psi_{1j})}\bar{Z} = 1 \quad (j=1,2,\ldots 5) \quad [2\text{-}5]$$

$$\bar{X}\bar{Y}Z = X\bar{Y}\bar{Z} \quad [2\text{-}6]$$

$$X - \bar{X} + Y - \bar{Y} + Z - \bar{Z} = ik \quad (k \text{ REAL}, \; i=\sqrt{-1}, \text{ FROM EQ[2-5]ON}) \quad [2\text{-}7]$$

$$\nabla = \begin{vmatrix} 1 & -1 & 1 & -1 & 1 & -1 \\ e^{i\phi_{12}} & e^{-i\phi_{12}} & e^{i\psi_{12}} & e^{-i\psi_{12}} & e^{i(\phi_{12}-\psi_{12})} & e^{-i(\phi_{12}-\psi_{12})} \\ e^{i\phi_{13}} & e^{-i\phi_{13}} & e^{i\psi_{13}} & e^{-i\psi_{13}} & e^{i(\phi_{13}-\psi_{13})} & e^{-i(\phi_{13}-\psi_{13})} \\ e^{i\phi_{14}} & e^{-i\phi_{14}} & e^{i\psi_{14}} & e^{-i\psi_{14}} & e^{i(\phi_{14}-\psi_{14})} & e^{-i(\phi_{14}-\psi_{14})} \\ e^{i\phi_{15}} & e^{-i\phi_{15}} & e^{i\psi_{15}} & e^{-i\psi_{15}} & e^{i(\phi_{15}-\psi_{15})} & e^{-i(\phi_{15}-\psi_{15})} \end{vmatrix} \quad [2\text{-}8]$$

$(i\,j\,k\,l)$ = 4×4 DETERMINANT CONSISTING OF THE COMPLEX ELEMENTS OF THE $i^{TH}, j^{TH}, k^{TH}, l^{TH}$ COLUMNS OF ∇ IN THE ORDER $i\,j\,k\,l$ LEFT TO RIGHT

$(0,j,k\,l)$ = SAME AS PRECEDING EXCEPT THAT ALL 1^{st} COLUMN ELEMENTS ARE UNITY

∇_x = DETERMINANT OBTAINED BY REPLACING FIRST COLUMN ELEMENTS OF ∇ BY $(ik,1,1,1,1,1)$ IN THAT ORDER GOING DOWN

$$\tfrac{1}{2}\nabla = (3456)+(2356)+(2346)-(1456)-(1346)+(1256)+(1245)-(1236)+(1234) \quad [2\text{-}9]$$

$$\nabla_x = (3456)+(2456)+(2356)+(2346)+(2345)+ik[(3456)-(1456)+(2356)-(2346)+(2345)] + 2[(0256)+(0245)+(0234)-(0456)-(0346)-(0236)] \quad [2\text{-}10]$$

∇_y = OBTAINED BY INTERCHANGING COLUMN NUMBERS $1 \rightleftharpoons 3, 2 \rightleftharpoons 4$ IN ∇_x

∇_z = OBTAINED BY INTERCHANGING COLUMN NUMBERS $1 \rightleftharpoons 5, 2 \rightleftharpoons 6$ IN ∇_x

$$X = \nabla_x/\nabla \; ; \; Y = \nabla_y/\nabla \; ; \; Z = \nabla_z/\nabla \quad [2\text{-}11]$$

THESE CALCULATIONS INVOLVE 17, 4×4 COMPLEX DETERMINANTS

SINCE ∇, (1234), (1256) AND (3456) ARE REAL; (2345) AND (1346)–(1236) AND (1245) – (1456) AND (2356) HAVE (PAIRWISE) REALS OF OPPOSITE SIGN AND IDENTICAL IMAGINARIES. LET

$$\nabla_x = u_1 + iu_2 = (\alpha_1+\alpha_2 k) + i(\beta_1+\beta_2 k) \quad [2\text{-}12]$$

$$\nabla_y = v_1 + iv_2 = (\gamma_1+\gamma_2 k) + i(\delta_1+\delta_2 k) \quad [2\text{-}13]$$

$$\nabla_z = w_1 + iw_2 = (\lambda_1+\lambda_2 k) + i(\mu_1+\mu_2 k) \quad [2\text{-}14]$$

FROM EQ. [2-6]: $u_1w_1v_2 + u_1v_1w_2 - u_2v_1w_1 + u_2v_2w_2 = 0$ [2-15]

$$\left.\begin{aligned} &\text{LET } Q_1 = \gamma_1\mu_1 + \delta_1\lambda_1 \; ; \quad Q_4 = \gamma_2\mu_2 + \delta_2\lambda_2 \\ &Q_2 = -\gamma_1\lambda_1 + \delta_1\mu_1 \; ; \quad Q_5 = \gamma_1\mu_2 + \delta_1\lambda_2 + \gamma_2\mu_1 + \delta_2\lambda_1 \\ &Q_3 = \delta_2\mu_2 - \gamma_2\lambda_2 \; ; \quad Q_6 = -\gamma_2\lambda_2 + \delta_1\mu_2 - \gamma_2\lambda_1 + \delta_2\mu_1 \end{aligned}\right\} \quad [2\text{-}16]$$

$$\text{THEN } a_3k^3 + a_2k^2 + a_1k + a_0 = 0 \quad [2\text{-}17]$$

$$\left.\begin{aligned} &\text{WHERE } a_0 = \alpha_1Q_1 + \beta_1Q_2 \\ &a_1 = \alpha_1Q_5 + \beta_1Q_6 + \beta_2Q_2 \\ &a_2 = \alpha_1Q_4 + \beta_1Q_3 + \alpha_2Q_5 + \beta_2Q_6 \\ &a_3 = \beta_2Q_3 + \alpha_2Q_4 \end{aligned}\right\} \quad [2\text{-}18]$$

COMPUTE k AND THEN X, Y, Z FROM EQ. [2-11]:-

$$\text{LET } X = X_1 + iX_2 \; ; \; Y = Y_1 + iY_2 \; ; \; Z = Z_1 + iZ_2 \quad [2\text{-}19]$$

$$\left.\begin{aligned} p_1 &= -\sqrt{X_1^2+X_2^2} \\ p_2 &= \sqrt{Y_1^2+Y_2^2} \\ p_3 &= \sqrt{Z_1^2+Z_2^2} \end{aligned}\right\} \quad [2\text{-}20]$$

$$\left(\text{FOR NON-TRIVIAL SOLUTIONS: } \frac{1}{p_1^2} + \frac{1}{p_2^2} + \frac{1}{p_3^2} > \frac{1}{p_1p_2p_3}\right) \quad [2\text{-}21]$$

$$\tan\phi_1 = X_2/X_1 \; ; \; \tan\psi_1 = Y_2/Y_1 \quad [2\text{-}22]$$

$$\left.\begin{aligned} &\text{IF } a=1, \; b = p_3/p_2 \; ; \; d = p_3/p_1 \\ &c^2 = 1 + b^2 + d^2 - \tfrac{1}{2}d \end{aligned}\right\} \quad [2\text{-}23]$$

Table 3 Minimization of structural error by successive respacing of precision points

$$\psi = \psi_S + r_\psi\left\{f\left[\frac{\phi-\phi_S}{r_\phi} + x_S\right] - y_S\right\} \quad \text{(IDEAL FUNCTION)} \quad [3\text{-}1]$$

$$\phi_S = \phi_1 - r_\phi(x_1 - x_S) \quad [3\text{-}2]$$

$$\psi_S = \psi_1 - r_\psi(y_1 - y_S) \quad [3\text{-}3]$$

$$h^2 = a^2 + b^2 + 2ab\cos\phi \quad [3\text{-}4]$$

$$\cos\theta_1 = \frac{a^2+h^2-b^2}{2ah} \quad [3\text{-}5]$$

$$\cos\theta_2 = \frac{h^2+d^2-c^2}{2hd} \quad [3\text{-}6]$$

$$\psi_A = \theta_1 \pm \theta_2 \; , \quad \text{(GENERATED OR ACTUAL FUNCTION)} \quad [3\text{-}7]$$

ϵ = STRUCTURAL ERROR, REFERS TO ψ OR y THUS:

$\epsilon(\phi) = \psi - \psi_A$, $\epsilon(x) = f(x) - g(x)$

ϵ_{ij} = max absolute value of error in the interval (ϕ_i, ϕ_j) or (x_i, x_j)

$\epsilon_{06}\}$ = max. absolute value of error in the intervals (ϕ_0, ϕ_1) and (ϕ_5, ϕ_6)

ϕ_{ij}', x_i', y_i' = values of ϕ_{ij}, x_i, y_i after respacing precision points

$$\phi_{ij}' = \frac{(\phi_f - \phi_S)\phi_{ij}}{\sqrt[m]{\epsilon_{ij}}\sum_{i=0}^{n}\frac{\phi_{ij}}{\sqrt[m]{\epsilon_{ij}}}} \quad \begin{matrix}(j = i+1) \\ (m \text{ is a number} > 1, \\ \text{usually } m=3)\end{matrix} \quad [3\text{-}8]$$

where $\phi_{01} = \phi_1 - \phi_S$ [3-9]

and $\phi_{56} = \phi_f - \phi_S$ [3-10]

$$x_i' = x_S + \frac{1}{r_\phi}\phi_{01}' \quad [3\text{-}11]$$

$$x_i' = x_{i-1}' + \frac{1}{r_\phi}\phi_{(i-1)(i)}' \; , \quad i = 2,3,4,5 \quad [3\text{-}12]$$

$$y_i' = f(x_i') \quad i = 1,2,3,4,5 \quad [3\text{-}13]$$

ϕ_{12}', $\phi_{(i)(i+1)}'$ = as computed from eq [3-8] [3-14]

$$\phi_{1j}' = \phi_{1(j-1)}' + \phi_{(j-1)(j)}' \quad j = 3,4,5 \quad [3\text{-}15]$$

$$\psi_{1j}' = r_\psi(y_j' - y_1') \quad j = 2,3,4,5 \quad [3\text{-}16]$$

that $\phi_{23} = -\phi_{34}$, $\psi_{23} = -\psi_{34}$, $\phi_{13} = -\phi_{35}$, and $\psi_{13} = -\psi_{35}$. Cranks of zero length occur when the precision points possess central symmetry: $\phi_{23} = -\phi_{34}$, $\psi_{23} = \psi_{34}$, $\phi_{13} = -\phi_{35}$, and $\psi_{13} = \psi_{35}$; in that case, however, other values of k may exist leading to well-proportioned linkages, depending on the particular case. If the remainder in Equation (2–17) is used as a criterion for the correctness of k, an inaccurate value of k can occur when the remainder, regarded as a function of k, is nearly stationary and small. For this case, special consistency checks are required to refine the k value (or greater precision in the computation). There may be three real or one real root of Equation (2–17) and if the consistency criteria are satisfied these values of k are non-trivial.

3 Respacing of Precision Points for Minimum Error, Table 3. Fig. 2 shows the nature of the structural-error variation in a five-point approximation. A new choice of precision points (x_i, y_i) is sought so as to minimize the maximum error, which is defined as the difference between the ideal function, Equation (3–1), and the generated function, Equation (3–7). An interval length (ϕ_i, ϕ_j) is denoted by ϕ_{ij} and the numerical value of the maximum error within that interval by ϵ_{ij}. Primes denote respaced values.

Suppose the interval width $\phi_{ij}(j = i + 1)$, Fig. 2, is proportional to the mth root of ϵ_{ij}. Then

$$\frac{\phi_{ij}'}{\phi_{ij}} = \frac{\sqrt[m]{\epsilon_{ij}'}}{\sqrt[m]{\epsilon_{ij}}} \quad (8)$$

The maximum error is minimized when $\epsilon_{ij} = \epsilon_{\min}$ for all intervals (ϕ_i, ϕ_j). This condition, coupled with the requirement that $\Delta\phi$ remains constant, leads to Equation (3–8) and the subsequent respacing, Equations (3–15) and (3–16). The value of m can be adjusted for rapid convergence, usually to $m = 3$. The respaced input values can be used to calculate new mechanism proportions,

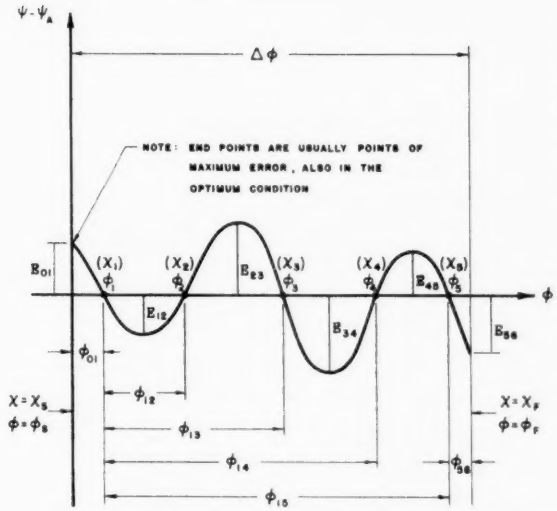

Fig. 2 Structural error variation in a five-point approximation

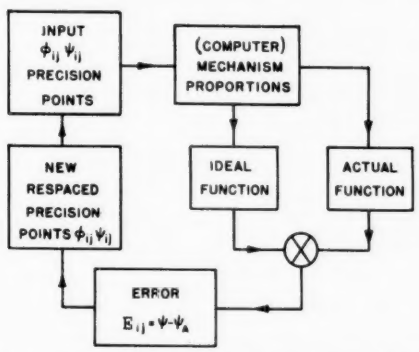

Fig. 3 Schematic of automatic computation setup with a digital computer

and the iteration can be continued until the maximum structural error has converged to its minimum value.

4 Digital Computer Setup. The nature of the feedback arrangement is shown in Fig. 3. A program usable in this fashion with the I.B.M. 650 Magnetic-Drum Data-Processing Machine, with the required logic circuits and double-precision accuracy for much of the computation, is available upon request from the author. The cubic equation (2–17) has been solved numerically by Sarafyan's method [13] which always converges and prescribes the "first guess" at the expense of slightly longer computation time. The rate of convergence to minimum error depends on the ideal function, the range, and the mechanism. In general, the smaller the angular velocity ratio and its variation, the faster the convergence. Five cycles have sufficed in the author's experience (see section Examples). Respacing theory can also be based upon the process of error linearization used by Svoboda [14], but in order to minimize the length of the program, as well as for its own sake, the method shown in Table 3 was developed.

Other Methods of Optimization

These can be based on the use of other orthogonal polynomials such as the trigonometric, Laguerre, and Legendre polynomials with their various least-square properties. For the Legendre polynomials the weight function in Equation (7) is unity if the T's are considered Legendre polynomials. Although the least-square integrated error is minimum, the maximum absolute value is not [9, 15], and the latter is believed to be the most frequently desired type of minimization. It can be shown[2] that approximations by means of series of orthogonal polynomials of degree $(n-1)$ for the highest-degree polynomials, possess at least n precision points (unless the approximation is exact), and have minimization properties similar to those of Equation (7) but with different weight functions.

Table 4 Levitskii's method for the three-point approximation

Let $p_0 = b/d$, $p_1 = -b/a$, $p_2 = \dfrac{a^2+b^2-c^2+d^2}{2ad}$ · [4-1]

Minimize $S_n = \sum_{i=1}^{n} [\cos\psi_i - p_0\cos\phi_i - p_1\cos(\phi_i-\psi_i) - p_2]$ · [4-2]

where (ϕ_i, ψ_i) are values obtained from the ideal function, Eq. [3-1], and $n \geq 4$. $\partial S_n/\partial p_i = 0$.

Let
$$C_{00} = \sum \cos^2\phi_i \quad \text{(all summations from 1 to n)}$$
$$C_{01} = \sum \cos\phi_i \cos(\phi_i-\psi_i)$$
$$C_{02} = \sum \cos\phi_i$$
$$C_{11} = \sum \cos^2(\phi_i-\psi_i)$$
$$C_{12} = \sum \cos(\phi_i-\psi_i)$$
$$C_{22} = n$$
$$C_{ij} = C_{ji}$$
[4-3]

Then
$$C_{00}p_0 + C_{01}p_1 + C_{02}p_2 = \sum_{i=1}^{n} \cos\psi_i\cos\phi_i$$
$$C_{10}p_0 + C_{11}p_1 + C_{12}p_2 = \sum_{i=1}^{n} \cos\psi_i\cos(\phi_i-\psi_i)$$
$$C_{20}p_0 + C_{21}p_1 + C_{22}p_2 = \sum_{i=1}^{n} \cos\psi_i$$
[4-4]

Solve for the eq. for the p_i's and compute linkage proportions from eq. [4-1]
Note that for all values of (ϕ_i, ψ_i) obtained from the actual function, eq. [3-7], S_n would be zero.

Least-square methods of a somewhat different type have been used by Levitskii [16], whose method leads to a closed-form solution when applicable; e.g., in a three-point approximation in a four-bar mechanism. The method is outlined in Table 4. The minimization applies to cos ψ rather than to ψ, and the integration is replaced by a summation. The number of summations can be reduced to one more than the number of precision points by adopting the following suggested addition to the Levitskii method:

The weight function required in Equation (7) with respect to integration disappears with respect to the summation

$$\sum_{\alpha=0}^{n=1} T_r(x_\alpha)T_s(x_\alpha) = 0, \; r, s < n, \; r \neq s$$

where x_α are the n roots of $T_n(x) = 0$ [17]. This suggests using, for the summation in Equation (4-2) Table 4, the four values of ϕ corresponding to the roots of $T_4(\phi) = 0$ as listed in Equations (1–3) and (1–4) of Table 1. This means that in a small interval the approximations obtained in this manner are not only least square in the sense just given, but, for sufficiently large n, also possess least maximum structural error. In most more complicated approximations, however, such as the five-point, a closed-form solution by the Levitskii method is no longer feasible due to nonlinearities in the equations, and a method of successive approximation, similar to Svoboda's [14] can be used.

The method of successive improvement as used in Table 3 can

[2] Private communication from Prof. G. Szegö, Stanford University.

Table 5 Examples of five-point approximations

FUNCTION	$\log_{10} x$	$\log_{10} x$	$\log_{10} x$	$\log_{10} x$	$\log_{10} x$	$\log_{10} x$	$\log_{10} x$	$\log_{10} x$	$-\log_{10} x$
x_s	1.0	1	1	1	1	1	1	1	1
x_f	10.0	2	2	2	2	2	2	2	2
$\Delta\phi$	60.0	60	60	60	60	60	60	60	60
$\Delta\psi$	90.0	60	60	60	60	60	60	60	60
x_1	1.000	1.02447	1.167	1.020	1.0120104	1.0153146	1.0140633	1.0144678	1.02447
x_2	1.431	1.20611	1.333	1.177	1.1166732	1.1415124	1.1323697	1.1355580	1.20611
x_3	2.307	1.50000	1.500	1.457	1.3537132	1.3836763	1.3787479	1.3842742	1.50000
x_4	4.180	1.79389	1.667	1.767	1.6883092	1.7172306	1.7094641	1.7104985	1.79389
x_5	8.577	1.97553	1.833	1.972	1.9593025	1.9641019	1.9629220	1.9627009	1.97553
ϕ_1 (deg)	19.372363	53.707936	63.186777	53.247315	52.36148	52.715795	52.578035	52.628390	61.170006
ψ_1 (deg)	-85.964738	259.19963	-89.485987	258.02325	259.16506	259.07868	259.08412	259.07749	99.393040
b/a	-1.2163005	-3.4325029	-3.480052	-3.4061202	-3.3255314	-3.3593430	-3.3480317	-3.3523485	-.28491374
c/a	2.8051365	.81539009	.73107648	.82519634	.85623419	.84289382	.84728507	.84560215	1.0359560
d/a	3.1917229	3.5589013	3.6189483	3.5336858	3.4624604	3.4917237	3.4816064	3.4855187	.25841210
ϵ_{01} (deg)	.00019	.01174	.09238	.00785	.00245	.00420	.00343	.0038	.00269
ϵ_{12} (")	.03728	.00820	.00112	.00637	.00274	.00403	.00357	.0037	.00194
ϵ_{23} (")	.02484	.00365	.00050	.00395	.00352	.00371	.00366	.0037	.000750
ϵ_{34} (")	.04106	.00177	.00015	.00243	.00426	.00339	.00387	.0036	.000162
ϵ_{45} (")	.16427	.00080	.00015	.00162	.00480	.00336	.00373	.0037	.00022
ϵ_{56} (")	.38222	.00080	.00015	.00134	.00512	.00331	.00375	.0036	.00030
m	-	-	-	-	2	2	2	3	-
TYPE OF SPACING	-	CHEBICHEV	EQUAL SPACING	MODIFIED CHEBICHEV	COLUMN 4 RESPACED PER CYCLE #2	COLUMN 5 RESPACED PER CYCLE # 3	COLUMN 6 RESPACED PER CYCLE #4	COLUMN 7 RESPACED TWICE PER CYCLE #6	CHEBICHEV
ESTIMATE OF ϵ_{min} (deg)		.0038 (SEE EQ. 11)							.0009
REMARKS	THIS CHECKS EXAMPLE IN REF. 3							OPTIMUM	6 PRECISION POINTS OBTAINED HERE! (SPACE $x_1 x_2 x_3 x_4 x_5$)
COLUMN NO	1	2	3	4	5	6	7	8	9

be used with any optimization criterion characterized by the minimization of the maximum absolute value in each interval $\phi_{i(i+1)}$ of any continuous function of x. If, for instance, the squared integrated area under each section of the error curve (A_{ij}) is to be a minimum, the only change in Table 3 is the substition of A_{ij} for the symbol ϵ_{ij}.

Application to Path Generation

The methods developed so far are applicable, with some modifications, to path generation. The distance between the ideal curve $f(x)$ and the generated curve $g(x)$ is, in general, not equal to $(f - g)$ which is the quantity minimized heretofore. The exact expression for the minimum distance between two curves involves the solution of a differential equation which may or may not be soluble, and the following approximate method is suggested:

Let (x, y) be a point on the ideal curve; let (x, y_1) and (x_2, y) be points on the generated curve. Then the minimum distance D between the curves is given approximately by the expression

$$\left[\frac{1}{D^2} = \frac{1}{(x_2 - x)^2} + \frac{1}{(y_1 - y)^2}\right]$$

This is the quantity which should be minimized. In the discussion of optimum spacing, the arc length of the curve takes the place of length along the x-axis. This is exact for small intervals and approximate for larger ones.

Examples

Table 5 lists sixteen linkages synthesizing the functions $\log x$, $\sin x$, and x^2 by means of five-point approximations obtained by means of the "650" I.B.M. computer. These examples illustrate the theory developed in the earlier part of this paper, as well as the accuracy and completeness of the obtainable information. One column represents several months on one desk computer and, once the program exists, it can be given to a computation section to grind out mechanisms.

Conclusion

The methods presented can be used in future work to develop an "atlas" of synthesized functions and paths having minimum structural error; such an atlas might be called "Approximations for Linkage Generators" (suggested also by K. Hain), similar in spirit to C. Hastings' "Approximations for Digital Computers" (Princeton University Press, Princeton, N. J., 1955).

Acknowledgments

The author is very greatly indebted to the Trustees of the Higgins Fund, the Watson Laboratory, and the Electronics Research Laboratories—all of Columbia University—the former for financial support and the latter for providing computation facilities. It is a particular pleasure to acknowledge the expert programming advice and help of Mr. Jonathan Robbin, whose skill and enthusiasm made this undertaking possible.

Table 5 Examples of five-point approximations (*continued*)

FUNCTION	$-\log_{10} x$	$\sin x$	$\sin x$	$\sin x$	$\sin x$	$\sin x$	x^2
x_5	1	0 (deg)	0 (deg)	0 (deg)	0 (deg)	0 (deg)	-1
x_f	2	90 (deg)	90 (deg)	90 (deg)	90 (deg)	90 (deg)	1
$\Delta\phi$	60	90	90	90	90	90	90
$\Delta\psi$	60	90	90	90	90	90	60
x_1	1.0166537	2.200 (deg)	2.9129988	2.6852580	2.7610490	2.7633673	-.94524490
x_2	1.1384432	18.55 (")	23.074985	21.451163	21.970803	21.988925	-.52592799
x_3	1.3704083	45.00 (")	49.875375	47.458635	48.213267	48.226892	.04921972
x_4	1.6816018	71.45 (")	72.415643	70.952447	71.404885	71.414168	.67282125
x_5	1.9567889	87.80 (")	87.737162	87.505346	87.555364	87.599570	.97667916
ϕ_1 (deg)	60.041818	118.44583	-62.932894	-61.961530	-62.25737	-62.263261	-21.176386
ψ_1 (deg)	100.01252	257.50621	74.553034	76.095608	75.619182	75.606709	-53.668212
b/a	-.28723765	-2.0753633	1.6928551	1.9040900	1.8357868	1.8343688	-.61016144
c/a	1.0344139	2.4107228	2.1324973	2.2911370	2.2395716	2.2385439	.56558925
d/a	.26145405	.75673805	-.65825785	-.71058516	-.69401338	-.69364556	.38040681
ϵ_{01} (deg)	.00121	.11966	.22149	.17614	.18982	.1902	1.791445
ϵ_{12} (")	.00107	.13796	.21725	.17851	.18983	.1902	2.4177010
ϵ_{23} (")	.00107	.20434	.19986	.18638	.19039	.1903	2.267000
ϵ_{34} (")	.00096	.28886	.17324	.19906	.19040	.1902	2.066015
ϵ_{45} (")	.00077	.23890	.16125	.20615	.19083	.1902	2.180213
ϵ_{56} (")	.00048	.19830	.15485	.20347	.18834	.1892	2.675985
m	2		2	2	3	3	
TYPE OF SPACING	COLUMN 9 RESPACED FURTHER	CHEBYCHEV	COLUMN 11 RESPACED - CYCLE 2	COLUMN 12 RESPACED - CYCLE #3	COLUMN 13 RESPACED CYCLE #4	COLUMN 14 RESPACED CYCLE #5	SHIFTED CHEB. SO AS TO BE UNSYMMETRICAL
ESTIMATE OF ϵ_{min} (deg)		.236					
REMARKS	LATER PRECISION POINT HAS VANISHED					OPTIMUM	HAS 3 REAL NON-TRIVIAL ROOTS
COLUMN NO.	10	11	12	13	14	15	16

References

1 N. I. Levitskii, "Sintez Mekhanizmov Po Chebicheva," Izdatelstvo Akademii Nauk USSR, Moscow-Leningrad, 1946, 168 pp.

2 N. I. Achieser, "Vorlesungen über Approximationstheorie," Akademie Verlag, Berlin, Germany, 1953, 309 pp., Chapter II, pp. 51–58 in particular.

3 F. Freudenstein, "Approximate Synthesis of Four-Bar Linkages," TRANS. ASME, vol. 77, 1955, pp. 853–861.

4 P. L. Chebichev, "Izbrannii Trudi," (Collected Works), Izdatelstvo Akademii Nauk USSR, Moscow, 1955, 926 pp.

5 S. Bernstein, "Leçons sur les Propriétés Extrémales et la Meilleure Approximation des Fonctions Analytiques d'une Variable Réelle," Gauthier-Villars, Paris, France, 1926, 207 pp.

6 Z. Kopal, "Numerical Analysis," John Wiley & Sons, New York, N. Y., 1955, 556 pp. (pp. 18–86 on polynomial approximations.)

7 S. Sh. Blokh, "Angenaeherte Synthese von Mechanismen," Verlag Technik, Berlin, Germany, 1951, 176 pp.

8 B. Skarski, "Das Ebene Gelenkviereck als Funktionsgetriebe," Thesis, Technische Hochschule Carolo Wilhelmina, Braunschweig, Germany, 1955—in particular p. 21.

9 F. B. Hildebrand, "Introduction to Numerical Analysis," McGraw-Hill Book Company, Inc., New York, N. Y., 1956, 511 pp.

10 I. I. Artobolevskii, S. Sh. Blokh, and V. V. Dobrovolskii, "Sintez Mekhanizmov," Gozudarstvennoe Izdatelstvo Tekhniko-Teoreticheskoi Literaturii, Moscow-Leningrad, 1944, 387 pp.

11 K. H. Sieker, "Zur Algebraischen Mass-Synthese Ebener Kurbelgetriebe," Ingenieur-Archiv, vol. 24, 1956; Part I, #3, pp. 188–215; Part II, #4, pp. 233–257.

12 K. H. Sieker, "Analytische Betrachtung des Gelenkviereckes, Insbesondere der Burmesterchen Punkte," *VDI Berichte*, vol. 5, (Getriebetechnik), 1955, pp. 55–60.

13 D. Sarafyan, "Nested Series, Computation of Square-Roots and Solution of Third-Degree Equations," *Mathematics Magazine*, Sept.-Oct., 1953, pp. 19–36.

14 A. Svoboda, "Computing Mechanisms and Linkages," M.I.T. Radiation Series #27, McGraw-Hill Book Company, Inc., New York, N. Y., 1948, first edition.

15 G. Szegö, "Orthogonal Polynomials," Colloquium Publications #23, American Mathematical Society, New York, N. Y., 1939, 401 pp.

16 N. I. Levitskii, "Proektirovanii Ploskikh Mekhanizmov Po Nishimi Parami," Izdatelstvo Akademii Nauk USSR, Moscow-Leningrad, 1950, 183 pp.

17 "Tables of Chebichev Polynomials $S_n(x)$ and $C_n(x)$," National Bureau of Standards, Applied Mathematics Series #9, Dec., 1952, U. S. Government Printing Office, Washington, D. C., 163 pp.

DISCUSSION

T. P. Goodman[3]

This paper is a landmark in the development of kinematic-synthesis techniques, since it presents for the first time a practical design procedure for finding the linkage which best approximates a given function. Particularly noteworthy is the author's digital-computer adaptation of Chebichev's mathematical approach.

Table 5 raises two practical questions:

1 Are the linkages given by Columns 8, 10, and 15 practical and useful (in which case they might well be the first entries

[3] Assistant Professor of Mechanical Engineering, Massachusetts Institute of Technology, Cambridge, Mass. Assoc. Mem. ASME.

in the atlas which the author suggests in his conclusion), or is there some factor not shown in Table 5 (such as unfavorable transmission angles) which limits their usefulness?

2 What are the approximate time and cost of the digital computations for a column of Table 5?

G. N. Sandor[4]

The author is to be congratulated on having added to his list of contributions in kinematic analysis and synthesis the very significant substance of the present paper. For example the method he modestly calls the "modified Chebichev spacing" is welcome as the first analytic procedure for the preselection of precision points, a task for which only general guide rules, also pronounced by himself [3], were previously available. Those of us who have spent weeks at the desk calculator on a single problem will especially appreciate his introduction of powerful automatic digital-computer techniques into the field of kinematic synthesis.

Using a new five-point approximation method, to be submitted shortly as an ASME paper by the author and the writer, the latter has applied the author's respacing formula (3-8) with $m = 3$ in the analytic synthesis of a path-generating linkage with noteworthy results. In a single step of respacing from an arbitrary initial spacing, not only was the maximum normal deviation between the generated and the ideal paths reduced from 0.007256 in. to 0.005598 in. along a 1.9-in. long arcuate segment of curvature radius 1.74 in., but also, the quality of the synthesized linkage was improved in two additional ways: (*a*) The ratio of maximum to minimum link length was reduced from 2.593 to 2.237; and (*b*) the ratio of maximum link length to the distance between the extreme points of the path also was decreased

These few results indicate that the author's suggestions of how to apply his newly developed theory to the optimization of path-generating mechanisms hold the promise of further worth-while achievements.

[4] Chief Engineer, TIME Inc., Springdale Laboratories, Springdale, Conn. Mem. ASME.

Author's Closure

The author is grateful to Drs. Goodman and Sandor for their discussions. The linkages given in columns 8, 10, and 15 are believed to be practical linkages. The ratio of maximum to minimum link length is about four to one; the most unfavorable transmission angle is about forty-five degrees; all three linkages are double-rockers. Since for most purposes these mechanisms are used only within the given range of mechanization, complete rotations would not be required. The proportions and transmission angles are reasonably good and thus these mechanisms could, it is thought, become the first entries in an atlas of computing linkages.

The time of computation of one column (one cycle) of Table 5 is about one hour on the IBM 650. At current rates this amounts to about $120.

It is gratifying to learn of Dr. Sandor's successful application of respacing theory to path-generation and it is conceivable that an atlas of optimum path-generating linkages would also serve a useful purpose.

While the computer provides us with a powerful tool, much work still remains to be done on predicting transmission angles and total crank ranges. As in other fields of endeavor the solution of one problem raises a host of new ones and thereby keeps the subject fascinating.

The Design of Linkages to Generate Functions of Two Variables[1]

C. W. ALLEN

Engineer, General Electric Company, Richland, Wash. Assoc. Mem. ASME

Graphical methods are presented for designing linkages that have two inputs and one output. Two basic approaches are developed. The desired function is matched at a limited number of positions with the maximum number being seven. Designs are also developed which match the derivatives of the desired function at a single point. The designs were developed with ease of solution and broadness of application as primary considerations.

Introduction

THE synthesis of linkages to generate functions of one variable has been the subject of numerous investigations in the past and undoubtedly will continue to be a subject of wide interest for some time. The extension of the problem of designing linkages to include functions of two variables presents the designer with a new and versatile tool. Svoboda [1][2] has presented a possible design procedure, but this has not been widely applied—perhaps due to the difficulty of the design or the resulting complexity of the final linkage. Pike and Silverberg [2] have given a method of solving the problem by using function generators of a single variable and adders. The resultant mechanism will contain more parts and occupy more space than can be allowed in many problems. The following designs are based upon two basic requirements: First, that the resulting linkage shall be a plane linkage containing as few parts as practical; second, that the design shall be as simple as practical, yet fulfilling the basic requirements of the problem.

The Linkage

An investigation of possible linkages resulted in choosing a single type of linkage for this investigation. This linkage has three fixed pivots and therefore can easily represent the output and two inputs as rotations with respect to the fixed link. By requiring that a crank have an infinite effective radius, straight line translation is obtained instead of rotation. The linkage represents the minimum number of links having three links rotating relative to the fixed link and having two degrees of freedom. The basic linkage to be used is shown in Fig. 1.

Expressing the Function in Design Form

The general function $z = f(x, y)$ is best expressed as three functions of one variable for design purposes. Then

$$Z_1 = F_1(x) \text{ when } y = y_1$$
$$Z_2 = F_2(x) \text{ when } y = y_2$$
$$Z_3 = F_3(x) \text{ when } y = y_3$$

Then Z_1, Z_2, and Z_3 can be plotted as curves. This will be helpful in choosing the design positions and also in evaluating the final design. The design points will be taken as points on these curves. For purposes of computation the values of the variables at the design points can be presented in tabular form.

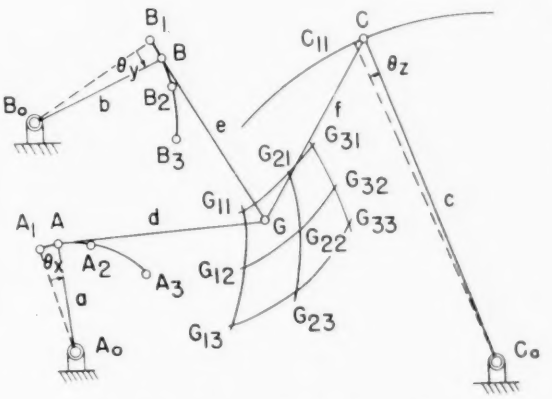

Fig. 1 The basic linkage and nomenclature

Nomenclature

Fig. 1 shows the linkage and the letters for the designation of links and pin joints. The following is a definiton of symbols:

z = output variable
x, y = the two input variables
$Z = f(x, y)$ = the desired function
x_1, x_2, etc. = values of the input variable x
y_1, y_2, etc. = values of the input variable y
z_{11}, z_{12}, z_{23}, etc. = values of the output variable $z_{12} = f(x_1, y_2)$
θ_z = output angle or distance (degrees or inches) measured from the theoretical position, $z = z_{11}$
θ_x = input angle or distance (degrees or inches) measured from the position, $x = x_1$
θ_y = input angle or distance (degrees or inches) measured from the position, $y = y_1$
k_x, k_y, k_z = scale factors
C_x, C_y, C_z = constants
$z = k_z\theta_z + C_z$, $y = k_y\theta_y + C_y$, $x = k_y\theta_y + C_x$ = relations for the input and output variables in terms of scale factors, angles, and constants
a = input crank or slider corresponding to variable x

[1] This paper is based on the author's PhD dissertation at Purdue University, Lafayette, Ind.

[2] Numbers in brackets designate References at end of paper.

Contributed by the Machine Design Division and presented at the Semi-Annual Meeting, Detroit, Mich., June 15-19, 1958, of THE AMERICAN SOCIETY OF MECHANICAL ENGINEERS.

NOTE: Statements and opinions advanced in papers are to be understood as individual expressions of their authors and not those of the Society. Manuscript received at ASME Headquarters, April 9, 1958. Paper No. 58—SA-57.

b = input crank or slider corresponding to variable y

c = output crank or slider

A_0, B_0, C_0 = fixed pivots for links a, b, and c

A, B, C = the movable ends of a, b, and c

G = the pin joint common to links d, e, and f

G_{11}, G_{12}, G_{23}, etc. = particular positions of point G; G_{12} is the position of G when $x = x_1$ and $y = y_2$

Design Considerations

It is desirable that any method of generating the desired function should be applicable to as broad a class of functions as possible. To be included in the class of functions will be empirical functions given only in the form of the curves. The only restrictions are that the functions in the range under consideration be bounded, single valued, and continuous.

The generation of the desired function will be approximate in all linkage designs of this type. The error between the desired and actual functions can be reduced to zero at only a finite number of positions. The number of positions of zero error is limited by the number of linkage parameters to be determined. Therefore there will, in general, exist an error in the output function compared to the desired function.

A function of two variables will be plotted as a series of curves with each curve representing a different value of one input variable. The method of solution will be to attempt to generate a function such that, when plotted as curves, will approximate the desired curves. No attempt will be made to find a particular type of linkage that will theoretically generate a function exactly.

FINITELY SEPARATED DESIGN POSITIONS

In this section consideration is given to matching the desired function in magnitude at a limited number of positions.

Starting the Design

To start the design a considerable portion of the linkage is chosen. The location A_0 and C_0; the lengths of links a, d, f, and c; and the locations of A_1 and C_{11} are chosen. The scale factors k_x and k_z are chosen. From previous equations values of θ_x and θ_z can be computed to locate A_2, A_3, and the necessary C points. (Just how many and which C points are necessary depends upon the particular design.) Then the G points corresponding to the C points are located. It is the location of the G points that forms the basis of the design.

With such a large number of variables to be chosen, the possible number of solutions to any problem is limited only by the number of solutions the designer is willing to complete. The large number of solutions allows a choice of solutions as well as the possibility of satisfying other conditions such as transmission angles.

For a given value of the y input, one, two, or three G points are located. If three G points (such as G_{12}, G_{22}, and G_{32}) are chosen, then B_2 is the center of a circle passing through the three points. If two points (such as G_{13}, G_{33}) are chosen, then B_3 is located equal distance from G_{13} and G_{33} (B_3 is on the perpendicular bisector of the line $G_{13}G_{33}$). If only one G point (such as G_{21}) is chosen, then the point B_1 is located on an arc with center G_{21} and radius BG. By combining these possibilities, solutions to the problem are obtained.

Completing the Design

Let N_1 be the number of values of the y input for which only one G point is given, N_2 be the number of values of the y input for which there are two G points, and N_3 be the number of values of the y input for which there are three G points. These G points are all that are to be used, not the number that can be found. There exist four solutions of interest as shown in Table 1. Each solution is based upon the location of one to three G points for each of the three values of y.

Table 1 Some *N* combinations having solutions to the design

Solution number	N_1	N_2	N_3
I	0	2	1
II	1	1	1
III	2	0	1
IV	1	2	0

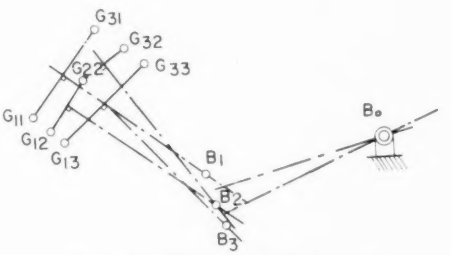

Fig. 2 Determination of B_1, B_2, B_3, and B_0

Solution I. This solution has seven design positions. There exists the disadvantage of having the y input scale nonlinear. For this solution three G points are located corresponding to one value of y and two G points located corresponding to each of two other values of y. The points G_{11}, G_{31}, G_{12}, G_{22}, G_{32}, G_{33}, and G_{13}, as shown in Fig. 2, will be used as an illustration for the completion of the design. The points G_{12}, G_{22}, and G_{32}, corresponding to the curve $y = y_2$, determine a circle with center B_2 and radius BG. Point B_1 lies on the perpendicular bisector of line $G_{11}G_{31}$ a distance BG from G_{11} and G_{31}. Similarly B_3 lies on the perpendicular bisector of line $G_{13}G_{33}$ a distance BG from G_{13} and G_{33}. Points B_1, B_2, and B_3 determine a circle with center B_0—thus completing the design.

Solution II. By reducing the number of design positions by one the scales can all be linear, thus only six G points are used. To obtain the linear scale it is convenient that $y_3 - y_2 = y_2 - y_1$. Let the points be the same as before except that for $y = y_3$ the point G_{22} is used instead of the two previous points. In Fig. 3 B_2 and B_1 are located as in the previous solution. The locus of point B_3 is a circle of radius BG and center G_{23}. Since $y_3 - y_2 = y_2 - y_1$, the arc distance from B_3 to B_2 will equal the arc distance from B_2 to B_1. Thus B_3 is found as the intersection of an arc about G_{23} of radius BG and an arc about B_2 of radius B_1B_2. Locating B_0 as the center of a circle passing through B_1, B_2, and B_3 completes the design.

Solution III. If the scale factor k_y for the crank pivoted at B_0 is not free to be determined in the design, then one more design position must be sacrificed to obtain a solution. Five G points are to be used: One for $y = y_1$, three for $y = y_2$, and one for $y = y_3$. The five G points are shown in Fig. 4. The point B_2 is located as the center of the circle determined by the three points G_{12}, G_{22}, and G_{32}. Arcs of radius BG are drawn about the G_{21} and G_{23} points. These arcs form the loci of the B_1 and B_3 points. Let the arc about G_{21} be labeled b_1 and the arc about G_{23} be labeled b_3.

The following construction is shown in Fig. 5. A locus for the point B_0 can be determined using B_2 and b_1. Choose any point R on b_1 and construct an isosceles triangle with base B_2R and vertex angle ϕ_{12}, where ϕ_{12} is the difference between θ_y for $y = y_1$ and θ_y for $y = y_2$. The vertex of this triangle is a point on the locus of B_0. Let the vertex be denoted by P. Since there are two possible locations for P as shown in Fig. 5, one location will be denoted

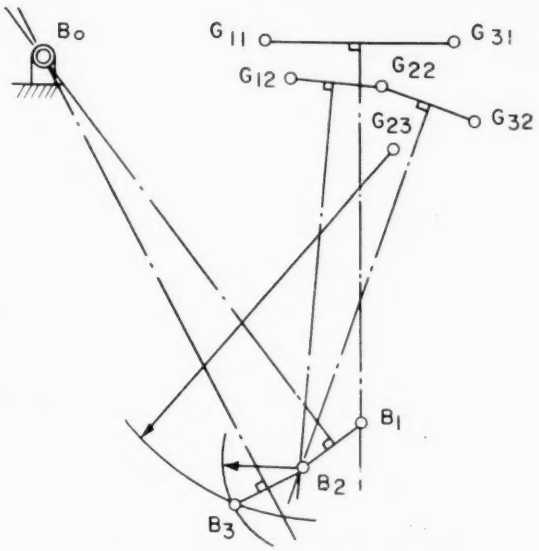

Fig. 3 Construction to locate B_1, B_2, B_3, and B_0

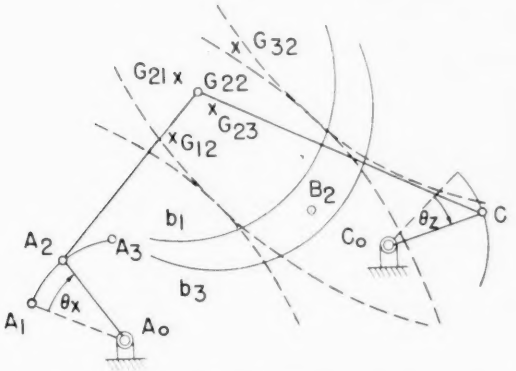

Fig. 4 The initial linkage with curves shown for locating B_0

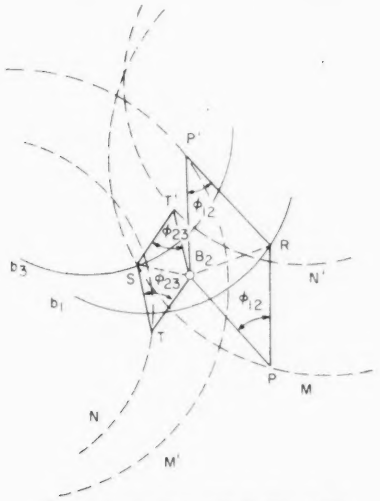

Fig. 5 Construction of M, N, M', and N'

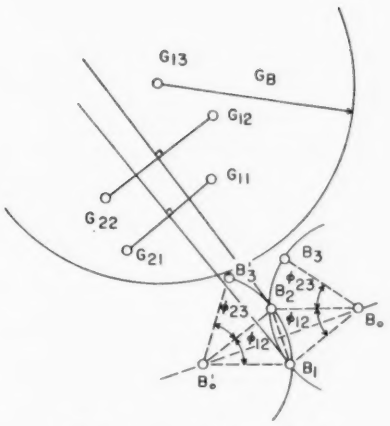

Fig. 6 Construction for solution IV

as P and one location will be denoted as P'. Choosing several R points enables the designer to determine a locus consisting of all points P and a locus consisting of all points P'. Let the locus of P points be M and the locus of P' points be M'. Thus the point B_0 may be any point on M or M'. Choosing points on b_3 and following a similar construction determines two more loci for B_0. Let the points on b_3 be denoted as S and the vertex of the triangles as T and T'. The loci of all points T and T' are N and N'. The vertex angles being θ_{23}, the difference between θ_y for $y = y_3$ and θ_y for $y = y_2$.

The loci M, M', N, and N' are circles [3] but are usually more easily constructed by individual points than by circle arcs. The intersection of one of the M loci with one of the N loci is a possible location for the B_0 point. Once the B_0 point is determined, an arc with center B_0 and radius BB_0 is drawn. The intersection of this arc with b_1 and b_3 determines the points B_1 and B_3. Because of the possibility of multiple solutions, care should be taken that the locations of B_0, B_1, B_2, and B_3 are such they fulfill the requirements of the problem.

Solution IV. Again only five positions are satisfied in the design, therefore resulting in a case limited in precision, but able to fulfill additional requirements. This solution is similar to Solution II except that the scale factor for both input cranks can be specified. For two values of y, two G points are located, and for the remaining value of y, one G point. Let these G points be G_{11}, G_{12}, G_{21}, G_{22}, and G_{31} as shown in Fig. 6. B_0 is located at some point on the perpendicular bisector of $G_{11}G_{21}$ and B_2 located at some point on the perpendicular bisector of $G_{12}G_{22}$. The point B_3 will be located on a circle about G_{13}.

To complete the solution a trial distance is shown for GB. Points B_1 and B_2 are located and a circle of radius GB is drawn about G_{31}. If the scale factor k_x has been chosen, then the angles ϕ_{12} and ϕ_{23} are known (ϕ angles are the same angles described in Solution III). The angle ϕ_{12} and the points B_1 and B_2 are used to locate two possible locations for point B_0 as shown in Fig. 6. By constructing the angle ϕ_{23} two points B_3' and B_3'' are located. If either of these points is located on the arc about G_{31}, then a solution has been found. Since in general this will not happen, another attempt must be made. It has been found convenient to draw a curve of the minimum distances from B_3' and B_3'' to the circle about G_{31}, denoted by e_1 and e_2, versus the chosen distance GB. Solutions are obtained when the value of e_1 or e_2 is zero.

Although the solution is obtained by a trial and error process, by accurate construction and careful plotting of the e values on a graph, solutions can be obtained that are as accurate as graphical methods allow.

Improving the Original Linkage Choice

The previous methods are based upon choice of most of the link lengths for a major portion of the linkage to locate the G points. In the first three methods three G points were used to determine the length of the link GB. The following involves eliminating these three points from the solution and choosing the original linkage such that four or five positions are satisfied. This is accomplished by designing a linkage to generate a function of one input for a fixed value of the second input. Links are then added in such a fashion that the precision of the original design is retained in the final linkage.

Procedures for designing a linkage to generate a function of one variable are well known [1, 4]. Any of these methods can be used to design a four-bar linkage to generate the desired function for a given value of y. Thus if $y = y_2$, then a linkage can be designed to generate z as a function of x. This is accomplished and the resulting linkage might appear as A_0AGB_2 in Fig. 7.

To the original four-bar linkage two more links are added such as to form a parallelogram linkage as shown by links GC and CC_0. The link GB_2 is momentarily disregarded and the remaining links are the portion of the linkage necessary to start the design. G points are located for $y = y_1$ and $y = y_3$. The design is completed as in Methods I, II, or III excepting that no points are necessary for $y = y_2$ as the length GB has been determined.

This procedure allows a very good design to be obtained for $y = y_2$.

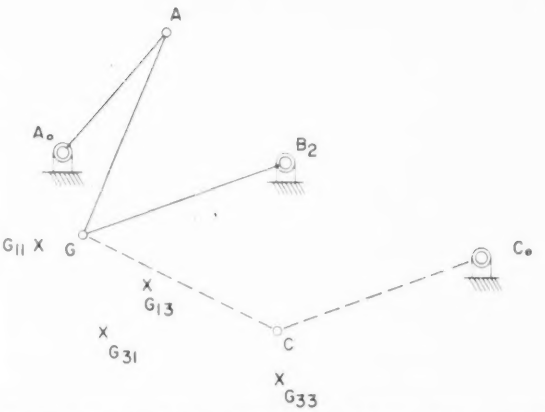

Fig. 7 A four-bar linkage with added parallelogram linkage added

DESIGN AT A SINGLE POINT

Instead of specifying that the desired function shall be matched at a number of separated points, there also exist designs which match a number of derivatives of the desired function at a single point. This approach has been used with good results for generating functions of a single variable [4, 5]—especially when the range of motion is small.

Derivatives of the Desired Function

For the following designs the derivatives of the desired function are related to the velocity and acceleration of points on the linkage. First let us consider the derivatives of the desired function. The function and the first two derivatives of the function are:

$$z = f(x, y) \tag{1}$$

$$\frac{dz}{dt} = \frac{\partial z}{\partial x}\frac{dx}{dt} + \frac{\partial z}{\partial y}\frac{dy}{dt} \tag{2}$$

$$\frac{d^2z}{dt^2} = \frac{\partial^2 z}{\partial x^2}\left(\frac{dx}{dt}\right)^2 + \frac{\partial^2 z}{\partial y^2}\left(\frac{dy}{dt}\right)^2 + \frac{\partial z}{\partial x}\frac{d^2x}{dt^2} + \frac{\partial z}{\partial y}\frac{d^2y}{dt^2} + 2\frac{\partial^2 z}{\partial x \partial y}\frac{dx}{dt}\frac{dy}{dt} \tag{3}$$

In the application of these equations to the linkage it is convenient to use special cases of both equations (2) and (3). These are:

$$\frac{dz}{dt} = \frac{\partial z}{\partial x}\frac{dx}{dt} \quad \text{when} \quad \frac{dy}{dt} = 0 \tag{4}$$

$$\frac{dz}{dt} = \frac{\partial z}{\partial y}\frac{dy}{dt} \quad \text{when} \quad \frac{dx}{dt} = 0 \tag{5}$$

$$\frac{d^2z}{dt^2} = \frac{\partial^2 z}{\partial x^2}\left(\frac{dx}{dt}\right)^2 + \frac{\partial z}{\partial x}\frac{d^2x}{dt^2} \quad \text{when} \quad \frac{dy}{dt} = \frac{d^2y}{dt^2} = 0 \tag{6}$$

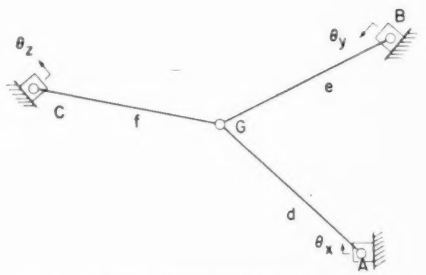

Fig. 8 The basic linkage with infinite crank lengths

$$\frac{d^2z}{dt^2} = \frac{\partial^2 z}{\partial y^2}\left(\frac{dy}{dt}\right)^2 + \frac{\partial z}{\partial y}\frac{d^2y}{dt^2} \quad \text{when} \quad \frac{dx}{dt} = \frac{d^2x}{dt^2} = 0 \tag{7}$$

Equations (4) through (7) will be used as the basis of the following designs.

Equations of Motion of Points on the Linkage

In the previous examples the input and output of the linkage has been an angular motion. For simplicity in the following design the input and output can be considered to be motion along a straight line. This corresponds to making cranks a, b, and c infinite in length. If angular motion is desired, then the proper adjustment is made before starting the solution.

In Fig. 8 the linkage to be considered is shown. The symbols θ_z, θ_y, and θ_x have been retained, but in this case represent linear motion. The following velocity relations are obtained from the usual velocity analysis [6, 7].

When $V_B = 0$,

$$V_C{}^A = V_G{}^A + V_{CG}{}^A \tag{8}$$

$$V_G{}^A = V_A{}^A + V_{GA}{}^A \tag{9}$$

The superscript has been introduced to avoid confusing certain terms with similar terms in the following equations.

When $V_A = 0$,

$$V_C{}^B = V_G{}^B + V_{CG}{}^B \tag{10}$$

$$V_G{}^B = V_B{}^B + V_{GB}{}^B \tag{11}$$

The following equations can be obtained from a similar acceleration analysis:

When $V_B = A_B = 0$,

$$A_C{}^A = A_{CG}{}^{NA} + A_{CG}{}^{TA} + A_G{}^A \quad (12)$$

$$A_G{}^A = A_{GB}{}^{NA} + A_{GB}{}^{TA} \quad (13)$$

$$A_G{}^A = A_{GA}{}^{NA} + A_{GA}{}^{TA} + A_A{}^A \quad (14)$$

When $V_A = A_A = 0$,

$$A_C{}^B = A_{CG}{}^{NB} + A_{CG}{}^{TB} + A_G{}^B \quad (15)$$

$$A_G{}^B = A_{GA}{}^{NB} + A_{GA}{}^{TB} \quad (16)$$

$$A_G{}^B = A_{GB}{}^{NB} + A_{GB}{}^{TB} + A_B{}^B \quad (17)$$

From a physical interpretation of equations (4) through (17) we can obtain the following relations:

$$\frac{dx}{dt} = k_x \frac{d\theta_x}{dt} = k_x V_A \quad (18)$$

$$\frac{d^2x}{dt^2} = k_x \frac{d^2\theta_x}{dt^2} = k_x A_A \quad (19)$$

$$\frac{dy}{dt} = k_y \frac{d\theta_y}{dt} = k_y V_B \quad (20)$$

$$\frac{d^2y}{dt^2} = k_y \frac{d^2\theta_y}{dt^2} = k_y A_B \quad (21)$$

$$\frac{dz}{dt} = k_z \frac{d\theta_z}{dt} = kV_C \quad (22)$$

$$\frac{d^2z}{dt^2} = k_z \frac{d^2\theta_z}{dt^2} = kA_C \quad (23)$$

If links a, b, and c are to be of finite length with θ_x, θ_y, and θ_z being angles, then A_A, A_B, and A_C are the tangential components of the acceleration.

Solving the Velocity and Acceleration Equations

The partial derivatives are evaluated at the design position. The design position is normally chosen as the middle of the ranges of both x and y. When the partial derivatives have been evaluated and the scale factors chosen, the magnitudes of the velocities and accelerations of points A, B, and C can be determined for the two cases of point A stationary and point B stationary.

Solution V. The solution of only the velocity equations can be easily accomplished by a graphical solution. The magnitude of $V_C{}^A$, $V_A{}^A$, $V_C{}^B$, and $V_B{}^B$ must first be determined. The directions of links d, e, and f are chosen. The solution is based upon a velocity polygon.

About the pole for the proposed velocity polygon three circles are drawn. One circle has a radius of unit magnitude. This circle will represent the magnitude of $V_C{}^A$ and $V_C{}^B$. The other two circles have radii proportional to $V_A{}^A/V_C{}^A$ and $V_B{}^B/V_C{}^B$. These circles represent the magnitude of $V_A{}^A$ and $V_B{}^B$, respectively. To start the polygon the direction of motion of one point is chosen. The solution of equations (8), (9), (10), and (11) can easily be accomplished, noting that $V_C{}^A$ is parallel to $V_C{}^B$. A completed velocity polygon is shown in Fig. 9.

The completion of the polygon determines the directions of the velocities of the two remaining points. There is still considerable freedom for the designer in completing the linkage. The lengths of the links are arbitrary as well as the sense of the points A, B, and C from the point G. Thus this design does not give a definite solution to the problem, but yields a class of linkages satisfying the design conditions.

Solution VI. The previous method is valuable in determining only a class of linkages, but may be extended to give a specific solution by including more design conditions. Thus the second derivatives can be satisfied by solving equations (12) through (17).

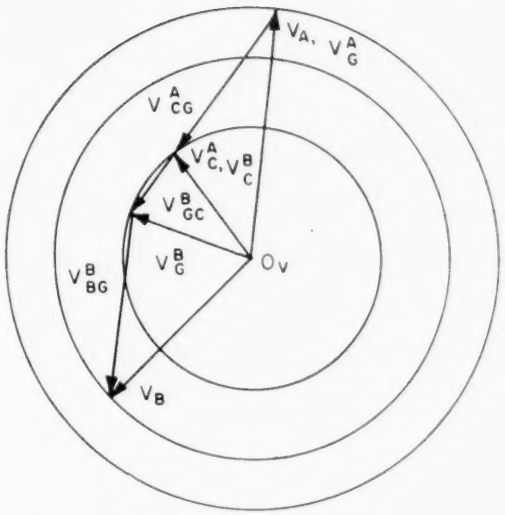

Fig. 9 The velocity polygon

A graphical solution of these equations can be obtained only by placing a restriction upon the direction of one velocity component. For a solution either V_A is taken perpendicular to link e, or V_B is taken perpendicular to link d. This restriction does not prove to be a serious restriction in the application. The first part of the design is accomplished by completing the previous velocity design. Using the values of the second derivatives of the desired function at the design position and the scale factors, the values of the tangential second derivatives of the points A, B, and C can be computed.

To solve the acceleration equations the paths of points A, B, and C must be known. The paths of these points will be either circle arcs or straight lines in a linkage. If the paths are circles, the radii of the circles must be known to compute the values of the normal accelerations. Starting with the point whose velocity is perpendicular to an intermediate link, the equations can be solved. The special choice of direction for one velocity results in a normal relative acceleration being zero. (If V_A is perpendicular to link e, then $A_{GA}{}^N = 0$ when $V_B = 0$.) The length of link d or e, depending upon how the design is started, must be chosen by the designer.

The velocity solution shown in Fig. 9 was started with V_A perpendicular to link e. This choice enables the solution to be

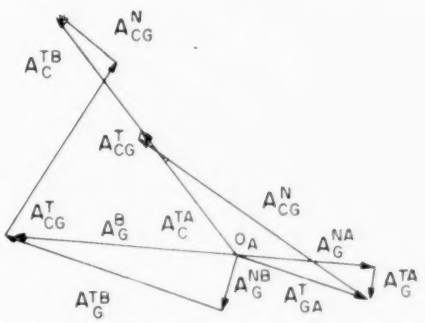

Fig. 10 The acceleration polygon

carried further and the accelerations satisfied. The completed acceleration polygon is shown in Fig. 10. Once the acceleration polygon is complete, the lengths of the remaining links can be determined. The acceleration polygon will also determine the sense of these links.

Results of an Example Problem

The details of solving a problem are simple, but step by step explanations are of such length that they must be omitted here. The results of applying the design procedure to a specific example are shown. The function used in this example is $z = x^2y^{1.2}$, for $1 \leq x \leq 1.4$ and $1 \leq y \leq 2$. The method given in Solution I for separated design positions was applied to this problem and the results are shown in Fig. 11. The design positions are not points of zero error due to drawing inaccuracies.

The same problem was solved by the method of Solution VI for design at a single point and the results are shown in Fig. 12. In this application the design is very good in a region about the design point ($x = 1.2$, $y = 1.5$) and the error becomes greater away from this point.

Summary

The preceding designs are presented as an approach to the solution of designing two degree-of-freedom linkages. Compared to present methods of synthesis for single degree-of-freedom linkages the approach may appear simple and the results crude. One cannot hope to find procedures for a more complicated linkage that will compare in simplicity and accuracy with the simpler four-bar linkage. The design procedures were developed with the intention of finding a general configuration of the linkage and certain dimensions to help the designer fit the final linkage to his particular application. The errors that result from the designs may eliminate the application of these procedures to some problems. Since the designs are quickly accomplished, several may be completed in a search for one fulfilling the allowable tolerance. One cannot hope to obtain errors of the magnitude possible in a four-bar linkage without considerable luck. In the many applications where the tolerances are more liberal, satisfactory solutions can be obtained. Perhaps future work will present methods of reducing the maximum error as has been done for the four-bar linkage.

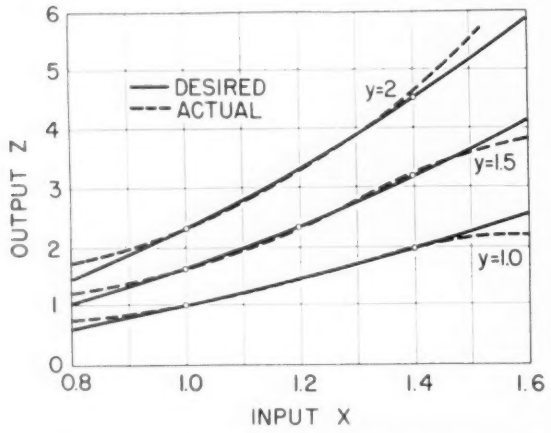

Fig. 11 Comparison of the actual and desired functions for an example of Solution I

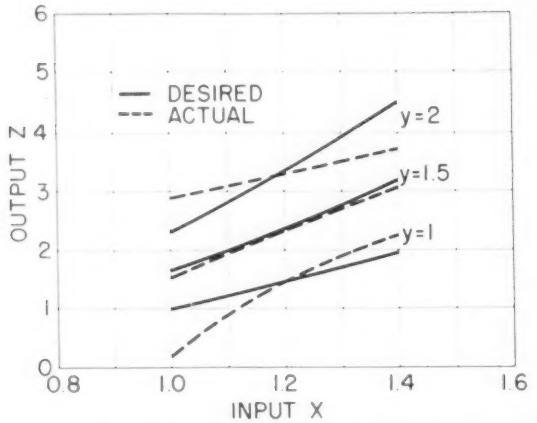

Fig. 12 Comparison of the actual and desired functions for an example of Solution VI

References

1 Antonin Svoboda, "Computing Mechanisms and Linkages," McGraw-Hill Book Company Inc., New York, N. Y., 1948.

2 E. W. Pike and T. R. Silverberg, "Designing Mechanical Computers," *Machine Design*, July, 1952, pp. 131–137.

3 Nathan Altshiller-Court, "College Geometry," Johnson Publishing Company, New York, N. Y., 1925, p. 48.

4 F. Freudenstein, "Approximate Synthesis of Four-Bar Linkages," TRANS. ASME, vol. 77, 1955, pp. 853–859.

5 J. C. Wolford, "Four-Bar Linkages as Function Generators," *Product Engineering*, October, 1955, pp. 166–171.

6 A. R. Holowenko, "Dynamics of Machinery," John Wiley & Sons, Inc., New York, N. Y., 1955.

7 A. H. Church, "Guillet's Kinematics of Machines," John Wiley & Sons, Inc., New York, N. Y., 1950.

DISCUSSION

F. Freudenstein[3]

Linkages with two degrees of freedom possess challenging design possibilities both in path and function generation as, for instance, in applications currently utilizing three-dimensional cams. The design of such linkages is complex and the author is to be commended for being among the first to investigate this subject and for having reduced it to the simplest possible geometrical terms. In the author's mechanism there are 9 link lengths, 3 scale-factors and 3 zero values (constants), and hence 14 precision points exist in theory in the general case. It will be of interest to consider whether some of the techniques of synthesis developed in recent times could be used to increase the number of precision points obtained by the author thus far. Furthermore, if the graphical techniques presented in this paper can be expressed analytically in a manner suitable for computer programming, the usefulness of the results might be increased. In any case, this work represents an encouraging beginning in a difficult field of endeavor.

T. P. Goodman[4]

This paper is a good beginning in a difficult field. Linkages which mechanize functions of two variables should be useful in automatic controls, especially in "adaptive" or "self-adjusting" controllers in which a second input variable is used to adjust the gain of the primary variable. The mechanical simplicity with which nonlinear functions of two variables can be obtained by these linkages, as shown by the example at the end of the paper, should represent a significant advantage over

[3] Columbia University, New York, N. Y. Assoc. Mem. ASME.

[4] Assistant Professor of Mechanical Engineering, Massachusetts Institute of Technology, Cambridge, Mass. Assoc. Mem. ASME.

conventional mechanical and electronic computing elements in control applications.

The solution of the problem for both finitely separated positions and infinitesimally close positions is a logical extension of the kinematic-synthesis techniques developed for the single-variable problem.[5,6] For infinitesimally close positions, the use of velocity and acceleration vectors to synthesize the desired values of the displacement derivatives $\partial z/\partial x$, $\partial z/\partial y$, $\partial^2 z/\partial x^2$, and $\partial^2 z/\partial y^2$ is an ingenious procedure. For finitely separated positions, since all constructions used depend on drawing a circle through three points, it appears that the method of point-position reduction[7] could be used to design more complex linkages to match a larger number of points. For both types of solutions, a digital computer undoubtedly could be used for further refinements.

[5] R. Beyer, "Kinematische Getriebesynthese," Springer Verlag, Berlin, Germany, 1953.

[6] F. Freudenstein, "Approximate Synthesis of Four-Bar Linkages," TRANS. ASME, vol. 77, 1955, pp. 853–861.

[7] K. Hain, "Angewandte Getriebelehre," Hermann Schroedel Verlag, Hannover and Darmstadt, Germany, 1952, chapter N.

Helical Springs of Hollow Circular Cross Section[1]

C. W. BERT

Principal Mechanical Engineer, Applied Mechanics, Battelle Memorial Institute, Columbus, Ohio. Assoc. Mem. ASME

A theoretical and experimental investigation of elastic shear stresses and deflection in an axially loaded helical spring having a hollow circular section is reported in this paper. Two analyses are presented: An approximation of the stresses by strength-of-materials theory and a more accurate elasticity-theory solution for stresses and deflection. The results are compared with strain and deflection measurements on an actual tubular spring.

Introduction

THE PROBLEM of determining elastic stresses in helical springs of solid circular cross section has been treated mathematically by many investigators. The analysis made by Wahl [1][2] is one of the most widely accepted analyses based on strength-of-materials theory. Wahl used a method analogous to Winkler's method [2] for finding bending stresses in curved beams. In solving the differential equations of equilibrium and compatibility by an iterative method, Göhner [3] made probably the first complete and generally applicable elasticity-theory analysis of the stresses and deflection.

In 1884, Smith [4] made perhaps the first suggestion that helical springs be coiled from tubing. Actual manufacture of such a spring was probably first mentioned in the literature by Berry [5] in 1938, when he described a hollow spring which carried lubricating oil to the supporting mechanism.

In apparently the only published analysis which treats elastic stresses and deflection of hollow springs, Reissner [6] analyzed an infinitely-thin-walled spring by the membrane theory of thin-walled shells of revolution.

[1] Based, in part, on a portion of an unpublished thesis submitted in partial fulfillment of the requirements for the Master of Science degree at The Pennsylvania State University, August, 1956.

[2] Numbers in brackets designate References at end of paper.

Contributed by the Machine Design Division and presented at the Semi-Annual Meeting, Detroit, Mich., June 15–19, 1958, of THE AMERICAN SOCIETY OF MECHANICAL ENGINEERS.

NOTE: Statements and opinions advanced in papers are to be understood as individual expressions of their authors and not those of the Society. Manuscript received at ASME Headquarters, February 25, 1958. Paper No. 58—SA-18.

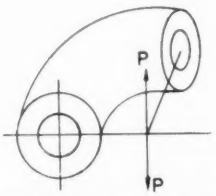

Fig. 1 Ring sector cut from a thick-walled helical spring

Springs of solid circular section and springs of thin-walled circular section are the two extremities of the present problem, which includes springs of any arbitrary wall thickness. The weight-saving characteristic of relatively thin-walled structural members has been used in aircraft structures for some time. However, springs having relatively thick walls are of importance because they have a weight advantage over solid springs and yet, unlike thin-walled springs, they neither crinkle flexurally during coiling nor buckle by torsional shear crippling in operation. For instance, Bruch [7] has recently conducted fatigue tests of thick-walled steel springs. The purpose of this paper is to present analyses applicable to this type of spring. Fig. 1 shows a ring sector cut from such a spring.

Derivation by Strength-of-Materials Theory

This derivation is an extension of Wahl's analysis of a solid spring. Helix angle is not considered. Fig. 2 shows the co-ordinate system and elemental area. The total shear stress is assumed to consist of a stress due to a pure torsional couple and

Nomenclature

B = bore ratio (ratio of inside to outside section diameter)
C = spring index (ratio of mean coil diameter to outside section diameter)
C_E = a constant
D = mean coil diameter
d_i, d_o = respective inside and outside section diameters
e = distance from center of torsional rotation to geometric center of section
F = total axial deflection of spring, measured from free height
G = modulus of rigidity
K = shear-stress factor of any point on spring surface
K_A, K_B = respective maximum and minimum total shear-stress factors
K_{max} = maximum combined shear-stress factor, including pitch effect
N = number of active coils
P = applied axial load
p = tangent of helix angle
R = mean coil radius
r = radius to any point in section, Fig. 4
r_i, r_o = respective inside and outside cross-sectional radii
x, y = rectangular co-ordinates of any point in section, Figs. 2 and 4
β = positional angle of any point in section, Fig. 4
ν = Poisson's ratio
ρ = radius from helix axis to any point in spring
τ = shear stress at any point on spring surface
τ_d = direct shear stress
τ_{tA}, τ_{tB} = maximum and minimum torsional shear stresses
τ_x, τ_y = shear stresses normal to and parallel to helix axis
ϕ = shear-stress function
ψ_u, ψ_p = respective uncorrected and pitch-corrected deflection factors

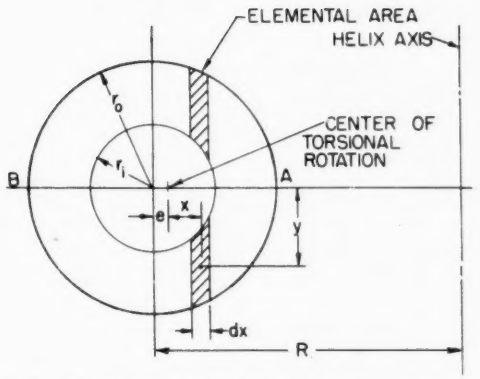

Fig. 2 Co-ordinate system used in the analysis according to strength-of-materials theory

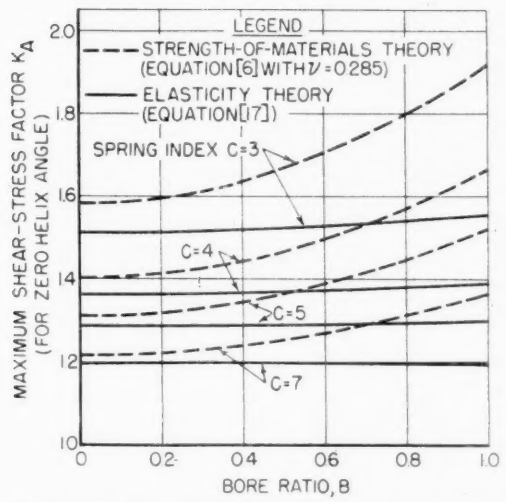

Fig. 3 Effect of bore ratio on maximum shear-stress factors obtained by strength-of-materials and elasticity theories

another due to direct shear load. The torsional stress at points A and B in Fig. 2 may be expressed as

$$\tau_{tA} = \frac{r_o - e}{R - r_o}\,\frac{2}{\pi}\,\frac{PR^2}{r_o^4 - r_i^4}, \quad \tau_{tB} = \frac{r_o + e}{R + r_o}\,\frac{2}{\pi}\,\frac{PR^2}{r_o^4 - r_i^4} \tag{1}$$

Equating the area integral of the torsional stress component parallel with the helix axis to zero, integrating, and simplifying, yields

$$e = \frac{1 + B^2}{4C}\,r_o \tag{2}$$

Substitution of Equation (2) into (1) and simplification gives

$$\tau_{tA} = \frac{4C - 1 - B^2}{4C - 4}\,\frac{8}{\pi}\,\frac{PDd_o}{d_o^4 - d_i^4}$$

$$\tau_{tB} = \frac{4C + 1 + B^2}{4C + 4}\,\frac{8}{\pi}\,\frac{PDd_o}{d_o^4 - d_i^4} \tag{3}$$

The following equation for the direct or transverse shear stress at the outer edges of the horizontal diameter of a straight, hollow, circular beam subjected to a symmetrical vertical load was obtained by applying Saint-Venant's elasticity-theory flexure analysis as reported by Sokolnikoff [8].

$$\tau_d = \frac{4}{\pi}\left(\frac{3 + 2\nu}{1 + \nu}\right)\left(\frac{1 + 2\nu}{3 + 2\nu} + B^2\right)\frac{Pd_o^2}{d_o^4 - d_i^4} \tag{4}$$

The stress at any point on the spring surface may be expressed as

$$\tau = \frac{8}{\pi}\,\frac{KPDd_o}{d_o^4 - d_i^4} \tag{5}$$

where the dimensionless shear-stress factor K is the ratio of the stress at the desired point on the spring surface to the nominal stress, which is the torsional stress on the surface of a straight member having an identical section and subjected only to a pure torsional couple of magnitude PR.

The maximum total shear stress, which is at A, is the sum of the torsional and direct-shear stresses. The corresponding K factor is

$$K_A = \frac{4C - 1 - B^2}{4C - 4} + \left(\frac{1 + 2\nu}{3 + 2\nu} + B^2\right)\frac{3 + 2\nu}{(1 + \nu)2C} \tag{6}$$

In Fig. 3 dotted curves show this relation for a Poisson's ratio ν of 0.285.

The total shear-stress factor at B is

$$K_B = \frac{4C + 1 + B^2}{4C + 4} - \left(\frac{1 + 2\nu}{3 + 2\nu} + B^2\right)\frac{3 + 2\nu}{(1 + \nu)2C} \tag{7}$$

Derivation by Theory of Elasticity

This derivation is based on Göhner's analysis of a solid spring. Fig. 4 shows the co-ordinate system. Helix angle is not considered here, since Ancker [9] has shown that it does not affect shear stress. Its effect on combined shear stress will be discussed later. The basic differential equation is

$$\frac{\partial^2\phi}{\partial\rho^2} + \frac{\partial^2\phi}{\partial y^2} - \frac{3}{\rho}\,\frac{\partial\phi}{\partial\rho} + 2C_E = 0 \tag{8}$$

The only boundary condition in the solid spring is that the resultant surface shear stress must be tangent to the surface. Here a similar condition is imposed at both inside and outside surfaces. This requires that along each boundary the stress function ϕ be equal to a constant, chosen to make the displacements single-valued. On the outside, ϕ is chosen to be zero for simplicity; thus on the inside it must have some other value.

The resulting expressions for the fourth approximations of ϕ and the shear-stress components, respectively normal to and parallel to the helix axis, are

$$\phi = -\frac{3C_E x}{512R^3}(x^2 + 5y^2 + 10r_o^2)(x^2 + y^2 - r_o^2) \tag{9}$$

$$\tau_z = -C_E G\left(y + \frac{5}{4}\,\frac{xy}{R} + \frac{45}{16}\,\frac{x^2y}{R^2} + \frac{281}{128}\,\frac{x^3y}{R^3} + \frac{5}{16}\,\frac{y^3}{R^2} - \frac{5}{8}\,\frac{r_o^2y}{R^2} + \frac{95}{128}\,\frac{xy^3}{R^3} - \frac{305}{256}\,\frac{r_o^2xy}{R^3}\right) \tag{10}$$

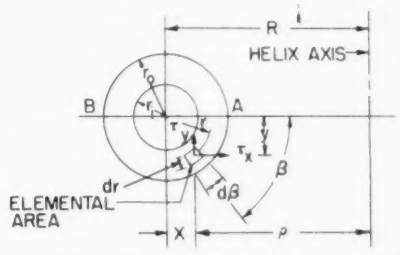

Fig. 4 Co-ordinate system used in the analysis according to elasticity theory

$$\tau_y = -C_K G\left(x + \frac{7}{8}\frac{x^2}{R} + \frac{13}{16}\frac{x^3}{R^2} + \frac{399}{512}\frac{x^4}{R^3} - \frac{3}{8}\frac{y^2}{R} + \frac{3}{8}\frac{r_o^2}{R} - \frac{9}{16}\frac{xy^2}{R^2} + \frac{r_o^2 x}{4R^2} - \frac{165}{256}\frac{x^2y^2}{R^3} + \frac{145}{512}\frac{r_o^2x^2}{R^3} + \frac{15}{512}\frac{y^4}{R^3} + \frac{15}{512}\frac{r_o^2y^2}{R^3} - \frac{5}{256}\frac{r_o^4}{R^3}\right) \quad (11)$$

Constant C_E is found by converting Equations (10) and (11) to polar co-ordinates and equating external torque to internal resisting torque. Thus

$$PR = -\int_{r_i}^{r_o}\int_0^{2\pi} r^2(\tau_z \sin\beta + \tau_y \cos\beta)\, d\beta\, dr \quad (12)$$

For the fourth approximation

$$PR = \frac{\pi}{2} C_E G(r_o^4 - r_i^4)\left(1 + \frac{13}{64}\frac{r_o^2}{R^2} - \frac{25}{64}\frac{r_i^2}{R^2}\right) \quad (13)$$

Axial spring deflection may be deduced from Equation (13) and expressed by using a deflection factor ψ_u analogous to shear-stress factor K in Equation (5). Thus

$$F = \frac{8\psi_u PD^3N}{G(d_o^4 - d_i^4)} \quad (14)$$

In obtaining Equation (13), the coefficients of the last two terms inside the last parentheses fluctuated around 3/16 and −3/8. Using these values instead of 13/64 and −25/64 and substituting B and C yields

$$\psi_u = 1 - \frac{3}{16C^2} + \frac{3B^2}{8C^2} \quad (15)$$

Curves showing this relation are given in Fig. 5.

At point A in Fig. 4, y and τ_z are zero and $x = r_o$. Then

$$K_A = \frac{1 + \frac{5}{4}\frac{r_o}{R} + \frac{17}{16}\frac{r_o^2}{R^2} + \frac{272}{256}\frac{r_o^3}{R^3}}{1 + \frac{13}{64}\frac{r_o^2}{R^2} - \frac{25}{64}\frac{r_i^2}{R^2}} \quad (16)$$

Using the same reasoning as in Equation (15), (16) may be approximated by

$$K_A = 1 + \frac{5}{4C} + \frac{7}{8C^2} + \frac{3B^2}{8C^2} \quad (17)$$

The solid curves in Fig. 3 represent the relationship of Equation (17).

The approximation for the shear-stress factor at point B is

$$K_B = 1 - \frac{5}{4C} + \frac{7}{8C^2} + \frac{3B^2}{8C^2} \quad (18)$$

For comparative purposes, Fig. 6 gives K_A and ψ_u versus C for springs of infinitely-thin-walled circular section according to Reissner's theory and also according to the expressions derived in this paper.

Effect of Spring Pitch

By considering deformation of a thin slice of a solid spring by elasticity methods, Ancker obtained an expression for the maximum bending stress, which occurs at A. Upon combining this stress with the shear stress at A by the usual method, he found that the maximum combined shear stress was larger than the uncombined shear stress by only the factor $^1/_2\, p^2$. Since this factor is small, the hole in a hollow spring will affect its value little

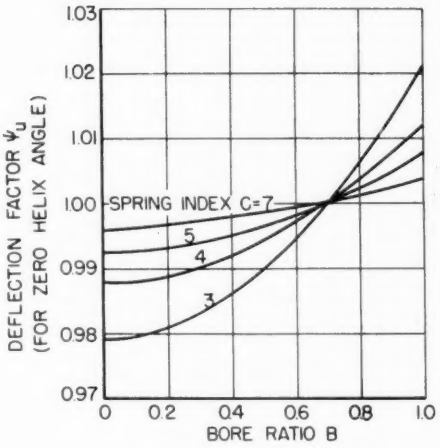

Fig. 5 Effect of bore ra io on deflection factor

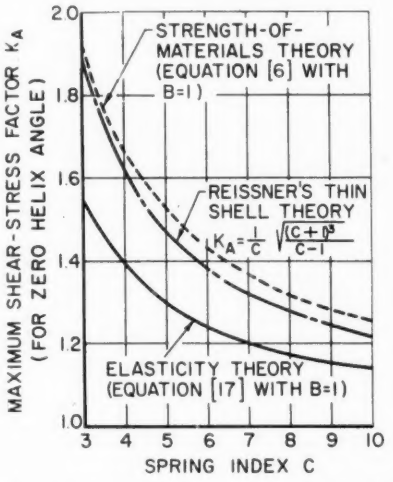

Fig. 6 Maximum shear-stress factor by three theories for a helical spring of thin-walled circular cross section

compared to the other terms in the expression. Therefore this term may be added to Equation (17) to obtain the maximum combined shear-stress factor K_{max}. Thus

$$K_{max} = 1 + \frac{5}{4C} + \frac{7}{8C^2} + \frac{3B^2}{8C^2} + \frac{1}{2}p^2 \quad (19)$$

Likewise another term derived by Ancker may be added to Equation (15) to provide for pitch effect on deflection. Then

$$\psi_p = 1 - \frac{3}{16C^2} + \frac{3B^2}{8C^2} + \frac{3+\nu}{2(1+\nu)}p^2 \quad (20)$$

Description of Test

To check these equations, deflection and SR-4 strain-gage measurements were made on a thick-walled helical compression spring. Its dimensions, in inches, were: D, 4.05; d_o, 0.570; d_i, 0.283; solid height, 6.50; and free height, 14.50. There were $11^1/_2$ total coils. The SAE 8740 steel spring was coiled cold, preset with 0.5-in. permanent set, heat treated to an ultimate

tensile strength of 200,000 to 220,000 psi, shot blasted, cadmium plated 0.0003 in. minimum, and hydrogen relieved at 375 F for three hours. Although these processes were beneficial to fatigue life, they were detrimental to strain-gage determination of elastic shear-stress factors.

Three sets of Type A-7 gages were equally spaced around a coil at approximately the center of the spring height. This enabled effects of load eccentricity to be removed by averaging and reduced the possibility of adverse end effects. These sets were mounted on the spring surface at A. One other set was mounted at B, but circumferentially in line with one of the point-A sets, in order to compare readings at A and B directly. In each set, one gage was mounted 45 deg above the tubing center line and the other 45 deg below.

The spring was compressed between parallel platens of a conventional universal testing machine. Load, deflection, and strain readings were taken at loads from 800 to 1300 lb.

Experimental Results

The average spring rate P/F, based on seven measurements, was 218 lb/in. with a 0.8 per cent standard deviation. The calculated nominal spring rate, using Equation (14) with deflection factor $\psi = 1$ and assuming $G = 11{,}500{,}000$ psi and $N = 9.75$, was 220 lb/in. Thus the average ψ_p obtained experimentally was 1.01. The theoretical ψ_p values calculated by Equation (20), using pitch values corresponding to each load, also averaged 1.01. Thus the actual difference between experimental and theoretical ψ_p values was zero. Table 1 lists possible sources of error and their estimated effects on the various results. The estimated probable error of 3.2 per cent for ψ_p indicated either that the errors were over-estimated or that the errors cancelled each other.

The average K_A was 1.00, based on six readings. However, K_A values based on readings taken later in the test were lower than those based on earlier readings. This was true of readings from all gages, so the effect was not just local. Apparently plastic flow, creep, or a combination of both, was occurring in the strain-gage cement bond, in the bond between the cadmium plating and the steel spring, or in the plating itself. The possibility of flow in the first two instances was improbable. However, in the third material this was entirely possible, since a 2611-microin./in. compressive strain, which was well above the 1200-microin./in. yield strain of cadmium, had already been reached at the surface when the first reading was taken. Furthermore, Andrade and Jolliffe [10] reported that cadmium exhibited large transient creep in shear at room temperature. Thus the K_A value corresponding to the first reading was probably the most valid. This was 1.03, which was still far below the 1.19 theoretical value calculated by use of Equation (17). Due to lack of information on the stress-strain relation of cadmium in the plastic range and also on account of the fact that the time at which the various readings had been taken was not observed, it was not possible to calculate the effect of plastic flow of the cadmium plating. Nevertheless, on account of the very good agreement between the respective experimental and theoretical ψ_p and K_A/K_B values, it is believed that the flow of the cadmium plating was the principal source of experimental error.

Fig. 7 shows the difference between the theoretical values by Equation (17) and experimental K_A values, expressed as a per cent of the theoretical value, for tests conducted by Wahl, Ferris [13], Thurston [14], and the present investigator. It

Table 1 Sources of variation between experimental and theoretical values

Source	ψ_p	Per cent effect on K_A/K_B	K_A
Errors in Measurement of Shear Strain:			
1 Finite gage length (0.25 in.)	0	−1.0	−0.6
2 Transverse sensitivity (−0.01 in tension)	0	0	+0.6
3 Effect of gage stiffness	(Negligible due to high G of steel)		
4 Angular misalignment (0 to ±2° in each gage)	0	0 to ±0.1	0 to −0.1
5 Positional misalignment (0 to ±0.03 in.)	0	0 to ±0.9	0 to −0.1
6 Miscellaneous gage error[a]	0	0 to ±4.0	0 to ±2.8
Errors in Determination of Spring Dimensions:			
7 Error in d_o (0 to ±0.001 in.)	0 to ±0.7	0	0 to ±0.5
8 Error in d_i (0 to ±0.001 in.)	0 to ±1.4	0	0 to ±1.4
9 Error in D (0 to ±0.002 in.)	0 to ±1.5	0	0 to ±0.05
10 Cross-sectional eccentricity (0 to −0.003 in.)[b]	0	0 to −1.5	0 to −0.7
11 Error in pitch (0 to ±0.03 in.)[c]	0 to ±0.5	0	0
12 Error in N	0 to ±1.0	0	0
Adverse Spring-Material and Plating-Material Effects:			
13 Error in G[d]	0 to ±5.0	0	0 to ±5.0
14 Error in ν (0 to −40 per cent) (affects value of item 2)	0	0	0 to ±1.0
15 Direct effect of residual stress	(0 due to use of differential values)		
16 Alteration of surface properties due to peening	(Not possible to calculate)		
17 Local inclusions	(Negligible due to finite gage length)		
18 Stress relaxation due to creep in plating	0	Small	Large
Load and Deflection Measurement Errors:			
19 Error in P (±25 lb)	0 to ±3.0	0	0 to ±3.0
20 Error in F (±0.02 in.)	0 to ±0.6	0	0
Maximum total error (algebraic sum)	±10.7	−7.5	−12.6+
Probable error (rms value)	± 3.2	±2.4	± 3.4+

[a] Based on a ±2.0 per cent error specified by the gage manufacturer for each individual gage.
[b] Calculated by using equations derived by Wilson [11].
[c] Affects theoretical values only. All other errors affect experimental values only.
[d] According to results of various tests reported by Wahl [12]. It was impossible to obtain a straight-tube sample of the spring material.

SPRING NO.	TYPE	PRESET	SHOT PEENED	MATERIAL	SOURCE
1	Solid	Unknown	No	Steel	Wahl, 1929
2	Same	No	No	Same	Ferris, 1942
3, 4, 5	Same	Yes	No	Same	Same
6	Same	Yes	No	Carbon steel	Thurston, 1951
7P	Same	Yes	Yes	Same	Same
8	Same	Yes	No	Same	Same
9	Same	Yes	No	Cr-V steel	Same
10P	Same	Yes	Yes	Same	Same
11	Same	Yes	No	Si-Mn steel	Same
12P	Same	Yes	Yes	Same	Same
13P	Hollow	Yes	Yes	Cr-Ni-Mo steel	Present investigator

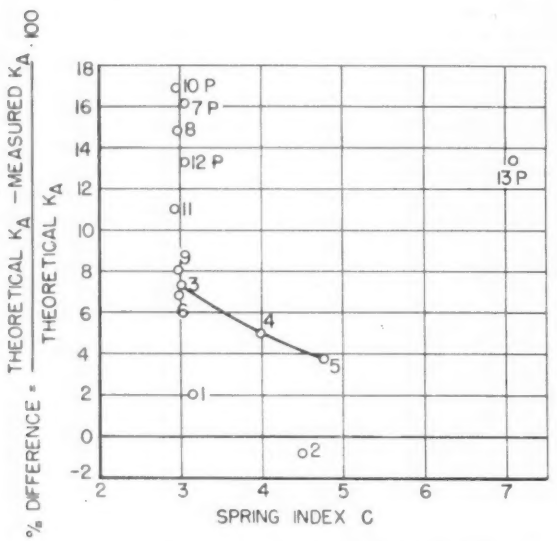

Fig. 7 Differences between theoretical and experimental maximum shear-stress factors of helical springs as found by various investigators

should be noted that in every case except one, the experimental K_A was lower than the theoretical one. The effects of presetting and shotpeening on increasing this difference are apparent. These values are plotted versus C to show the interesting effect of C on per cent difference in the results obtained by Ferris. This relationship may be misleading, however, since the section diameters of the springs tested by Ferris are not known and the well-known size effect, which depends on stress gradient and the material, may be the actual causal factor. Compared with the results obtained by Thurston on preset, shotpeened springs, the results of the present test appear to be reasonable. It is recommended that in future tests of hollow springs those having relatively thin walls and low index and which have not been preset, shotpeened, or plated, be used in order to minimize extraneous effects and to exaggerate effects of B and C.

An average compressive bending strain at A equal to 7.5 per cent of the average shear strain at the same point was observed. Assuming that there was no tensile or compressive strain at A normal to the tubing axis and using the Mohr strain circle, this bending strain was combined with the shear strain. The resulting combined shear strain, and thus the combined shear stress, was 1.0 per cent greater than the uncombined value. This compared favorably with a theoretical increase of 0.8 per cent produced by the $\frac{1}{2}\ p^2$ factor of Equation (19).

An effective load eccentricity as high as $0.127R$ was calculated from shear and bending strains from the three point-A gage sets by using equations developed by Thomas [15]. Thus in designing long compression springs, such as the one tested, the factor of safety should be increased at least 0.13 to provide for the increased stresses at one point around the perimeter of the coil.

Conclusions

1 For all practical values of spring index, the effect of the hole in a helical spring of hollow circular cross section is to increase the shear-stress and deflection factors only slightly as compared with the corresponding values for a solid-circular-section spring of the same index. Therefore the saving in weight of a hollow spring due to its larger polar moment of inertia per pound of spring weight, compared with a solid spring, can be utilized to great advantage in applications where weight saving is important.

2 The list of design equations included at the end of the paper may be used to calculate the deflection and maximum combined shear stress for hollow springs with considerable accuracy.

3 The design equations have been checked experimentally and found to be correct within the limits of accuracy of such experimental determinations.

List of Design Equations

The maximum combined shear stress produced by an axial load P, including effects of load eccentricity and helix angle, is

$$\tau = \frac{8}{\pi}\,\frac{K_{\max} P D d_o}{d_o^4 - d_i^4}\left(1 + \frac{\text{load eccentricity}}{R}\right)$$

where

$$K_{\max} = 1 + \frac{5}{4C} + \frac{7}{8C^2} + \frac{3B^2}{8C^2} + \frac{1}{2}\ p^2$$

This value may be obtained by adding the value of $\frac{1}{2}\ p^2$ to the value of K_A in the solid-line curves of Fig. 3.

The total axial spring deflection produced by the same load is

$$F = \frac{8\psi_p P D^3 N}{G(d_o^4 - d_i^4)}$$

where

$$\psi_p = 1 - \frac{3}{16C^2} + \frac{3B^2}{8C^2} + \frac{3+\nu}{2(1+\nu)}\ p^2$$

This may be obtained by adding the last term to ψ_u values given in Fig. 5.

Acknowledgments

The author is indebted to W. J. Eaton of Bendix Products Division, Bendix Aviation Corporation, South Bend, Ind., for providing the test spring. Appreciation is due J. N. Marsden of Fairchild Aircraft Division, Fairchild Engine and Airplane Corporation, Hagerstown, Md., for providing facilities. The author wishes to acknowledge the guidance of Prof. M. S. Gjesdahl of The Pennsylvania State University, under whose supervision this research was conducted, and the advice of various members of the staff of the Battelle Memorial Institute.

References

1 A. M. Wahl, "Stresses in Heavy Closely Coiled Helica Springs," TRANS. ASME, vol. 51, 1929, pp. 185–200.

2 S. Timoshenko, "Strength of Materials," part II, D. Van Nostrand and Company, New York, N. Y., second edition, 1941, pp. 65–74.

3 O. Göhner, "Schubspannungsverteilung in Querschnitt einer Schraubenfeder," *Ingenieur-Archiv*, vol. 1, 1930, pp. 619–644. Also S. Timoshenko and J. N. Goodier, "Theory of Elasticity," McGraw-Hill Book Company, New York, N. Y., second edition, 1951, pp. 391–395.

4 "Helical Springs," discussion by O. Smith, TRANS. ASME, vol. 5, 1884, p. 191.

5 "Practical Problems in Spring Design," discussion by W. R. Berry, *Proceedings of The Institution of Mechanical Engineers*, vol. 139, 1938, p. 480.

6 E. Reissner, "Note on the Problem of Twisting of a Circular Ring Sector," *Quarterly of Applied Mathematics*, vol. 7, 1949, pp. 342–347.

7 P. E. Bruch, "Fatigue Test of Tubular Centering Spring for B-47 Front Main Landing Gear," Bendix Products Division, Bendix Aviation Corporation, South Bend, Ind., Report No. 1248, April 22, 1954.

8 I. S. Sokolnikoff, "Theory of Elasticity," McGraw-Hill Book Company, New York, N. Y., second edition, 1956, pp. 228, 229.

9 C. J. Ancker, Jr., "Combined Curvature and Pitch Correction for Stress and Deformation in Helical Springs," unpublished doctoral dissertation, Stanford University, 1955.

10 E. N. daC. Andrade and K. H. Jolliffe, "The Flow of Polycrystalline Metals Under Simple Shear," *Proceedings of the Royal Society of London*, series A, vol. 213, 1952, pp. 3–26.

11 T. S. Wilson, "The Eccentric Tube," *Aircraft Engineering*, vol. 14, 1942, pp. 76–79.

12 A. M. Wahl, "Mechanical Springs," Penton Publishing Company, Cleveland, Ohio, 1944, pp. 83–85, 157–159.

13 E. A. Ferris, "An Experimental Study of Stress Concentrations in Helical Coil Springs," unpublished master's thesis, Massachusetts Institute of Technology, 1942.

14 R. C. A. Thurston, "Strength Characteristics of Helical Springs," *Canadian Mining and Metallurgical Bulletin*, vol. 44, 1951, pp. 658–668; supplemental information by private letter from R. C. A. Thurston, June 11, 1956.

15 W. N. Thomas, "Helical Springs," *Proceedings of The Institution of Mechanical Engineers*, 1920, pp. 869–889.

DISCUSSION

W. B. Diboll, Jr.[3]

The author has done an excellent job of extending Mr. Wahl's strength-of-materials analysis of a solid spring and of Mr. Gochner's theory-of-elasticity analysis for a solid spring to that of a spring of hollow cross section. To be commended especially is the carrying of his analysis to a fourth approximation in the theory-of-elasticity approach.

In both plots of the maximum-shear-stress factor K_A, Fig. 3 and Fig. 6, there is a large difference between the strength-of-materials theory and the elasticity theory, and it would be most helpful if the experimental results could have verified either one or the other.

It is unfortunate that the manufacture of the experimental spring did not match the assumptions made in the theoretical analysis. Perhaps in the future, springs without cadmium plating and without shotpeening could be tested, which would bring us in line with the analysis made. It would indeed be worth while to cover a larger range of spring sizes which would allow a little more information concerning the deflection factor ψ_u as shown in Fig. 5. For the particular spring under test which had a bore ratio of 0.496, and a spring index of 7.105, the curve of ψ_u versus bore ratio B is so flat that an appreciable change of bore ratio B would not affect the factor ψ_u appreciably. In conjunction with this, it is extremely interesting to note that the bore ratio B has very little effect on the maximum-shear-stress factor K_A, as shown in Fig. 3.

It would be interesting to see some charts or figures on the actual weight savings that result from using hollow springs. This would involve particular examples as far as size of spring is concerned and the stress loading is concerned, and it would be most interesting to see this plotted in order to get an idea of exactly how much weight might be saved by using hollow springs. Since the stress measured was so much below the theoretical stresses expected, it would hardly be worth while for the particular spring involved to calculate the weight saving although it could be done on a completely theoretical basis.

[3] Lecturer, Mechanical Engineering Department, Washington University, St. Louis, Mo.

In general, the saving of weight in a spring, by any means, is certainly worth while. The author has done an excellent job of presenting the theoretical approach to this, and it is hoped we will see many more applications in this particular line. Another method of increasing the load capacity of springs is by stressing them beyond the yield point before installation. Some very conclusive analytical and experimental work has been done along this line by Mr. Thomas Atterbury, formerly of Washington University, now at Battelle Institute. Either of these methods is certainly worth while considering for any installation where weight is a serious factor.

Author's Closure

The author wishes to thank Professor Diboll for his worthwhile comments and will attempt to reply to them in the space available.

The difficulty due to the cadmium plating on the spring unfortunately did not permit checking of the absolute values of the shear-stress factors K_A and K_B. However, since the same phenomenon occurred both at point A and at point B, it is believed that the value obtained experimentally for the ratio K_A/K_B is valid.

The average experimental value of K_A/K_B was 1.392, from the raw data. In Table 1 the only constant or bias errors on the K_A/K_B value were those due to finite gage length (−1 per cent) and cross-sectional eccentricity (an estimated average value of −0.7 per cent). However, since writing the paper the author has discovered one other source of bias error: Cross-sectional out-of-roundness, which accounts for +1.7 per cent, estimated from the analysis of a solid spring of elliptical cross section by Biezeno and Grammel [16]. Since the sum of the bias errors is zero, no correction need be made to the raw value of 1.392.

As calculated by the strength-of-materials equations, the K_A/K_B value for the particular spring geometry tested is 1.600, which is 14.9 per cent higher than the experimental value. According to the elasticity-theory solution, including the effect of pitch, the ratio is 1.415, which is only 1.7 per cent higher than the measured value. Thus it is apparent that the experimental results quite definitely verified the elasticity-theory solution.

The author heartily agrees with the writer that it would be very worth while to test a larger range of spring sizes, using springs which are not electroplated and not shotpeened. However, the spring tested by the author was the only one which was then available. It had been manufactured on an experimental basis for simulated service tests under rather severe fluctuating-load conditions. Therefore it had been subjected to the usual treatments which are beneficial to fatigue life. Unfortunately, these treatments were very detrimental to experimental stress measurements.

Information on the actual weight saving which can result from the use of hollow springs was omitted for brevity. However, it may be mentioned that the spring used in the experimental work and described in the paper was designed to replace a nest of two conventional helical compression springs of solid round wire. The space occupied by the two different installations was identical. The outer spring in the nest had a mean coil diameter and wire diameter of 4.15 inches and 0.500 inch, respectively; the inner, 3.10 inches and 0.375 inch. The performance data for the two installations are:

Installation	Total weight, pounds	Max total operating load, pounds	Max operating stress, psi
Two solid springs	11.75	1576	109,000
One hollow spring	7.50	1700	120,000

Thus, in this particular instance, use of a hollow spring in place of two solid springs resulted in a weight saving of 36 per cent.

(However, the designs were not exactly comparable since the maximum operating load in the hollow spring was 7.9 per cent greater and its stress level 10.1 per cent higher than in the solid spring.) If the space requirements had been such that a larger-size, yet thinner-walled, hollow spring could have been used, the weight saving would have been considerably more. In fact, it appears to be inherent that hollow springs save weight, but not space, in comparison to solid springs.

Another way of comparing spring designs is on the basis of energy-storage capacity per unit weight U. It can be shown that the ratio of U for a single hollow spring to that for a single solid spring of the same material and stressed to the same maximum stress is given by:

$$U_{\text{hollow}}/U_{\text{solid}} = (1 + B^2)(K_{A_{\text{solid}}}/K_{A_{\text{hollow}}}) \qquad (21)$$

Using Equation (21) and the appropriate values of the stress multiplication factors, the potential increase in energy-storage capacity of a thin-walled spring, as compared to a solid spring, approaches 95 per cent for a spring having an index as low as 3.

The author is familiar with Mr. Atterbury's research on the effect of presetting and is looking forward to its publication in the literature.

Reference

16 C. B. Biezeno and R. Grammel, "Engineering Dynamics," vol. II, Blackie and Son Ltd., London, England, 1956, pp. 121–122.

R. T. HINKLE

Professor of Mechanical Engineering, Michigan State University, East Lansing, Mich. Mem. ASME

I. E. MORSE, JR.

Assistant Professor of Mechanical Engineering, Michigan State University, East Lansing, Mich.

Design of Helical Springs for Minimum Weight, Volume, and Length

In the design of helical springs where the load, deflection, allowable stress, and material are specified, there are an infinite number of solutions. In this paper, equations and graphs are presented for the selection of a spring index that will result in a spring of minimum weight, volume, or length. If, an addition to these requirements, the inside or outside diameter of the spring is fixed, there is only one solution. Equations and graphs are included for the selection of the spring index which will satisfy this additional requirement.

Introduction

A COMMON PROCEDURE in spring design is to assume an allowable stress that is based on the material, severity of loading, and estimated wire size; assume a reasonable spring index, then determine the size of the spring. If the wire size does not fall in the assumed range, a new allowable stress is assumed and the spring recalculated. If it is necessary that the spring have minimum volume, minimum weight, minimum length, a specified inside diameter, or specified outside diameter, various values of spring index are assumed until the desired result is obtained. The purpose of this paper is to eliminate the trial and error procedure of this last step. Equations are derived for the determination of the correct spring index for the five conditions listed. Since these equations are long, curves have been plotted to facilitate the selection of the spring index.

The torsional strain energy in a cubic inch of material, in the form of a solid circular rod, is

$$U = \frac{\tau^2}{4G} \tag{1}$$

When the required strain energy and allowable shear stress for a helical spring are known, Equation (1) can be used to determine the absolute minimum volume of material, and hence the weight that is required. This minimum weight can never be obtained in a coil spring because of the wire curvature and direct shear, which are accounted for in design by the Wahl factor and the number of inactive end coils. A spring with a large index C will not be appreciably affected by the Wahl factor but the per cent of weight in the end coils may be large. In the following development, the effects of end coils and Wahl factor are related and then minimized.

Contributed by the Machine Design Division and presented at the Semi-Annual Meeting, Detroit, Mich., June 15–19, 1958, of THE AMERICAN SOCIETY OF MECHANICAL ENGINEERS.

NOTE: Statements and opinions advanced in papers are to be understood as individual expressions of their authors and not those of the Society. Manuscript received at ASME Headquarters, September 3, 1957. Paper No. 58—SA-9.

Minimum Weight

The weight of a spring is

$$W = \rho(n + Q)\pi D \frac{\pi d^2}{4} \tag{2}$$

This can be written in the form

$$\frac{4W}{\rho\pi^2} = nCd^3 + QCd^3 \tag{3}$$

The design equations for stress and deflection are

$$\tau = \frac{8KPC}{\pi d^2} \quad \text{or} \quad d = \left(\frac{8KPC}{\pi\tau}\right)^{1/2} \tag{4}$$

$$\delta = \frac{8PC^3n}{Gd} \quad \text{or} \quad n = \frac{\delta Gd}{8PC^3} \tag{5}$$

Substituting Equations (4) and (5) into Equation (3) and clearing the right-hand side of all terms (symbols) except the variables K and C gives

$$\frac{4}{\sqrt{\pi}\sqrt{\rho Q}}\left(\frac{\tau}{8P}\right)^{3/2} W = BK^2 + K^{3/2}C^{5/2} \tag{6}$$

Equation (6) is differentiated with respect to C, giving

$$\frac{4}{\sqrt{\pi}\sqrt{\rho Q}}\left(\frac{\tau}{8P}\right)^{3/2}\frac{dW}{dC} = 2BK\frac{dK}{dC} + \frac{3}{2}C^{3/2}K^{1/2}\frac{dK}{dC} + \frac{5}{2}C^{3/2}K^{3/2} \tag{7}$$

$\frac{dW}{dC}$ is set equal to zero and the equation is solved for B

$$B = -\frac{1}{4}C^{3/2}K^{1/2}\left[\frac{3C\frac{dK}{dC} + 5K}{K\frac{dK}{dC}}\right] \tag{8}$$

Nomenclature

C = spring index, D/d
d = wire diameter, in.
D = mean coil diameter, in.
D_i = inside coil diameter, in.
D_o = outside coil diameter, in.
δ = deflection corresponding to load P, in.
Δ = δ + clearance, in. (clearance equals the difference between the deflection to solid length and the maximum working deflection)
G = torsional modulus of elasticity, psi
K = Wahl factor
L = length of spring, in.
n = number of active coils
P = maximum spring load, lb
Q = number of inactive coils (end coils)
ρ = density of spring wire material (for steel, 0.284 lb per cu in.)
τ = maximum allowable shear stress, psi
U = strain energy, in lb per cu in.
V = volume occupied by spring, cu in.
W = weight of spring, lb
B = $\frac{\delta G}{Q(8P\pi\tau)^{1/2}}$ a design constant

The Wahl factor [1][1] is

$$K = \frac{4C - 1}{4C - 4} + \frac{0.615}{C} \quad \text{or} \quad K = \frac{C^2 + 0.365\,C - 0.615}{C(C - 1)} \tag{9}$$

When differentiated this becomes

$$\frac{dK}{dC} = \frac{-1.365\,C^2 + 1.230\,C - 0.615}{(C^2 - C)^2} \tag{10}$$

Substituting Equations (9) and (10) into (8) gives

$$B = \frac{C^3(C^3 - 0.635\,C^2 - 0.980\,C + 0.615)^{1/2}\,(5\,C^3 - 7.27\,C^2 - 1.21\,C + 1.23)}{4(1.365\,C^4 - 0.732\,C^3 - 0.673\,C^2 + 0.981\,C - 0.378)} \tag{11}$$

Any spring that satisfies Equation (11) has minimum weight. The graph for this equation is plotted as "minimum weight" in Fig. 1.

Minimum Volume

The space required for the solid length of a spring is

$$V = (n + Q)d\,\frac{\pi}{4}\,d^2(C + 1)^2 \tag{12}$$

Substitution of Equations (4) and (5) into Equation (12) gives

$$\frac{4V}{\pi Q}\left(\frac{\pi\tau}{8P}\right)^{3/2} = (C + 1)^2\left[B\,\frac{K^2}{C} + (KC)^{1/2}\right] \tag{13}$$

Differentiating, setting $\frac{dV}{dC} = 0$, and solving for B give

$$B = -\frac{C}{2}\left(\frac{C}{K}\right)^{1/2}\left[\frac{3C\,\frac{dK}{dC} + K\left(\frac{7C + 3}{C + 1}\right)}{2\,\frac{dK}{dC} + \frac{K}{C}\left(\frac{C - 1}{C + 1}\right)}\right] \tag{14}$$

Substituting Equations (9) and (10) into Equation (14) gives

$$B = \frac{C^4}{2}\left(\frac{C - 1}{C^2 + 0.365\,C - 0.615}\right)^{1/2}\left[\frac{7\,C^3 - 5.54\,C^2 - 8.9\,C + 3.21}{-C^4 + 4.365\,C^3 + 0.615\,C^2 - 2.825\,C + 1.845}\right] \tag{15}$$

The positive branch of this curve which is asymptotic to the line $C = 4.39$ is plotted as "minimum volume" in Fig. 1. The negative branch for larger values of C has no physical meaning.

Minimum Length

The free length of a spring is

$$L = (n + Q)d + \Delta \tag{16}$$

Substituting Equations (4) and (5) into Equation (16) gives

$$\left(\frac{\pi\tau}{8P}\right)^{1/2}\frac{L}{Q} = B\,\frac{K}{C^2} + (KC)^{1/2} + \left(\frac{\pi\tau}{8P}\right)^{1/2}\frac{\Delta}{Q} \tag{17}$$

Differentiating, setting $\frac{dL}{dC} = 0$, solving for B give

$$B = -\frac{C^3\left(K + C\,\frac{dK}{dC}\right)}{2(KC)^{1/2}\left(C\,\frac{dK}{dC} - 2K\right)} \tag{18}$$

[1] Numbers in brackets designate References at end of paper.

Substitution of Equations (9) and (10) into Equation (18) gives

$$B = \frac{C^4}{2}\left(\frac{C - 1}{C^2 + 0.365\,C - 0.615}\right)^{1/2}\left(\frac{C^2 - 2C + 0.250}{2C^3 + 0.095\,C^2 - 3.19\,C + 1.845}\right) \tag{19}$$

The graph of this equation is plotted as "minimum length" in Fig. 1. The term containing Δ is a constant and becomes zero when differentiated, hence a spring with a minimum solid length will have a minimum length in working position.

Example 1

Given the following conditions:

$P = 75$ lb
$\delta = 0.5$ in.
$G = 12 \times 10^6$ psi
$\tau = 40{,}000$ psi
$Q = 2$

Design springs of minimum weight, volume, and length. The design constant is

$$B = \frac{G\delta}{Q(8P\pi\tau)^{1/2}} = \frac{(0.5)(12 \times 10^6)}{2[(8)(75)(\pi)(40{,}000)]^{1/2}} = 344$$

From Fig. 1, the values of C for minimum weight, volume, and length are 5.82, 3.8, and 19, respectively. For minimum weight, using Equations (4) and (5)

$$d = \left(\frac{8KPC}{\pi\tau}\right)^{1/2} = \left[\frac{(8)(1.26)(75)(5.82)}{(\pi)(40{,}000)}\right]^{1/2} = 0.187 \text{ in.}$$

$$n = \frac{\delta G d}{8PC^3} = \frac{(0.5)(12 \times 10^6)(0.187)}{(8)(75)(5.82)^3} = 9.5 \text{ coils}$$

The weight, volume, and solid length of this spring are determined from Equations (2), (12), and (16). These values are shown in Fig. 2 where the spring is drawn to scale.

The springs for minimum volume and length are determined in a similar manner. These springs are also shown in Fig. 2. In order to make a more exact comparison of the three springs, the values were not rounded out as would be done in practice.

For this example, the increase in weight, volume, and length for different values of C are shown in Fig. 3. The ordinate is the ratio of the actual value to the optimum. The weight and volume curves intersect at $C = 4.75$. If this value is used in the design of the spring, the weight and volume will both be 5 per cent above the optimums.

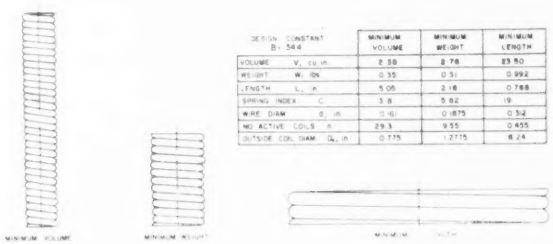
DESIGN CONSTANT B = 344
MINIMUM VOLUME
MINIMUM WEIGHT
MINIMUM LENGTH
VOLUME V, cu in. 2.38 2.76 83.80
WEIGHT W, lbs 0.35 0.31 0.992
LENGTH L, in 5.05 2.18 0.788
SPRING INDEX C 5.8 5.82 19
WIRE DIAM. d, in 0.161 0.1875 0.312
NO. ACTIVE COILS n 29.3 9.55 0.455
OUTSIDE COIL DIAM. D, in 0.775 1.2775 6.24

Fig. 2 Springs designed for minimum volume, weight, and length, using the data from Example 1

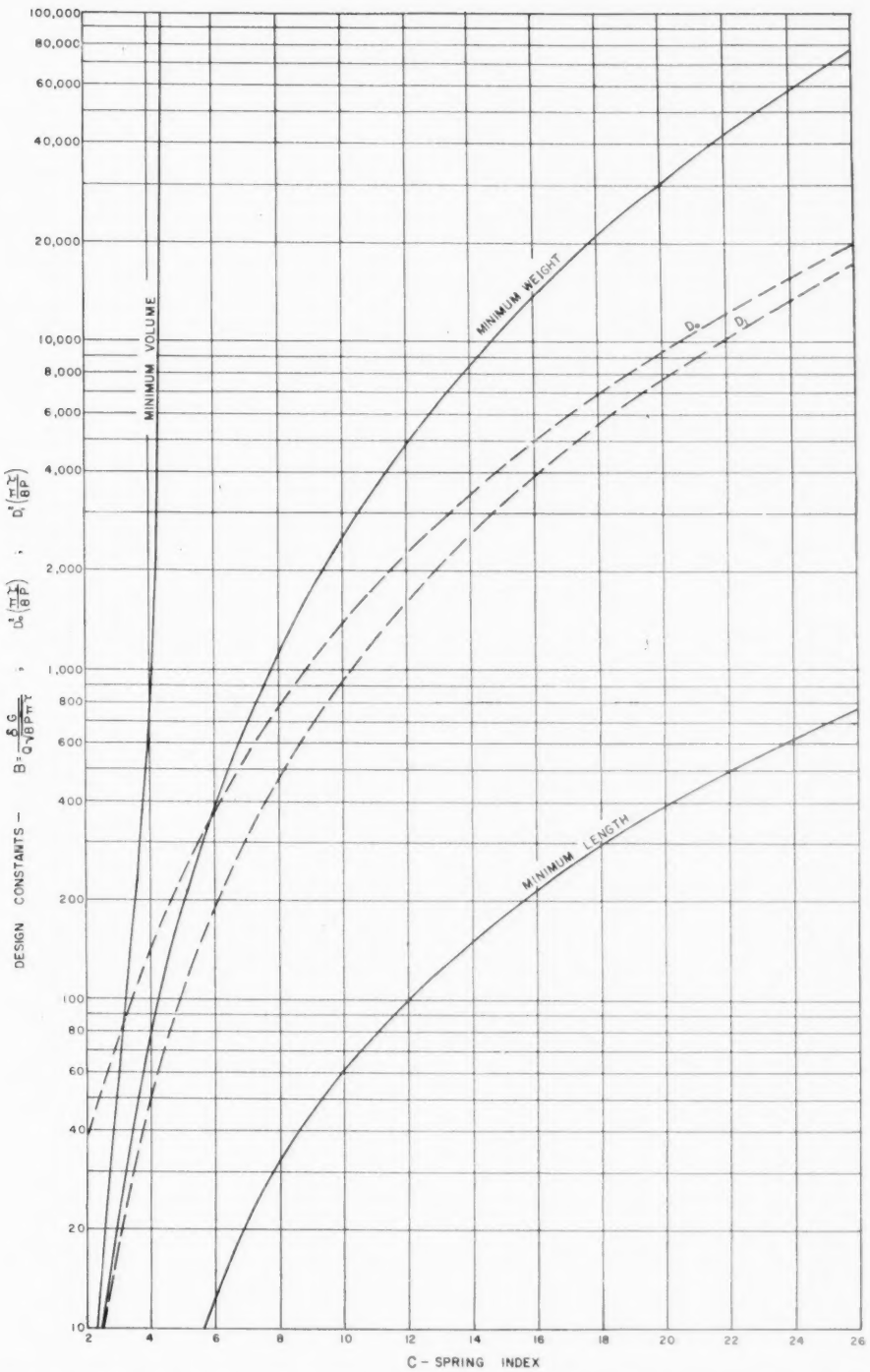

Fig. 1 Design curves for the selection of the spring index for a spring of minimum weight, volume, length, or for a spring with specified outside or inside diameter

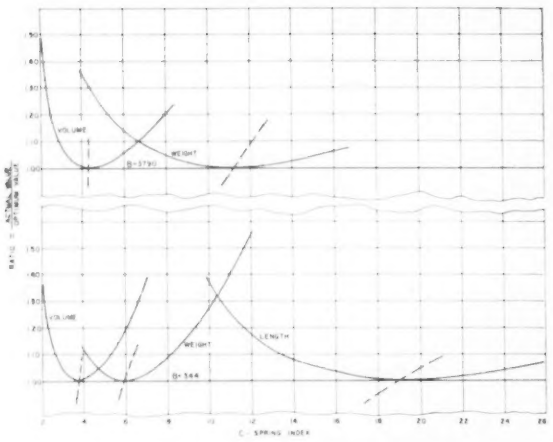

Fig. 3 The upper set of curves is for the data of Example 2 and the lower set is for Example 1. The points of tangency of the curves are for the optimums of the examples. The curves show, in general, and exactly for these examples, how the volume, weight, and length change when values different from the optimum spring index are used.

Example 2

Given the following:

$P = 50$ lb $\qquad \tau = 50{,}000$ psi
$\delta = 5$ in. $\qquad Q = 2$
$G = 12 \times 10^6$ psi

The design constant is

$$B = \frac{\delta G}{Q(8P\pi\tau)^{1/2}} = \frac{(5)(12 \times 10^6)}{2[(8)(50)(\pi)(50{,}000)]^{1/2}} = 3780$$

From Fig. 1, the values of C for minimum weight and volume are 11.2 and 4.3, respectively. For minimum weight, $d = 0.179$ in. and $n = 19.15$, giving a spring with $D_o = 2.18$ in. and $L = 3.78$ in. For minimum volume, $d = 0.122$ in. and $n = 231$, giving a spring with $D_o = 0.647$ in. and $L = 28.4$ in. The change in weight and volume for different values of C are shown in Fig. 3.

These examples show that a spring designed for minimum volume or length may not be practical. If the spring is not practical, a designer, with the aid of Figs. 1 and 3, would be able to make a compromise and select a spring index which gives a spring of practical proportions, and also nearly fulfills the requirement of minimum volume or length.

In other cases it is specified that the spring fit over a rod or in a hole which requires that the spring be made with a given inside or outside diameter. If, in addition to P, δ, G, and τ, a diameter is specified, there is only one solution. The spring cannot be minimized for volume, weight, or length.

Outside Diameter Specified

When D_o is fixed, the corresponding value of C can be determined as follows

$$D_o = D + d = d(C + 1) = \left(\frac{8PKC}{\pi\tau}\right)^{1/2}(C + 1) \qquad (20)$$

Substituting Equation (9) into Equation (20) and squaring both sides gives

$$D_o^2\left(\frac{\pi\tau}{8P}\right) = \frac{C^3 + 2.365\,C^2 + 1.115\,C - 0.867\,C - 0.615}{C - 1} \qquad (21)$$

The graph of this equation is plotted as D_o in Fig. 1.

Inside Diameter Specified

$$D_i = D - d = d(C - 1) = \left(\frac{8PKC}{\pi\tau}\right)^{1/2}(C - 1) \qquad (22)$$

Substituting Equation (9) into Equation (22) and squaring both sides gives

$$D_i^2\left(\frac{\pi\tau}{8P}\right) = C^3 - 0.635\,C^2 - 0.98\,C + 0.615 \qquad (23)$$

The graph for this equation is plotted as D_i in Fig. 1.

Example 3

The conditions given in Example 1 are to apply and, in addition, the outside diameter of the spring is to be 3 in.

$$D_o^2\left(\frac{\pi\tau}{8P}\right) = (3)^2\left(\frac{(\pi)(40{,}000)}{(8)(75)}\right) = 1885$$

From Fig. 1, the corresponding value of C is 11.2.

$$d = \left(\frac{8KPC}{\pi\tau}\right)^{1/2} = \left[\frac{(8)(1.127)(75)(11.2)}{(\pi)(40{,}000)}\right]^{1/2} = 0.246 \text{ in.}$$

This can be checked

$$D_o = d(C + 1) = (0.246)\ (11.2 + 1) = 3 \text{ in.}$$

In some applications an intermediate load is specified and the maximum load is arbitrary. Spotts [2] has shown that for this problem with an assumed value of C, a spring with minimum weight is obtained when the maximum load is made two times as large as the intermediate load. For this type of problem, the maximum load can be determined in this manner before selecting a value of C from Fig. 1.

Conclusion

The use of these curves to select a value for the spring index does not interfere with the usual procedure in spring design. All of the information that is needed for the selection is shown in Fig. 1. In these curves the full value of the Wahl factor was used.

Wahl [3] has considered the design of springs for minimum volume. He simplified the work by neglecting end coils which made it possible to investigate nests of springs. The results presented here agree closely with his work for a single spring. The reason for this can be seen from Fig. 2. A spring designed for minimum volume has a large number of active coils; hence the effect of end coils is not great. This is not true when a spring is designed for minimum weight or length.

References

1 A. M. Wahl, "Mechanical Springs," Penton Publishing Co., Cleveland, Ohio, 1944, p. 37.

2 M. F. Spotts, "Design of Helical and Leaf Springs for Minimum Weight," *Journal of Applied Mechanics*, vol. 20, TRANS. ASME, vol. 75, 1953, p. 435.

3 A. M. Wahl, "Combining Maximum Spring Deflection With Minimum Space," *Machine Design*, January, 1942.

DISCUSSION

E. S. Ault[2]

This paper is an excellent application of a procedure that always delights me—the combining and gathering together of interre-

[2] Professor of Machine Design, Purdue University, Lafayette, Ind.

lated variables into such a form that a relatively direct solution of a problem with many unknowns is possible.

The authors have accomplished this most successfully and have provided charts of design constants that facilitate their method. The paper is a welcome addition to the literature.

C. W. Bert[3]

The authors are to be commended for developing a very useful method for the optimum design of helical compression springs. Their method facilitates rapid design because they have succeeded in grouping all of the fixed requirements into a single design constant, B.

It is the practice of some spring-design engineers to apply the full Wahl stress-concentration factor to only the variable-stress component in springs subject to fluctuating loads. For static loading, they sometimes use a reduced stress factor which takes into account only the contribution of direct shear in increasing the stresses in a spring and which neglects the effect of coil curvature. Although this practice may not be justified theoretically, it is the common belief that its use has been verified experimentally. Those who prefer to use reduced stress factors can use the same general method as outlined in the paper to arrive at another set of curves analogous to those in Fig. 1. If this is done, it will be found that the curves will be moved to the left.

As the authors state, they derive their expressions for the design problem in which the maximum load and maximum deflection are specified. The comments in this paragraph are intended to supplement their work in reference to its application to the design problem in which an intermediate working load P_1 is specified and the maximum working load P_2 is arbitrary. In applying their results to this problem, the authors referred to the work of Spotts (reference [2] in the paper), where it was shown that a spring having minimum weight is obtained when P_2/P_1 is equal to 2. However, Spotts neglected the effect of the inactive end coils. Account of the end-coil effect on the load ratio P_2/P_1 for minimum weight was made by Jennings.[4] Using the notation of this paper, his expression was

$$P_2/P_1 = 2(3Q)/(2n + 3Q) \tag{24}$$

The load ratio approaches a value of 2 only when the number of active coils is excessively large. According to Jennings, Equation (24) also gives a spring which occupies a minimum volume of space, assuming that the minimum clearance between coils is proportional to the solid height of the spring.

It is interesting to note a basic difference between the optimum analysis by Jennings and that by the authors. Jennings[4] arrived at an optimum design for the problem he considered without taking into account the Wahl factor, while in the analysis by Hinkle and Morse the Wahl factor and its variation with spring index are necessary to achieve an optimum.

Another factor of importance in helical spring design is the well-known decrease in allowable stress with increase in wire diameter for most materials. Faires[5] has observed that the allowable torsional stress is inversely proportional to the wire diameter raised to an exponential power. For the usual spring materials, this exponent varies from 0.125 to 0.22. When the exponent is 0.22, the size effect is of equal importance to that of the Wahl factor. It has been shown by the writer[6] that the Wahl factor is inversely proportional to the spring index raised to the 0.22 power, within an accuracy of about 3 per cent over the range of spring indexes from 4 to 10.

Of course, a trial-and-error method in which a trial wire size and corresponding allowable stress are selected can always be used. However, to save design time, it would be desirable to develop design charts in which the effect of wire diameter on allowable stress is incorporated.

In many design situations, the final design chosen must necessarily be a compromise among a number of choices, each of which is an "optimum" for one particular characteristic only. Some characteristics in addition to these considered in the paper include:

1 Minimum spring cost. Obviously this is particularly important in high-production applications.

2 Resistance to buckling. This is of importance only for unguided helical compression springs.

3 Natural frequency. This is often of importance in dynamic applications.

4 Ejection velocity or energy-release rate.

5 Maximum spring life under fluctuating load or fluctuating elevated temperatures.

It would be quite worth while to develop a universal spring-design chart or series of charts in terms of nondimensional parameters which would show the effect of considering each of the foregoing criteria.

P. H. Black[7]

In the field of mechanical design there is a large number of comparatively simple elements, such as springs, the design of which has been too much of a trial-and-error procedure. In contrast, considerable work has been done and progress made in the analysis and design procedure in more complicated areas such as lubrication and bearing design, and in metal cutting. The authors deserve special commendation for this contribution to the rationalization of the design of the helical spring, a neglected element.

One point that occurs to the writer is that the authors might well include a discussion of the effect of pitch of the coils on the length of the spring; for instance, that a specified clearance between coils at the maximum-load condition, $(\Delta - \hat{\delta})/n$, would have a marked increase in the length of a spring of minimum volume, medium increase for minimum weight, and least for minimum length. It might be well also to use subscripts for spring length L to avoid confusion, for instance, between L in Equation (16) which stands for the free length, and L in Fig. 2 which is the compressed-solid length.

G. H. Howell[8]

The authors have indicated that a spring designed for minimum volume or length may not be practical. This is not to say that there is no practical value to the determination of these extremes because these do provide a pair of limiting conditions which as a general rule we would not even want to approach.

The minimum-volume extreme will tend toward a spring which will buckle while the minimum length will give an inordinately high spring index. Note also, in Example 1, the large number of active coils in the first as compared to the low number in the second. This, of course, leads to the interesting conclusion that in the minimum-volume spring each coil deflects only 0.017 in

[3] Principal Mechanical Engineer, Applied Mechanics Division, Battelle Memorial Institute, Columbus, Ohio. Assoc. Mem. ASME.

[4] J. Jennings, "Springs of Minimum Weight," *Machinery*, vol. 52, 1938, pp. 707–709.

[5] V. M. Faires, "Design of Machine Elements," The Macmillan Company, New York, N. Y., third edition, 1955, pp. 173–174.

[6] C. W. Bert, "Analysis and Optimum Design of Helical Compression Springs," unpublished MS thesis, The Pennsylvania State University, 1956, pp. 68–69.

[7] Chairman, Department of Mechanical Engineering, Ohio University, Athens, Ohio. Mem. ASME.

[8] Professor, Mechanical and Industrial Engineering Department, Wayne State University, Detroit, Mich. Mem. ASME.

while in the minimum-length spring the deflection per coil is 1.1 in.

The minimum-weight spring presents some even more interesting aspects. The authors have indicated that the torsional strain energy in a cubic inch of material in the form of a circular rod is

$$U = \frac{T^2}{4G}$$

Based on the conditions of Example 1 where the stress is 40,000 psi, this becomes

$$\frac{4^2 \times 10^3}{4 \times 12 \times 10^6} = 33 \text{ in-lb/in.}^3$$

which defines the absolute minimum volume of material for a given load-deflection combination. In the example given the energy input is

$$\frac{75 \times 0.5}{2} = 18.75 \text{ in-lb}$$

Thus, the theoretical minimum volume of material is

$$\frac{18.75}{33} = 0.57 \text{ cu in.}$$

Note how this figure compares with the actual volume contained in the three springs calculated:

$$\text{Minimum volume, } \frac{0.35}{0.284} = 1.23 \text{ cu in. (218 per cent)}$$

$$\text{Minimum weight, } \frac{0.31}{0.284} = 1.09 \text{ cu in. (193 per cent)}$$

$$\text{Minimum length, } \frac{0.99}{0.284} = 3.50 \text{ cu in. (620 per cent)}$$

These figures indicate the truth of the authors' statement that the minimum theoretical weight can never be obtained. However, it would appear that the reasons are not fully enough explained.

Going back to the original equation for torsional strain energy (or resilience) and for purposes which will be evident later using total strain energy of the active coils, the equation becomes

$$U = \frac{T^2 V_a}{4G}$$

This equation is predicated on all of the energy being "returnable" as the wire is "unwound" when the torque producing force is removed and becomes an absolute maximum when T is equal to the yield point stress.

When we relate this equation to a circular rod wound in the form of a helical spring, two extraneous factors enter the determination of the maximum fiber stress, the first is stress due to the wire curvature and the second is the direct shear. Both are included in the maximum shear stress existent when Wahl's factor is applied but neither develops "returnable" types of energy. The returnable energy is determined by the stress S_s/k and the equation takes the form

$$U = \frac{S_s^2 V_a}{4Gk^2}$$

This equation also can be developed from the basic stress, load, and deflection formulas for springs including the Wahl factor.

Now if we substitute for V_a, the total spring volume, V_t divided by x, the ratio of total volume to active volume, the equation becomes

$$U = \frac{S_s^2 V_t}{4Gk^2 x}$$

From this equation and for given conditions of Example 1, it then becomes possible to compute the expected actual volume as a percentage of the theoretical volume. The tabulation indicates the values of k, k^2, and x for the example given:

	Minimum volume	Minimum weight	Minimum length
k	1.429	1.262	1.075
k^2	2.042	1.593	1.156
x	1.07	1.21	5.4

From these figures, by using $V_t = k^2 x V$, and comparing to the actual volumes determined from the results of the example given, we can determine the relative accuracy of the theories evolved:

Minimum volume, $2.042 \times 1.07 = 218$ per cent
Minimum weight, $1.593 \times 1.21 = 193$ per cent
Minimum length, $1.56 \times 5.4 = 620$ per cent

The accuracy noted leads us to say again that while the springs are not practical, *per se*, the theories can have a very practical application. Added to this, the development of the single-solution curves for a given ID or OD can be of invaluable assistance to the designer.

Authors' Closure

Professors Ault and Black, both being Machine Design teachers, are fully aware of the shock that many students receive when they move from Strength of Materials to Machine Design where the problems are not presented so that there is a single, simple solution, but are met head on. They therefore welcome any contribution that eases their burden.

The use of a reduced Wahl factor for statically loaded springs may result from the time-honored custom of neglecting stress concentration in a statically loaded member, but including all stresses that can be determined from equations giving nominal stress. In many applications this is correct. When the distribution of the stresses in a spring is examined it will be seen that those due to curvature and direct shear have the same effect on the stress due to torsion, i.e., their detrimental effect is significant in the same small region on the inside of the coil. Hence, we believe that, if there is justification for neglecting one, there is also justification for neglecting the other. However, or Mr. Bert suggests, curves can be made for all types of stress factors.

Jenning's paper was not available to us. We appreciate Mr. Bert's inclusion of equation (24).

In this paper we assumed zero clearance at the maximum load condition. In practice a small clearance would be required. If a large clearance is necessary, the derivation of new equations would be required as suggested by Professor Black.

Professor Howell has discussed some of the aspects more fully. His equations and examples should help the reader to obtain a deeper insight into the physical concepts of the problem.

We wish to thank the discussers for their interest and their contributions. Because of time, we confined ourselves to the problems presented here. We hope that this paper, and the discussions, will encourage others to continue the work in optimum design. Mr. Bert has listed five problems that could be investigated.

Stress and Strain in Spinning Paraboloid Dishes

M. J. COHEN

Leaturer, Northampton College of Advanced Technology, London, England

The following is an investigation to determine completely the state of stress and strain in spinning paraboloid dishes both whole and holed at the center. The material of the dish is homogeneous and its thickness is constant. The results comprise expressions for the radial, hoop, and shear stresses, the bending moments, and deformation induced by the spinning of the dish in terms of the angular distance from the center of the dish. Tables at the end of the paper make the actual evaluation of these stresses, moments, and deformations a matter of simple arithmetic.

Introduction

THE INVESTIGATION DESCRIBED in the paper affords a ready means of determining the stresses and strains induced in paraboloid dishes spinning with angular velocity Ω. The problem is of some interest for example in such systems where the spinning paraboloid mirror is also used as the inertial rotor unit in a gyroscopic arrangement. In such a case it is important ideally that the mirror be truly paraboloid in its deformed state and hence slightly off the parabolic shape when at rest. The amount of the deviation from the parabolic generator, is, of course, a function of the stresses induced in the dish by its rotational motion. Both the stresses and resultant strains can be determined to very good approximations using relatively simple theory.

Statement of Problem

Referring to Fig. 2, and the element of the spinning dish shown, it is required to determine the radial stress p, the hoop stress f, and the shear stress s, distributions as functions of θ, subject to specified boundary conditions at rim and hub.

Two main assumptions are made:

(a) The paraboloid is considered shallow enough to justify an approximation to a spherical cap.

(b) No distinction is made between the dimensions of the element in the deformed and undeformed states, in the derivation of the equation of compatibility of strains.

Assumption (a) will lead to some small error in the quantitative use of the results; this error will be considered acceptable for mirror apertures of up to 60 deg.

Contributed by the Machine Design Division and presented at the Semi-Annual Meeting, Detroit, Mich., June 15-19, 1958, of THE AMERICAN SOCIETY OF MECHANICAL ENGINEERS.

NOTE: Statements and opinions advanced in papers are to be understood as individual expressions of their authors and not those of the Society. Manuscript received at ASME Headquarters, January 28, 1957. Paper No. 58—SA-8.

Assumption (b) will lead to some of the boundary conditions remaining ideally unfulfilled; it will, however, be found that practically the errors involved at the rim are small; e.g., about one per cent of the maximum radial stress occurring in the dish for the radial stress at the rim which of course should be zero.

Making use of the geometry of Fig. 1, and with the foregoing provisos accepted, the statement of the problem in mathematical form follows.

Equations of Stress Equilibrium. From a resolution of forces along the radius OB

$$\frac{d(s\theta)}{d\theta} - p\theta = (f - \rho\Omega^2R^2\theta^2)\theta \qquad (\theta, \text{small}) \qquad \text{(i)}$$

From a resolution of forces along the tangent to the dish normal to OB

$$\frac{d(p\theta)}{d\theta} + s\theta = f - \rho\Omega^2R^2\theta^2 \qquad (\theta, \text{small}) \qquad \text{(ii)}$$

Stress-Strain Relations

$$\epsilon_\theta = \frac{p}{E} - \frac{\sigma f}{E} \qquad \text{(iii)}$$

$$\epsilon_\phi = \frac{f}{E} - \frac{\sigma p}{E} \qquad \text{(iv)}$$

Equation of Compatibility of Strains

$$\epsilon_\theta = \frac{d(\epsilon_\phi\theta)}{d\theta} \qquad \text{(v)}$$

Shear-Bending Moment Relation

$$\frac{d(M_\theta\theta)}{d\theta} - M_\phi = -s\theta \cdot Rh \qquad \text{(vi)}$$

Bending Moment-Normal Deflection Relations

$$M_\theta = \frac{Eh^3}{12(1-\sigma^2)}\left\{\frac{d^2\Delta}{R^2d\theta^2} + \frac{\sigma}{R\theta}\left(\frac{d\Delta}{Rd\theta} + \int_0^\theta \epsilon_\theta d\theta\right)\right\} \qquad \text{(vii)}$$

Nomenclature

ϵ_θ = radial strain
ϵ_ϕ = tangential strain
E = Young's modulus
f = hoop stress
ϕ = tangential circular measure in polar co-ordinates
M_θ = bending moment across faces of an element normal to a radius
M_ϕ = bending moment across faces of an element normal to a tangent
h = uniform thickness of dish
O = center of spherical cap, at twice the focal distance of the paraboloid dish from apex P of the dish
p = radial stress or pressure
P = apex of dish
r = radial distance of point on dish from apex P
r_1 = inner radius of holed dish
r_2 = outer radius of holed dish
R = radius of spherical cap on the undeformed state
s = shear stress tangential to the sides of the element
σ = Poisson's ratio
α = angular semiaperture of dish
α_1 = angular semiaperture at outer rim of holed dish
α_2 = angular semiaperture at inner rim of holed dish
Δ = deflection of dish normal to its undeformed surface

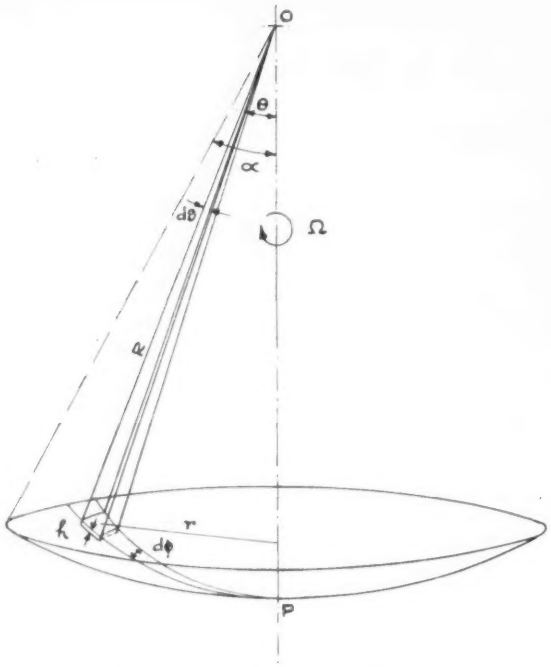

Fig. 1 Type-element of a spinning dish (geometry)

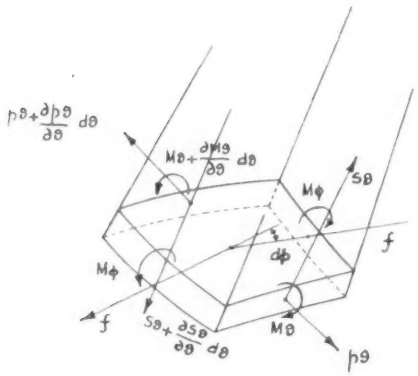

Fig. 2 Type-element of a spinning dish (forces and moments)

$$M_\phi = \frac{Eh^3}{12(1-\sigma^2)}\left\{\frac{1}{R\theta}\left(\frac{d\Delta}{Rd\theta} + \int_0^\theta \epsilon_\theta d\theta\right) + \frac{\sigma}{R^2}\frac{d^2\Delta}{d\theta^2}\right\} \quad \text{(viii)}$$

Boundary Conditions. Two sets of boundary conditions, corresponding to two distinct problems, will be used:

(a) Solid paraboloid dish

$$\left.\begin{aligned} s = M_\theta = p = 0 \quad & \text{at } \theta = \alpha \\ s = 0 \quad & \text{at } \theta = 0 \end{aligned}\right\} \quad \text{(ix)}$$

(b) Paraboloid dish holed at the center:

$$\left.\begin{aligned} s = M_\theta = p = 0 \quad & \text{at } \theta = \alpha_2 \\ s = p = M_\theta = 0 \quad & \text{at } \theta = \alpha_1 \end{aligned}\right\} \quad \text{(x)}$$

Equations (i) to (viii) are eight differential equations in the eight unknowns: s, p, f, M_θ, M_ϕ, ϵ_θ, ϵ_ϕ, Δ, to be solved subject to the boundary conditions (ix) or (x).

Solution to Problem A

An exact solution to the foregoing system of eight equations, subject to the stipulated boundary conditions, is certainly impossible with the equation of compatibility of strains as given by (v). This equation represents an approximate relation between ϵ_θ and ϵ_ϕ obtained by relating radial and circumferential elongations evaluated from the strains ϵ_θ and ϵ_ϕ, respectively, by multiplying these strains by the deformed element lengths and integrating, whereas strictly speaking it is the undeformed element lengths which should be involved. Also θ is considered small enough ($\theta \leq 30°$) to justify $\sin\theta \approx \theta$ and $\cos\theta \approx 1$.

Problem A. Solid paraboloid dish. Boundary conditions (ix). A solution for s, the shear stress, of the form

$$s = \sum_1^\infty a_r\theta^r \quad (1)$$

is assumed; $a_0 = 0$, to satisfy the second of (ix). Then

$$s\theta = \sum_1^\infty a_r\theta^{r+1} \quad (2)$$

and, to satisfy the first of (ix)

$$\sum_1^\infty a_r\alpha^r = 0 \quad (I)$$

The series (2) can now be used in (i) and (ii) to determine p and f in terms of θ. Thus

$$\frac{d(s\theta)}{d\theta} = \sum_1^\infty (r+1)a_r\theta^r$$

Substituting this in (i) yields

$$\sum_1^\infty (r+1)a_r\theta^{r-1} = p + f - \rho\Omega^2R^2\theta^2 \quad (3)$$

Also substituting for $s\theta$ from (2) in (ii) gives

$$\frac{d(p\theta)}{d\theta} + \frac{p\theta}{\theta} = 2a_1 + 3a_2\theta + \sum_1^\infty [(r+3)a_{r+1} - a_r]\theta^{r+1} \quad (4)$$

a first-order differential equation in $p\theta$ which integrated gives

$$p\theta = \frac{1}{\theta}\left[\int\left\{2a_1\theta + 3a_2\theta^2 + \sum_1^\infty [(r+3)a_{r+2} - a_r]\theta^{r+2}\right\}d\theta + b_1\right]$$

Since p or $p\theta$ cannot be infinite at $\theta = 0$, $b_1 = 0$, and, performing the integration

$$p = a_1 + a_2\theta + \sum_1^\infty \left[a_{r+2} - \frac{a_r}{r+3}\right]\theta^{r+1} \quad (5)$$

Substituting for p from (5) in (3) yields f; i.e.

$$f = \sum_1^\infty \left[(r+2)a_{r+2} + \frac{a_r}{r+3}\right]\theta^{r+1} + a_1 + 2a_2\theta + \rho\Omega^2R^2\theta^2 \quad (6)$$

Also since $p = 0$ when $\theta = \alpha$

$$a_1 + a_2\alpha + \sum_1^\infty \left[a_{r+2} - \frac{a_r}{(r+3)} \right] \alpha^{r+1} = 0 \qquad \text{(II)}$$

As hinted in the foregoing, following the assumptions made, (I) and (II) are incompatible since the pair will reduce to two equations in one unknown only, namely a_1, once the a_r's are made functions of a_1 using a recurrence relation between a_r and a_{r+2} to be derived. Thus either (I) or (II) can be chosen as the binding boundary condition and (I) will be chosen as it leads to simpler arithmetic, resulting, however, in an error at the boundary for p of the order of 1 per cent of the maximum p in the dish and this will be considered acceptable.

Derivation of the Recurrence Relation. It now becomes necessary to determine the a_1's in (5) and (6) to make the values of p, f, and s determinate; to that end (iii), (iv), and (v) yield in turn, after substitution of p and f, from (5) and (6)

$$\epsilon_\theta = \frac{1}{E}\left\{(1-\sigma)a_1 + (1-2\sigma)a_2\theta + \sum_1^\infty \left[(1 - \overline{r+2}\cdot\sigma)a_{r+2} - \frac{(1+\sigma)}{(r+3)} a_r \right] \theta^{r+1} - \sigma\rho\Omega^2R^2\theta^2 \right\} \qquad (7)$$

$$\epsilon_\phi = \frac{1}{E}\left\{(1-\sigma)a_1 + (2-\sigma)a_2\theta + \sum_1^\infty \left[(\overline{r+2} - \sigma)a_{r+2} + \frac{(1+\sigma)}{(r+3)} a_r \right] \theta^{r+1} + \rho\Omega^2R^2\theta^2 \right\} \qquad (8)$$

and

$$(1-\sigma)a_1 + (1-2\sigma)a_2\theta + \sum_1^\sigma \left[(1 - \overline{r+2}\cdot\sigma)a_{r+2} - \frac{(1-\sigma)}{(r+3)} a_r \right] \theta^{r+1} - \sigma\rho\Omega^2R^2\theta^2 = (1-\sigma)a_1 + 2(1-2\sigma)a_2\theta + \sum_1^\infty \left[(\overline{r+2}^2 - \overline{r+2}\cdot\sigma)a_{r+2} + \frac{(1+\sigma)(r+2)}{(r+3)} a_r \right] \theta^{r+1} + 3\rho\Omega^2R^2\theta^2 \qquad (9)$$

From (9) it follows that a_1 is still arbitrary,

$$a_2 = 0$$

$$a_3 = -\frac{(1+\sigma)}{8} a_1 - \frac{(3+\sigma)}{8} \rho\Omega^2R^2$$

and, generally,

$$a_{r+2} = \frac{-(1+\sigma)}{(r+2)^2 - 1} a_r \qquad (10)$$

with r odd and ≥ 3.

Equation (10) gives the required recurrence relation between a_{r+2} and a_r. Alternatively (10) can be written

$$a_{r+2} = \frac{[-(1+\sigma)]^{\frac{r-1}{2}}}{(r+3)(r+1)^2(r-1)^2 \ldots 4} \left\{ -\frac{(1+\sigma)}{8} a_1 - \frac{(3+\sigma)}{8} \rho\Omega^2R^2 \right\} \quad r \geq 1, \text{ odd} \qquad (11)$$

Determination of a_1. Substituting for a_{r+2} from (11) in (I) yields

$$a_1 + \sum_3^\infty \frac{[-(1+\sigma)]^{\frac{r-1}{2}} \alpha^{r-1}}{(r+1)(r-1)^2 \ldots 4^2 \cdot 2} \cdot a_1 - \sum_3^\infty \frac{[-(1+\sigma)]^{\frac{r-3}{2}} (3+\sigma)}{(r+1)(r-1)^2 \ldots 4^2 \cdot 2} \rho\Omega^2R^2\alpha^{r-1} = 0$$

and solving for a_1, gives

$$a_1 = \frac{\sum_3^\infty \frac{[-(1+\sigma)]^{\frac{r-3}{2}} \alpha^{r-3}}{(r+1)(r-1)^2 \ldots 4^2 \cdot 2} \times (3+\sigma)\rho\Omega^2R^2\alpha^2}{1 + \sum_3^\infty \frac{[-(1+\sigma)]^{\frac{r-1}{2}} \alpha^{r-1}}{(r+1)(r-1)^2 \ldots 4^2 \cdot 2}} \qquad (12)$$

with r odd, or

$$a_1 = f_1(\alpha, \sigma) \frac{3+\sigma}{8} \rho\Omega^2R^2$$

with

$$f_1(\alpha,\sigma) = \frac{\sum_3^\infty \frac{[-(1+\sigma)]^{\frac{r-3}{2}} \alpha^{r-1}}{(r+1)(r-1)^2 \ldots 4}}{1 + \sum_3^\infty \frac{[-(1+\sigma)]^{\frac{r-1}{2}} \alpha^{r-1}}{(r+1)(r-1)^2 \ldots 4^2 \cdot 2}}$$

It follows from (10), that

$$\left.\begin{aligned} a_3 &= -\left[\frac{(1+\sigma)}{8} f_1(\alpha,\sigma) + 1\right] \frac{3+\sigma}{8} \rho\Omega^2R^2 \\ &= f_3(\alpha,\sigma) \frac{3+\sigma}{8} \rho\Omega^2R^2 \\ a_5 &= \frac{(1+\sigma)}{6.4} \left[\frac{(1+\sigma)}{8} f_1(\alpha,\sigma) + 1\right] \frac{3+\sigma}{8} \rho\Omega^2R^2 \\ &= f_5(\alpha_1\sigma) \frac{3+\sigma}{8} \rho\Omega^2R^2 \\ a_7 &= \frac{-(1+\sigma)^2}{8 \cdot 6^2 \cdot 4} \left[\frac{(1+\sigma)}{8} f_1(\alpha+\sigma) + 1\right] \\ &\quad \times \frac{3+\sigma}{8} \rho\Omega^2R^2 = f_7(\alpha,\sigma) \frac{3+\sigma}{8} \rho\Omega^2R^2 \end{aligned}\right\} \qquad (13)$$

and generally

$$a_{r+2} = \frac{[-(1+\sigma)]^{\frac{r-1}{2}}}{(r+3)(r+1)^2 \ldots 4} \left[\frac{(1+\sigma)}{8} f_1(\alpha+\sigma) + 1\right] \times \frac{3+\sigma}{8} \rho\Omega^2R^2 = f_{r+2}(\alpha,\sigma) \frac{3+\sigma}{8} \rho\Omega^2R^2$$

Since $\alpha \leq 0.5$, the series for s, f, and p is very rapidly convergent. Thus, for s,

$$\lim_{r \to \infty} \left| \frac{a_{r+2}}{a_r} \right| \alpha^2 = \lim_{r \to \infty} \frac{1+\sigma}{[(r+2)^2 - 1]} = 0$$

Owing to the rapidity of the convergence it will be considered sufficient to take only three terms in the three series for s, p, and f. Thus f_7/f_5 is of the order of 0.001, and neglecting terms of higher order will not involve errors of more than 0.1 per cent. The functions f_1, f_3, and f_5 are tabulated in Table 1 for a range of values of

α and σ. With the foregoing values of a_1, a_3, and a_5, the expressions for s, p, and f become

$$\left.\begin{aligned} s &= [f_1\theta + f_3\theta^3 + f_5\theta^5]\frac{(3+\sigma)}{8}\rho\Omega^2R^2 \\ p &= \left[f_1 + \left(f_3 - \frac{f_1}{4}\right)\theta^2 + \left(f_5 - \frac{f_3}{6}\right)\theta^4\right]\frac{(3+\sigma)}{8}\rho\Omega^2R^2 \\ f &= \left[f_1 + \left(3f_3 + \frac{f_1}{3} + \frac{8}{3+\sigma}\right)\theta^2 + \left(5f_5 + \frac{f_3}{5}\right)\theta^4\right]\frac{(3+\sigma)}{8}\rho\Omega^2R^2 \end{aligned}\right\} \quad (14)$$

Note: The case of the flat disk can be derived as a special case of the foregoing by writing $r_2 = R\alpha = \lim_{\substack{R\to\infty \\ \alpha\to 0}} R\alpha$. Then

$$\left.\begin{aligned} s &= 0 \\ p &= \frac{(3+\sigma)}{8}\rho\Omega^2r_2^2\left[1 - \left(\frac{r}{r_2}\right)^2\right] \\ f &= \frac{(3+\sigma)}{8}\rho\Omega^2r_2^2\left[1 - \frac{(1+3\sigma)}{(3+\sigma)}\left(\frac{r}{r_2}\right)^2\right] \end{aligned}\right\} \quad (15)$$

Moments in and Normal Deflection of Dish. Substituting for M_θ, M_ϕ, and s in (vi) from (vii), (viii) and (1) yields after some arithmetic the following differential equation for Δ:

$$\theta^3\frac{d^3\Delta}{d\theta^3} + \theta^2\frac{d^2\Delta}{d\theta^2} - \theta\frac{d\Delta}{d\theta} = R\theta\int_0^\theta \epsilon_\theta d\theta - \sigma R\theta^2\epsilon_\theta - \frac{sR^2h\theta^3}{D} \quad (16)$$

where

$$D = \frac{Eh^3}{12(1-\sigma^2)}$$

Now, from (7) and (1),

$$\theta\int_0^\theta \epsilon_\theta d\theta = \frac{1}{E}\left\{(1-\sigma)a_1\theta^2 + \sum_1^\infty\left[\left(\frac{1}{r+2} - \sigma\right)a_{r+2} - \frac{1+\sigma}{(r+2)(r+3)}\cdot a_r\right]\theta^{r+3} - \frac{\sigma}{3}\rho\Omega^2R^2\theta^4\right.$$

$$\epsilon_\theta\theta^2 = \frac{1}{E}\left\{(1-\sigma)a_1\theta^2 + \sum_1^\infty\left[(1 - \overline{r+2}\cdot\sigma)a_{r+2} - \frac{1+\sigma}{(r+3)}\cdot a_r\right]\theta^{r+3} - \sigma\rho\Omega^2\theta^2\theta^4\right.$$

with r_1 odd, and

$$s\theta^3 = \sum_1^\infty a_r\theta^{r+3}, \quad \text{with } r \text{ odd.}$$

An examination of the order of the coefficients in the terms on the right-hand side of (16) shows that the only term that needs to be considered is

$$\frac{-12R(1-\sigma^2)}{E}\cdot\left(\frac{R}{h}\right)^2 a_1\theta^4$$

neglecting higher powers of θ. Thus

$$\theta^3\frac{d^3\Delta}{d\theta^3} + \theta^2\frac{d^2\Delta}{d\theta^2} - \theta\frac{d\Delta}{d\theta} = \frac{-12R(1-\sigma^2)}{E}\left(\frac{R}{h}\right)^2 a_1\theta^4 \quad (16a)$$

The solution to (16a) is

$$\frac{d\Delta}{d\theta} = A_1\theta - \frac{3R(1-\sigma^2)}{2E}\left(\frac{R}{h}\right)^2 a_1\theta^3 \quad (17)$$

neglecting higher orders of small quantities.

The constant A_1 in (17) is derived from the first of boundary conditions (ix). Thus substituting for $d\Delta/d\theta$ in (vii) and setting $M_\theta = 0$ when $\theta = \alpha$ gives

$$0 = (1+\sigma)A_1 - \frac{3R(1-\sigma^2)}{2E}\left(\frac{R}{h}\right)^2(3+\sigma)\alpha^2 a_1$$

i.e.,

$$A_1 = \frac{3R(1-\sigma)}{2E}\left(\frac{R}{h}\right)^2(3+\sigma)\alpha^2 a_1 \quad (18)$$

after, again, neglecting higher orders of small quantities.

Finally integrating (17) with respect to θ gives

$$\Delta = A_0 + \frac{A_1\theta^2}{2} - \frac{3R(1-\sigma^2)}{8E}\left(\frac{R}{h}\right)^2 a_1\theta^4$$

The constant A_0 is arbitrary in the sense that it represents the displacement of the center of the solid disk vertically in the absence of constraints. This could be determined by the additional consideration that the CG of the deformed dish coincides with the CG of the undeformed dish, there being no vertical forces acting on the dish. This, however, is not relevant to our problem and it will be assumed without loss of generality that $A_0 = 0$. Then

$$\frac{\Delta}{R} = \frac{3a_1(1-\sigma^2)}{8E}\left(\frac{R}{h}\right)^2\theta^2\left[2\left(\frac{3+\sigma}{1+\sigma}\right)\alpha^2 - \theta^2\right] \quad (19)$$

and $\Delta_{\max}$ occurs at

$$\theta^2 = \frac{3+\sigma}{1+\sigma}\alpha^2$$

i.e., at

$$\theta = \left(\frac{3+\sigma}{1+\sigma}\right)^{1/2}\alpha$$

Since this is outside the dish rim, the maximum value of Δ occurs at the rim where $\theta = \alpha$; then

$$\left(\frac{\Delta}{R}\right)_{\max} = \frac{3(5+\sigma)(1-\sigma)a_1}{8E}\left(\frac{R}{h}\right)^2\alpha^4 \quad (20)$$

or

$$\left(\frac{\Delta}{R}\right)_{\max} = \frac{3(5+\sigma)(1-\sigma)a_1}{8E}\left(\frac{r_2}{h}\right)^2\alpha^2 \quad (20a)$$

where $r_2 = R\alpha$.

Also using (18) in (17) gives for $d\Delta/d\theta$

$$\frac{d\Delta}{d\theta} = \frac{3R}{2E}(1-\sigma^2)\left(\frac{R}{h}\right)^2 a_1\theta\left[\left(\frac{3+\sigma}{1+\sigma}\right)\alpha^2 - \theta^2\right]$$

With

$$\frac{d^2\Delta}{d\theta^2} = \frac{3R}{2E}(1-\sigma^2)\left(\frac{R}{h}\right)^2 a_1\left[\left(\frac{3+\sigma}{1+\sigma}\right)\alpha^2 - 3\theta^2\right]$$

But

$$M_\theta = \frac{E}{12(1-\sigma^2)}\left(\frac{h}{R}\right)^2 h\left\{\frac{d^2\Delta}{d\theta^2} + \frac{\sigma}{\theta}\frac{d\Delta}{d\theta}\right\}$$

With

$$M_\phi = \frac{E}{12(1-\sigma^2)}\left(\frac{h}{R}\right)^2 h\left\{\frac{1}{\theta}\frac{d\Delta}{d\theta} + \sigma\frac{d^2\Delta}{d\theta^2}\right\}$$

neglecting higher orders of small quantities

Hence

$$M_\theta = Rha_1(\alpha^2 - \theta^2)\frac{3+\sigma}{8}$$

and

$$M_\phi = Rha_1\left[\alpha^2 - \left(\frac{3\sigma+1}{3+\sigma}\right)\theta^2\right]\frac{3+\sigma}{8}$$

i.e.

$$\boxed{\begin{aligned} M_\theta &= \frac{3+\sigma}{8}Rha_1[\alpha^2 - \theta^2] \\ M_\phi &= \frac{3+\sigma}{8}Rha_1\left[\alpha^2 - \left(\frac{1+3\sigma}{3+\sigma}\right)\theta^2\right] \end{aligned}} \quad (21)$$

When

$$\theta = 0, \quad M_\theta = M_\phi = \frac{3+\sigma}{8}Rha_1\alpha^2$$

When

$$\theta = \alpha, \quad M_\theta = 0 \quad \text{and} \quad M_\phi = \frac{(1-\sigma)}{4}Rha_1\alpha^2$$

The set of equations (14), (19), and (21) completely determines the values of the stresses, moments, and normal displacement anywhere in the dish. The strains, if required, would follow from (7) and (8).

Problem B

Stress and Strain in a Centrally Holed Paraboloid Dish Spinning at Angular Velocity Ω. Following a treatment parallel to that adopted for problem A, assume a solution for s, the shear stress, of the form

$$s = \sum_0^\infty a_r\theta^r \quad (1a)$$

$\alpha = \alpha_1$, defines the aperture, at the dish center, of the hole.
$\alpha = \alpha_2$, defines the aperture, at the dish center, of the dish rim.

To satisfy the second of (x)

$$\sum_0^\infty a_r\alpha_1^r = 0 \quad (1a)$$

and to satisfy the first of (x)

$$\sum_0^\infty a_r\alpha_2^r = 0 \quad (1b)$$

Also (1a) can be used in (i) and (ii) to determine p and f in terms of θ.

Thus

$$\frac{d(s\theta)}{d\theta} = \sum_0^\infty (r+1)a_r\theta^r$$

and substituting this for $d(s\theta)/d\theta$ in (i) yields

$$\sum_0^\infty (r+1)a_r\theta^{r-1} = p + f - \rho\Omega^2R^2\theta^2 \quad (3a)$$

Also substituting for $s\theta$ in (ii) yields

$$\frac{d(p\theta)}{d\theta} + \frac{(p\theta)}{\theta} = p + f - \rho\Omega^2R^2\theta^2 - \sum_0^\infty a_r\theta^{r+1}$$

or

$$\frac{d(p\theta)}{d\theta} + \frac{(p\theta)}{\theta} = \frac{a_0}{\theta} + 2a_1 + \sum_0^\infty [(r+3)a_{r+2} - a_r]\theta^{r+1} \quad (4a)$$

Integrating (4a) for p gives

$$p = \frac{b_0}{\theta^2} + \frac{a_0}{\theta} + a_1 + \sum_0^\infty\left[a_{r+2} - \frac{a_r}{r+3}\right]\theta^{r+1} \quad (5a)$$

Substituting for p from (5a) and (3a) gives

$$f = \sum_0^\infty (r+1)a_r\theta^{r-1} - \sum_0^\infty\left(a_{r+2} - \frac{a_r}{r+3}\right)\theta^{r+1} - \frac{b_0}{\theta^2} - \frac{a_0}{\theta} - a_1 + \rho\Omega^2R^2\theta^2$$

i.e.

$$f = -\frac{b_0}{\theta^2} + a_1 + \sum_0^\infty\left[(r+2)a_{r+2} + \frac{a_r}{r+3}\right]\theta^{r+1} + \rho\Omega^2R^2\theta^2 \quad (6a)$$

and since $p = 0$ when $\theta = \alpha_2$,

$$b_0 + a_0\alpha_2 + a_1\alpha_2^2 + \sum_0^\infty\left[a_{r+2} - \frac{a_r}{r+3}\right]\alpha_2^{r+3} = 0 \quad (11a)$$

Similarly since $p = 0$ when $\theta = \alpha_1$

$$b_0 + a_0\alpha_1 + a_1\alpha_1^2 + \sum_0^\infty\left[a_{r+2} - \frac{a_r}{r+3}\right]\alpha_1^{r+3} = 0 \quad (11b)$$

Derivation of Recurrence Relation. Using (iii), (iv), (v) in turn yields, after substituting for p and f, from (5a) and (6a),

$$\epsilon_\theta = \frac{1}{E}\left[a_1(1-\sigma) + \frac{b_0(1+\sigma)}{\theta^2} + \frac{a_0}{\theta} + \sum_0^\infty\left[(1 - \overline{r+2}\cdot\sigma)a_{r+2} - \left(\frac{1+\sigma}{r+3}\right)a_r\right]\theta^{r+1} - \sigma\rho\Omega^2R^2\theta^2\right] \quad (7a)$$

$$\epsilon_\phi = \frac{1}{E}\left[a_1(1-\sigma) - \frac{b_0(1+\sigma)}{\theta^2} - \frac{a_0}{\theta} + \sum_0^\infty\left[(\overline{r+2} - \sigma)a_{r+2} + \left(\frac{1+\sigma}{r+3}\right)a_r\right]\theta^{r+1} + \rho\Omega^2R^2\theta^2\right] \quad (8a)$$

and

$$\frac{a_0}{\theta} + \sum_0^\infty \left[a_{r+2}(1 - \overline{r+2}\,\sigma) - \left(\frac{1+\sigma}{r+3}\right) a_r \right] \theta^{r+1} - \sigma\rho\Omega^2R^2\theta^2 = \sum_0^\infty \left[a_{r+2}(\overline{r+2} - \sigma)(r+2) + \frac{(1+\sigma)(r+2)}{(r+3)} a_r \right] \theta^{r+1} + 3\rho\Omega^2R^2\theta^2 \quad (9a)$$

Hence, a_1 and b_0 are still arbitrary, and $a_0 = 0$.
Also, the coefficients of θ^r must be zero, yielding

$$a_3 = -\left[\frac{(1+\sigma)}{8} a_1 + \frac{(3+\sigma)}{8}\rho\Omega^2R^2\right] = -\left[\frac{(1+\sigma)}{8} f_1 + 1\right]\frac{(3+\sigma)}{8}\rho\Omega^2R^2 = f_3\frac{3+\sigma}{8}\rho\Omega^2R^2$$

where $$a_1 = f_1\frac{3+\sigma}{8}\rho\Omega^2R^2$$

and $$a_{r+2} = \frac{-(1+\sigma)}{[(r+2)^2 - 1]} a_r, \; r \text{ odd} \geq 3 \quad (10a)$$

Since $a_0 = 0$, the coefficients a_r with even suffixes are all zero and $s = \sum_1^\infty a_r\theta^r$, involves only odd powers of θ.

Determination of a_1 and b_0. In this problem we shall choose to satisfy (IIa) and (IIb) rather than (Ia) and (Ib). The errors in s involved at the dish edges are of the order of 1 per cent of the maximum value of s in the dish. These errors, as explained in the foregoing, arise from the nondiscrimination in the values of α_1 and α_2 of the dish, in the deformed as distinct from the undeformed state. Hence the equations to determine a_1 and b_0 follow from (IIa) and (IIb). Thus equation (5a) can be rewritten, making use of the results in the previous paragraph, as

$$b_0 + a_1\left[\theta^2 - \sum_1^\infty \frac{(r+2+\sigma)[-(1+\sigma)]^{\frac{r-1}{2}}}{(r+3)(r+1)^2\ldots 4^2\cdot 2}\theta^{r+3}\right] + \frac{(3+\sigma)}{4(1+\sigma)}\rho\Omega^2R^2\left[\theta^4 - 4\sum_1^\infty \frac{(r+2+\sigma)[-(1+\sigma)]^{\frac{r-1}{2}}}{(r+3)(r+1)^2\ldots 4^2\cdot 2}\theta^{r+3}\right] = 0$$

at the dish rim, where $\theta = \alpha_1$ and $\theta = \alpha_2$, i.e.

$$b_0 + a_1\left[\alpha_2^2 - \sum_1^\infty A_r\alpha_2^{r+3}\right] + \frac{3+\sigma}{4(1+\sigma)}\left[\alpha_2^4 - 4\sum_1^\infty A_r\alpha_2^{r+3}\right]\rho\Omega^2R^2 = 0 \quad (\text{II}a)$$

$$b_0 + a_1\left[\alpha_1^2 - \sum_1^\infty A_r\alpha_1^{r+3}\right] + \frac{3+\sigma}{4(1+\sigma)}\left[\alpha_1^4 - 4\sum_1^\infty A_r\alpha_1^{r+3}\right]\rho\Omega^2R^2 = 0 \quad (\text{II}b)$$

where

$$A_r = \frac{(r+2+\sigma)[-(1+\sigma)]^{\frac{r-1}{2}}}{(r+3)(r+1)^2\ldots 4^2\cdot 2}$$

Also, $A_1 = (3+\sigma)/8$.

Solving (IIa) and (IIb) for b_0 and a_1, gives, after some arithmetic,

$$a_1 = -\frac{(3+\sigma)}{4(1+\sigma)}\rho\Omega^2R^2\alpha_2^2\frac{\left\{\left[1+\left(\frac{\alpha_1}{\alpha_2}\right)^2\right] - 4\sum_1^\infty \frac{A_r\alpha_2^{r-1}}{\left[1-\left(\frac{\alpha_1}{\alpha_2}\right)^2\right]} + 4\frac{\alpha_1^4}{\alpha_2^4}\sum_1^\infty \frac{A_r\alpha_1^{r-1}}{\left[1-\left(\frac{\alpha_1}{\alpha_2}\right)^2\right]}\right\}}{\left\{1 - \sum_1^\infty \frac{A_r\alpha_2^{r+1}}{\left[1-\left(\frac{\alpha_1}{\alpha_2}\right)^2\right]} + \frac{\alpha_1^2}{\alpha_2^2}\sum_1^\infty \frac{A_r\alpha_1^{r-1}}{\left[1-\left(\frac{\alpha_1}{\alpha_2}\right)^2\right]}\right\}} \quad (12a)$$

$$b_0 = \frac{(3+\sigma)}{4(1+\sigma)}\rho\Omega^2R^2\alpha_2^2\alpha_1^2\frac{\left\{1 - (4-\alpha_1^2)\sum_1^\infty \frac{A_r\alpha_2^{r-1}}{\left[1-\left(\frac{\alpha_1}{\alpha_2}\right)^2\right]} + \frac{\alpha_1^2}{\alpha_2^2}(4-\alpha_2^2)\sum_1^\infty \frac{A_r\alpha_1^{r-1}}{\left[1-\left(\frac{\alpha_1}{\alpha_2}\right)^2\right]}\right\}}{\left\{1 - \sum_1^\infty \frac{A_r\alpha_2^{r+1}}{\left[1-\left(\frac{\alpha_1}{\alpha_2}\right)^2\right]} + \frac{\alpha_1^2}{\alpha_2^2}\sum_1^\infty \frac{A_r\alpha_1^{r+1}}{\left[1-\left(\frac{\alpha_1}{\alpha_2}\right)^2\right]}\right\}} \quad (12b)$$

Note that as the dish becomes flatter and tends to a flat disk with a hole in the center,

$$R\alpha_2 \to r_2, \quad \frac{\alpha_1}{\alpha_2} \to \frac{r_1}{r_2}, \quad \alpha_1 \to 0, \text{ and } \alpha_2 \to 0.$$

Then,

$$b_0 \to 0$$

and

$$a_1 \to \frac{(3+\sigma)}{8}\rho\Omega^2r_2^2\left[1+\left(\frac{r_1}{r_2}\right)^2\right]$$

Thus the case of the flat disk can be derived as a special case of the foregoing, leading to

$$\left.\begin{aligned} s &= 0 \\ p &= \frac{(3+\sigma)}{8}\rho\Omega^2r_2^2\left\{\left[1+\left(\frac{r_1}{r_2}\right)^2\right] - \left[\frac{r_1^2}{r^2} + \frac{r^2}{r_2^2}\right]\right\} \end{aligned}\right\} \quad (15a)$$

$$f = \frac{(3+\sigma)}{8}\rho\Omega^2 r_2^2\left\{\left[1+\left(\frac{r_1}{r_2}\right)^2\right] + \left[\frac{r_1^2}{r^2} - \left(\frac{1+3\sigma}{3+\sigma}\right)\frac{r^2}{r_2^2}\right]\right\} \quad (15a)\ (cont.)$$

Thus at $r = r_1$, $p = 0$ and

$$f = \frac{(3+\sigma)}{4}\rho\Omega^2 r_2^2\left[1+\left(\frac{1-\sigma}{3+\sigma}\right)\left(\frac{r_1}{r_2}\right)^2\right]$$

If $r_1 \to 0$,

$$f \to \frac{(3+\sigma)}{4}\rho\Omega^2 r_2^2$$

which shows for the holed dish the familiar doubling of the amount of the central hoop stress present in a solid dish, resulting from the removal of the constraint at the center.

Moments in and Normal Deflection of Dish. The analysis here follows an argument similar to that adopted in a previous similar section, and the result (17) is adopted here to avoid unnecessary repetition of analysis. Thus the normal deflection Δ of the dish will be given by

$$\frac{d\Delta}{d\theta} = \frac{B_1}{\theta} + A_1\theta - \frac{3R(1-\sigma^2)}{2E}\left(\frac{R}{h}\right)^2 a_1\theta^3 \quad (17a)$$

neglecting second order of small quantities.

The slope is not zero at either $\theta = \alpha_1$ or $\theta = \alpha_2$ and hence the additional constant of integration B_1, which was dropped in (17) because $d\Delta/d\theta = 0$ at $\theta = 0$, is inserted. A_1 and B_1 are determined from the first of boundary condition (x), i.e., from the fact that $M_\theta = 0$ when $\theta = \alpha_1$ and $\theta = \alpha_2$; i.e.

$$\left.\begin{aligned}&(1+\sigma)A_1\alpha_2^2 - (1-\sigma)B_1 - \frac{3(1-\sigma^2)}{2E}\left(\frac{R}{h}\right)^2 Ra_1(3+\sigma)\alpha_2^4 = 0\\ &(1+\sigma)A_1\alpha_1^2 - (1-\sigma)B_1 - \frac{3(1-\sigma^2)}{2E}\left(\frac{R}{h}\right)^2 Ra_1(3+\sigma)\alpha_1^4 = 0\end{aligned}\right\} \quad (18a)$$

Solving (18a) for A_1 and B_1 gives

$$A_1 = \frac{3(1-\sigma^2)}{2E}\left(\frac{R}{h}\right)^2 Ra_1\left(\frac{3+\sigma}{1+\sigma}\right)\frac{\left[1-\left(\frac{\alpha_1}{\alpha_2}\right)^4\right]}{\left[1-\left(\frac{\alpha_1}{\alpha_2}\right)^2\right]}\alpha_2^2 \quad (18b)$$

and

$$B_1 = +\frac{3(1-\sigma^2)}{2E}\left(\frac{R}{h}\right)^2 Ra_1\frac{(3+\sigma)}{(1-\sigma)}\alpha_1^2\alpha_2^2 \quad (18c)$$

Equation (17a) can now be integrated with A_1 and B_1 now determined. This done results in

$$\Delta = B_1\ln|\theta| + \frac{1}{2}A_1\theta^2 - \frac{3R(1-\sigma^2)}{8E}\left(\frac{R}{h}\right)^2 a_1\theta^4$$

setting the quite arbitrary constant of integration to zero, as has been done on the previous occasion.

Substituting for B_1 and A_1, and gathering like terms finally yields

$$\frac{\Delta}{R} = \frac{-3}{8}a_1\frac{(1-\sigma^2)(3+\sigma)}{\sigma E}\left(\frac{R}{h}\right)^2\left\{-\frac{4\sigma\alpha_1^2\alpha_2^2}{(1-\sigma)}\ln|\theta| - \frac{2\sigma\alpha_2^2}{(1+\sigma)}\left[1+\left(\frac{\alpha_1}{\alpha_2}\right)^2\right]\theta^2 + \frac{\sigma}{(3+\sigma)}\theta^4\right\} \quad (19a)$$

From (19a), by differentiation,

$$\frac{d\left(\frac{\Delta}{R}\right)}{d\theta} = \frac{-3a_1(1-\sigma^2)(3+\sigma)}{8\sigma E}\left(\frac{R}{h}\right)^2\left\{-\frac{4\sigma\alpha_1^2\alpha_2^2}{(1-\sigma)\theta} - \frac{4\sigma\alpha_2^2}{(1+\sigma)}\left[1+\left(\frac{\alpha_1}{\alpha_2}\right)^2\right]\theta + \frac{4\sigma}{(3+\sigma)}\theta^3\right\}$$

or

$$\frac{d\left(\frac{\Delta}{R}\right)}{d\theta} = \frac{-3a_1(1-\sigma^2)(3+\sigma)}{2\sigma E}\left(\frac{R}{h}\right)^2\left\{-\frac{\sigma\alpha_1^2\alpha_2^2}{(1-\sigma)\theta} - \frac{\sigma\alpha_2^2}{(1+\sigma)}\left[1+\left(\frac{\alpha_1}{\alpha_2}\right)^2\right]\theta + \frac{\sigma}{(3+\sigma)}\theta^3\right\}$$

and the slope at $\theta = \alpha_1$ and $\theta = \alpha_2$ follows by simple substitution. Also

$$\frac{d^2\left(\frac{\Delta}{R}\right)}{d\theta^2} = \frac{3a_1(1-\sigma^2)(3+\sigma)}{2\sigma E}\left(\frac{R}{h}\right)^2\left\{-\frac{\sigma\alpha_1^2\alpha_2^2}{(1-\sigma)\theta^2} + \frac{\sigma\alpha_2^2}{(1+\sigma)}\left[1+\left(\frac{\alpha_1}{\alpha_2}\right)^2\right] - \frac{3\sigma}{(3+\sigma)}\theta^2\right\}$$

and since

$$\left.\begin{aligned}M_\theta &= \frac{E}{12(1-\sigma^2)}\left(\frac{h}{R}\right)^2 h\left\{\frac{d^2\Delta}{d\theta^2} + \frac{\sigma}{\theta}\frac{d\Delta}{d\theta}\right\}\\ \text{and}\quad M_\phi &= \frac{E}{12(1-\sigma^2)}\left(\frac{h}{R}\right)^2 h\left\{\frac{1}{\theta}\frac{d\Delta}{d\theta} + \sigma\frac{d^2\Delta}{d\theta^2}\right\}\end{aligned}\right\} \text{ neglecting higher orders of small quantities}$$

expressions for M_θ and M_ϕ can be obtained explicitly as

$$\left.\begin{aligned}M_\theta &= \frac{(3+\sigma)}{8}a_1Rh\left\{-\frac{\alpha_1^2\alpha_2^2}{\theta^2} + (\alpha_2^2+\alpha_1^2) - \theta^2\right\}\\ \text{and}\quad M_\phi &= \frac{(3+\sigma)}{8}a_1Rh\left\{-\frac{\alpha_1^2\alpha_2^2}{\theta^2} + (\alpha_2^2+\alpha_1^2) - \left(\frac{1+3\sigma}{3+\sigma}\right)\theta^2\right\}\end{aligned}\right\} \quad (21a)$$

The first of (21a) shows $M_\theta = 0$ at $\theta = \alpha_1$ and $\theta = \alpha_2$.

The second of (21a) gives the values of M_ϕ at $\theta = \alpha_1$ and $\theta = \alpha_2$.

In both equations (21a), a_1 is given by (12a). Equations (19a) and (21a) are given in terms of the angular measure θ. Alternative forms can be obtained, where Δ, M_θ, and M_ϕ are expressed in terms of the radial distance from the center of the dish thus:

$$\Delta = +\frac{3a_1(1-\sigma^2)(3+\sigma)}{8Eh^2R}\left\{\frac{4}{(1-\sigma)}r_1^2r_2^2\log_e\left|\frac{r}{R}\right| + \frac{2}{(1+\sigma)}(r_2^2+r_1^2)r^2 - \frac{1}{(3+\sigma)}r^4\right\}$$

Table 1 The functions: f_1, f_2, f_3. Whole dish.

σ	α_1, deg	f_1	$-f_2$	f_3
0.1	10	0.0306	1.0046	0.0460
	20	0.1234	1.0170	0.0466
	30	0.2808	1.0386	0.0475
0.2	10	0.0306	1.0046	0.0502
	20	0.1235	1.0185	0.0509
	30	0.2814	1.0422	0.0521
0.3	10	0.0306	1.0050	0.0544
	20	0.1236	1.0206	0.0552
	30	0.2814	1.0458	0.0566
0.4	10	0.0306	1.0054	0.0586
	20	0.1237	1.0216	0.0595
	30	0.2826	1.0494	0.0612

$$M_\theta = \frac{3+\sigma}{8}\frac{ha_1}{R}\left\{-\frac{r_1^2 r_2^2}{r^2} + (r_1^2 + r_2^2) - r^2\right\}$$

$$M_\phi = \frac{3+\sigma}{8}\frac{ha_1}{R}\left\{-\frac{r_1^2 r_2^2}{r^2} + (r_1^2 + r_2^2) - \frac{(1+3\sigma)}{(3+\sigma)}r^2\right\}$$

In particular,

$$M_\phi = \frac{(1-\sigma)ha_1 r_1^2}{4R} \quad \text{at} \quad r = r_1$$

$$M_\phi = \frac{(1-\sigma)ha_1 r_2^2}{4R} \quad \text{at} \quad r = r_2$$

This completes the examination of this problem. In both solutions, p, f, s, M_θ, M_ϕ, and Δ have been determined in terms of the immediate geometry of the dish and of the coefficients a_r. M_θ, M_ϕ, and Δ are functions of a_1 only, the a_r's for $r > 1$ having been left out as being coefficients of a higher order of small quantities. The coefficients b_0 and $f_r (1 \leq r \leq 5,\ r,\ \text{odd})$ are tabulated in Table 2 in certain ranges of σ, α_1, α_2, and α_1/α_2.

Conclusions

The departure in the profile of a paraboloid dish from a spherical profile is less than 5 per cent of the sphere radius at the outer rim for a dish of semiaperture 30 deg. This will be considered to justify the use of the results derived in previous sections for the assessment of stresses and strains in the spinning paraboloid dish. Thus (19) and (19a) which represent the radial deformation of the spinning dish could be used to design a dish which is parabolic in the spinning condition; this could be achieved by using a template for the dish profile which departs radially from the parabolic shape negatively by amounts (19) and (19a), respectively, for the cases of the unholed and holed dishes.

Normally the problem is rather more involved than that treated here, especially as regards constraints at the hub introduced by the flanges necessary to support the dish and the possibility that the dish be not homogeneous either in material or in thickness. However, these further complications can be undertaken by methods not different from the foregoing, which method thus provides a useful angle of attack on problems which might incorporate them.

Finally, as an example of the extreme arithmetical simplicity involved in the use of the results derived, one can verify that a whole spinning paraboloid steel dish of angular aperture 60 deg at the center, focal distance 6 in., $^1/_2$ in. thickness, and spinning at 6000 rpm will experience the following various maximum stresses, moments and deformations:

$$s_{max} = 7650 \text{ psi at } \theta = 17.2 \text{ deg}$$

$$f_{max} = p_{max} = 38{,}200 \text{ psi at } \theta = 0 \qquad \text{Equations (14)}$$

Table 2 The functions: f_1, f_3, f_5, b_0. Holed dish.

σ	α_1/α_2	α_2, deg	f_1	$-f_3$	f_5	$-b_0$
0.1	0.1	10	0.0311	1.0043	0.0460	0.0003
		20	0.1264	1.0174	0.0466	0.0013
		30	0.2921	1.0401	0.0477	0.0031
	0.2	10	0.0322	1.0044	0.0400	0.0012
		20	0.1312	1.0180	0.0466	0.0052
		30	0.3047	1.0419	0.0478	0.0124
	0.3	10	0.0346	1.0047	0.0461	0.0028
		20	0.1416	1.0195	0.0467	0.0117
		30	0.3322	1.0457	0.0479	0.0281
	0.4	10	0.0386	1.0053	0.0461	0.0050
		20	0.1594	1.0219	0.0468	0.0208
		30	0.3780	1.0520	0.0482	0.0502
0.2	0.1	10	0.0310	1.0047	0.0502	0.0003
		20	0.1262	1.0189	0.0509	0.0013
		30	0.2920	1.0437	0.0522	0.0031
	0.2	10	0.0321	1.0048	0.0502	0.0012
		20	0.1302	1.0197	0.0510	0.0052
		30	0.3042	1.0458	0.0523	0.0124
	0.3	10	0.0343	1.0051	0.0503	0.0028
		20	0.1419	1.0214	0.0511	0.0117
		30	0.3304	1.0501	0.0525	0.0281
	0.4	10	0.0383	1.0058	0.0503	0.0050
		20	0.1583	1.0238	0.0512	0.0208
		30	0.3758	1.0563	0.0528	0.0502
0.3	0.1	10	0.0311	1.0051	0.0521	0.0003
		20	0.1266	1.0206	0.0530	0.0013
		30	0.2933	1.0475	0.0545	0.0031
	0.2	10	0.0322	1.0052	0.0522	0.0012
		20	0.1320	1.0214	0.0531	0.0052
		30	0.3050	1.0496	0.0546	0.0124
	0.3	10	0.0342	1.0056	0.0523	0.0028
		20	0.1407	1.0229	0.0532	0.0117
		30	0.3309	1.0537	0.0548	0.0281
	0.4	10	0.0383	1.0058	0.0503	0.0050
		20	0.1583	1.0238	0.0512	0.0208
		30	0.3758	1.0563	0.0528	0.0502
0.4	0.1	10	0.0311	1.0054	0.0586	0.0003
		20	0.1268	1.0224	0.0596	0.0013
		30	0.2940	1.0514	0.0613	0.0031
	0.2	10	0.0321	1.0056	0.0586	0.0012
		20	0.1311	1.0229	0.0597	0.0052
		30	0.3060	1.0535	0.0615	0.0124
	0.3	10	0.0341	1.0060	0.0587	0.0028
		20	0.1406	1.0246	0.0598	0.0117
		30	0.3300	1.0578	0.0617	0.0281
	0.4	10	0.0379	1.0066	0.0587	0.0050
		20	0.1572	1.0275	0.0599	0.0208
		30	0.3733	1.0653	0.0621	0.0502

$$M_{\theta max} = M_{\phi max} = 26{,}000 \text{ lb-in./in. at } \theta = 0 \qquad \text{Equations (21)}$$

$$(\Delta/R)_{max} = 0.063 \text{ at } \theta = 30 \text{ deg} \qquad \text{Equations (19)}$$

The last results show the considerable maximum normal deformation of the dish due to the spinning; it amounts to 6.3 per cent of the radius R; i.e., $^3/_4$ in. for this particular dish. Conditions are obviously critical at the center and holing the dish at the center to remove the constraints would not be indicated.

Acknowledgment

The author wishes to record his sincere appreciation of the very competent and expeditious help given by Mrs. J. Abbott, of the Civil and Mechanical Department, in the preparation of the typescripts

References

I. S. Sokolnikoff, "Mathematical Theory of Elasticity," McGraw-Hill Book Co., Inc., New York, N. Y., 1946.

S. Timoshenko, "Theory of Elastic Stability," McGraw-Hill Book Co., Inc., New York, N. Y., first edition, 1936.

Torispherical Shells—A Caution to Designers

G. D. GALLETLY

Shell Development Company,
Emeryville Research Center,
Emeryville, Calif.
Assoc. Mem. ASME

It has recently become apparent, through a rigorous stress analysis of a specific case that designing torispherical shells by the current edition of the ASME Code on Unfired Pressure Vessels can lead to failure during proof-testing of the vessel. The purpose of the present paper is to show in what respects the Code fails to give accurate results. As an illustrative example, a hypothetical pressure vessel with a torispherical head having a diameter-thickness ratio of 440 was selected. The supports of the vessel were considered to be either on the main cylinder or around the torus. The vessel was subjected to internal pressure and the elastic stresses in it were determined rigorously and by the Code. A comparison of the two revealed that the Code predicted stresses in the head which were less than one half of those actually occurring. Furthermore, the Code gave no indication of the presence of high compressive circumferential direct stresses which exceeded 30,000 psi for practically the entire torus. If the head had been fabricated using a steel with a yield point of 30,000 psi, then a limit analysis shows that it would have failed or undergone large deformations, whereas the Code would have predicted that it was safe. The Code's rules for torispherical heads are thus in need of revision for certain geometries. The implications of the foregoing results are currently being studied by the ASME; in the interim, however, designers should exercise care in applying the Code to torispherical shells.

It is also shown in the paper that the use of the membrane state as a particular solution of the differential equations is not a good approximation for toroidal shells of the type considered.

Introduction

Just over a year ago a large pressure vessel collapsed while undergoing its hydrostatic proof-test. The bottom head of the vessel, which had been designed in accordance with the provisions of the ASME Code for Unfired Pressure Vessels [1][1] was of the torispherical type and was supported by a cylindrical skirt.

Since many pressure vessels are used in refineries and chemical plants it was felt desirable to undertake a study of this type of head. In particular, it was desired to ascertain whether the current edition of the Code adequately portrayed the state of stress in torispherical heads, and whether supporting a pressure vessel around its bottom head produced larger stresses than supporting it from its cylindrical body.

In order to have a specific example to discuss, a hypothetical pressure vessel design incorporating a torispherical head was selected. This vessel was then subjected to pressure loading and the stresses in it were determined both by the ASME Code and also by integrating the differential equations of the problem. For both cases the dead weight of the vessel was neglected, as were any initial out-of-roundness, welding stresses, defects, etc. A comparison of the two methods then indicated in what respects the current Code was deficient. These points are discussed in more detail later.

During the course of the investigation it also became apparent that an approximation commonly used in shell theory was producing poor results when applied to the toroidal shell of the numerical example. The approximation referred to is the practice of using the membrane forces and deformations as particular integrals of the nonhomogeneous differential equations. Numerical results are given later which show the discrepancies caused by use of the approximation.

Details of Example Vessel and Loadings Considered

The vessel chosen for illustrative purposes is shown in Fig. 1. The bottom head, upon which most interest will be concentrated, consists of a spherical cap joined to the main cylindrical body of the vessel by a fairly sharp radius toroidal transition piece. The over-all dimensions of the vessel are 62 ft high × 23 ft diameter. Other pertinent dimensions are given in Fig. 1.

The continuous circumferential support for the vessel will be considered to be located at one of two positions. These are:

1 On the main cylindrical body of the vessel. The exact position of these supports is immaterial as long as they are far enough away so that they do not produce any discontinuity effects at the cylinder-torus junction.

2 Around the horizontal circle at $\phi = 75$ deg on the torus.

The vessel itself is supposed to be designed for a pressure of 40 psig. However, the loadings to be investigated herein correspond to those which would exist during proof-testing of the vessel. Thus the two loadings which will be considered are:

1 A constant pressure of 60 psig and

2 The vessel completely filled with water and an additional pressure of 34 psig applied.

Loading (2) corresponds to a pressure of 59 psig at the cylinder-torus junction and 61 psig at the crown of the spherical cap. It also corresponds to the usual hydrostatic proof-test.

It will also be assumed that the material from which the vessel is constructed has an allowable stress of 13,750 psi, a yield point of 30,000 psi, and that the joint efficiency of the welds is 1.0.

[1] Numbers in brackets designate References at end of paper.

Contributed by the Petroleum Division and presented at the Petroleum-Mechanical Engineering Conference, September 21–24, 1958, Denver, Colo., of The American Society of Mechanical Engineers.

Note: Statements and opinions advanced in papers are to be understood as individual expressions of their authors and not those of the Society. Manuscript received at ASME Headquarters, August 7, 1957. Paper No. 58—PET-3.

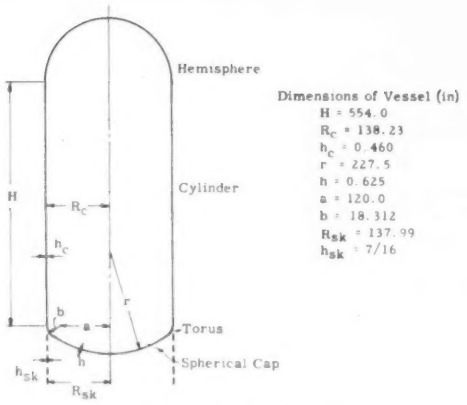

(a) Over-all view of vessel

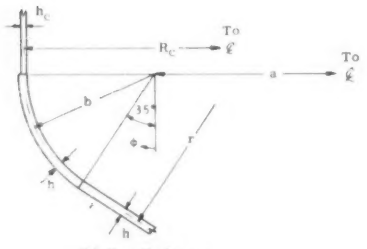

(b) Detail of torus

Fig. 1 Example vessel used for analysis

Provisions of the ASME Code for Unfired Pressure Vessels

Torispherical Heads

The provisions of the Code, in so far as it relates to torispherical heads, may be summarized as follows.

Geometrical Requirements

1 The inside radius of the spherical cap shall not exceed the outside diameter of the skirt of the head.

2 The inside radius of the torus (or knuckle) shall not be less than 6 per cent of the outside diameter of the skirt. It also must not be less than three times the head thickness.

Stresses Due to Pressure

From Paragraph UA-4(*d*) of the Code the following formula is obtained for the stress in torispherical heads due to internal pressure:

$$\sigma = \frac{p}{\eta}\left(0.5M\,\frac{R}{t} + 0.1\right) \qquad (1)^2$$

where

σ = stress in vessel wall, psi
p = internal pressure, psig
R = inside crown radius (radius of spherical cap), in.
t = thickness of head, exclusive of corrosion allowance, in.
M = factor tabulated in Table UA-4.2 of the Code
η = joint efficiency (assumed to be unity herein)

[2] When the toroidal radius is 6 per cent of the crown radius, M = 1.77. For this particular case, equation (1) then agrees with the equation given in Paragraph UG-32(*e*) of the Code. For the example vessel under discussion, M = 1.65.

The Code does not state whether the stress given by equation (1) is meridional or circumferential, or whether it is tensile or compressive. Some discussion concerning its derivation would thus appear to be in order.

Usually the Code attempts to predict only the direct (i.e., membrane) stresses due to pressure. Examples of such cases are the Code formulas for evaluating stresses in cylindrical or spherical shells. The Code's attitude with regard to bending stresses is as follows:

> "It is recognized that high localized and secondary bending stresses may exist in vessels designed and fabricated in accordance with these rules. In so far as practical, design rules for details have been written to hold such stresses at a safe level consistent with experience."

The situation with regard to the Code stress formula for torispherical shells appears to be somewhat different from that outlined. Reference [2], which includes a history of the design of pressure vessel heads, states that the formula is not based on computed stresses in torispherical heads. Instead, it is based on tests of heads of various geometries in which the stress intensification coefficients (ratio of the maximum stress in the head to the membrane stress in the spherical cap, i.e., the factor M) were determined by observation of the pressure at which yielding occurred on the outside of the torus. The fact that yielding first began on the inside of the torus, for some of the tests at least, was ignored, as also was the fact that the onset of yielding is influenced by both meridional and circumferential stresses. Thus the Code formula for stress in torispherical heads is only approximate; it includes both direct and bending stresses, but to which point in the head it is supposed to apply remains a moot point.

Suggested Good Practice Regarding Design of Supports

In the nonmandatory Appendix G of the Code it is mentioned that for vessels supported on skirts

> ". . . localized longitudinal bending and circumferential compressive stresses of high order may exist in the metal of the shell and skirt near the circle of skirt attachment, if the skirt reaction is not substantially tangent to the vessel wall."

The Code appears to prefer attaching the cylindrical skirt above the junction of the head with the main cylindrical shell. When the attachment is below this junction, localized stresses are introduced in proportion to the component of skirt reaction which is normal to the head at the point of attachment. However, the Code proceeds:

> ". . . when the mean diameter of skirt and shell approximately coincide and a generous knuckle radius is used (e.g., a 2:1 ellipsoidal head) the localized stresses are minimized and are not considered objectionable. In other cases, an investigation of local effects may be warranted depending on the magnitude of the loading, location of skirt attachment, etc., and an additional thickness of vessel wall or compression rings may be necessary."

Stresses in Example Vessel as Predicted by the Code

For the proof-test it is not necessary to subtract the corrosion allowance in the value for t. Thus the following dimensions apply for the vessel:

Inside radius of spherical cap	=	227.2 in.
Inside radius of torus	=	18.0 in.
Thickness of head	=	0.625 in.

Considering first the case where the vessel is supported from

the cylindrical body, and a constant internal pressure of 60 psig is applied, equation (1) gives $\sigma = 18{,}000$ psi. A similar value for the stress would also be obtained with the second type of loading (hydrostatic loading plus an additional pressure of 34 psig).

While the Code does not require the maximum localized stress in the head to be calculated, some idea of its magnitude can be obtained from Reference [2], which is a publication of the PVRC (Pressure Vessel Research Committee). In Fig. 11 of the PVRC report the maximum measured stresses from a limited series of tests on torispherical heads are plotted in dimensionless form against the ratio

$$\frac{\text{radius of torus}}{\text{radius of spherical cap}}$$

For the head under discussion this ratio equals 0.0795; from the PVRC report one would then estimate the maximum localized stress in the head to be 45,000 psi.[3]

Turning now to the case where the vessel is supported around the torus at $\phi = 75$ deg, the additional dimension of interest is the outside diameter of the skirt, which equals 276.42 in. As the inside spherical cap radius is less than this value, and the inside toroidal radius is 6.5 per cent of it, two of the geometrical requirements of the Code are satisfied.

The next problem facing the designer is to decide whether an investigation of local effects is warranted at the skirt-torus junction (cf. the earlier remarks on "Suggested Good Practice Regarding Design of Supports"). The mean diameters of skirt and cylinder approximately coincide for this vessel and the skirt reaction (located at $\phi = 75$ deg) is substantially tangent to the vessel wall. The radius of curvature of the knuckle (torus) is about one half that of a 2:1 ellipsoid at the location of the skirt attachment, decreasing to 1/5 at the torus-spherical cap junction. Thus the curvature of the torus in question is not as generous as the example cited by the Code. However, since the supports meet the other requirements, it will be assumed herein that the designer would compromise on the curvature suggestion and not make an investigation of local effects.[4]

The Code, however, still requires that the direct stress due to the skirt reaction be taken into account. For the case where the vessel is subject to a constant internal pressure, the skirt reaction equals zero (neglecting the dead weight of the vessel). Thus the additional direct stress equals zero for this case.

When the vessel is filled with water it can be shown that the weight of water above the level of the skirt attachment is 1.406×10^6 lb while that below is 6.24×10^4 lb. As the horizontal radius at the skirt attachment is approximately 138 inches, the following values are obtained for the meridional direct stresses in the torus due to the skirt reaction:

Above the skirt attachment: $\Delta\sigma = -2685$ psi

Below the skirt attachment: $\Delta\sigma = 120$ psi

The previously calculated value of $\sigma = 18{,}000$ psi should now be added to one of these two values of $\Delta\sigma$. As the Code does not specify the location of σ, the worst case is obtained by adding $|\Delta\sigma| = 2{,}685$ psi. Thus when the vessel is supported around the torus, the Code would predict a stress of $18{,}000 + 2{,}685 = 20{,}685$ psi in the torispherical head.

[3] This value can be considered only approximate for the head considered herein. This is because the diameter-thickness and toroidal radius-thickness ratios of the test vessels in Reference [2] were considerably smaller than those of the example vessel.

[4] Since the curvature suggestion appears in a nonmandatory appendix, this does not seem unreasonable.

Stresses Predicted by the Accurate Analyses

The details of the accurate analyses are given in the Appendix. Briefly, what is given there is as follows: First, the differential equations for the bending of a surface of revolution with constant thickness and constant meridional radius of curvature (as given, for example, in Reference [3]) were extended to include the effects of nonuniform internal pressure. The two second-order differential equations so obtained were then reduced, in the usual manner, to a single, complex second-order nonhomogeneous differential equation. This latter equation was then specialized to apply to spherical and toroidal shells. A high-speed electronic computer was then utilized to obtain the homogeneous and particular solutions for the torus, and the homogeneous solutions for the spherical cap. The particular solution for the spherical cap was obtained in closed form, as were the homogeneous and particular solutions for the cylinder.

Having these solutions available it is then possible to compute the edge displacements and rotations of the various shells in terms of the unknown edge moments and shears. Use of the compatibility equations then yields a set of simultaneous linear algebraic equations for the unknown edge moments and shears. Solution of this system of equations determines the unknowns at the edges of the shells and then the stress distributions can be determined in the usual manner.

The manner in which the vessel was cut apart for stress analysis purposes when it was supported around the toroidal shell is shown in Fig. 2. When the vessel was supported from the cylinder, cuts were made only at the cylinder-torus and torus-spherical cap junctions.

The elastic stress distributions throughout the toroidal shell, as calculated by the methods outlined in the Appendix, have been obtained for three cases. These are:

1 Constant pressure of 60 psig, supports on cylinder.

2 Constant pressure of 60 psig, supports on torus.

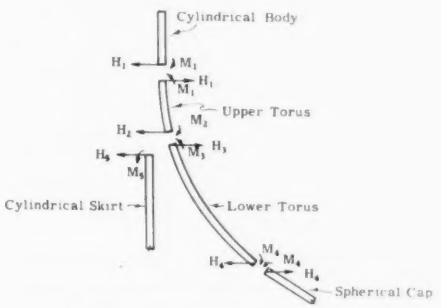

(a) Unknown edge moments and horizontal shears

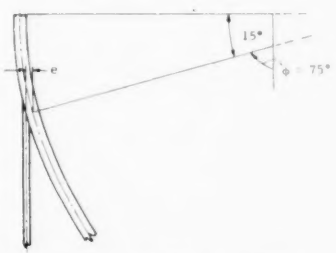

(b) Detail at skirt-torus junction

Fig. 2 Method of analyzing the vessel when supported around the torus at $\phi = 75$ deg

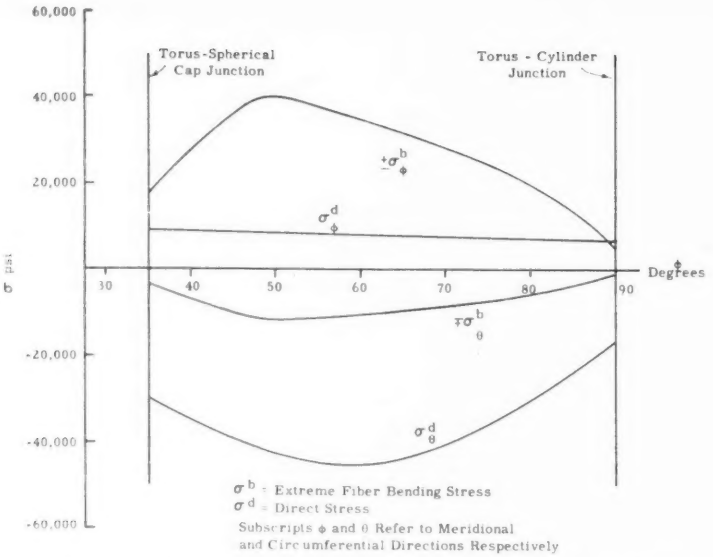

Fig. 3 Stresses in torus. Constant internal pressure of 60 psig, supports on cylinder.

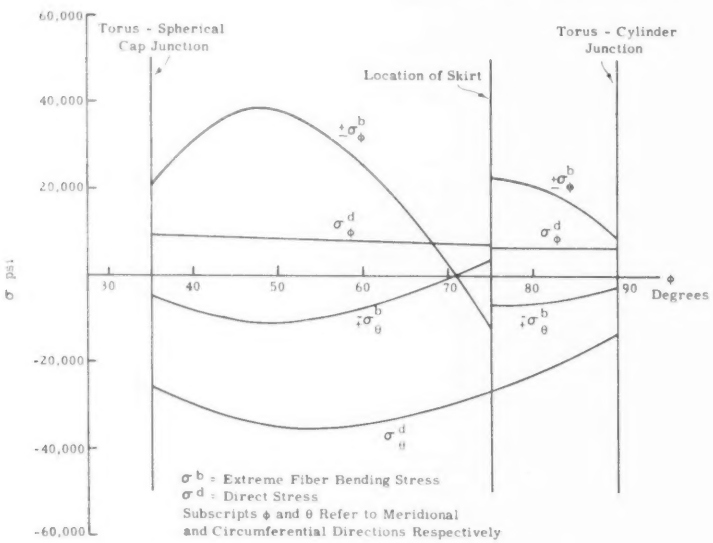

Fig. 4 Stresses in torus. Constant internal pressure of 60 psig, supports on torus.

3 · Hydrostatic loading plus an additional constant pressure of 34 psig, supports on torus.

The corresponding stress distributions are given in Figs. 3–5. The positions of the elastically deformed torus for cases (1) and (3) are also shown in Fig. 6. It can be seen that the maximum deflection is only about 1/3 of the shell thickness. Thus small-deflection theory, which was used in the analyses, should be quite accurate.

The stress distributions throughout the spherical cap and cylinder have not been plotted since they were not as severe as the stresses in the torus. The stresses in the skirt for case (3) are, however, given in Fig. 7.

In what follows the salient points about cases (1), (2), and (3) will be briefly summarized. The fact that the vessel material was assumed to have a yield point of 30,000 psi will be ignored temporarily.

Constant Pressure—Supports on Cylinder

From Fig. 3 it can be seen that:

(*a*) The maximum value of the circumferential direct stress $\sigma_\theta{}^d$, is 45,000 psi compression. Also, between 35 deg $< \phi <$ 80 deg, the circumferential direct stress is greater than 30,000 psi.

(*b*) The meridional bending stress $\sigma_\phi{}^b$ has a maximum value of $\pm$40,000 psi (tension on the inside of the torus) and it is greater than $\pm$30,000 psi over an arc of 30 deg.

(*c*) The meridional direct stress, $\sigma_\phi{}^d$, is quite small, having a maximum value of 9,000 psi.

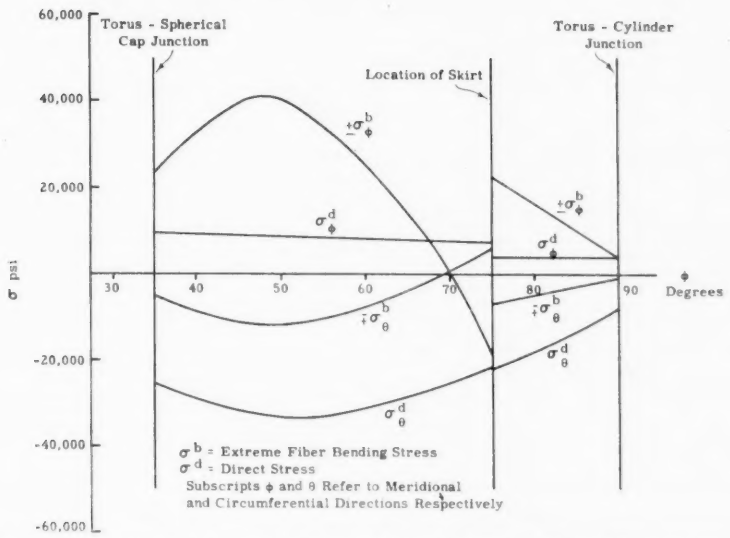

Fig. 5 Stresses in torus. Hydrostatic plus constant internal pressure of 34 psig, supports on torus.

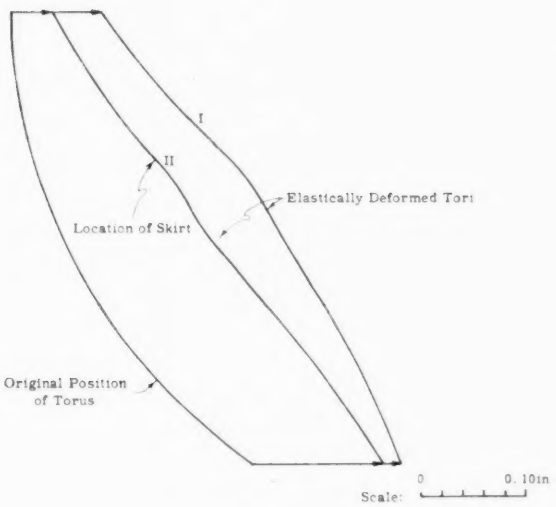

I = Constant Internal Pressure of 60 psig - Supports on Cylinder
II = Hydrostatic Plus Constant Internal Pressure of 34 psig - Supports on Torus

Fig. 6 Deflected positions of elastic tori

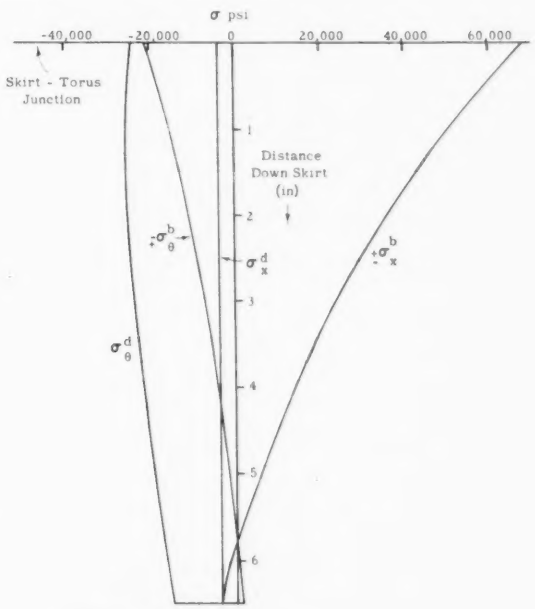

$\sigma^b = $ Extreme Fiber Bending Stress
$\sigma^d = $ Direct Stress
Subscripts x and θ Refer to Axial and Circumferential Directions Respectively

Fig. 7 Stresses in cylindrical skirt. Hydrostatic plus constant internal pressure of 34 psig, supports on torus

Constant Pressure—Supports on Torus

Comparing Figs. 3 and 4 it can be seen that the skirt has the effect of reducing the maximum value of $\sigma_\theta{}^d$ from 45,000 psi to 36,000 psi. The maximum value of $\sigma_\phi{}^b$ is also decreased slightly and the locations of the two maximums are changed somewhat.

The skirt also considerably alters the distribution of the meridional and circumferential bending stresses. The maximum value of $\sigma_\phi{}^b$ at the location of the skirt attachment is 23,000 psi, which is not an excessive discontinuity stress.

Hydrostatic Plus Constant Pressure—Supports on Torus

Actually there is not much difference between the stress distributions of cases (2) and (3). The maximum values of $\sigma_\phi{}^b$ and $\sigma_\theta{}^d$ differ by only ± 2000 psi. The stresses at the cylinder-torus junction for case (2) are nearly twice as high as those for case (3); however, they are small anyway. The compressive value of $\sigma_\phi{}^b$ at the skirt attachment is 50 per cent higher for case (3) than for case (2). The value of $\sigma_\theta{}^d$ is also slightly lower at this location.

The stresses in the skirt for this case are quite substantial as can be seen from Fig. 7. The maximum bending stress is ±68,000 psi and the maximum circumferential direct stress is about −26,000 psi. Similar stresses are found in the skirt for case (2) loading also.

Comparison of Code Predictions and the Results of the Accurate Stress Analyses

Supports on Cylinder

For the case where the supports were on the cylinder, and the vessel was subjected to a constant internal pressure of 60 psig, it has been seen that the ASME Code predicted a stress in the torispherical head of 18,000 psi.[6] Further, using some results given in the PVRC report [2], it has been estimated that the maximum localized stress was about 45,000 psi.

From the preceding section, it has been shown that the maximum direct stress for the constant pressure case was −45,000 psi. The maximum meridional stresses in the torus were 48,000 psi (inside) and −32,000 psi (outside), and the maximum circumferential stress was −55,000 psi (outside). Thus if the material did not yield, the Code would have predicted a stress which was less than one half the maximum meridional and circumferential stresses that actually occurred. The estimate of maximum localized stress, which is not considered by the Code, is also somewhat low. However, the way in which the Code errs most seriously is in not bringing the designer's attention to the large circumferential direct stresses which occurred in this example. As mentioned hitherto, they are greater than 30,000 psi for practically the entire arc length of the torus.

It has been assumed that the actual vessel material has a yield point of 30,000 psi. Thus the stress distributions given in Fig. 3 will not occur. If the meridional stresses are neglected, then an approximate estimate of the pressure p at which the vessel wall first reaches the fully plastic distribution (in the circumferential direction, at $\phi = 60$ deg) can be obtained from the relation:

$$\sigma_y^2 = \sigma_d^2 + \frac{2}{3}\sigma_y\sigma_b \qquad (2)$$

where

σ_y = yield point of material, psi
σ_d = direct stress, psi
σ_b = bending stress, psi

Use of equation (2) and the results of Fig. 3 indicates that p = 37 psig. Because of the presence of the meridional stresses, the vessel wall will become fully plastic somewhat before this value. After this occurs, the circumferential stress at this point will maintain its yield point value despite the increasing pressure. Other points will begin to yield and the equations of equilibrium have to be modified for the circumferential areas which have become plastic. The problem becomes rather complex because parts of the shell are fully plastic while other parts are still fully elastic. Instead of attempting to deal with the elastoplastic shell, it was decided that a better approach to the problem would be to determine the limit load of the shell. This was calculated by Profs. D. C. Drucker and R. T. Shield of Brown University. Their approach will be briefly described.

The limit analysis is concerned with predicting an upper bound for the maximum pressure the shell can carry without failing due to plastic action. A possible deformation pattern of the shell is first assumed, consisting of a yield hinge in the cylindrical shell, at the mid-point of the torus, and in the spherical cap. The rate at which energy is dissipated due to plastic action is then calculated and an upper bound for the collapse pressure is found from the following theorem of limit analysis:

External rate of doing work = rate of plastic dissipation of energy.

Using this procedure, Drucker and Shield calculated that the collapse pressure for the case under consideration would be about 49 psig [5].

Thus for the torispherical head under a constant internal pressure of 60 psig, with the supports on the cylinder, the situation may be summarized as follows:

1 The Code predicts a fairly modest stress and thus the vessel would be considered safe.

2 The accurate stress analysis predicts high circumferential direct stresses and fairly high meridional bending stresses. If the vessel material has a yield point of 30,000 psi, then a fully plastic stress distribution occurs in the circumferential direction at a pressure lower than 40 psig. If the material has a high yield point, then it appears possible that the shell might buckle elastically in the circumferential direction.

3 The limit analysis predicts a collapse pressure of 49 psig. Thus the subject vessel, if made of a brittle material with no appreciable strain-hardening, would have failed during the proof-test. If the material had been ductile and tested at 60 psig, then large deformations, many times the shell thickness, would have occurred.

Hence for the case under discussion it can be concluded that the provisions of the current ASME Code, as it relates to torispherical heads, can lead to unsafe design.

It may also be mentioned, in connection with item (3), that as larger vessels are built for the same internal pressure, so the method of testing the vessel becomes more important. This is because of the tendency of notch ductility to decrease, and transition temperature to increase, with increasing plate thickness. The present Code (Paragraph UG-99(h)) recommends that the minimum test temperature be 60 F. As this recommended temperature may be lower than the transition temperature of the thicker plate thicknesses (>3/4 inch), caution should be exercised in deciding the temperature at which a test should be conducted.

Supports on Torus

In applying the Code it was assumed that an investigation of local effects was not warranted when the vessel was supported around the torus. Thus for the constant pressure case, the Code's predictions of stress will be the same as when the vessel is supported from the cylinder. For the hydrostatic plus constant pressure case, with the supports on the torus, the Code would have predicted somewhat higher stresses than for the constant pressure case.

The accurate analyses, however, show that the maximum meridional stresses are approximately the same for all the cases. Also, the direct circumferential stress decreases by about 20 per cent when the supports are on the torus. Use of equation (2) (and neglecting, as before, the meridional stresses) then indicates that the vessel wall becomes fully plastic in the circumferential direction at a pressure of 47 psig. Also, neglecting the circumferential stresses, use of equation (2) and the results of Fig. 7 indicates that a yield hinge will form at the skirt-torus junction at a pressure of 39 psig.

Unfortunately, a limit analysis of the vessel with the supports around the torus has not been made as yet. However, the values of the pressures quoted in the preceding paragraph for the formation of yield hinges indicate that the collapse pressure of the vessel with the supports around the torus should not be too different from that with the supports on the cylinder. Thus for

[6] It is of interest to note that application of the British Code [4] to this case gives σ = 25,000 psi.

this case also, it is apparent that the Code does not give an adequate representation of the stresses which occur.

Comments on Two Approximations Commonly Used in Shell Theory

In analyzing shells subjected to both internal pressure and edge bending loads, approximations are frequently made in shell theory with regard to a particular solution of the nonhomogeneous differential equations. Two common approximations are:

(*a*) The transverse shear Q_ϕ and the rotation V, are both set equal to zero, and the stress resultants N_ϕ and N_θ are given by their membrane values.

(*b*) Same as (*a*), except that the rotation V is given by the membrane rotation V_m.

The approximation (*a*) for toroidal shells is discussed by Clark [6] who points out that it is not valid in the neighborhood of $\phi = 0, \pm \pi$. Hildebrand [7] discusses both approximations in connection with his paper on asymptotic integration. His work indicates that, for the case to be considered later, the assumption that V_m is an adequate particular integral for V should be quite good.

Both approximations were used to calculate the stress distributions ($\sigma_\phi{}^b$ and $\sigma_\theta{}^d$) throughout the torus of the torispherical head of the example vessel. The homogeneous solutions used in each case were those previously obtained by numerical integration. The loading considered was a constant internal pressure of 60 psig and the supports were assumed to be on the cylinder. For constant internal pressure the membrane rotation of the torus is given by the expression:

$$EV_m = -\frac{ph \cot \phi}{2h} \cdot \frac{\lambda}{\sin \phi}\left(1 + \frac{\lambda}{\sin \phi}\right)\left(\frac{2\lambda}{\sin \phi} - 1\right) \quad (3)$$

Equation (3) was used in connection with the approximation (*b*) just mentioned; when using it the membrane moments were also neglected.

The end results of the two approximations are given in Fig. 8. These curves should be compared with the $\sigma_\phi{}^b$ and $\sigma_\theta{}^d$ curves obtained by numerical integration of the complete differential equation, which are given in Fig. 3. It can be seen that approximation (*a*), while giving maximum values of $\sigma_\phi{}^b$ and $\sigma_\theta{}^d$ which are approximately correct, gives an entirely different stress distribution to that actually occurring. Approximation (*b*) gives a reasonable maximum value for $\sigma_\theta{}^d$ and the distribution is not too far off; the meridional bending stress distribution, however, is incorrect by a factor of two or more. Thus neither approximation can be considered satisfactory for the shell under discussion.

The reason the approximations do not give good results in this case is because the membrane rotations are very large at the lower end of the shell ($\phi = 35$ deg). The membrane moments then become of importance and the assumption that $Q_\phi = 0$ in the particular solution is no longer reasonable. This is in line with Hildebrand's general results where he shows that setting $V = V_m$, $Q_\phi = 0$ as a particular solution neglects a resultant of order of magnitude $k^{-4}EhV_m$ where k, for a torus, is given by

$$k^2 = [3(1 - \nu^2)]^{1/2} \frac{b}{h(1 + \lambda/\sin \phi)_{\text{ref}}} \quad (4)$$

Taking the reference station at $\phi = 90$ deg and substituting the numerical values gives $k = 2.53$. Since this is a relatively low value of k, and as EhV_m is so large for the values of ϕ toward the lower edge of the shell, the neglected resultant is quite substantial.

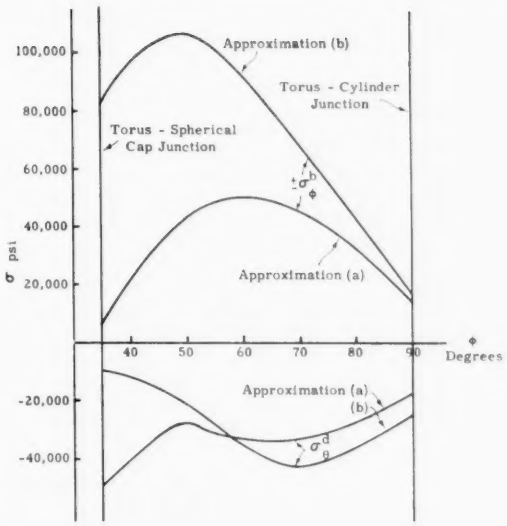

σ_ϕ^b = Extreme Fiber Meridional Bending Stress

σ_θ^d = Circumferential Direct Stress

Approximation (a) Neglects Membrane Rotations

Approximation (b) Includes Membrane Rotations

Fig. 8 Stresses in torus using approximate particular integrals. Constant internal pressure of 60 psig, supports on cylinder.

Conclusions

Since only one torispherical shell geometry has been investigated, the following conclusions really apply only to it. It is believed, however, that further study will show them to be valid for a range of shell geometries.

1 Assuming the head remained elastic, the current edition of the Code predicted a stress which was less than one half the maximum meridional and circumferential stresses actually present. Of greater significance, however, is the fact that the Code gave no indication of the high circumferential direct stresses which were present over practically the entire torus.

2 For similar heads, constructed from materials with relatively low yield points and designed in accordance with the Code, either the head will fail during the proof-test or large deformations will result. The first circumstance will happen if a defect is present and the material of the head is notch-brittle, the second if it is notch-ductile.

3 For heads made from a high yield point material, it appears possible that elastic buckling might take place.

4 Supporting the vessel around the bottom head in the manner discussed herein did not increase the elastic stresses in the head. The bending stresses remained about the same and the direct circumferential stress decreased.

5 Care should be taken in evaluating a particular solution of the differential equations for toroidal shells, even when the colatitude angle ϕ is as large as 35 deg.

Until further research has established the ranges over which the present Code formula is applicable, and amended it for other ranges, it is recommended that caution be exercised when designing torispherical shells by the Code. This is especially so if the vessel has geometric ratios which differ substantially from past practice. In this connection it might be mentioned that Drucker and Shield, of Brown University, are currently calcu-

lating limit loads for torispherical shells of various geometries and yield points. This work, when it becomes available, should be of considerable value to designers.

Acknowledgments

The author would like to acknowledge the assistance he has received from J. R. M. Radok and L. B. Rall of the Emeryville Research Center in numerically integrating the differential equations of equilibrium for the torus and the spherical cap.

APPENDIX

Differential Equations of Equilibrium for Surfaces of Revolution Subjected to Nonuniform Internal Pressure

By extending the analysis given in Timoshenko [3], the following differential equations are obtained for constant thickness shells of revolution subjected to nonuniform internal pressure p and edge bending loads:[6]

$$L(U) + \frac{\nu}{r_1} U - EhV = g(\phi) \tag{5}$$

$$L(V) - \frac{\nu}{r_1} V + \frac{U}{D} = 0 \tag{6}$$

where

$$L(\ldots) = \frac{r_2}{r_1^2}(\ldots)'' + \frac{1}{r_1}\left[\left(\frac{r_2}{r_1}\right)' + \frac{r_2}{r_1}\cot\phi\right](\ldots)' - \frac{\cot^2\phi}{r_2}(\ldots) \tag{7}$$

and the primes indicate differentiation with respect to ϕ. The notation used is similar to that of Timoshenko and is as follows:

$U = r_2 Q_\phi$
Q_ϕ = transverse shearing force
V = angle of rotation of a tangent to a meridian
h = shell thickness
r_1 = meridional radius of curvature
r_2 = radius of curvature in the normal plane perpendicular to a meridian
D = bending rigidity of shell $= Eh^3/12(1 - \nu^2)$
E = modulus of elasticity
ν = Poisson's ratio
ϕ = angle measured from the vertical axis of revolution

The right-hand side of equation (5) is given by:

$$g(\phi) = -\frac{1}{r_2 \sin^2\phi}\left[\left(1 - \frac{r_2^2}{r_1^2}\right)\cot\phi + \frac{r_2}{r_1}\left(\frac{r_2}{r_1}\right)'\right]\Lambda + \frac{1}{r_1}(pr_2^2)' \tag{8}$$

where p is the internal pressure.

The function Λ in equation (8) is given by:

$$\Lambda = \frac{1}{2}\int p\frac{d}{d\phi}(r_2^2 \sin^2\phi)\,d\phi = \int pr_1 r_2 \sin\phi\cos\phi\,d\phi \tag{9}$$

For shells of constant thickness whose meridional radius of curvature r_1 is also constant, equations (5) and (6) can be reduced to a single second-order complex differential equation. This reduction is quite well known (see, for example, Reference [8]) and will be described only briefly.

[6] These equations can also be obtained from equations (12), (13), and (14) of Reference [7].

Let a quantity Z be introduced such that:

$$Z = U + kV \tag{10}$$

where k is a constant defined by:

$$k = -\frac{D}{r_1}(\nu \pm i\mu^2 r_1) \tag{11}$$

and

$$\left.\begin{aligned}\mu^2 r_1 &= \left[m^4\left(\frac{r_1}{h}\right)^2 - \nu^2\right]^{1/4}\\ m^4 &= 12(1 - \nu^2)\\ i &= \sqrt{-1}\end{aligned}\right\} \tag{12}$$

Multiplying equation (6) by k, adding it to equation (5), and using equations (10), (11), and (12), yields the following equation in Z:

$$L(Z) \mp i\mu^2 Z = g(\phi) \tag{13}$$

If the two linearly independent solutions of

$$L(Z) - i\mu^2 Z = g(\phi) \tag{14}$$

are

$$\left.\begin{aligned}Z_1 &= x_1 + iy_1 + (P + iQ)\\ Z_2 &= x_2 + iy_2 + (P + iQ)\end{aligned}\right\} \tag{15}$$

where $(P + iQ)$ is a particular solution of equation (14), then the complex conjugates $\bar{Z}_1$ and $\bar{Z}_2$ are solutions to:

$$L(Z) + i\mu^2 Z = g(\phi) \tag{16}$$

Thus Z_1 and Z_2, together with their complex conjugates, represent the complete system of independent solutions of equation (13).

From equation (10)

$$\left.\begin{aligned}Z &= U + kV\\ \bar{Z} &= U + \bar{k}V\end{aligned}\right\} \tag{17}$$

Adding and subtracting the relations (17) and using equation (11)

$$\left.\begin{aligned}DV &= i(Z - \bar{Z})/2\mu^2\\ U &= \frac{1}{2}(Z + \bar{Z}) + \nu r_1 DV\end{aligned}\right\} \tag{18}$$

The solution to equation (14) may be written as

$$Z = (A_1 + iB_1)(x_1 + iy_1) + (A_2 + iB_2)(x_2 + iy_2) + P + iQ \tag{19}$$

or, alternatively,

$$Z = (A_1x_1 - B_1y_1 + A_2x_2 - B_2y_2 + P) + i(A_1y_1 + B_1x_1 + A_2y_2 + B_2x_2 + Q) \tag{20}$$

where $A_1 \ldots B_2$ are arbitrary constants.

Use of equations (17) and (20) then determines U and V in terms of $A_1 \ldots B_2$. It is somewhat more convenient to define new constants such that

$$\left.\begin{aligned}C_1 &= A_1 - \nu B_1/\mu^2 r_1\\ D_1 &= -\nu A_1/\mu^2 r_1 - B_1\end{aligned}\right\} \tag{21}$$

etc.

The solutions for U and V then become:

$$U = C_1x_1 + D_1y_1 + C_2x_2 + D_2y_2 + P - \nu Q/\mu^2 r_1 \tag{22}$$

$$Ehr_1V = C_1(\nu x_1 - \mu^2 r_1 y) + D_1(\nu y_1 + \mu^2 r_1 x_1) + C_2(\nu x_2 - \mu^2 r_1 y_2) + D_2(\nu y_2 + \mu^2 r_1 x_2) - m^4 r_1 Q/\mu^2 h^2 \quad (23)$$

Knowing U and V the stress resultants can be found from the following equations:

$$\left.\begin{aligned} N_\phi &= -U \cot \phi/r_2 + \frac{\Lambda}{r_2 \sin^2 \phi} && (a)\\ N_\theta &= -U'/r_1 - \frac{\Lambda}{r_1 \sin^2 \phi} + pr_2 && (b)\\ M_\phi &= -D(V'/r_1 + \nu V \cot \phi/r_2) && (c)\\ M_\theta &= -D(V \cot \phi/r_2 + \nu V'/r_1) && (d)\\ Q_\phi &= U/r_2 && (e)\\ H_\phi &= \frac{Q_\phi}{\sin \phi} && (f) \end{aligned}\right\} \quad (24)$$

For shells with constant r_1 the function $g(\phi)$ can also be written as:

$$g(\phi) = \frac{\cot \phi}{r_2 \sin^2 \phi}\left(2\frac{r_2}{r_1} + 1\right)\left(\frac{r_2}{r_1} - 1\right)\Lambda - 2pr_2 \cot \phi\left(\frac{r_2}{r_1} - 1\right) + \frac{p' r_2^2}{r_1} \quad (25)$$

The horizontal displacement δ can be found from the relation:

$$E\delta = \frac{r_2 \sin \phi}{h}(N_\theta - \nu N_\phi) \quad (26)$$

Before specializing these general equations so that they apply to toroidal and spherical shells under hydrostatic plus constant internal pressure, the closed-form solution for the cylinder will first be given.

Deformations of Cylinder

The cylinder referred to is the cylindrical body of the pressure vessel shown in Fig. 1. The moment and shear acting on the cylinder at its junction with the torus are, from Fig. 2(*b*), M_1 and H_1. From the equations of static equilibrium the axial force in the cylinder is found to be (neglecting the dead weight of the cylinder):

$$N_x = \frac{1}{2} R_c(\bar{p} + \gamma_w R_c/3) \quad (27)$$

where

$\bar{p}$ = constant internal pressure, psig
R_c = radius of cylinder, in.
γ_w = density of water, lb/in.^{2}/in.

Extending the analysis given in Reference [3] to include the effect of a constant axial force, the following are obtained for the displacement and rotation at the lower end of the cylinder:

$$Eu_c = R_c^2/h_c\left[\bar{p}(1 - \nu/2) + \gamma_w\left(H + R_c - \frac{\nu R_c}{6}\right)\right] + \frac{1}{2\beta^3 D_c}(\beta M_1 + H_1) \quad (28)$$

$$EV_c = R_c^2 \gamma_w/h_c + \frac{1}{2\beta^2 D_c}(2\beta M_1 + H_1) \quad (29)$$

where

u_c = edge radial displacement (+ outwards)
$V_c = d/dx(u_c)$ = edge rotation (+ when tangent rotates outwards)

$D_c = Eh_c^3/12(1 - \nu^2)$
$\beta^4 = 3(1 - \nu^2)/R_c^2 h_c^2$
H = height of cylinder

If the vessel is supported above the cylinder-torus junction, N_x is increased by

$$\Delta N_x = W/2\pi R_c \quad (30)$$

where

W = weight of vessel and contents

Equation (28) must then be modified accordingly.

The Spherical Cap

For this case $r_1 = r_2 = r$. Thus from equations (7) and (8)

$$\left.\begin{aligned} L(\ldots) &= \frac{1}{r}[(\ldots)'' + \cot \phi\,(\ldots)' - \cot^2 \phi\,(\ldots)]\\ \text{and } g(\phi) &= rp' \end{aligned}\right\} \quad (31)$$

The pressure at any angle ϕ from the vertical on the spherical cap is given by

$$p = k + \gamma_w r \cos \phi \quad (32)$$

where

$$k = \bar{p} + \gamma_w[H + R - (r - b)\cos \alpha] \quad (33)$$

b = meridional radius of curvature of torus
α = value of ϕ at spherical cap-torus junction

Hence the differential equation for the spherical cap becomes, from equations (14), (31), and (32):

$$Z'' + \cot \phi Z' - \cot^2 \phi Z - i\mu^2 r Z = -\gamma_w r^3 \sin \phi \quad (34)$$

From equations (9) and (32):

$$\Lambda = \frac{kr^2}{2}\sin^2 \phi - \frac{\gamma_w r^3}{3}\cos^3 \phi + C \quad (35)$$

From equations (24*a*) and (35):

$$N_\phi = -\frac{U}{r}\cot \phi + \frac{kr}{2} - \frac{\gamma_w r^2 \cos^3 \phi}{3 \sin^2 \phi} + \frac{C}{r \sin^2 \phi} \quad (36)$$

At $\phi = 0$, $U = 0$ (from symmetry considerations).
Thus

$$C = \gamma_w r^3/3 \quad (37)$$

and

$$N_\phi = -\frac{U}{r}\cot \phi + \frac{kr}{2} + \frac{\gamma_w r^2}{3 \sin^2 \phi}(1 - \cos^3 \phi) \quad (38)$$

From equations (24*b*), (32), (35), and (37):

$$N_\theta = -\frac{U'}{r} + kr/2 + \frac{\gamma_w r^2}{3 \sin^2 \phi}(3 \cos \phi - 2 \cos^3 \phi - 1) \quad (39)$$

The Toroidal Shells

The toroidal shell joining the cylindrical body with the spherical cap will be considered in two parts in what follows. The upper torus, with $75° < \phi < 90°$, lies between the cylindrical body and the skirt. The lower torus, with $35° < \phi < 75°$, lies between the skirt and the spherical cap.

For a torus, the principal radii of curvature are given by [see Fig. 1(*b*)]:

$$\left.\begin{aligned} r_1 &= b\\ r_2 &= b(1 + \lambda/\sin \phi) \end{aligned}\right\} \quad (40)$$

where

$$\lambda = a/b$$

Inserting the relations (40) into equations (7) and (8) there follows:

$$L(\ldots) = \frac{f(\phi)}{b}(\ldots)'' + \frac{\cot\phi}{b}(\ldots)' - \frac{\cot^2\phi}{bf(\phi)}(\ldots)$$

and

$$g(\phi) = \frac{\lambda\cot\phi}{b\sin^3\phi f(\phi)}\left(\frac{2\lambda}{\sin\phi} + 3\right)\Lambda + b[pf^2(\phi)]' \qquad (41)$$

where

$$f(\phi) = 1 + \frac{\lambda}{\sin\phi}$$

The function Λ has to be evaluated for the upper and lower tori separately. The lower torus will be considered first.

The pressure at any angle ϕ in the torus is:

$$p = q + \gamma_w b\cos\phi \qquad (42)$$

where

$$q = \bar{p} + \gamma_w(H + R) \qquad (43)$$

From equations (9) and (42)

$$\Lambda = \frac{qr_2^2\sin^2\phi}{2} - \frac{\gamma_w b^3}{3}\cos^3\phi + \gamma_w\lambda b^3(\phi/2 + 1/4\sin 2\phi) + C_1 \qquad (44)$$

From equations (24a) and (44), N_ϕ for the lower torus can be determined. Equating N_ϕ for the spherical cap and the torus at $\phi = \alpha$ enables C_1 to be found. One obtains:

$$C_1 = \gamma_w\left\{\frac{r^3}{3}(1 - \cos^3\alpha) + b^3\left[1/3\cos^3\alpha - \lambda\left(\frac{\alpha}{2} + 1/4\sin 2\alpha\right)\right] - \frac{\lambda b r^2}{4}\sin 2\alpha\right\} \qquad (45)$$

This value of C_1 applies throughout the entire torus ($35° < \phi < 90°$) if the vessel is supported above the torus-cylinder junction. However, when the skirt is located at $\phi = 75$ deg on the torus, it does not apply for the upper torus. The constant applicable to this latter area is obtained by equating N_ϕ for the torus at $\phi = 90$ deg with N_z for the cylinder [given by equation (27)]. The constant for this case, C_2, is then given by:

$$C_2 = -\gamma_w(1/2\,HR_c^2 + 1/3\,R_c^3 + 1/4\,\pi\lambda b^3) \qquad (46)$$

The differential equations for the two toroidal shells become:

$$Z'' + \frac{\cot\phi}{f(\phi)}Z' - \left(\frac{\cot\phi}{f(\phi)}\right)^2 Z - \frac{i\mu^2 b}{f(\phi)}Z = G(\phi) \qquad (47)$$

where $G(\phi)$ is given by:

$$G(\phi) = \frac{qb^2\lambda}{2}\frac{\cot\phi}{\sin\phi}\left(\frac{2\lambda}{\sin\phi} - 1\right) - 2\gamma_w\lambda b^3\cot^2\phi - \gamma_w b^3\sin\phi f(\phi) + \frac{\lambda\cot\phi}{f^2(\phi)\sin^3\phi}\left(\frac{2\lambda}{\sin\phi} + 3\right)\left[C + \gamma_w\lambda b^3\left(\frac{\phi}{2} + \frac{1}{4}\sin 2\phi\right) - 1/3\gamma_w b^3\cos^3\phi\right] \qquad (48)$$

where C is given by either equation (45) or (46).

If the internal pressure has the constant value q, e.g., if produced by a gas, then $C_1 = C_2 = 0$. The function $G(\phi)$ then reduces to:

$$G(\phi) = \frac{qb^2\lambda}{2}\frac{\cot\phi}{\sin\phi}\left(\frac{2\lambda}{\sin\phi} - 1\right) \qquad (49)$$

Solution of the Differential Equations of Equilibrium

In the remainder of the Appendix, details will be given of the most complicated problem discussed in the paper, i.e., hydrostatic plus a constant internal pressure of 34 psig, with the supports on the torus. The other two problems considered in the paper can either be solved similarly or much more simply. This latter situation occurs if the supports are on the cylinder.

Equations (34) and (47) are nonhomogeneous, second-order, linear complex ordinary differential equations. As they are complex equations the complete solution will contain [as shown by equation (19)] four solutions of the homogeneous equation plus a particular solution. An accurate and easy-to-use solution of the equations is, particularly for the tori, rather difficult to obtain. There are various approximate techniques that could be used. However, since a high-speed electronic digital computer was available, this was used instead.

For the spherical cap a particular solution can easily be found in closed form. This is given by:

$$Z = \frac{\gamma_w r^3}{1 + i\mu^2 r}\sin\phi \qquad (50)$$

Substituting $Z = x + iy$ in equation (34) with the right-hand side set equal to zero, and equating the real and imaginary parts,

$$x'' = -\cot\phi x' + \cot^2\phi x - \mu^2 ry$$
$$y'' = -\cot\phi y' + \cot^2\phi y + \mu^2 rx \qquad (51)$$

The homogeneous solutions were obtained by numerically integrating the two simultaneous differential equations (51). Since the spherical cap includes the angle $\phi = 0$, only one complex solution has to be determined. This is because it is known, from the analytic solution, that one of the complex homogeneous solutions becomes infinite at $\phi = 0$. The results of the numerical integration for selected values of ϕ are given in Table 1.

Table 1 Homogeneous solutions for the spherical cap

ϕ, degrees	x	x'	y	y'
5	−0.092702	−2.85901	0.049929	−1.10091
10	0.007229	15.8382	−0.647489	−14.0242
15	3.86274	28.3553	2.44011	149.791
20	−30.6797	−1070.25	14.6522	−410.560
25	31.1898	7076.07	−259.039	−5318.66
30	1579.91	5654.52	1295.75	69390.0
35	−15434.1	−491281	5044.38	−258157

As far as the two toroidal shells are concerned, both the homogeneous and the particular solutions were obtained by numerical integration. The equations to be integrated are obtained in a similar manner to those for the spherical cap. The end results, for the three problems discussed in the body of the paper, are given in Tables 2 and 3 for selected values of ϕ.

For both the spherical cap and the tori the relevant differential equations were integrated at 1/2-degree intervals. They have been tabulated at selected values only in the interest of brevity.

Deformations of Spherical Cap and Tori in Terms of Edge Moments and Shears

From the numerical integration results, and equations (22)

Table 2 Homogeneous solutions for the torus

ϕ [degrees]	x_1	$\dot{x}_1$	y_1	$\dot{y}_1$	x_2	$\dot{x}_2$	y_2	$\dot{y}_2$
90	138.312	0	0	0	0	100.000	0	0
80	137.436	19.9667	26.9497	−308.088	−17.4430	99.5732	−1.13201	19.4121
75	133.919	66.6582	60.4184	−458.036	−26.0540	97.3145	−3.80263	43.3145
65	105.254	296.827	164.522	−723.376	−41.7541	78.1068	−17.2784	116.148
55	16.5967	760.072	305.984	−867.735	−51.0473	19.9084	−45.6552	211.045
45	−173.285	1447.04	452.979	−764.113	−45.2079	−97.8301	−90.8128	303.265
35	−495.256	2246.90	551.354	−296.931	−13.1170	−279.601	−149.353	358.455

and (24), one can obtain the moments M_ϕ and horizontal shears H_ϕ at the various cut edges in terms of $C_1 \ldots D_2$ and the particular solutions. Equations are obtained of the form:

$$\{x\} = [a]\{y\} + \{b\} \tag{52}$$

where the vectors x, y, and b represent the edge moments and shears, the constants $C_1 \ldots D_2$, and the particular solutions, respectively; the elements of the square matrix a are obtained from equations (24c) and (24f) and the numerical integration results.

Three equations similar to equation (52) will be obtained: One for the upper torus, one for the lower torus, and one for the spherical cap. The vectors and matrices will be different for each shell, of course. Solving equation (52) in the usual way one obtains:

$$\{y\} = [a^{-1}]\{x - b\} \tag{53}$$

Thus the constants C_1, etc., can be determined in terms of the edge moments and shears and certain numerical values. From equations (23), (26), and (53) the edge values of the rotation and horizontal displacement of the shells can then be obtained in terms of their respective edge moments and shears and certain constants.

As an illustration of the foregoing procedure, consider the lower toroidal shell. Using the results of Tables 2 and 3, equations (24c) and (24f), the following relations may be written:

Table 3 Particular solutions for the torus

(a) = Constant pressure of 60 psig.
(b) = Hydrostatic + constant pressure of 34 psig. C given by equation (45).
(c) = Hydrostatic + constant pressure of 34 psig. C given by equation (46).

(a)

ϕ [degrees]	P	$\dot{P}$	Q	$\dot{Q}$
90	138.312	0	0	0
80	853.904	−12401.7	40.7612	−703.820
75	2591.18	−28630.4	165.339	−2462.30
65	12065.4	−86161.0	1514.10	−16183.8
55	35347.6	−190311	7549.58	−60000.9
45	83105.9	−375583	25751.0	−160617
35	176856	−747203	68826.7	−351001

(b)

ϕ [degrees]	P	$\dot{P}$	Q	$\dot{Q}$
90	138.312	0	0	0
80	835.426	−12230.3	40.0718	−688.835
75	2557.64	−28467.7	162.212	−2418.71
65	12020.4	−86251.6	1495.71	−16048.7
55	35372.0	−191112	7501.86	−59822.3
45	83385.9	−377885	25685.6	−160662
35	177775	−752624	68829.8	−351875

(c)

ϕ	P	$\dot{P}$	Q	$\dot{Q}$
90	138.312	0	0	0
80	447.354	−5502.27	32.5907	−474.487
75	1226.70	−12024.9	105.382	−1333.12

$$\begin{pmatrix} H_3 \\ -M_3 \\ H_4 \\ -M_4 \end{pmatrix} = \begin{pmatrix} 0.972627 & 0.438807 & -0.189225 & -0.027618 \\ 4.72629 & 0.688086 & -0.443837 & 1.00366 \\ -3.79498 & 4.22484 & -0.100511 & -1.14444 \\ 2.94168 & 23.0205 & -3.65787 & -2.88106 \end{pmatrix} \begin{pmatrix} C_1 \\ D_1 \\ C_2 \\ D_2 \end{pmatrix} + \begin{pmatrix} 18.5720 \\ 24.9655 \\ 1362.23 \\ 3610.01 \end{pmatrix} \tag{54}$$

Solving equation (54) one finds:

$$\begin{pmatrix} C_1 \\ D_1 \\ C_2 \\ D_2 \end{pmatrix} = \begin{pmatrix} 3.31740 & -0.462363 & 0.965474 & 0.254244 \\ 0.747874 & -0.511039 & 0.734428 & 0.120877 \\ 14.8947 & -3.55566 & 6.95393 & 1.66642 \\ -9.54783 & -0.041081 & -1.97482 & -0.543197 \end{pmatrix} \begin{pmatrix} H_3 \\ M_3 \\ H_4 \\ M_4 \end{pmatrix} + \begin{pmatrix} -470.531 \\ -590.741 \\ -3822.45 \\ 905.508 \end{pmatrix} \tag{55}$$

From Tables 2 and 3, and equations (23) and (26), $E\delta$ and EV can be obtained in terms of $C_1 \ldots D_2$ and numerical values. Inserting the values for C_1, etc., given by equation (55) into these relations yields the following:

$$\begin{pmatrix} EV^l_{75} \\ E\delta^l_{75} \\ EV^l_{35} \\ E\delta^l_{35} \end{pmatrix} = \begin{pmatrix} 1738.76 & -447.940 & 997.479 & 180.315 \\ -10984.5 & 1738.91 & -3839.42 & -1205.69 \\ 1272.11 & -190.27 & 1428.43 & 473.45 \\ 4050.20 & -1052.34 & 8043.90 & 1428.43 \end{pmatrix} \begin{pmatrix} H_3 \\ M_3 \\ H_4 \\ M_4 \end{pmatrix} - \begin{pmatrix} 752,700 \\ 4,317,510 \\ 847,335 \\ 12,663,650 \end{pmatrix} \tag{56}$$

The superscript l on the EV's, etc., refers to the lower torus.

Equations similar to equation (56) can also be obtained for the upper torus and the spherical cap.

Deformations of Cylindrical Skirt

The edge horizontal displacement and rotation of the skirt due to the edge moment M_b and edge shear H_b (see Fig. 2a) can be obtained from relations similar to equations (28) and (29) (and omitting the pressure terms). The skirt also has a vertical compressive force induced in it equal to

$$N_{sk} = -\frac{W}{2\pi R_{sk}} = -\frac{(C_1 - C_2)'}{R_{sk}} \tag{57}$$

where

W = weight of vessel and contents
R_{sk} = radius of skirt

and C_1, C_2 are given by equations (45) and (46), respectively.

Due to N_{sk} the skirt experiences an additional outward displacement given by

$$\Delta\delta_{sk} = -\frac{R_{sk}}{Eh_{sk}} \cdot \nu N_{sk} \tag{58}$$

The edge moment M_5 and shear H_5 can also be expressed in terms of the edge moments and shears on the tori at $\phi = 75$ deg. From Fig. 2 one finds

$$\left.\begin{aligned} H_5 &= (H_1 - H_2)\ \frac{r_{75}}{R_{sk}} \\ M_5 &= (M_2 - M_3)\ \frac{r_{75}}{R_{sk}} - |N_{sk}|e \end{aligned}\right\} \tag{59}$$

where

r_{75} = horizontal radius at $\phi = 75$ deg
e = horizontal distance between the line of action of N_{sk} and the middle surface of the torus at $\phi = 75$ deg.

The Equations of Compatibility

As has been indicated in the foregoing pages, it is possible to obtain all the necessary horizontal edge displacements and edge rotations in terms of $H_1 \ldots H_5, M_1 \ldots M_4$. The following equations summarize the deformations of the vessel considered herein, i.e., Fig. 1, skirt at $\phi = 75$ deg, hydrostatic pressure plus an additional pressure of 34 psig:

		H_1	M_1	H_2	M_2	H_3	M_3	H_4	M_4	Constant
Cylinder	$E\delta_c =$	13391.5	2158.71							2,220,700
	$EV_c =$	2158.71	695.968							1,500
Upper torus	$E\delta_{90} =$	−25728.2	8147.55	−12603.0	−8037.23					−2,466,530
	$EV_{90} =$	8146.92	−3471.33	7925.66	3353.99					−32,595
	$E\delta^u_{75} =$	12660.5	−7962.31	25152.3	8020.94					−2,627,085
	$EV^u_{75} =$	8072.98	−3369.18	8020.19	3465.95					−32,715
Skirt	$E\delta_{sk} =$			−14368.4	2377.10	14368.4	−2377.10			−1,058,040
	$EV_{sk} =$			2377.10	−786.536	−2377.10	786.536			403,100
Lower torus	$E\delta^l_{75} =$					−10984.5	1738.91	−3839.42	−1205.69	−4,317,510
	$EV^l_{75} =$					1738.76	−447.940	997.479	180.315	−752,700
	$E\delta_{35} =$					4050.20	−1052.34	8043.90	1428.43	−12,663,650
	$EV_{35} =$					1272.11	−190.27	1428.43	473.45	−847,335
Spherical cap	$E\delta_s =$							−5766.92	1115.66	966,295
	$EV_s =$							1115.54	−419.543	1,580

(60)

In the equations just given $E\delta$ is positive outwards and EV positive when the tangent rotates clockwise on the left-hand side of the vessel. The equations of compatibility are thus:

$$\left.\begin{aligned} E\delta_c &= E\delta_{90} & EV_c &= EV_{90} \\ E\delta^u_{75} &= E\delta_{sk} & EV^u_{75} &= EV_{sk} \\ E\delta^l_{75} &= E\delta_{sk} & EV^l_{75} &= EV_{sk} \\ E\delta_s &= E\delta_{35} & EV_s &= EV_{35} \end{aligned}\right\} \tag{61}$$

From equations (60) and (61) a system of eight linear simultaneous algebraic equations in the eight unknowns $H_1 \ldots M_4$ is obtained. Solving these in the usual way one obtains:

$$\left.\begin{aligned} H_1 &= -296.156 & M_1 &= 228.181 \\ H_2 &= -258.980 & M_2 &= 1434.42 \\ H_3 &= -852.253 & M_3 &= -1249.71 \\ H_4 &= 1107.41 & M_4 &= 1510.42 \end{aligned}\right\} \tag{62}$$

Using these values in conjunction with equation (59) the following are obtained for the shear and moment acting on the skirt:

$$H_5 = -591.974 \qquad M_5 = 2166.88 \tag{63}$$

Determination of the Stresses

Having found the unknown H's and M's, the next step is to determine the constants $C_1 \ldots D_2$ for the various shells. These constants are found from equation (55) and others similar to it. The various stresses throughout the shells are then found by utilizing these constants, Tables 1, 2, and 3, and equations (22), (23), and (24). The detailed calculation of the stresses will not be presented herein; however, the final stress distribution throughout the torus for the case being considered is shown in Fig. 5.

The stresses in the spherical cap and the cylindrical body of the vessel can be determined relatively easily. However, as they are not as large as the stresses in the torus, they were not calculated. The stresses in the skirt, at its point of attachment with the torus, are, however, quite substantial and were computed. The final stress distribution in the skirt is shown in Fig. 7.

References

1 "Rules for Construction of Unfired Pressure Vessels," 1956 edition, ASME, New York, N. Y.

2 "Report on the Design of Pressure Vessel Heads," Welding Journal Research Supplement, January, 1953.

3 S. Timoshenko, "Theory of Plates and Shells," McGraw-Hill Book Company, New York, N. Y., 1940.

4 "Fusion Welded Pressure Vessels," British Standard Code No. 1500: 1949 (Provisional), British Standards Association, London.

5 Brown University letter of December 26, 1956 (D. C. Drucker to G. D. Galletly).

6 R. A. Clark, "On the Theory of Thin Elastic Toroidal Shells," *Journal of Mathematics and Physics*, vol. 29, 1950, p. 146.

7 F. B. Hildebrand, "On Asymptotic Integration in Shell Theory," Proceedings, Symposium of Applied Mathematics, III, 1950, McGraw-Hill Book Company, New York, N. Y.

8 W. R. Burrows, "Pressure Vessel Heads Under Internal Pressure. Part I—General Considerations," 1950, Design Division Paper, Pressure Vessel Research Committee, New York, N. Y.

DISCUSSION

L. P. Zick[7]

The author has done an excellent job of analyzing a specific example of a torispherical head which has proportions that place it beyond the empirical torispherical head rules of the Code. Of particular interest is his comment on the high circumferential compressive stress over the entire knuckle region.

In 1944, Mr. H. C. Boardman [9][8] analyzed a sharp intersection between a cone head and a cylindrical shell, and he proposed rules for compression ring reinforcements. Par. UG-32(g) and UA-4(f) of Section VIII of the ASME Boiler and Pressure Vessel (UPV) Code provide similar reinforcement rules for sharp intersections of conical heads having a half apex angle of 30 deg or less. These rules are based upon the premise that the compressive stress of the composite compression ring region should not exceed the allowable tension stress value. The same limit is specified in Par. UG-23(b)(1) for the allowable compressive stress in a cylindrical shell.

If the circumferential compressive stress in a 6 per cent torispherical knuckle ($L = 2R$) is limited to the allowable tensile stress as it is in other parts of the UPV Code, then such heads having a cylindrical radius/head thickness ratio greater than 35 appear to be underdesigned when present Code head rules are used. Fig. 9 has been developed empirically to point up the region where this becomes important.

[7] Research Engineer, Chicago Bridge & Iron Company, Chicago, Ill. Mem. ASME.

[8] Numbers in brackets from 9 to 12 designate References at end of discussion.

Fig. 10 gives the proportions for an ASME standard (6 per cent) torispherical head and an assumed shape to permit analysis of the head similar to that used for sharp conical head intersections. The spherical portion is continued to its intersection with the cylindrical shell. The unbalanced inward force at the junction is $0.866PR$ where P is the internal pressure and R is the cylindrical radius. The internal pressure acting on the vertical projection of the effective compression region reduces this inward, unbalanced force.

If the knuckle alone is assumed to resist the unbalanced force at a compressive stress equal to the allowable tensile stress, all 6 per cent torispherical heads would have to be about 2.5 times as thick as now required by the Code. However, the effective area is greater than just the knuckle region in the smaller diameter thicker heads. Also, the very large thin heads are not stressed uniformly throughout the knuckle region so an area less than the knuckle region is effective.

Therefore, the curve in Fig. 9 for the 6 per cent torispherical head is based upon the assumed effective compression region shown in Fig. 10 for the assumed shape. The material within a distance of 0.7 times the square root of the product of the tangent radius and the actual thickness on either side of the junction is included. The internal pressure acting over a vertical height of $1.2\sqrt{RT}$ will reduce the inward unbalanced force. The net unbalance will produce a circumferential compressive force F in lb which is given by the following equation:

$$F = 0.866PR^2 - 1.2\,PR^2\sqrt{T/R} \tag{64}$$

The compressive circumferential stress over the assumed effective region is

$$S = \frac{F}{A} = PR^2\,\frac{0.866 - 1.2\sqrt{T/R}}{1.7TR\sqrt{T/R}} \tag{65}$$

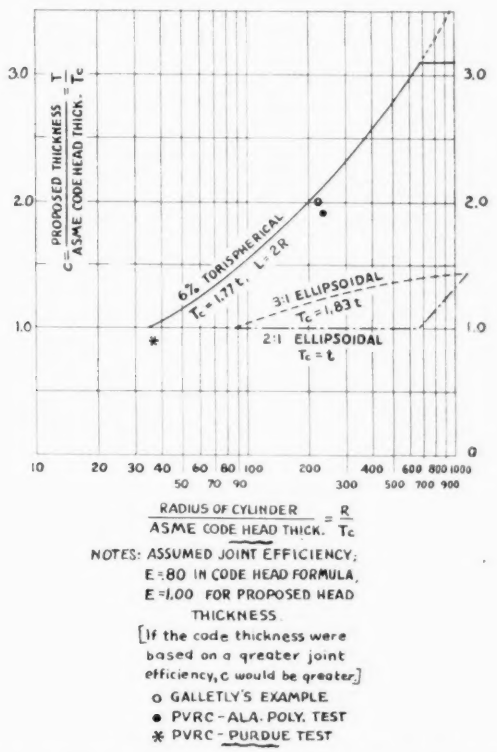
C = PROPOSED THICKNESS / ASME CODE HEAD THICK. = T/Tc
3.0
2.0
1.0
6% TORISPHERICAL
Tc = 1.77 t, L = 2R
3:1 ELLIPSOIDAL
Tc = 1.83 t
2:1 ELLIPSOIDAL
Tc = t
10 20 30 40 60 80 100 200 400 600 800 1000
50 70 90 300 500 700 900
RADIUS OF CYLINDER / ASME CODE HEAD THICK. = R/Tc
NOTES: ASSUMED JOINT EFFICIENCY;
E = 80 IN CODE HEAD FORMULA,
E = 1.00 FOR PROPOSED HEAD THICKNESS
[If the code thickness were based on a greater joint efficiency, C would be greater.]
o GALLETLY'S EXAMPLE
• PVRC - ALA. POLY. TEST
* PVRC - PURDUE TEST

Fig. 9 Proposed correction factor to be applied to required code head thickness

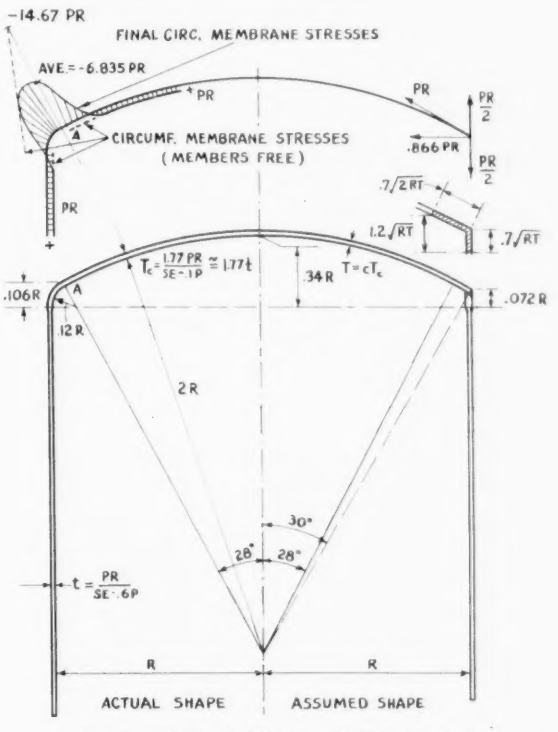

Fig. 10 ASME standard (6 per cent) torispherical head [See Par. UG-32(e) and (j)]

Then

$$T = \frac{PR}{S}\left[0.510\sqrt{\frac{R}{T}} - 0.706\right] \tag{66}$$

If the circumferential compressive stress S is not to exceed the allowable, the required thickness of the head is obtained from equation (66). Since the compressive stress governs, a joint efficiency $E = 100$ per cent is assumed.

On the other hand, the thickness of the torispherical head, according to UPV Code, is

$$T_c = \frac{1.77PR}{SE - 0.10P} \tag{67}$$

which for low pressures reduces to

$$T_c = \frac{1.77PR}{SE} \tag{67a}$$

The UPV Code does not recognize the maximum stress as compressive so the joint efficiency is based upon tension.

If the allowable stresses in compression and tension are assumed to be the same and E, the joint efficiency in tension, is 0.80, the ratio between these computed thicknesses is given by

$$c = \frac{T}{T_c} = \frac{0.80}{1.77}\left[0.510\sqrt{\frac{R}{T_c c}} - 0.706\right] \tag{68}$$

or

$$\sqrt{c}\,(c + 0.319) = 0.23\sqrt{\frac{R}{T_c}} \tag{68a}$$

The values of c for various R/T_c values have been plotted in Fig. 9 for torispherical heads with 6 per cent knuckles and $L = 2R$. The coefficient c represents the maximum factor by which the Code thickness of the head should be increased to limit the circumferential compressive stress to the allowable stress value.

It might be argued that this curve represents a head made of a spherical segment (plus a flange) having a spherical radius twice as great as the cylindrical radius. On the other hand, the correctness of this approach is partially substantiated by plots of the examples listed as follows:

	Cylindrical shell		Torispherical head: Spherical rad. = L,	Torispherical head: Knuckle rad. = r,		
Source	R, in.	t, in.	in.	in.	T_c in.	Remarks
Galletly	138.23	0.460	227.5	18.31	0.625	Analysis
PVRC Ala. Poly. [10]	30.0	0.125	60.0	3.625	0.125	SR-4 measured
PVRC Purdue [11]	3.75	0.100	7.5	0.45	0.100	SR-4 measured

This approach does not account for benefits that are undoubtedly gained by increasing the knuckle radius above 6 per cent. Also a smaller spherical radius will reduce the unbalanced force and therefore the compressive stress in the knuckle.

Table UA-4.2 of the UPV Code gives values for the constant $M = 1/4(3 + \sqrt{L/r})$ in the formula for determining the required thickness of a torispherical head. If the average circumferential compressive stress at the sphere-knuckle junction (jt. A Fig. 10) is limited to the allowable tension stress, a correction factor c depending upon L/r should be applied to the Code thickness.

The primary membrane stresses on the side of the spherical element at junction A (if the members are cut at A) are the same both in the circumferential direction (T_2 lb/in.) and the meridional direction (T_1/ lb/in.). These are given by

$$T_2 = T_1 = \frac{PL}{2} = PR \tag{69}$$

On the knuckle side of junction A, the T_1 stress is the same as in the spherical portion. The T_2 stress (circumferential) is obtained from the equation

$$\frac{T_2}{L} + \frac{T_1}{r} = p \quad \text{or} \quad \frac{T_2}{L} + \frac{PL}{2r} = P \tag{70}$$

Then on the knuckle side

$$T_2 = PL\left(1 - \frac{L}{2r}\right) \tag{71}$$

This stress is the maximum calculated compressive circumferential membrane stress in the knuckle but does not exist. Since continuity exists between the knuckle and the spherical cap, the final circumferential stress in the head can be estimated to be the average of the T_2 values given by (69) and (71).

$$T_{2\,\text{avg}} = \frac{PL}{4}\left(3 - \frac{L}{r}\right) \tag{72}$$

If T_c is the head thickness as calculated according to the Code, and T the thickness of the head which would give stresses not to exceed the allowable tension, and c the ratio T/T_c, then the thickness of the head should be

$$T = cT_c = \frac{PL}{4S}(3 - L/r) \tag{73}$$

but from the Code

$$T_c = \frac{MPL}{2SE} \tag{74}$$

and combining (73) and (74)

$$c = \frac{E}{2M}(3 - L/r) \tag{75}$$

For the 6 per cent torispherical head shown in Fig. 10 with $E = 0.80$

$$c = \frac{0.8}{2(1.77)}\left[3 - \frac{2R}{0.12R}\right] = 3.1$$

From Fig. 9 it can be seen that the sharp intersection approach gives smaller c values except for R/T_c values in excess of 700. At the other extreme, an L/r value of 6.5 would result in a c value of 1 by averaging the circumferential membrane stresses at the discontinuity. In other words, Code designed torispherical heads having L/r ratios up to at least 6.5 appear to limit the circumferential compressive stress to the allowable tension stress or less for all values of R/T_c. As either or both ratios L/r and R/T_c increase, the present Code permits an increase in the circumferential compressive stress.

A 3:1 ellipsoidal head has about the same depth as an ASME standard (6 per cent) torispherical head. The minimum tangent radius is slightly greater than 6 per cent of the diameter of the cylinder. The tangent radius varies continuously, which elimi-

nates the discontinuity except at the head-to-cylinder junction. This discontinuity can be analyzed assuming the elements of the head to be beams on an elastic foundation [12]. The maximum circumferential compressive stress was determined for 3:1 ellipsoidal heads having various R/T_c ratios. The required head thickness was determined by limiting this maximum calculated stress to the allowable tension stress. c values were determined by comparing this thickness with the thickness required by the present Code. These are plotted in Fig. 9.

The present Code requires a 3:1 ellipsoidal head to be slightly thicker than the 6 per cent torispherical head having the same depth. However, it is apparent from Fig. 9 that the circumferential stress can be reduced substantially for high ratios of R/T_c by going to the ellipsoidal shape. Another approach would be to use more than one radius in the knuckle so that the discontinuity stresses are reduced and so that the unbalanced inward force is spread over a wider band of the head.

For very large R/T_c ratios, consideration should be given to the possibility of local buckling due to these circumferential compressive stresses. For values up to 1000, this should not be a problem in torispherical and 3:1 ellipsoidal heads. However, it may start to govern the 2:1 ellipsoidal head at $R/T_c = 650$. The maximum circumferential compressive stress in a 2:1 ellipsoidal head has the same magnitude as the circumferential tension stress in the cylinder when they are the same thickness. Since the knuckle approximates a torus, which in turn becomes a cylinder as the diameter of the center line of the torus approaches infinity, the allowable compressive stress should be limited as now required for cylindrical shells in Par. UG-23(b)(2).

Although this discussion has not included toriconical heads and reducers, the same general approach is applicable. This crude approach is offered in an attempt to define the region where caution is warranted. A series of calculations such as those presented by the author and/or a series of measured stresses would be more appropriate and would bring out the effect of increasing the knuckle radius.

The writer assumes that the author is considering the high local bending stresses in the meridional direction when he determines the collapse by his limit analysis and when he refers to brittle fracture. This is implied since he speaks of choosing yield hinge points at the mid-point of the torus, etc. The stresses in this direction are tension on one surface and the writer assumes that such stresses are required in speaking of brittle fracture. Does the high circumferential compressive stress in the knuckle region contribute in any way to the collapse pressure or brittle failure determined by the author's limit analysis? Although a defect is mentioned in the conclusions, the writer gets the impression from reading the paper that the limit analysis predicts failure of a brittle material even though the so-called defect is limited to the nonhomogeneity of the material and/or weld metal.

The writer has been unable to find in the literature a tie-in between biaxial stresses and brittle failure where one of the stresses is compressive. On the other hand, a high compressive stress would contribute to the transverse strain due to Poisson's ratio.

References

9 H. C. Boardman, "Stresses at Junction of Cone and Cylinder in Tanks With Cone Bottoms or Ends," *The Water Tower*, January, 1944.

10 Alabama Polytechnic Institute, Final Report on Vessel One to Pressure Vessel Research Committee, December, 1957.

11 Purdue University, Final Report to Pressure Vessel Research Committee, August, 1952.

12 M. Hetenyi, "Beams on Elastic Foundation," University of Michigan, Ann Arbor, Mich., 1947.

R. T. Shield[9]

The author is to be congratulated for an excellent contribution. There is no need to stress the significance and practical value of his work.

The writer would like to mention that since this problem was brought to their attention by the author, Prof. D. C. Drucker and the writer have used limit analysis to predict the limit strength of thin-walled pressure vessels with an ASME standard head.[10]

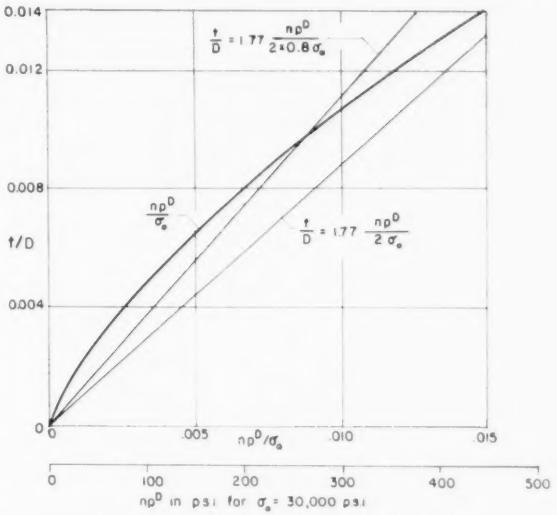

Fig. 11 Limit pressure for ASME standard head

The ASME standard torispherical head is such that the radius of the toroidal knuckle is 6 per cent of the radius of the spherical cap which in turn is equal to the diameter D of the cylinder. The results of the work show that the present ASME Code for Unfired Pressure Vessels is unsuitable when the design or working pressure is low (less than 100 psi, approximately, for steel plate). The limit pressure np^D predicted by limit analysis for a head of uniform thickness t is given by the full curved line in Fig. 11, which is a plot of t/D versus np^D/σ_0. A scale is also given for np^D with the value 30,000 psi for the yield stress σ_0. p^D is the design pressure and n the factor of safety against collapse. The two straight lines marked $t/D = 1.77np^D/2 \times 0.8\sigma_0$ and $t/D = 1.77np^D/2\sigma_0$ show the thickness ratio t/D as specified by two interpretations of the ASME Code. It may be seen that for np^D in the vicinity of 100 psi and below, the safety factor against reaching the limit pressure at operating pressures may be dangerously low for a head designed according to the Code.

Author's Closure

The author wishes to thank Messrs. Zick and Shield for their generous comments on his work and also for their contributions to the paper.

Even though it was derived on an approximate basis, Mr. Zick's Fig. 9 should be of value to the designer as it delineates the geometries where caution is required. As Mr. Zick states, it would be most helpful to conduct experiments and make

[9] Brown University, Providence, R. I.

[10] R. T. Shield and D. C. Drucker, "Limit Strength of Thin-Walled Pressure Vessels With an ASME Standard Torispherical Head," to appear in the Proceedings of the Third U. S. National Congress of Applied Mechanics.

accurate calculations in order to check the validity of Fig. 9 for various percentages of knuckle-radius head-diameter ratios. In so far as the calculations are concerned, the author might mention that he has calculated, on a computer, the influence coefficients for a number of toroidal shell geometries which will make the accurate analysis of torispherical shells much easier. The author hopes to present this work in the near future.

The additional limit analysis results cited by Professor Shield are most interesting. In reference [10], Professors Shield and Drucker also gave another interpretation of these results and it seems to be their feeling that the provisions of the Code give a smaller factor of safety than that desired for $D/t \approx 60$ and above. This is in rough agreement with Mr. Zick's estimate of $D/t = 35$ and above.

The high circumferential compressive stress does play a part in the determination of the limit load and the author refers Mr. Zick to reference [10] for further details.

There is also a minor error in the paper which the author would like to correct at this time. When the vessel is filled with water, the meridional direct stresses in the torus due to the skirt reaction (see page 53 of the paper) should read as follows:

Above the skirt attachment: $\Delta\sigma = 165$ psi

Below the skirt attachment: $\Delta\sigma = 4180$ psi

These values can be checked from Equations (24*a*), (44), (45), and (46); the new values do not affect the conclusions of the paper.

Drilling by Vibration

R. SIMON

Consultant, Applied Mechanics Division, Battelle Memorial Institute, Columbus, Ohio

An analysis is presented of the process of vibratory drilling, based on the assumption that the load presented by the bit vibrating on the rock to the vibration generator, a magnetostriction transducer, can be represented by a force-displacement characteristic with hysteresis. The conclusions reached are compared with experimental observations on the performance of vibratory drilling systems.

Introduction

DRILLING by vibration[1] is accomplished by superimposing longitudinal vibrations, at some frequency in the range of about 100 to about 1000 cycles per second, onto the drill bit of an otherwise conventional rotary drilling system.

A number of laboratory and field models of vibratory drilling machines have been designed, constructed, and used in experimentation. The latest version encompasses a magnetostriction transducer that follows a $10^1/_2$-in-diam rotary bit down the drilled hole. Details of the designs and performances of these systems are described elsewhere [1, 2].[2]

The basic feature of all the models of vibratory drilling systems is a column which is vibrated longitudinally at or near the resonant frequency of its fundamental mode. One end of the column is essentially free, as far as the vibrations are concerned, and the other end is loaded by the bit acting on the rock. Since the effective impedance of this load is small compared with the characteristic impedance of the column, the fundamental mode of vibration of the column is close to that of a free-free bar, one half wavelength long.

Magnetostriction transducers were employed to drive the vibrating column for most of the experimental work in vibratory drilling, although some preliminary work was done with electrodynamic transducers. Use of electroacoustic devices to generate the vibrations affords the distinct advantage of the absence of sliding or rolling bearing surfaces which must be sealed off from the abrasive drilling fluid. On the other hand, they require means for generating and controlling up to about 200 kw of electric power and for transmitting it down the drill string. The magnetostriction transducer is more readily adapted to the requirements imposed by operation down a hole being drilled than the electrodynamic transducer, considering the limitations on lateral dimensions and the need for transmitting large steady forces and torques through the transducer.

The purpose of this paper is to present a comprehensive theory of vibratory drilling, in which the interaction between the load and the transducer is taken into account in determining performance. The theory presented in this paper is developed for the case of a magnetostriction transducer, but the same analytical techniques would be applicable to the uses of other types of transducers.

[1] This new method of drilling was investigated at Battelle under the sponsorship of Drilling Research, Inc., an organization supported by a number of companies associated with oil production for the purpose of studying new methods of drilling.

[2] Numbers in brackets designate References at end of paper. It is planned to prepare for future publication the significant contents of those references cited that are not readily available to the general reader.

Contributed by the Petroleum Division and presented at the Petroleum-Mechanical Engineering Conference, Denver, Colo., September 21–24, 1958, of THE AMERICAN SOCIETY OF MECHANICAL ENGINEERS.

NOTE: Statements and opinions advanced in papers are to be understood as individual expressions of their authors and not those of the Society. Manuscript received at ASME Headquarters, July 17, 1958. Paper No. 58—PET-21.

Nomenclature

A_{Ni} = cross-sectional area of nickel in the transducer, in.^{2}

A_{tr} = cross-sectional area of nickel and steel in the transducer, in.^{2}

$C = 2\pi^2 f Z_c / K_1 Q_{ti}$, dimensionless parameter

D = bit diameter, in.

E = vibratory energy input to rock per cycle of vibration, in-lb

E_r = rotary energy input to rock per effective loading of the bit teeth on the rock in presence of vibration, in-lb

E_t = rotary energy input to rock per effective loading of the bit teeth on the rock in absence of vibration, in-lb

F = instantaneous force between the bit and the rock, lb

F_m = amplitude of fundamental component of magnetostrictive driving force, lb

F_{ns} = maximum safe amplitude of force alternation at center of the transducer, lb

F_0 = peak value of the force between the bit and the rock, lb

f = resonant frequency of loaded transducer, also the operating frequency, cycles/sec

$f(\text{opt})$ = optimum value of operating frequency, cycles/sec

$f(\alpha, \beta) = E/(1/2)K_1\xi_0^2$, dimensionless function of α and β

g = acceleration of gravity, in./sec^2

$g(\alpha, \beta) = W/K_1\xi_0$ dimensionless function of α and β

$h(\alpha, \beta) = (L_v/L)(W/K_1\xi_0)^2$, dimensionless function of α and β

K_1 = stiffness of rock for downward motion of bit, lb/in.

K_2 = stiffness of rock for upward motion of bit, lb/in.

K_{eq} = equivalent stiffness of rock for fundamental component of force waveform, lb/in.

K_{tr} = longitudinal stiffness of the transducer, lb/in.

L = torque required to rotate bit in absence of vibration, in-lb

L_v = torque required to rotate bit in presence of vibration, in-lb

(Continued on next page)

Theory of Transducer Operation

Magnetostriction transducers convert electrical power to vibratory mechanical power (and vice versa) by application of the magnetostriction effect. This effect is the change in dimensions of certain ferromagnetic materials when magnetized and, also conversely, the change in magnetic properties which occur when the materials are strained mechanically.[3]

The transducers used for vibratory drilling are constructed of nickel, which shrinks in the direction of the applied field when magnetized, up to a maximum strain of about -37×10^{-6} for annealed nickel at magnetic saturation. In order to obtain the maximum amount of vibratory power output from the transducer at least sacrifice in electromechanical conversion efficiency, the transducer is operated with a suitable combination of bias and alternating magnetic fields so as to vary the magnetic induction from about zero to a reasonable approach to saturation. These magnetic fields are provided by direct and alternating current, respectively, in copper windings.

Despite the nonlinearity of the transducer operation associated with high power levels and despite the nonlinearity of the rock load, much of the linear theory of transducer operation can be applied to obtain good approximations to the performances of the transducers used in vibratory drilling. This occurs essentially because the transducer vibrates predominantly in its fundamental mode when the driving frequency is tuned to the fundamental resonant frequency of the transducer. The resonant frequencies of the higher modes of vibration are harmonically related to that of the lowest mode only for the special case of a uniform characteristic impedance along the length of the vibrating column and a purely resistive load. Under practically all circumstances of vibratory drilling, the stress variations at the node of the transducer are found to be reasonably sinusoidal.

The excitation of the transducer is conveniently expressed for the purposes of the subsequent analyses in terms of F_m, the amplitude of the fundamental component of the magnetostrictive driving force. The magnetostrictive driving force is defined as the force which would have to be exerted to obtain complete constraint to magnetostrictive strain. Since the maximum amplitude of the fundamental component of the magnetostrictive strain variation would be about 15×10^{-6} for nickel, the maximum value of F_m would be about 450 psi A_{Ni}, where A_{Ni} is the cross-section area of the nickel portion of the transducer.

At fundamental resonance, the amplitude of the displacement at the ends of the transducer, ξ_0, assumed to be sinusoidal, is given by [2]

$$\xi_0 = (2/\pi^2)QF_m/fZ_c \tag{1}$$

where f is the resonant frequency and Z_c is the characteristic impedance of the transducer. Z_c is given by

$$Z_c = \sqrt{W_{tr}K_{tr}/g} \tag{2}$$

where W_{tr} is the weight of the transducer and K_{tr} is the longitudinal stiffness of the transducer.

Equation (2) is a good approximation if the weight per unit length and the stiffness of a unit length do not vary too much along the length of the transducer. Z_c is customarily expressed in terms of cross-section area, density, and either Young's modulus or sound velocity, but the form given is more useful for a composite structure of nickel laminations, copper windings, electrical transmission lines, steel jackets, and bonding, insulating, and impregnating materials.

Equation (1) for ξ_0 applies, strictly speaking, only to the case where the entire length of the half-wavelength vibrating column is occupied by the transducer and if the nickel of the transducer is uniformly excited magnetically along the entire length of the transducer. Equation (1) could be applied, however, to cases which depart from these ideal conditions by suitably defining effective values of F_m that are less than its ideal value for uniform excitation of the entire column. Analytical procedures for computing the effective value of F_m can be developed from the general theory presented in reference [4]. The effective value of F_m for any actual system is related to the effective value of the coefficient of electromechanical coupling for that system, which latter quantity can be determined from motional impedance measurements [2]. With this understanding regarding the use of an effective F_m, the terms "transducer" and "vibrating column" are used interchangeably throughout this paper.

Q in Equation (1) is defined as 2π times the ratio of the stored vibratory energy in the transducer at the fundamental frequency to the total energy dissipated per cycle of vibration, the energy dissipated into all internal and external sources of energy loss. If E is the energy output per cycle of vibration into the rock load

[3] Reference [3], for example, contains a comprehensive account of the magnetostriction effect.

Nomenclature

N = effective number of applications of loadings of the bit teeth on the rock per revolution, dimensionless

P = vibratory power output from the transducer to the rock, in-lb/sec

$P(\max)$ = maximum value of vibratory power output from the transducer to the rock, in-lb/sec

Q = 2π times ratio of vibratory energy stored in transducer at resonance to the total amount of vibratory energy dissipated per cycle, dimensionless parameter

Q_i = 2π times the ratio of vibratory energy stored in the transducer at resonance to the amount of vibratory energy dissipated everywhere per cycle except into useful work in the rock load, dimensionless parameter

R = rate of penetration of the bit, in/sec

S = drilling strength of the rock, lb/in.[2]

t = time, sec

W = weight on the bit, lb

W_{tr} = weight of the transducer, lb

y = instantaneous displacement of the bit into the rock, in.

y_0 = peak value of the displacement of the bit into the rock, in.

Z_c = characteristic impedance of the transducer, lb-sec/in.

α = K_1/K_2, dimensionless parameter

β = ξ_e/ξ_0, dimensionless parameter

ξ_e = mean position of vibrating bit with respect to rock surface, in.

ξ_0 = amplitude of sinusoidal vibration of bit, in.

θ = $2\pi ft$, dimensionless

σ_n = amplitude of stress variation at the center of the transducer, lb/in.[2]

σ_{ns} = maximum safe value of stress level amplitude at center of the transducer, lb/in.[2]

and Q_i is 2π times the ratio of stored energy to that dissipated into all other sources except into the useful load, then [2]

$$(1/Q) = (1/Q_i) + E/\pi^3 f Z_c \xi_0^2, \tag{3}$$

since the stored energy is $(\pi^2/2)\, fZ_c\xi_0^2$.

The elimination of Q between Equations (1) and (3) would establish a relationship between E and ξ_0 as determined by the characteristics of the transducer. The establishment of an additional relationship between E and ξ_0, as imposed by the characteristics of the system consisting of the bit acting on the rock, would enable both E and ξ_0 to be computed, and hence, also the vibratory power output to the rock, $P = fE$.

Fundamentals of Rock Drilling

The results of an experimental and theoretical study of the basic action involved in rock drilling by mechanical means, the momentary loading of chisel-like tools on the surface of the rock at the bottom of the drilled hole, demonstrated that the volume of rock fractured out in rock drilling should be just about proportional to the mechanical energy input to the rock over a wide range of operating and design conditions [5]. The rate of penetration should, hence, be proportional to the mechanical power input to the rock per unit area of hole. An approximate formula developed in reference [5] for the rate of penetration R of a bit is

$$R = 2.0P/D^2S \tag{4}$$

where P is the power input to the rock, D the diameter of the hole, and S is the drilling strength. S is the ratio of impact energy to volume of rock broken out by the impact of a sharp chisel with an included angle of 90 deg onto the smooth surface of a rock sample. The value of S, averaged over several impacts, is a constant independent of the energy level or of the length of the chisel, for depths of penetration considerably less than the length of the chisel.

It follows from these considerations that the attainment of substantial increases in the rate of penetration depends upon the development of means whereby the rate at which the rock will accept mechanical energy could be appreciably increased. This is the intended function of vibratory drilling. The results of the fundamental study indicate that little would be gained by attempting to improve the efficiency of utilization of mechanical energy to break rock under the types of loading imposed by down-hole conditions and within the strength limitations of present bit materials.

Bit Force—Displacement Characteristic

It was found in the fundamental study of rock drilling that the relationships among the force, displacement, and volume of rock broken out for a chisel are only a very slowly changing function of the rate of loading. This is in agreement with the known behaviors of other brittle materials [6]. However, this conclusion would not be expected to be valid for rocks which exhibit a significant degree of ductility prior to fracture, such as a few rocks do at atmospheric pressure, and as many rocks do at the temperatures and confining pressures of some bottom-hole conditions.

This result suggests that, for the brittle state of rock at least, the characteristics of a given bit vibrating on a given rock could be represented by a relationship between the force between the bit and the rock, F, and the displacement of the bit into the rock, y, such as shown in Fig. 1(a). This relationship is taken to consist of two straight lines in order to simplify the analysis. The actual shapes of the curves for a rotary bit are not known; but there is some evidence, to be discussed later, that they cannot be straight lines. However, the salient features of the analysis can be

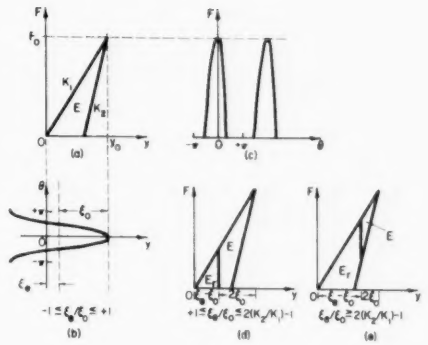

Fig. 1

demonstrated equally well and many significant conclusions can be obtained by using the assumed straight-line relationships.

The assumed force-displacement relationship is represented analytically, for a given maximum displacement y_0, by

$$\left.\begin{aligned} &F = K_1 y, \text{ for } 0 \leqslant y \leqslant y_0 \text{ and } dy/dt > 0 \\ &F = K_2 y - (K_2 - K_1)y_0, \\ &\qquad \text{for } y_0 \geqslant y \geqslant (1 - K_1/K_2)y_0 \\ &\qquad \text{and } dy/dt < 0 \\ &F = 0, \text{ for } (1 - K_1/K_2)y_0 \geqslant y \geqslant 0 \text{ and } dy/dt < 0 \end{aligned}\right\} \tag{5}$$

Fig. 1(b) shows the displacement of the bit as a function of time, t, in terms of $\theta = 2\pi ft$. The bit is assumed to undergo a sinusoidal displacement of amplitude ξ_0 about some mean position ξ_e, represented analytically for one complete cycle by

$$y = \xi_0 \cos\theta + \xi_e, \text{ for } -\pi \leqslant \theta \leqslant +\pi \tag{6}$$

Fig. 1(c) shows the relationship between F and θ for two successive cycles of vibration. This is the type of waveform between the bit and the rock that is observed experimentally in vibratory drilling. The fraction of the cycle for which the force is different from zero is termed the "on-time"; Fig. 1(c) illustrates an on-time of about 50 per cent.

If ξ_e and ξ_0 are varied so that $\xi_e + \xi_0 = y_0$ remains constant, the peak force F_0 would be constant but the on-time would vary. This is done in practice by adjusting the amplitude of vibration and the weight on the bit. The energy input to the rock per cycle, E, the area of the indicator diagram of Fig. 1(a), would then remain constant, and hence, so would the power input to the rock $P = Ef$, if the frequency is not changed. The experimental observation that the rate of penetration obtained at a given level of peak force is essentially independent of on-time, up to a certain value of the on-time, contributes some evidence for the validity of the basic assumption regarding the existence of force-displacement characteristics with no significant rate of loading effect for brittle rock. Above a certain value of on-time the rate of penetration either increases or decreases with on-time or remains approximately constant, depending upon the circumstances discussed hereafter.

It is seen from Figs. 1(d and e), the latter figure representing 100 per cent on-time, that complications arise when ξ_e is greater than ξ_0. Only the portion of the area of the indicator diagrams labelled E on the figures represents energy supplied by the vibration of the bit; the remainder, labelled E_r, is supplied by the loading and unloading of each tooth of the bit as the bit rolls.

The fact that the force-displacement relationship for the teeth that are in the process of loading as the bit rolls is not the same as that for the teeth that are simultaneously unloading produces

a moment which tends to resist rotation. The mechanical power input to the rock in conventional rotary drilling is supplied by the torque which must be applied to counteract this moment to rotate the bit. It is thus seen that the basic mechanisms of conventional rotary drilling and of vibratory drilling are quite similar. Whether the total power developed at a given peak force level increases or decreases for on-times corresponding to $\xi_e > \xi_0$ would depend upon the effective number of cycles of E_r per second as compared with the vibration frequency, f. The former quantity would depend upon such factors as the rate of rotation, the diameter of the bit, and tooth spacing.

A conceptual difficulty is associated with the assumed indicator diagrams of Figs. 1(*d*) and (*e*), in regard to the instantaneous increase of vibratory force from zero to some finite value at the end of one cycle of vibration and the beginning of the next. This difficulty arises from the fact that y is not equal to zero at the beginning of the cycle for $\xi_e > \xi_0$. The difficulty may be formally obviated by considering that the bit is first loaded to the displacement $\xi_e - \xi_0$, a cycle of vibration takes place, and then the bit is unloaded to $y = 0$ and reloaded to $y = \xi_e - \xi_0$ on another portion of the rock before the commencement of the next cycle of vibration.

It is understood, of course, that this formalism is not intended to be descriptive of the actual details of the vibratory drilling process. Although the weight on the bit is nominally constant, but may actually fluctuate violently under some down-hole circumstances, the loads on individual teeth of the bit increase and then decrease more or less slowly compared with the frequency of vibration, depending upon the speed of rotation of the bit and the radial position on the bit of the tooth in question. Hence each cycle of vibration encounters a different loading condition as far as an individual tooth is concerned. The formalism mentioned, however, enables an analysis to be made from certain assumptions regarding the action of the bit as a whole without regard to the details of the actual process, which would be practically impossible to take into account. However, because of these details, the force-displacement characteristics of a given bit would be expected to be a function of the ratio of the rotation frequency to the vibration frequency.

Computations of Power Output to the Rock

The energy per cycle, E, is readily shown to be given by

$$E = (1/2)K_1\xi_0^2 f(\alpha, \beta) \tag{7}$$

wherein $\alpha = K_1/K_2$ and $\beta = \xi_e/\xi_0$. The dimensionless function $f(\alpha, \beta)$ is given by

$$\left.\begin{aligned} f(\alpha, \beta) &= (1 - \alpha)(1 + \beta)^2, \text{ for } -1 \leqslant \beta \leqslant +1 \\ &= (1 - \alpha)(1 + \beta)^2 - (1 - \beta)^2 \text{ for } +1 \leqslant \beta \\ &\leqslant (2/\alpha) - 1 \\ &= 4[(1/\alpha) - 1] \text{ for } \beta \geqslant (2/\alpha) - 1 \end{aligned}\right\} \tag{8}$$

$f(\alpha, \beta)$ is shown as a function of β for four different values of α in Fig. 2.

Substitution of Equation (7) for E into Equation (3) for Q, and Equation (3) into Equation (1) for ξ_0, results in the following determining equation for ξ_0:

$$F_m/K_1\xi_0 = (1/4\pi)[f(\alpha, \beta) + C] \tag{9}$$

where the dimensionless parameter C is given by

$$C = 2\pi^3 f Z_e/K_1 Q_s \tag{10}$$

The power output of the transducer to the rock is given by substituting for ξ_0 given by Equation (9) into Equation (7) for E and multiplying by f, resulting in

$$P = [8\pi^2 F_m^2 f/K_1]/\left[\sqrt{f(\alpha, \beta)} + C/\sqrt{f(\alpha, \beta)}\right]^2 \tag{11}$$

P has a maximum value of

$$P(\max) = F_m^2 Q_s/\pi Z_e \tag{12}$$

when $f(\alpha, \beta) = C$. In terms of $P(\max)$, Equation (11) may be rewritten as

$$P/P(\max) = 4/\left[\sqrt{f(\alpha, \beta)/C} + \sqrt{C/f(\alpha, \beta)}\right]^2 \tag{13}$$

It is of interest to note that the value of $P(\max)$, as given by Equation (12), corresponds to $Q = Q_s/2$; that is, the power output to the load is maximum when the load is so adjusted that the dissipation of energy into the load and in the generator are the same, in agreement with the well-known result of linear theory.

It is significant that the value of $P(\max)$ depends only upon the characteristics of the transducer and not upon the characteristics of the rock. $P(\max)$ is also independent of frequency. This means that, provided it is possible to adjust operating conditions so that $f(\alpha, \beta) = C$, the same amount of vibratory power can be fed into any type of rock. Nor is this adjustment of $f(\alpha, \beta)$ too critical, since P is only 11 per cent less than $P(\max)$ for $f(\alpha, \beta) = 2C$ or $(1/2)C$.

The conclusion that the vibratory power output should be insensitive to variations in rock characteristics, if conditions of operation are somewhere near optimum, implies that the rate of penetration in vibratory drilling should be approximately inversely proportional to the drilling strength of the rock, according to Equation (4). On the other hand, for conventional rotary drilling, the torque required to rotate the bit will be shown later to be proportional to $W^2[(1/K_1) - (1/K_2)]$, where W is the weight on the bit. Hence the rotary power output to the rock, 2π times the product of the torque and the rate of rotation of the bit, should decrease rapidly as the rock gets harder (larger values of K_1 and K_2) or as the relative number of tooth loadings that break out large fragments decreases (K_2 closer in value to K_1). For rotary drilling, therefore, the rate of penetration should decrease more rapidly than inversely proportional to S at constant weight on the bit.

These deductions are in agreement with experience. When drilling through inhomogeneous formations the rates of penetration obtained by vibratory drilling fluctuate much less rapidly than those obtained by rotary drilling. For example, in the tests with the down-hole transducer, fluctuations in penetration rates of about 2.5 to 1 were obtained by vibratory drilling as compared with about 7 to 1 for rotary drilling in the same formation.

Incidentally, this variation of torque with W^2 would imply

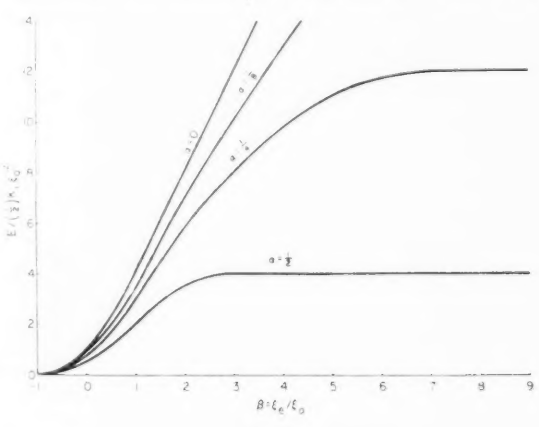

Fig. 2

that the rate of penetration of a rotary bit should increase as W^2. In practice, the rate of penetration of a rotary bit is found to be an approximately linear function of W which extrapolates to a positive intercept on the W-axis. This indicates that the use of straight lines to represent the force-displacement characteristic of a rotary bit is an oversimplification.

Effect of Weight on the Bit

It has been noted that the maximum power output is obtainable if the vibratory load on the transducer could be suitably chosen. The coupling between the vibrating transducer and the rock can be adjusted by changing the weight on the bit, since the weight on the bit determines the value of $\beta = \xi_s/\xi_0$. If the bit is advancing into the rock at a constant rate of penetration, the equilibrium position ξ_s must so adjust itself that the average value of the force between the bit and the rock equals the weight on the bit. This has been verified experimentally for the observed force waveforms. Thus,

$$W = (1/2\pi) \int_{-\pi}^{+\pi} F d\theta \tag{14}$$

resulting in

$$W/K_1\xi_0 = g(\alpha, \beta) \tag{15}$$

$g(\alpha, \beta)$ is a rather complex function that changes in algebraic form at $\beta = 0$, 1, $(1/\alpha) - 1$, and $(2/\alpha) - 1$. The required integrations within each range of values of β are relatively straightforward, however. $g(\alpha, \beta)$ is shown as a function of β for four values of α in Fig. 3.

Using β as a computational parameter, the value of $P/P(\max)$, as given by Equation (13), can be plotted as a function of W/F_m, the latter obtained by taking the ratio of Equation (15) to Equation (9). The result is shown in Fig. 4 for $C = 0.31$ and for the four assumed values of α. This particular value of C corresponds to $f = 300$ cps, $Z_c = 6000$ lb sec/in., $Q_i = 100$, and $K_1 = 3.6 \times 10^6$ lb/in. The values of the first three variables represent approximately the characteristics of the down-hole transducer; the value of K_1 was chosen as representative of its order of magnitude for a 10-in-diam rotary bit on hard rock. $W/F_m = 0$ corresponds to $\beta = -1$ and the maximum power output is obtained at values of β between $-1/2$ and $-1/4$.

An outstanding feature of these curves is the fact that $P/P(\max)$ is a multivalued function of W/F_m in a narrow range of values of W/F_m to the right of the maxima. This is in agreement with experience. What distinguishes the various values of $P/P(\max)$ at a given value of W/F_m is the resonant frequency, which increases monotonically along the curves from $W/F_m = 0$. This is explained by the fact that the equivalent stiffness of the rock load, given by $K_{eq} = (1/\pi\xi_0) \int_{-\pi}^{+\pi} F \cos\theta \, d\theta$ increases monotonically with β. The change in resonant frequency of the transducer is given by $+ (1/2\pi^2)K_{eq}/Z_c$ for small changes in frequency compared with the frequency of the unloaded transducer. Frequency shifts in agreement with experience are obtained for values of K_{eq} of the order of 3×10^6 lb/in. and for $Z_c = 6000$ lb sec/in.

Since all points on the curves of Fig. 4 correspond to resonance, it should be possible to obtain as many as three resonances in the region of multivalued power as the frequency is varied at constant W and constant level of excitation of the transducer. It is not difficult in practice to obtain two resonances in this region, with the low frequency resonance at a higher level of vibration than the high frequency one. The third resonance has not been observed, probably because the lowest peak could easily be masked by the finite width of the neighboring higher peak. However, systematic attempts to find evidence for the existence of a third peak have not been made.

Under certain conditions of operation a state of vibration may be obtained for which successive force peaks between the bit and the rock are alternately high and low. A subharmonic of the driving frequency is thus generated, similar to that obtainable electronically with bistable circuits. For solid bits with radial wings, such as those commonly used for percussion drilling, vibrating on hard rock, it is relatively easy to generate the second subharmonic, and with care, as low as the eighth subharmonic has been produced. Hence the region of multiple values of P can probably be more extensive and the curves more complicated in form than indicated in Fig. 4, probably for values of C less than 0.31.

Fig. 5 shows $P/P(\max)$ as a function of W/F_m for $C = 2.00$.

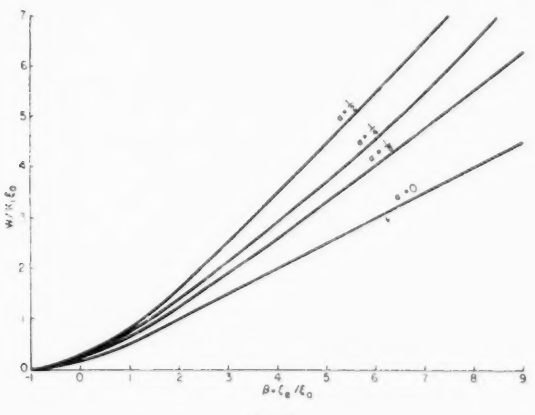

Fig. 3

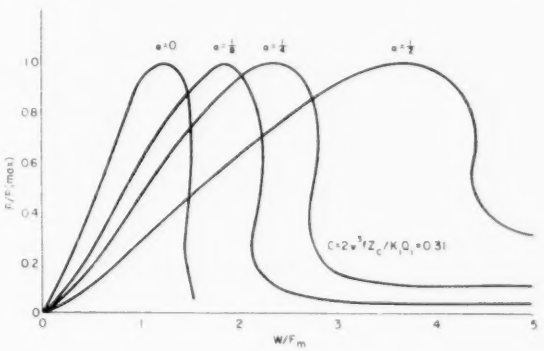

Fig. 4

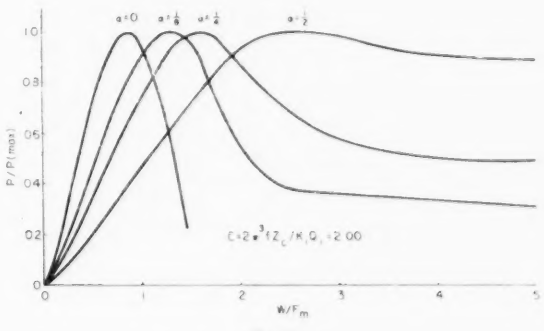

Fig. 5

It is noted that a region of multiplicity of values of $P/P(\max)$ does not exist and that the power output does not drop as precipitously with increasing W/F_m to the right of each maximum as for $C = 0.31$. The maxima occur for this case at values of β ranging between $+0.5$ to $+1.0$, that is, at higher on-times.

It would apparently be advantageous if P would rise up to its maximum value as W/F_m were increased and remain at that level as W/F_m were further increased, such as is approximated by the curve for $\alpha = 1/2$ in Fig. 5. The value of the weight on the bit would then not be critical, as long as it exceeded a certain multiple of the magnetostrictive driving force. It is readily demonstrated that this would occur for $C = 4[(1/\alpha) - 1]$ and that the minimum value of W/F_m required would be $(\pi/4)(3 - \alpha)/(1 - \alpha)$. It is seen from Fig. 5 that the optimum value of C would not be critical, since the desired condition is almost obtained for $C = 2.00$, whereas the optimum C would be 4.00 for $\alpha = 1/2$. Operation on the plateau of the curves is at 100 per cent on-time.

The only variable in the parameter C, given by Equation (10), that can be changed to any great extent is the resonant frequency f. It would certainly be desirable to keep the ratio Q_i/Z_c as high as feasible because $P(\max)$ is directly proportional to Q_i/Z_c, according to Equation (12). Q_i is increased by reducing all sources of vibratory energy dissipation to as low levels as feasible. Not much can be done about Z_c since it is desirable to fill up as much of the available space as possible with nickel in order to increase F_m.

From the condition that $C = 4[(1/\alpha) - 1]$ the optimum operating frequency, at which the power output of the transducer should be independent of weight on the bit above a minimum weight would be

$$f(\text{opt}) = (2/\pi^3)(K_2 - K_1)Q_i/Z_c \qquad (16)$$

Limitations of Results

There are many limitations that must be considered before attempting to apply the results of this analysis to practical design. Some of these limitations are understandably imposed by the deviations of the basic assumptions from reality. The conditions under which the basic assumptions represent sufficiently close approximations to reality must be outlined as concisely as necessary and the analysis should be extended to include first-order corrections, at least, for the deviations. In addition, there are other limitations on the analytical results imposed by such practical considerations as stress and temperature limits which may prevent operation at $P = P(\max)$.

Nodal Stress. The amplitude of the fundamental component of the nominal stress alternation at the node is given by [2]

$$\sigma_n = (4/\pi)QF_m/A_{tr} \qquad (17)$$

where A_{tr} is the area of the high modulus materials in the cross section of the transducer, that is, the nickel and steel casing.

If σ_n exceeds the maximum safe operating stress for $Q = Q_i/2$, it is necessary to operate at a lower power output than $P = P(\max)$. The maximum safe operating stress would be less than the fatigue strength of the nickel laminate by an amount that depends upon such considerations as the presence of points of stress concentration and of residual stresses in the structure of the transducer along almost its entire length, not only at the node. This is because the fundamental component of the stress amplitude does not decrease by more than $(1 - \sqrt{3}/2) = 13$ per cent over a distance of 1/3 the length of the transducer centered about the node, because the even harmonics (particularly the second harmonic), which contribute practically nothing to the stress at the center of the transducer, become important away from the center, and because of the stresses produced by the force pulses at the bit.

For one modification of the down-hole transducer, the effective value of F_m was about 11,000 lb, with $A_{tr} = 37$ in.^{2} and $Q_i = 125$. Hence, at $Q = Q_i/2$, the nominal value of the nodal stress amplitude would be 24,000 psi, as given by Equation (17), which is just above the fatigue strength of annealed nickel. 10,000 psi was found to be a safe operating value for the nominal nodal stress amplitude for the laboratory transducers.

If σ_n exceeds the maximum safe operating stress it must be reduced by decreasing Q, not by decreasing F_m. The latter expedient would reduce the power output in proportion to F_m^2, whereas the former would produce much less of a decrease in power output.

This is illustrated in Fig. 6. The upper solid curve of Fig. 6 represents the relationship between $P/P(\max)$ and Q/Q_i at a constant value of F_m. If the stress level at $P/P(\max) = 1$ is too high by a factor of 2.5, for example, reducing F_m by a factor of 0.4 would reduce the power output by a factor of 0.16, down to the lower solid curve at $Q/Q_i = 0.50$. However, by maintaining the maximum F_m and decreasing Q by a factor of 0.4 the power output is reduced by only 35 per cent, at the intersection of the two solid curves. The lower solid curve to the right of the point of intersection represents power output to the load as a function of Q at constant nodal stress level (decreasing F_m with increasing Q).

Expressed analytically, if σ_{ns} is the maximum safe value of the stress level at the node and $F_{ns} = A_{tr}\sigma_{ns}$ is the corresponding force level at the node, the maximum power output subject to the stress limitation is obtained when [2]

$$Q(\text{opt}) = (\pi/4)F_{ns}/F_m \qquad (18)$$

and has the value

$$P_s(\max) = [1 - Q(\text{opt})/Q_i]F_{ns}F_m/Z_c \qquad (19)$$

This variation of power output with Q, subject to a maximum stress amplitude at the node, was verified experimentally with a transducer terminated on one end with a variable friction brake load.

Efficiency. The over-all efficiency of conversion of input electrical power into the vibratory power in the rock load was not considered in the analysis. Altho gh maximum power output is the primary consideration, too low a conversion efficiency is distinctly undesirable because of the increased costs of operation necessitated by the excessively large power generating equipment required. The greater space required by the electrical transmission line in the drill string would also necessitate more powerful pumps for the drilling fluid. Hence, some sacrifice in power output is warranted if a distinct improvement in efficiency is thereby effected.

The dashed lines of Fig. 6 represent the total mechanical power generated by the transducer as a function of Q, including both the useful power output to the load and all the vibratory power dissipated elsewhere. The total power generated is proportional to Q, as shown by the straight line from the origin, if there is no limitation on the nodal stress level. However, the total power generated becomes inversely proportional to Q, as shown by the lower dashed line, for operation at a constant safe maximum nodal stress. It is to be noted that only 50 per cent of the total mechanical power output represents power into the load at $Q = Q_i/2$; whereas at $Q = Q_i/4$, for example, the efficiency of utilization of mechanical power is increased to 75 per cent and the power output to the load is decreased by only 25 per cent below $P(\max)$. The over-all conversion efficiency from electrical input power to the transducer to mechanical power in the load would also be increased thereby by almost the same factor for a well-designed transducer.

It would seem, therefore, that from both the viewpoints of nodal stress and improved efficiency, it would be preferable to

operate at values of Q less than $Q_i/2$; that is, to the right of the maxima of the curves of Figs. 4 and 5. The optimum shape of the curve of P as a function of W/F_m would then be one for which the plateau to the right of the peak is approximately 25 per cent or so lower than the peak; that is, for $C \cong 2[(1/\alpha) - 1]$ rather than $4[(1/\alpha) - 1]$. The curve for $\alpha = 1/2$ of Fig. 5 would represent this condition. The optimum value of the operating frequency would then be approximately half of that given by Equation (16).

Frequency. An upper limit to the frequency of vibration is determined by the ability of the transducer to dissipate heat and by the allowable temperature rise. Because $P(\max)$, as given by Equation (12), is independent of frequency, operation at $P(\max)$ or at some specified power level below $P(\max)$, as limited by stress or efficiency considerations, implies a greater rate of generation of heat per unit volume of transducer for higher frequency transducers, because of the decrease in length of the transducer with increasing frequency. Internal heat is generated not only by the internal damping of mechanical vibrations but by ohmic resistance, eddy current, and magnetic hysteresis losses.

Lower limits to the frequency are imposed by the increased length, and hence, increased cost of the transducer. It would be undesirable also from the viewpoint of ease in handling to have a transducer much longer than a section of drill collar (about 30 ft). The use of two or more sections for the transducer coupled by threaded joints is undesirable because of the excessive incidence of failure and excessive vibratory power losses in such joints unless they are fabricated to much greater precision than tolerable for repeated making and breaking in the field.

Operation at given amplitude of nodal force F_n implies a particular value of the amplitude of the fundamental component of velocity at the ends of the transducer, given by F_n/Z_c, which is independent of frequency. Operation at $P = P(\max)$ likewise implies a certain velocity amplitude which is the same at all frequencies for a half-wavelength transducer. Consequently, the amplitude of vibration under optimum operating conditions would decrease with increasing frequency. For example, for $\sigma_n = 10{,}000$ psi, the velocity amplitude is about 66 in/sec. This makes ξ_0 only 0.035 in. at 300 cps.

It would not matter how small the displacement amplitude is if the force-displacement characteristic assumed in this paper, as illustrated in Fig. 1(a), were strictly valid. Operation at higher frequencies and correspondingly lower displacements would merely imply lower peak forces and less energy per cycle, but the same power level. There is much indirect evidence, however, that there are effective thresholds in the actual force-displacement characteristics of bits on rocks that preclude the use of too low a vibration amplitude for the purpose of doing mechanical work on the rock. Experimental results indicate that this limitation is apparently already attained for solid-head bits with rounded tungsten carbide cutting edges at frequencies above about 100 cps, but not for rotary bits up to about 500 cps. There may indeed be no such limitations for rotary bits operated with $\xi_0 > \xi_0$ because the threshold force levels would be exceeded by the weight on the bit. Clearances and excessive damping in the cone bearings may set the upper frequency limit of rotary bits.

Other Transducer Configurations. The various relationships presented in this paper are applicable only for half-wavelength transducers. Some of the advantages and disadvantages of using multiple half-wavelength transducers are discussed in reference [2], and a more complete analysis of the interaction of the transducer with the rock load should include the possibility of such other configurations, particularly for use at higher frequencies.

A common type of transducer configuration employed, for example, in the ultrasonic drilling of hard materials, includes a steel tapered section of decreasing cross-section area from the magnetostriction generator to the tool. Greater amplitudes of vibration are thus attained at the load for a given stress amplitude at the node of the transducer. Excellent results have been obtained experimentally in vibratory drilling of shallow holes in rock smaller in diameter than that of the transducer by use of such an impedance transformer. It is doubtful that much, if anything, can be gained by terminating a down-hole transducer with a tapered section to the bit. Since the bit must be larger in diameter than the transducer, the inertia load of the bit and its sub might be great enough to prevent attainment of the increased amplitude of vibration resulting from tapering. However, this remains to be investigated.

Effect of Vibrations on Torque. In the process of rotary drilling without vibration, the nominally steady weight on the bit, W, displaces the bit a distance W/K_1 into the rock. Each tooth rolls into contact with the rock, penetrates it to the distance W/K_1, and rolls out again. The work done in rolling through an angle between one set of tooth contacts and the next is given by the area of the indicator diagram of Fig. 1(a) with $F_0 = W$, obtaining

$$E_t = (W^2/2K_1)(1 - \alpha) \tag{20}$$

The situation is actually more complicated than this because of the variation in angular spacing between successive teeth with radial position. However, if N is some effective value of the number of loadings per revolution, which will not be precisely defined, the torque required to turn the bit would be given by

$$L = (N/2\pi)(W^2/2K_1)(1 - \alpha) \tag{21}$$

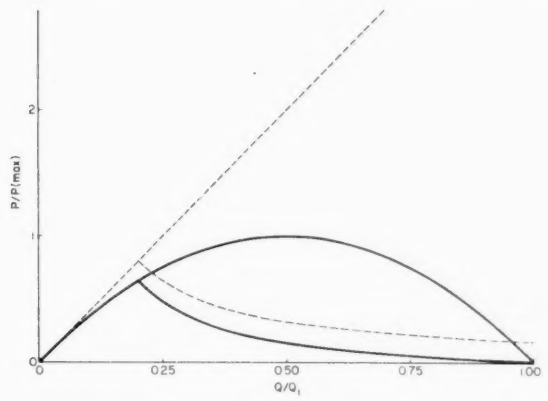

Fig. 6

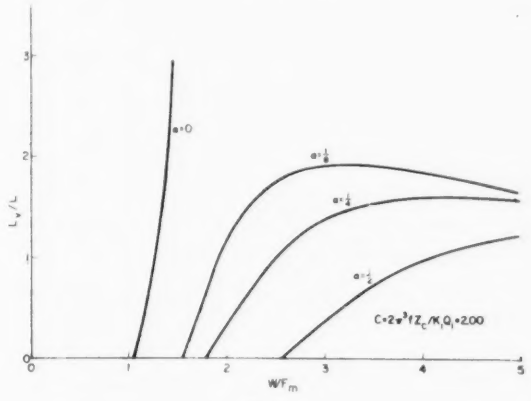

Fig. 7

Reference to Figs. 1(*a*, *d*, and *e*), respectively, show that when vibrating, the torque required to turn the bit would be given by

$$\left.\begin{aligned} L_v &= 0, \text{ for } -1 \leqslant \beta \leqslant +1, \\ &= (N/2\pi)(1/2)K_1\,\xi_0^2\,(\beta - 1)^2 \\ &\qquad \text{for } +1 \leqslant \beta \leqslant (2/\alpha) - 1 \\ &= (N/2\pi)(1/2)K_1\,\xi_0^2[(\beta - 1)^2 - \alpha(\beta + 1 - 2/\alpha)^2] \\ &\qquad \text{for } \beta \geqslant (2/\alpha) - 1 \end{aligned}\right\} \quad (22)$$

Hence, the ratio of the torque with vibration to that without vibration would be (the indefinite quantity N cancelling out)

$$L_v/L = (K_1\xi_0/W)^2 h(\alpha, \beta) \quad (23)$$

where $h(\alpha, \beta) = 0$, $(\beta - 1)^2/(1 - \alpha)$, or $[(\beta - 1)^2 - \alpha(\beta + 1 - 2/\alpha)^2]/(1 - \alpha)$ for the three respective ranges of β in Equation (22). Since $(K_1\xi_0/W)^2$ and W/F_m are known functions of β and α, L_v/L can be plotted as a function of W/F_m, obtaining Fig. 7 for the case of $C = 2.00$.

It is noted from Fig. 7 that, over certain ranges of values of W/F_m, the torque with vibration is less than that without vibration and for other ranges of values it is greater. This is in agreement with experiment. The ratio of the torques approaches unity as W/F_m increases indefinitely, as would be expected for either increasing W or decreasing F_m.

Comparison of Figs. 6 and 7 indicates that the torque begins to differ from zero at just about the positions for peak vibratory power. This occurs in this special case of $C = 2.00$ because the peaks come at values of β between 1/2 and 1, but it would not be true in general.

A zero or small value for the torque is a desirable condition for drilling with solid bits with radial wings, since bit wear would be thereby greatly reduced. A solid head bit is rotated mainly for the purpose of indexing the positions of impacts on the surface of the rock at the bottom of the hole. However, for rotary drilling, operation at zero or small torque means only that vibratory power is being substituted for rotary power. There is no point in substituting an expensive form of power for a less expensive form unless some other appreciable gain is achieved thereby, such as greatly reduced bit wear or a substantial net increase in power level. What little evidence exists on the rate of wear of rotary bits in vibratory drilling indicates that this rate is about the same as for rotary drilling at the same penetration rate. Substantial net increases in power level are obtained with vibratory drilling in hard rock, but the same increases can also be obtained at values of W/F_m for which L_v/L is approximately maximum by suitable choice of C. Operation at maximum L_v/L would imply that not only would the vibrations themselves feed appreciable amounts of power into the rock, but also the power produced by rotation would also be substantially increased with no increase in rate of rotation or weight on the bit.

It is seen from Fig. 7 that the ratio of L_v/L may be quite high for values of α of 1/8 or less. Since the value of α would depend upon both the characteristics of the rock and the geometry of the bit, it may be possible to control the value of α to some extent by suitable bit design.

Evaluation of Vibratory Drilling

In order for vibratory drilling to become economically competitive with rotary drilling, it would probably have to result in at least tripling the rate of penetration achievable by optimum rotary drilling techniques in medium to medium-hard formations [2]. The reason for this is essentially that the average cost of drilling a foot of hole depends on the ratio of the average cost of operation per unit time to the average rate of advance of the hole per unit time, round trips included. The former factor would also increase appreciably for vibratory drilling as compared with conventional rotary drilling.

For rotary drilling of a 10-in. hole in a medium hard rock like Columbus limestone (S = 40,000 psi), the operating values of the weight on the bit and rate of rotation as set by safe and economical drilling practice might be 40,000 lb and 60 rpm, respectively, resulting in a rate of penetration of about 40 ft/hr. This would require a power output to the rock of 40 hp, according to Equation (4). The problem of tripling this rate to 120 ft/hr involves the feeding of an additional 80 hp into the rock.

For a transducer of 33 in. of cross-section area of nickel operating at a maximum nodal stress level of 10,000 psi, the maximum power output available is 70 hp, according to Equation (19). In making this computation, F_m was chosen to be 0.7 of its maximum theoretical value for uniform excitation (15,000 lb), which would represent a good practical transducer for such an elongated shape. The value of $Q_i = 100$ was also assumed as representative of that achievable with careful design to reduce internal and extraneous external power losses. For the value of W given, $W/F_m = 3.8$, so that the torque might be expected to increase about 50 per cent or so, depending upon the value of α, thus contributing an additional 20 hp. With suitable choice of operating frequency, again depending upon α, it should be possible to obtain maximum vibratory power under the same conditions as the maximum torque increase, resulting in a total power output to the rock of 130 hp.

It is seen from these considerations that the required increase in power output to a medium hard rock might just about be achievable under optimum conditions of design and operation for a transducer that follows the bit down the hole. In extremely hard rock, however, it is a relatively simple matter to multiply the rate of penetration several times with vibratory drilling, even with a transducer of poor design operating under far from optimum conditions. However, the primary interest in oil-well drilling is apparently in the economical drilling of rocks of medium hardness.

Conclusions

(1) An analytical technique has been developed for predicting the performances of vibratory drilling systems by considering the interaction between the generator of the vibrations, a magnetostriction transducer operated at resonance, and assumed force-displacement characteristics with hysteresis for the mechanical system consisting of the bit vibrating on the rock.

(2) Most of the phenomena observed in laboratory and in field tests with vibratory drilling are predicted by this analysis. Among these phenomena are the waveform of the force between the bit and the rock, the dependence of the penetration rate on peak force and on-time, the comparative magnitudes of the fluctuation in penetration rates achieved by vibratory and rotary drilling in inhomogeneous formations, the double resonances and generation of subharmonics which occur under certain conditions of operation, the variation in power output with weight on the bit, the change in torque when vibrating, and the change in resonant frequency of the transducer produced by the rock load.

(3) An important dimensionless parameter for the process of vibratory drilling, C, combining variables associated with the transducer and variables associated with the system consisting of the bit vibrating on the rock, has been established. Its value determines the natures of the curves of power output as a function of the ratio of the weight on the bit to the magnetostrictive driving force. Some optimization analysis has been performed with respect to this parameter, resulting in an expression for the optimum operating frequency in terms of certain characteristics

of the transducer and of the system consisting of the bit vibrating on the rock.

(4) The analytical techniques developed herein should be applicable to rock drilling with resonant mechanical systems driven by other means than by magnetostrictive transducers. They should also have more general applicability to predict the performances of resonant systems with nonlinear loads other than rock, particularly for the types of loads for which tension forces between the vibrating system and the load cannot exist.

(5) It is tentatively concluded that vibratory drilling in rock of medium hardness may be just about economically competitive with conventional rotary drilling. In order to obtain a more definite conclusion in this regard, the following research is required:

(*a*) Experimental measurements of the force-displacement characteristics of bits on rocks, with due consideration to their possible dependences on the relative frequencies of rotation and vibration for each given bit geometry and to the possible existence of significant rate of loading effects for some rocks under some conditions of operation.

(*b*) Theoretical and experimental work to correlate the force-displacement characteristics of bits as a whole with the relationships among the forces, energies, and volumes of rock fractured out by the individual teeth of the bits.

(*c*) Extension of the present theory to include transducer configurations other than the half-wavelength vibrator and transducers other than magnetostrictive.

(*d*) Investigation of the possibility of developing bit designs more suitable for vibration drilling than standard rotary bits.

References

1 Collected Reports, Drilling Research, Inc., vol. 1–6, 1949–1954.

2 Summary Report, "Vibratory Drilling of Oil Wells," from Battelle Memorial Institute to Drilling Research, Inc., December 31, 1957.

3 R. M. Bozorth, "Ferromagnetism," D. Van Nostrand, Inc., New York, N. Y., chapter 13, 1951.

4 A. Lubinski, "Theoretical Investigation of Vibrations in a Magnetostrictive Transducer," Stanolind Oil and Gas Company, Research Department Report, January 24, 1956.

5 R. Simon, "Theory of Rock Drilling," Proceedings of the Sixth Annual Drilling and Blasting Symposium, University of Minnesota, October 11–13, 1956.

6 A. Nadai, "Theory of Flow and Fracture of Solids," vol. 1, second edition, McGraw-Hill Book Company, New York, N. Y., p. 188.

DISCUSSION

L. W. Ledgerwood, Jr.[4]

The author is to be congratulated for summarizing the analytical work done for Drilling Research, Inc., and for placing this summary in the public record for future use by other researchers.

It should be re-emphasized that this is a mathematical analysis of vibratory drilling. The author states that the analysis is developed for magnetostriction transducers but would be applicable to other types of transducers, but it appears that perhaps further evidence should be developed to support this statement. Because of the lack of experimental work reported in the paper, we feel that perhaps a better paper title might be "An Analytical Study of Magnetostriction Drilling."

We note that the author limits the applicability of this work frequency to above 100 cps and below 1000 cps. We would like to have the author discuss the applicability of this analysis to sinusoidal force displacement systems below 100 cps and in particular between 5 and 10 cps. Secondly, we also note that this is also confined to sinusoidal systems. We should like to have the author discuss its applicability to impact systems, that is, ones such as the Gulf hammer drill, the Hughes percussor, etc.

We are fully aware of the reasoning leading to the choice of 300 cps for the final form of the magnetostriction tool. With respect to this paper, however, we have several specific questions which we would like to ask:

1 If the results of this mathematical analysis had been available, would 300 cps have been chosen as *the* desirable frequency for the magnetostriction tool? In other words, does this analysis predict that 300 cps is an optimum desirable condition?

2 Concerning Conclusion 3, is it possible for an operator to use this mathematical analysis to (*a*) use a vibratory tool already designed in a better manner than is possible now, or (*b*) design a better operating tool? That is, how is the Factor C discussed in the paper applied to a real case?

3 Concerning Conclusion 4, would the author care to elaborate on the general applicability to other resonant mechanical systems? We do not believe there is sufficient evidence in this paper to show its applicability to such systems.

We most certainly agree with the author's conclusion concerning the need for further research on vibratory drilling, in particular, the items listed at the end of his paper.

[4] Jersey Production Research Company, Tulsa, Okla. Assoc. Mem. ASME.

Author's Closure

The author wishes to thank Mr. Ledgerwood for his thoughtful comments and agrees that the title Mr. Ledgerwood suggests would be more pertinent to the contents of this paper. The author had originally intended to present a paper outlining the results of the laboratory and field experiments in vibratory drilling under the present title, and hopes to have the opportunity to do so in the near future. However, the author developed the analysis presented in this paper after the completion of the experimental research program for Drilling Research, Inc., and felt that the early publication of this analysis would be of greater value to future researchers in this field than publication of a summary of the experimental results already reported in References [1] and [2].

The frequency range of about 100 to about 1000 cps is mentioned in the opening sentence of this paper in order to give the reader a concept of the approximate frequency range encompassed by the term "vibratory drilling" as distinguished from the developments of drilling systems by other investigators at frequencies primarily below this range, using both sinusoidal and nonsinusoidal displacement systems. It was not intended to limit the applicability of the subject analysis to any particular frequency range; the analysis would be applicable to any frequency range in which the assumption that the action of the vibrating bit on the rock could be represented by a force-displacement characteristic with hysteresis is a sufficiently good approximation to reality. In particular, this assumption might well be a much better approximation to reality for some types of rocks in combination with some types of bits at frequencies between 5 and 10 cps than at the higher frequencies, as could be ascertained by performing the experimental measurements suggested in Conclusion (5).

The particular analysis presented herein would not be applicable to nonresonant mechanical systems. However, it should be possible, in principle, to develop suitable analyses for such systems based on the assumptions presented in this paper regarding the nature of the interaction between the bit and the rock. The analytical development for a given mechanical impact system might be carried out as follows: (1) Start with a displacement versus time waveform for the bit as determined by

the driving mechanism, (2) compute the force versus time waveform as determined by the assumed force versus displacement characteristic for the bit vibrating on the rock and by the applied weight on the bit, (3) ascertain what effects, if any, the computed reaction force on the bit would have on the displacement waveform of the mechanism, (4) use the possibly modified displacement waveform to recompute the force waveform and repeat until successive approximations are in reasonable agreement, and finally (5) compute the mechanical power output to the rock.

The answers to the three specific questions are:

(1) The analysis predicts that the value of the maximum mechanical power output to the rock should be independent of frequency, subject to the limitations discussed in the paper. This is in agreement with experiment. The optimum frequency discussed in the paper is the frequency at which the value of the weight on the bit should not be critical for obtaining operation at $P(\max)$ or at some usable fraction of $P(\max)$. There would be no way of ascertaining the value of this optimum frequency from the results of the analysis alone, since the unknown constants K_1 and K_2 are involved in the expression for $f(\text{opt})$. The values of these constants would be measured by the suggested experiments.

(2) The dimensionless parameter C has been discovered as a result of this analysis as an important parameter in determining the nature of the curves of $P/P(\max)$ as functions of W/F_m. It would be premature at present to say how this parameter might be used to obtain improved performance of present vibratory tools or to design better tools. The full ramifications of the effects of the numerical value of C remain to be investigated; only two values of C were used by the author in computing curves of $P/P(\max)$ as functions of W/F_m and only a single value of C for computing curves of L_c/L as a function of W/F_m. The author did not consider it worth while to investigate the effects of the value of C more thoroughly until more experimental evidence is available on the nature of the force-displacement relationships of bits vibrating on rocks. If the assumed straight-line relationships of Fig. 1(a) do not represent sufficiently good approximations to reality, the definition of C would have to be revised to incorporate the physical constants descriptive of the revised characteristics.

(3) The analysis developed is strictly applicable to the particular case of a column vibrating longitudinally at the resonant frequency of its fundamental mode and driven by magnetostrictive action distributed uniformly along its length. However, only slight modifications of the analysis would be required to make the analysis applicable to other mechanical resonant systems for which the rock load would not react on the system sufficiently to distort the sinusoidal waveform of the motion of the bit to any appreciable extent. These modifications are: (a) The reformulation of Equation (1) to an expression for the pertinent relationship between the amplitude of the displacement of the bit ξ_0, the Q of the new system, and the amplitude F_r of the Fourier component of the lumped or distributed driving force at the resonant frequency of the new system, and (b) the reformulation of Equation (3) to incorporate the new pertinent expression for the stored energy as a function of ξ_0. All of the rest of the analysis would remain the same. The same curves of $P/P(\max)$ as functions of W/F_r would be obtained, as illustrated in Figs. 4 and 5, with a different numerical scale for the abscissa because of the use of W/F_r instead of W/F_m, and a different definition of C to include F_r and the mechanical characteristics of the new system analogous to Z_c. These two modifications would also be the only ones needed to cover magnetostrictive drive systems other than half-wave vibrators or magnetostrictive drive systems incorporating mechanical transition elements between the vibrator and the bit. Furthermore, if the reaction of the rock load were great enough to alter appreciably the sinusoidal nature of the motion of the bit, the successive approximation technique outlined here for use in the analyses of nonresonant systems could be employed also in the analyses of resonant systems.

Vibrations of Vertical Pressure Vessels

C. E. FREESE

Mechanical Engineer, The Fluor Corporation, Ltd., Los Angeles, Calif. Mem. ASME

This paper is primarily concerned with the vibration of vertical pressure vessels known as columns or towers.

The procedure for estimating the period of the first mode of vibration for columns which are the same diameter and thickness for their entire length is outlined. A graph is included for this purpose which recommends limits between vessels considered to be static structures and those considered dynamic.

A method for designing vessels considered as dynamic structures is described as well as a detailed procedure for estimating the period of vibration of multithickness (stepped shell) vessels and/or vessels built to two or more diameters with conical transitions where the difference in diameter is small.

There is a brief résumé of the "Karman vortexes" effect and a discussion regarding vibration damping by liquid loading and the benefit of ladders and platforms which help reduce the effect of periodic eddy shedding.

The design procedure outlined will be useful to the practical vessel designer confronted with the task of investigating vibration possibilities in vertical pressure vessels.

Introduction

FOR MANY YEARS it was customary to apply guy wires to tall, slender pressure vessels. In recent years, refinery and petro-chemical officials have demanded self-supporting vessels from the standpoint of plant appearance and safety.

In order to design a self-supporting vessel of this type, the following problems must be carefully analyzed:

1 When is it necessary to deviate from the common practice of designing a vertical vessel as a static structure and consider it as a dynamic structure?

2 What is the most practical method for designing to meet dynamic conditions?

3 Does the method used produce consistent results and does it provide additional strength to resist the force due to the mass-acceleration resulting from the motion of the vessel?

4 Is the period of vibration of the dynamically designed vessel such that prevailing winds are not apt to cause excessive movement?

5 Are the external attachments (such as piping, ladders, and platforms) distributed all around the vessel to guard against resonance due to eddy shedding in the "Karman vortex trail" at critical wind velocities?

These problems will be discussed during the outline of a design procedure presented in this paper.

Before proceeding, it should be pointed out that vessel vibrations induced by earthquakes are infrequent in occurrence and this paper is more concerned with vibrations induced by wind or other forces which may occur every day or many times during the day depending upon the location.

Contributed by the Petroleum Division and presented at the ASME Petroleum-Mechanical Engineering Conference, Denver, Colo., September 21–24, 1958, of THE AMERICAN SOCIETY OF MECHANICAL ENGINEERS.

NOTE: Statements and opinions advanced in papers are to be understood as individual expressions of their authors and not those of the Society. Manuscript received at ASME Headquarters, July 9, 1958. Paper No. 58—PET-13.

Nomenclature

f = lowest natural frequency of vibration, cycles per second

$T = \frac{1}{f}$ = period of vibration, sec

g = acceleration due to gravity

W = total weight of vessel or vessel section above horizontal plane under consideration, lb

W_s = shear load at end of section, lb

w = unit weight, lb/ft

w' = weight of vessel element or internal part, lb

L = total length, ft

l = length of element or section, ft

D = vessel diameter, ft

d = vessel diameter, in.

t = thickness of vessel shell, in.

$h = \frac{t}{12}$ = thickness of vessel shell, ft

y = deflection of element or section, ft

y' = distance from c.g. of vessel element or internal part (of weight w') to seam or horizontal plane under consideration, ft

F_s = seismic factor

$E' = 4320 \times 10^6$ = modulus of elasticity for steel, lb/ft²

E = welded joint efficiency

$I = \frac{\pi}{8} D^3 h$ = moment of inertia of vessel shell cross-sectional area, ft⁴

V = velocity, ft/sec

k = Strouhal number

θ = end slope of element in bending as a cantilever beam, radians (tan $\theta = \theta$)

P = internal pressure, psig

S = allowable stress of vessel material, psi

M = moment about vessel seam or horizontal plane under consideration, lb-ft

M_T = moment at end of vessel section resulting from weight of sections to the right of section under consideration

C = corrosion allowance

R = Reynolds number

Design Procedure

It is customary for most vessel designers to establish the minimum vessel shell and head thickness according to the pressure-temperature conditions and then calculate the thickness required at the bottom head seam due to bending moments imposed by wind or earthquake forces [9].[1] Stresses in the longitudinal direction are involved and the following notation may be used to summarize the thickness required:

$$t = \left| \pm \frac{Pd}{4SE + 0.8P} \pm \frac{48M}{\pi d^2 SE} - \frac{W}{\pi d SE} \right| + C \qquad (1)$$

The terms within the absolute value signs are positive for tensile stresses and negative for compressive stresses. The first term gives the thickness required for the longitudinal stress resulting from internal pressure and is positive for pressures above atmospheric and negative for pressures below atmospheric. The second term is the thickness required to resist the longitudinal bending stress and both positive and negative values exist at the same time. The third term is the thickness required for the weight of the vessel above the seam being investigated and, since this is a compressive stress, it has a negative value. The combination giving the highest value establishes the thickness required to resist the longitudinal stresses.

Consider equation (1) for a typical vessel operating at an internal pressure greater than atmospheric:

$$t = | + 0.275 \pm 0.307 - 0.063 | + 0.125$$

The required thickness within the absolute value signs will have two values; namely, +0.519 in. and −0.095 in. Therefore the minimum thickness required is 0.519 + 0.125 in. corrosion allowance = 0.644 in.

Next consider equation (1) to appear as follows for the same vessel operating under vacuum conditions:

$$t = | -0.123 \pm 0.307 - 0.063 | + 0.125$$

For this case, the two values within the absolute value signs are −0.493 and +0.121 in. resulting in a minimum thickness of 0.493 + 0.125 in. = 0.618 in.

As previously stated, the moment M is the longitudinal bending moment due to wind or earthquake, either of which may be combined with eccentric loads imposed by mounting heavy equipment on the vessel. All designers are accustomed to evaluating moments due to eccentric and wind loads, but there are a few who may not be familiar with the method used for estimating moments due to earthquake. Therefore, the following brief outline is presented because this method is recommended as a design procedure for vessels where dynamic considerations are required.

The weight of each vessel element (shell, head, tray, or internal part) is calculated and then multiplied by the vertical distance from the circumferential seam (or horizontal plane) under consideration to the center of gravity of the element. The summation of the moments so found is multiplied by the seismic factor for the area where the vessel is to operate, thereby yielding a moment due to earthquake or seismic disturbance. For vessels, the seismic factor will usually have a value of 0.03 to 0.12, depending upon the geographical location. Expressed mathematically,

$$M = F_s \Sigma w' y' \qquad (2)$$

After the vessel has been designed in the regular manner (considered as a static structure) it should be investigated regarding its possible behavior under vibration conditions. If the vessel shell is of constant diameter and thickness for its full length, the period of vibration may be easily found from the graph shown in Fig. 1. This graph is plotted from the general formula for the period of the first mode of vibration of a cantilever beam [7]:

$$T = \frac{2\pi}{3.52} \left(\frac{wL^4}{E'Ig} \right)^{1/2}$$

$$= 1.785 \left(\frac{wL^4}{E'Ig} \right)^{1/2} \qquad (3)$$

For a steel cylindrical shell, equation (3) may be written:

$$T = 7.64 \times 10^{-6} \left(\frac{wL^4}{D^3 h} \right)^{1/2} \qquad (4)$$

By rewriting equation (4) in the form:

$$T = 7.64 \times 10^{-6} \left(\frac{L}{D} \right)^2 \left(\frac{wD}{h} \right)^{1/2} \qquad (5)$$

the variables (L/D) and (wD/h) are used as parameters to plot the graph in Fig. 1.

One of the first graphs of equation (4) was issued by a major oil company for their refinery work. In its original form, all vessels having a period of vibration over 0.4 sec were ordered designed as dynamic structures and those having a vibration period of 0.4 sec or less were ordered designed as static structures. Experience has shown that a more practical limit for this division is a line drawn from 0.4 sec at the extreme left of the graph to 0.8 sec at the extreme right and considering vessels having a period of vibration above this line to require dynamic consideration and those below to require designing as a static structure. The reason for revising the former limit is the fact that many vessels having small (L/D) ratios and large values of (wD/h) have given satisfactory service although their period of vibration exceeded 0.4 sec. In general, vessels having an (L/D) ratio less than 15 are not apt to be critical from a vibration standpoint. One exception to this statement, unofficially reported to the author, involved two vessels operating near a railroad whereby they were vibrated by railroad equipment. Both vessels had a period of vibration considerably less than 0.4 sec and their frequency probably coincided with the frequency of the exciting force, thereby causing resonance. This type of response is difficult, if not impossible, to predict accurately and should be considered as a special case.

If investigation indicates that the vessel should be designed as a dynamic structure, the method of seismic analogy is recommended. This method consists of designing the vessel for earthquake conditions using a seismic factor $F_s = 0.20$, regardless of the geographical location. In most cases, the vessel will have thicker shell and head material in the lower section. As an example, consider a vessel 10 ft 0 in. diameter by $^{13}/_{16}$ in. thick by 190 ft 0 in. high which has an (L/D) ratio of 19, and a period of vibration (after being designed as a static structure) of 1.65 sec. This vessel, when designed as a dynamic structure by the method of seismic analogy, resulted in a shell thickness of $^{13}/_{16}$ in. for the upper 137 ft 0 in. and three lower sections consisting of $^{7}/_{8}$, $^{15}/_{16}$, and 1-in. thick material (the supporting skirt increased from 1 to $1^{9}/_{16}$ in.). The period of vibration was reduced to approximately 1.4 sec.

Whereas the application of this method actually consists of trial and error, the experienced pressure vessel designer becomes very proficient in estimating how far down the vessel he can utilize the material thickness which is based on pressure-temperature requirements, as well as the length of successive sections of thicker material. It is usually unnecessary to carry the seismic analogy into the design of the anchor bolts because this method is applied

[1] Numbers in brackets designate References at end of paper.

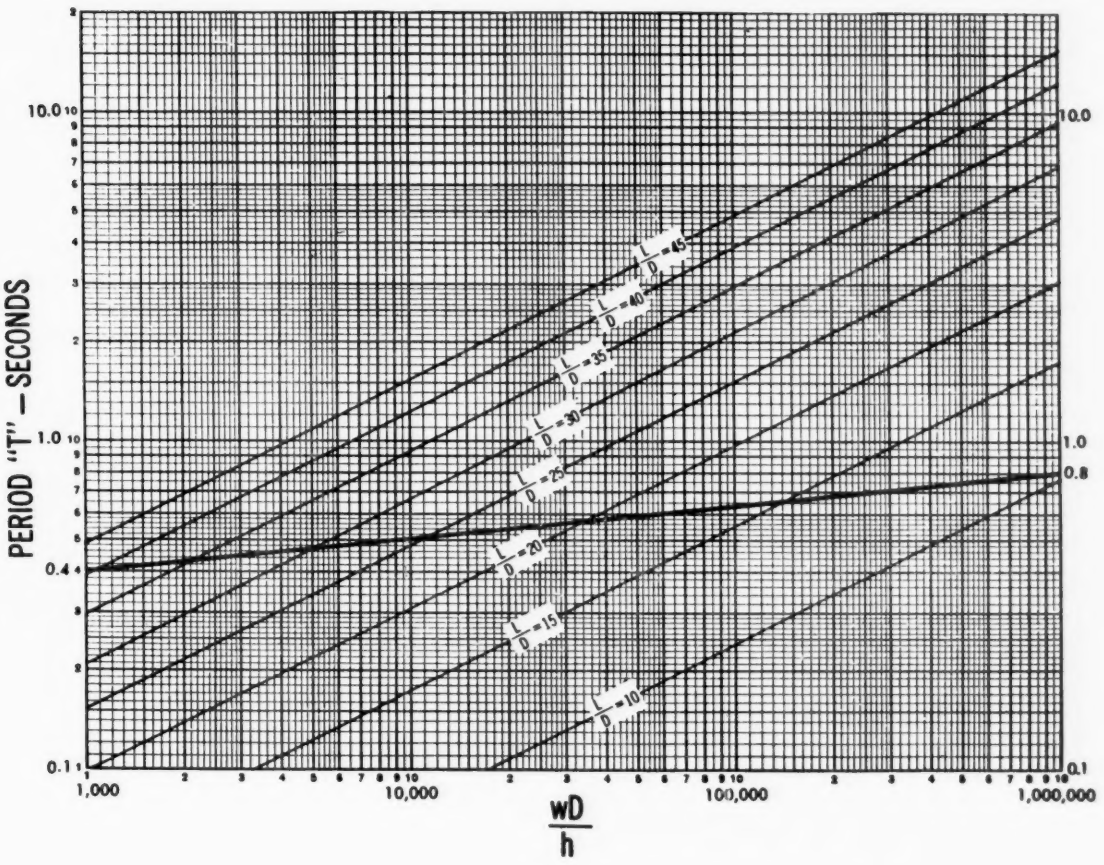

Fig. 1

only as a "yardstick" to provide reasonable protection with a minimum amount of additional material. However, anchor bolt stresses should be held low (15,000–16,000 psi) for these vessels or, if a higher stress is used, the design procedure outlined should be applied to them. Proper tightening of anchor bolts for vessels subject to dynamic behavior is of utmost importance and it is recommended that they should be pretightened to the predicted working stress to avoid stretching and loosening in service. It is definitely unnecessary to apply this method to the design of the foundation unless the vessel is operating in a seismic area.

The design procedure just outlined produces consistent results and also provides additional material to resist the force due to mass-acceleration of the vessel in motion. A number of years ago, approximate calculations indicated that the total force due to wind load plus the force due to mass acceleration was about 1.5 to 1.75 times the static force due to a 30 lb/ft² wind load for several different size vessels. It was found that the recommended design procedure resulted in shell thicknesses within a few thousandths of an inch of those obtained by the more lengthy approximation. Many critical vessels have been successfully installed which were designed to the seismic analogy method just described.

The same company that produced the first graph of equation (4) tentatively recommended the seismic design method using a 0.20 seismic factor for their vessels requiring dynamic design in order to be on the "safe side." Since this company was mainly interested in the response of vessels and other structures to earthquake induced vibration, they later revised their recommendations as follows:

Natural period of vibration	Earthquake coefficient
Less than 0.40 sec	0.20
0.40 sec to 1.0 sec	0.08 divided by period
Greater than 1 sec	0.08

Attention is again called to the fact that this paper is primarily concerned with vibrations induced by wind or other forces which occur more frequently than earthquakes and it should be noted that the vessel reported as Case II under Field Data is well within the later recommendations outlined here and vibration trouble was encountered. It is agreed that the current practice is probably adequate for earthquake design; however, all critical vessels (except the vessel reported as Case II) designed and installed by our company have been designed to the seismic analogy method using a 0.20 seismic factor.

Not all vessels designed as static structures have the same thickness of shell for their entire length and some vessels are of more than one diameter. These vessels, as well as many designed as dynamic structures cannot have their period of vibration estimated from the graph in Fig. 1 or equation (4). It is also desirable to know the change in the vibration period resulting from dynamic design. Of the several methods referred to in reference books on vibration [1, 2, 3] the numerical integration of the equation

$$T = 2\pi \left(\frac{\Sigma W y^2}{g \Sigma W y} \right)^{1/2} \tag{6}$$

is probably the easiest and safest method for the designer who is not a specialist in vibration to apply. This equation follows the Rayleigh method of approximation for finding the fundamental period of vibration as applied to a shaft or loaded beam on two supports. It will be shown that this equation is reasonably accurate for estimating the period of the first mode of vibration of vertical pressure vessels.

Equation (6) will result in an estimated period of vibration slightly lower than the actual period. The degree of accuracy is dependent upon the number of sections calculated in estimating the static deflections when the vessel is considered as a cantilever beam deflecting under its own weight. As an example, the period of vibration of a cylindrical shell 3 ft 0 in. diam by $^3/_4$ in. thick by 90 ft 0 in. high was estimated under two separate conditions. In order to eliminate nonuniformly distributed masses, this shell was considered to have tray sections at one-foot intervals from the top to the ground and the heads were omitted. When calculated to equation (4), the period of vibration was found to be 1.088 sec. Dividing the shell into nine sections, each 10 ft 0 in. long and calculating the period to equation (6) resulted in an estimated period of 1.08 sec which is 0.735 per cent low. On the other hand, when this same shell was divided into five sections having lengths of 30 ft 0 in., 20 ft 0 in., 15 ft 0 in., 15 ft 0 in., and 10 ft 0 in., the estimated period of vibration to equation (6) was 1.068 sec which is 1.84 per cent lower than the results from equation (4). Most vessels designed as dynamic structures have five to ten sections similar to the latter division and the weight is not always uniformly distributed. Field tests have shown the calculated period of vibration to be 1.5 to 4.5 per cent lower than the observed periods for several different size vessels. This is in good agreement for large structures and it is reasonable to assume that the period of vibration obtained by the numerical integration of equation (6) will be approximately 5 per cent lower than the actual period.

Equation (6) is not difficult to integrate numerically, but care must be exercised to make certain that all factors affecting deflection are included. Instead of following a complete numerical integration, some designers prefer to estimate the deflections at the center of each section graphically by either the area-moment or conjugate beam method. The same results will be obtained. The choice of method depends upon the personal preference of the individual. An outline for the numerical integration of equation (6) when applied to vertical pressure vessels is given in the Appendix of this paper.

Discussion of Wind Effects

Tall, cylindrical structures such as pressure vessels and stacks are subject to being put in oscillatory motion by wind currents. The motion is at right angles or normal to the direction of the wind. This phenomenon is usually referred to as resulting from the Karman vortex trail [4, 5, 6, 10]. The relationship between wind velocity and frequency of eddy shedding is given by the equation

$$V = \frac{fD}{k} = \frac{D}{Tk} \tag{7}$$

Since we are primarily concerned with the resonant condition which occurs when the frequency of eddy shedding equals or is in the neighborhood of the natural frequency of vibration for the vessel, the symbols for the vessel frequency and period of vibration are shown in equation (7). From this equation, we can estimate the critical wind velocity for most vessels.

The value for k was first determined in 1878 by V. Strouhal as 0.185 and is known as the Strouhal number [10]. It is assumed by some authorities to be within 0.18 to 0.27 and dependent upon the velocity of flow [4]. The reproduced graph shown in Fig. 2 gives the variation of the Strouhal number with the Reynolds number as obtained experimentally by Relf and Simmons [10]. Research engineers, employed by the same company as the author, reported the following values for k obtained from full size vessels after erection [12]:

k = 0.133, for a 7.67 O.D. insulated vessel at a wind velocity of 39.6 ft/sec (27 mph)

k = 0.189, for a 3.0 O.D. vessel at a wind velocity of 32.25 ft/sec (22 mph)

The difference between the values reported from field data and the graph is probably due to the size of cylinders tested and the method of support. When the velocity of the wind is such that the frequency f in the equation corresponds to the natural frequency of the vessel, resonance occurs and the vessel will oscillate at an excessive amplitude. Since aerodynamic stability theory and calculation methods are beyond the scope of this paper, the reader should refer to Steinman's paper [10] and similar publications for additional information on this subject.

One vessel, not designed to the seismic analogy method outlined herein, gave trouble due to wind induced vibration. This vessel is identified as Case II under Field Data. It was found to be free from vibration when the wind was blowing from a direction such that nearby equipment disturbed the flow pattern and it is conceded by some individuals that the external attachments also helped to reduce or nullify the effect of periodic eddy shedding. It is recommended that any vessel, where possible vibration trouble is indicated, should have the external appurtenances located around its circumference and not placed on only one or two sides as was done with this vessel. The break in vertical ladder runs demanded by some states helps to accomplish this because intermediate platforms and ladders are distributed circumferentially. The same vessel which gave trouble when empty has been satisfactory after liquid loading. Therefore the additional damping effect of liquid loading cannot be ignored—on the other hand, neither can too much confidence be put in it as a cure-all.

Some engineers are also concerned regarding the possibility of the vessel being vibrated at a frequency corresponding to its second mode of vibration. The second mode of vibration for a cantilever beam has a frequency of 6.37 times the frequency of the first mode [7]. This relationship will not necessarily hold true for multithickness and/or multidiameter vessels and more involved methods of analysis for the second mode frequency have to be employed. The Ritz method [8] which is a further development of Rayleigh's method can be used for these cases. It is sometimes referred to as the Rayleigh-Ritz method and should be applied by designers specializing in vibration problems. For the average vessel, it is not unreasonable to assume that the second mode frequency might occur between five to six times the frequency of the first mode. If a wind velocity of thirty miles an hour has been estimated to induce vibration in the first mode, it is reasonable to conclude that vibrations in the second mode will not be induced by any wind less than one hundred fifty miles per hour. On the other hand, a vessel subject to vibration in the first mode by winds of only ten miles an hour might be vibrated in the second mode by winds of fifty to sixty miles per hour if external attachments do not interfere with the periodic eddy shedding. Surrounding structures and terrain will also have some bearing on the considerations involved.

It is not the intention of this paper to overamplify the possibility of the second mode of vibration. Some engineers maintain that vibrations in the second mode could be catastrophic; how-

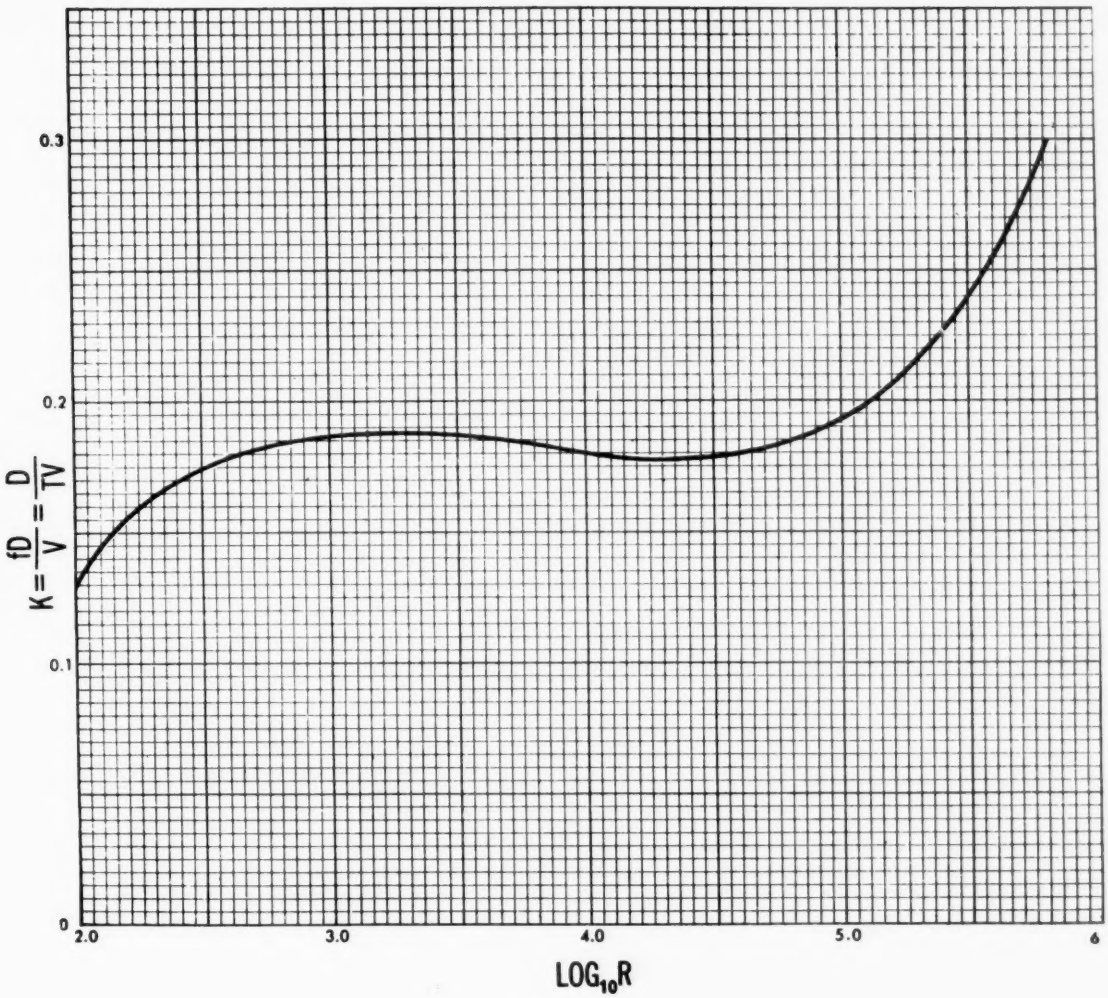

Fig. 2

ever, to the knowledge of this author no case of this type of failure has ever been recorded. In fact, no one has reported a second mode vibration in a self-supporting vertical pressure vessel and vessels are in service which have (L/D) ratios in the neighborhood of 40:1. Steinman's paper refers to the Meier-Windhorst tests at the Hydraulic Institute at Munich (1939) wherein the hydrodynamic oscillations of cylinders yielded sharply defined results for (a) the low velocity range, (b) critical range, and (c) high velocity range, and further states that, "In these vortex induced oscillations, there is no 'catastrophic range' of increasing amplification with unlimited increase of steam velocity" [13].

Discussion of Correction Methods

This paper would not be complete without a brief discussion of possible remedies if trouble occurs. One of the first things done to the vessel reported as Case II under Field Data was to try a spring loaded damping device originally designed by a large process engineering concern and shown in Fig. 3. This device had practically no effect on the behavior of the vessel. It can be argued that the spring load of 800 to 1000 lb results in a horizontal force of only about 200 to 300 lb at the top of the vessel and this small force will have very little effect on a moving vessel weighing 50,000 to 300,000 lb. If the spring load is doubled, the resisting load at the top of the vessel is still a small factor in reducing vibration or limiting the resulting deflection. However, if an accurate estimate can be made of the vertical expansion for the operating temperature involved, the spring could be designed and installed so that the assembly resulted in full cable tension during operation. This in turn becomes a hazard, because of possible cable breakage which would endanger personnel. It has been suggested that the spring could be entirely eliminated, but this does not appear attractive due to the thermal expansion of the vessel during operation and the subsequent danger of cable breakage just outlined. Carrying the wires over sheaves and then straight down to the foundation as shown in Fig. 4 has similar drawbacks. Aerodynamic paneling similar to that used on the pipeline suspension bridge [6] has also been suggested, but is not always desirable from other standpoints, such as appearance and easy access to all sections of the vessel. If paneling is used, the sections should be attached by bolting them to clips which

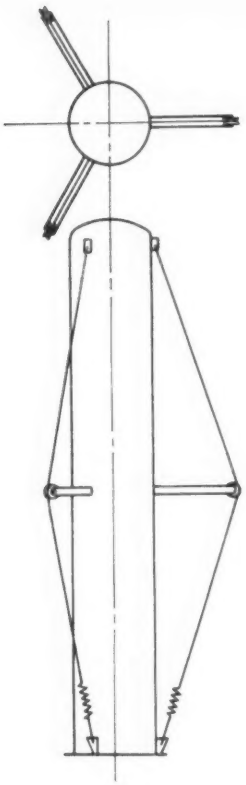

Fig. 3

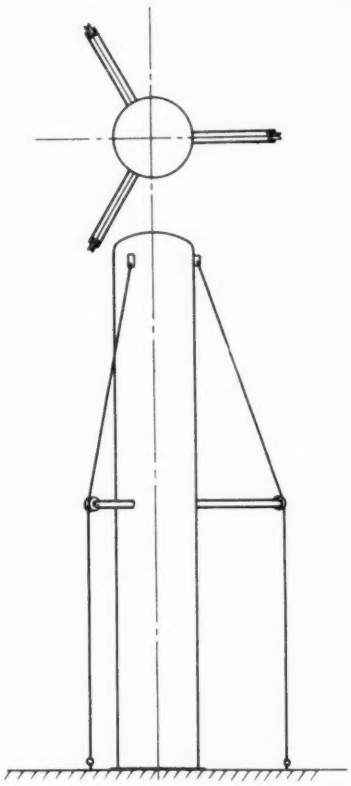

Fig. 4

have elongated or oversize holes to provide differential expansion during operation. In some cases additional rolled plate can be applied at the lower section which will increase the stiffness and lower the period of vibration. Vertical beams welded for the length of the vessel could be used, but are not recommended because of their restraining effect under thermal conditions and possible discontinuity stresses. One practical approach is to design the vessel so that there is a separate section in the top which can be partially filled with liquid (water or mercury if high density is required). The action of the liquid will rapidly dampen the vibration and help prevent excessive amplitude build-up, because at the instant the oscillatory motion has its maximum acceleration, the liquid is still moving in the opposite direction thereby creating a damping effect. This is the same effect (only of greater magnitude) as observed from the tray liquid reported in Case II under Field Data. Of course the choice of liquid and the possibility of using this type of damping is dependent upon the temperature involved. To date, it has not been necessary to resort to any of these methods for vessels designed to the method outlined in this paper.

Field Data

Case I 54 in. I.D. × 146 ft-0 in. High Vessel Shown in Fig. 5.

This vessel was designed to the seismic analogy method described in this paper. Field engineers checked the period of vibration by setting the vessel in motion and observing its frequency and amplitude with a surveyor's transit sighted on a target rod mounted horizontally at the top of the vessel. A stop watch was used to time the number of cycles. This vessel could be oscillated by two men exerting a back-and-forth motion at the top platform. Whereas formal data were not retained, the engineering records show that they found the period of vibration to be 1.67 sec. Calculating the period of vibration by the Rayleigh approximation (6), using six sections gives a period of vibration of 1.61 sec which is 3.6 per cent lower than the observed period.

Although the calculated wind velocity required to cause resonance is only 10–12 mph, this vessel has operated without any difficulty. The external attachments were well distributed about the circumference.

Case II 84 in. I.D. × 145 ft-6 in. High Vessel Shown in Fig. 6.

This vessel was not designed to the seismic analogy method. The thickness of the shell was increased in the lower section to withstand a high wind loading. During the construction period, this vessel was observed to be vibrating under certain wind conditions and, not only was the amplitude great enough to be alarming, but the anchor bolts stretched and an adjoining reboiler was loosened at its foundation.

Research engineers were sent to the field and made a comprehensive study of the installation. It was observed that resonance occurred at wind velocities in the neighborhood of 27 mph. As previously mentioned, critical vibration was induced when the wind came from a certain direction and, although the vessel could be mechanically vibrated from any direction, the vessel was "frequency-polarized" due to the orientation of the trays and welded downcomers. The maximum amplitude was 0.45 ft during resonance.

The vibration was recorded by strain gage-oscillograph equipment and accurate wind velocity readings were recorded at several different elevations. The recorded amplitude measurement was checked with a surveyor's target rod and transit as outlined under Case I.

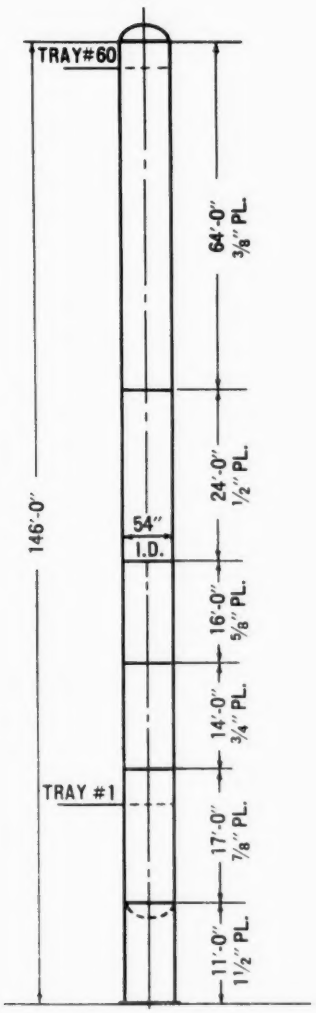

Fig. 5

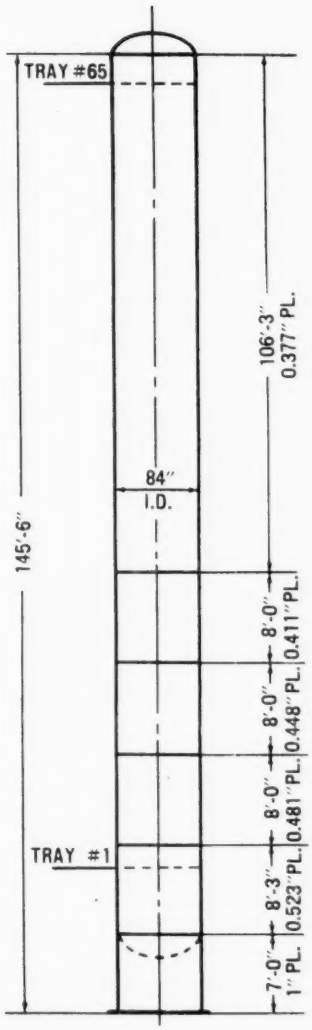

Fig. 6

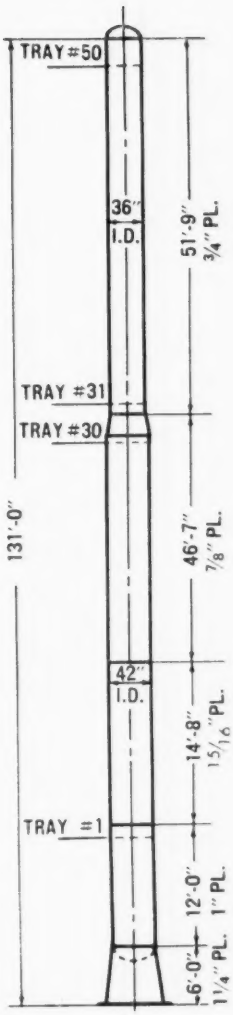

Fig. 7

During the investigation, the Strouhal number for this column (7.67 ft O.D. of insulation) and another 3 ft D column was obtained. These are reported in the Design Procedure section of this paper.

Using the term "per cent decrement," defined as each amplitude having a swing equal to a certain percentage less than that of its predecessor, this column was found to have a $3\frac{1}{2}$ per cent decrement when the vessel was empty and a 14 per cent decrement when the trays were liquid loaded.

The logarithmic decrement for this column is approximately 0.035 without liquid loading and approximately 0.133 loaded with liquid.

The calculated period of vibration of 1.42 sec is 4.05 per cent lower than the observed period of 1.48 sec.

Case III 36 in. I.D. × 42 in I.D. × 131 ft-0 in. High Vessel Shown in Fig. 7.

This vessel, which was designed to the seismic analogy method, has a calculated period of vibration of 1.61 sec. Field readings were taken in the manner outlined under Case I. The readings shown in Table I were taken before the insulation was applied. The average observed period of vibration is 1.64 sec.

The readings shown in Table II were taken after the insulation was applied. The column was also pressurized at 210 psig and had a bottom temperature of 340 F and a top temperature of 90 F. There was no liquid on the trays but there was about four feed of liquid in the bottom. Both sets of readings were taken in still air. The average observed period is 1.69 sec.

The calculated period of vibration is only 1.83 per cent lower than the average from Table I and 4.15 per cent lower than the average from Table II.

The numerical integration of equation (6) consisted of considering the skirt to be 51 in. average diameter and the 42 in. D section as extending to the top of the conical reducer. In addition, the upper 51 ft 9 in. consisting of $\frac{3}{4}$ in. thick plate was divided into three sections as was the 46 ft 7 in. of $\frac{7}{8}$-in. thick plate of the 42 in. D section, making a total number of 9 sections.

Calculations indicate a critical wind velocity in the neighborhood of 8–10 mph for this vessel. No excessive movement has

TABLE I						
Observer	Time – Seconds	Number of Cycles	Amplitude at Start – Feet	Amplitude at Finish – Feet	Period – Seconds	Percent Decr't.
1	38	24	0.15	0.05	1.58	4.66
2	51.5	31	0.20	0.05	1.66	4.52
3	49	30	0.20	0.05	1.64	4.67
1	67	40	0.20	0.03	1.67	4.75
2	50.2	30	0.20	0.05	1.68	4.67
3	50.4	31	0.20	0.05	1.62	4.52
				Aver. →	1.64	4.63

TABLE II						
Observer	Time – Seconds	Number of Cycles	Amplitude at Start – Feet	Amplitude at Finish – Feet	Period – Seconds	Percent Decr't.
3	31	19	0.25	0.05	1.63	8.55
1	33.2	20	0.30	0.05	1.66	9.00
3	38.2	22	0.30	0.05	1.74	8.18
1	38.2	22	0.30	0.05	1.74	8.18
				Aver. →	1.69	8.48

been reported and here again, the external attachments are well distributed about the circumference.

The increased per cent decrement in Table II is partly due to the addition of the insulation which would have a more noticeable effect on a small diameter column. Internal pressure is believed to increase the stiffness and probably was a contributing factor. Whereas the bottom liquid is near the base and would not be expected to contribute to the increase in per cent decrement, it could conceivably have some effect.

The corresponding logarithmic decrements for the two conditions are 0.045 and 0.082.

Conclusion

1 Self-supporting vertical pressure vessels should always be investigated regarding their possible behavior under vibrating conditions.

2 If the statically designed vessel has a period of vibration such that it is necessary to consider it as a dynamic structure, it should be designed to the seismic analogy method using a 0.20 seismic factor. It is not necessary to apply this analogy to anchor bolts, *if they are not stressed over 15,000–16,000 psi.*

3 The period of vibration of multithickness vessels and most multidiameter vessels may be estimated by the numerical integration of equation (6). The length of the sections used for solving equation (6) should not exceed twenty to twenty five feet in order to have the estimated period within approximately 5 per cent of the true period. Complicated units with long, conical transitions (making it impractical to consider the cone as a straight shell having uniform properties) require more involved methods of approximation, or recognition that the estimated period for these units, if estimated to equation (6), may be more than 10 per cent in error.

4 The evaluation of wind velocity effects should include considerations pertaining to the distribution of external vessel attachments as well as the surrounding equipment and terrain. It should be borne in mind that liquid loading in vessels having trays will help dampen vibration, but should not be relied upon as a cure-all.

5 Anchor bolts must be properly pretightened to a torque which will prestress them an amount equal to their estimated working stress, otherwise they may stretch sufficiently to affect the period of vibration and possibly work loose.

6 If vibration trouble does occur, careful analysis of any proposed remedy must be made in order to avoid trouble from some other source.

Acknowledgment

The author wishes to acknowledge and express his appreciation for the co-operation of the Standard Oil Company of California, Salt Lake Refining Company, and the Research Division of The Fluor Corporation. The assistance of Mr. R. C. Baird as well as many individuals of The Fluor Corporation helped to make this paper possible and is gratefully acknowledged.

References

1 J. P. Den Hartog, "Mechanical Vibrations," third edition, McGraw-Hill Book Company, Inc., New York, N. Y.

2 Stephen Timoshenko, "Vibration Problems in Engineering," second edition, D. Van Nostrand Company, Inc., New York, N. Y.

3 N. O. Myklestad, "Fundamentals of Vibration Analysis," first edition, McGraw-Hill Book Company, Inc., New York, N. Y.

4 Reference [1], p. 373.

5 R. L. Solnick and R. H. Bishop, "Noise, Vibration, and Measurement Problems, Resulting From Fluid-Flow Disturbances," TRANS. ASME, vol. 79, 1957, pp. 1045–1048.

6 R. C. Baird, "Wind-Induced Vibration of a Pipe-Line Suspension Bridge, and Its Cure," TRANS. ASME, vol. 77, 1955, pp. 797–804.

7 Reference [1], p. 459.

8 Reference [2], pp. 370 to 382 incl.

9 E. O. Bergman, "The Design of Vertical Pressure Vessels Subjected to Applied Forces," TRANS. ASME, vol. 77, 1955, pp. 863–867.

10 D. B. Steinman, "Problems of Aerodynamic and Hydrodynamic Stability," Proceedings, Third Hydraulic Conference, June, 1946, Univ. Iowa Bulletin No. 31, Page 139. Graph shown in Fig. 2 reproduced by permission.

11 R. C. Baird, "Aerodynamic Vibration of Tall Cylindrical Columns," Paper No. 58—PET-4.

12 Report of Fluor Research, unpublished.

13 Reference [10] pp. 144 and 145.

APPENDIX

I Estimating Period of Vibration

The weights of the following items are used for estimating the period of vibration when applying equation (4) (or the corresponding graph of this equation) or when numerically integrating equation (6):

1 Weight of Shell and Heads.
2 Weight of Trays, Caps, and Internals.
3 Weight of Manways and Nozzles.
4 Weight of Insulation and Fireproofing.

The total weight (items 1 through 4) of the vessel or vessel section is considered as a uniformly distributed load acting on the vessel when it is considered as a cantilever beam, i.e., a cantilever beam deflecting under its own weight. Note that equation (4) requires the total weight to be divided by the total length in feet to obtain the unit loading in pounds per foot, whereas equation (6) and the deflection equations shown in Fig. 9 are based on the total weight of each section under consideration.

The numerical integration of equation (6) is accomplished by dividing the vessel into the required number of sections—one section for each different thickness of plate with no section exceeding twenty or twenty-five feet in length, keeping in mind that the greater the number of sections, the more accurate will be the estimate.

After determining the weight and moment of inertia for each section, estimate the deflection at the c.g. of the section either

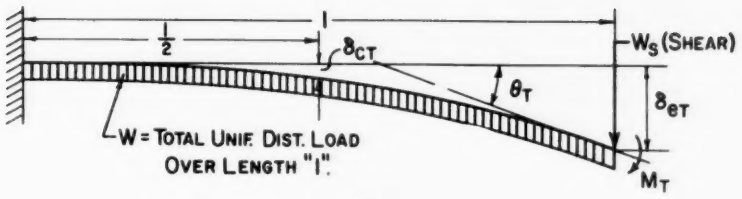

Fig. 8

TYPE OF LOADING	DEFL. AT c.g. (AT 1/2) In Ft.	DEFL. AT END In Ft.	END SLOPE "θ" IN RADIANS = tan θ
(a) UNIF. DIST. LOAD "W"	$\delta_C = \frac{17Wl^3}{384E'I}$	$\delta_e = \frac{Wl^3}{8E'I}$ $2.825\,\delta_C$	$\theta = \frac{Wl^2}{6E'I}$
(b) END MOMENT	$\delta_{CM} = \frac{M_T l^2}{8E'I}$	$\delta_{eM} = \frac{M_T l^2}{2E'I}$ $= 4.0\,\delta_{CM}$	$\theta_M = \frac{M_T l}{E'I}$
(c) SHEAR	$\delta_{CS} = \frac{5W_S l^3}{48E'I}$	$\delta_{eS} = \frac{W_S l^3}{3E'I}$ $= 3.2\,\delta_{CS}$	$\theta_S = \frac{W_S l^2}{2E'I}$
TOTAL PER SECT.	$\delta_{CT} = \delta_C + \delta_{CM} + \delta_{CS}$	$\delta_{eT} = \delta_e + \delta_{eM} + \delta_{eS}$	$\theta_T = \theta + \theta_M + \theta_S$

Fig. 9

graphically or by the numerical procedure outlined herein. When applying the numerical procedure, it is necessary to find for each section (except the last one at the free end) the deflection at the center, the deflection at the end, and the end slope due to (*a*) the uniformly distributed load W, (*b*) the end moment, and (*c*) the shear load. These are found from the standard deflection equations shown in Fig. 9. The last section at the free end requires only the deflection at its center due to its own weight. Reference to Fig. 8 will immediately disclose that the last section on the free end does not have an end moment M_T or a shear load W_s to take into consideration and the end deflection and end slope are not required to find the total deflection at the center. The center of gravity of each section is considered to be at its midpoint. Before proceeding with the deflection estimate, the designer should find all of the shear loads and end moments as shown in Fig. 10.

It is then a simple matter to find the total deflection of each section, square the deflection, and then tabulate the weight times the deflection and the weight times the deflection squared for each section, so that they may be added to find ΣWy and ΣWy^2 as shown in Fig. 11.

Equation (6) may be written

$$T = 1.108\left(\frac{\Sigma Wy^2}{\Sigma Wy}\right)^{1/2} \qquad (8)$$

to further simplify the arithmetic after the weight-deflection data are found.

As previously mentioned, many designers prefer to graphically estimate the deflection, but the numerical method is suggested for those who do not regularly use graphical methods. Actually either method requires about the same amount of arithmetic except those working graphically usually do not keep a detailed record of their areas and moments.

II Determination of Per Cent Decrement

Let X = amplitude of first swing

$$A = \left(1 - \frac{\%\text{ decrement}}{100}\right)$$

Note: A five per cent decrement means that each swing is 5 per cent less than its predecessor.

Then:

first swing amplitude = X
second swing amplitude = AX
third swing amplitude = A^2X

or

Nth swing amplitude = $A^{(N-1)}X$

and

per cent decrement = $100\,(1 - A)$

The term per cent decrement is of value when comparing the damping effect of different loading conditions for the same column.

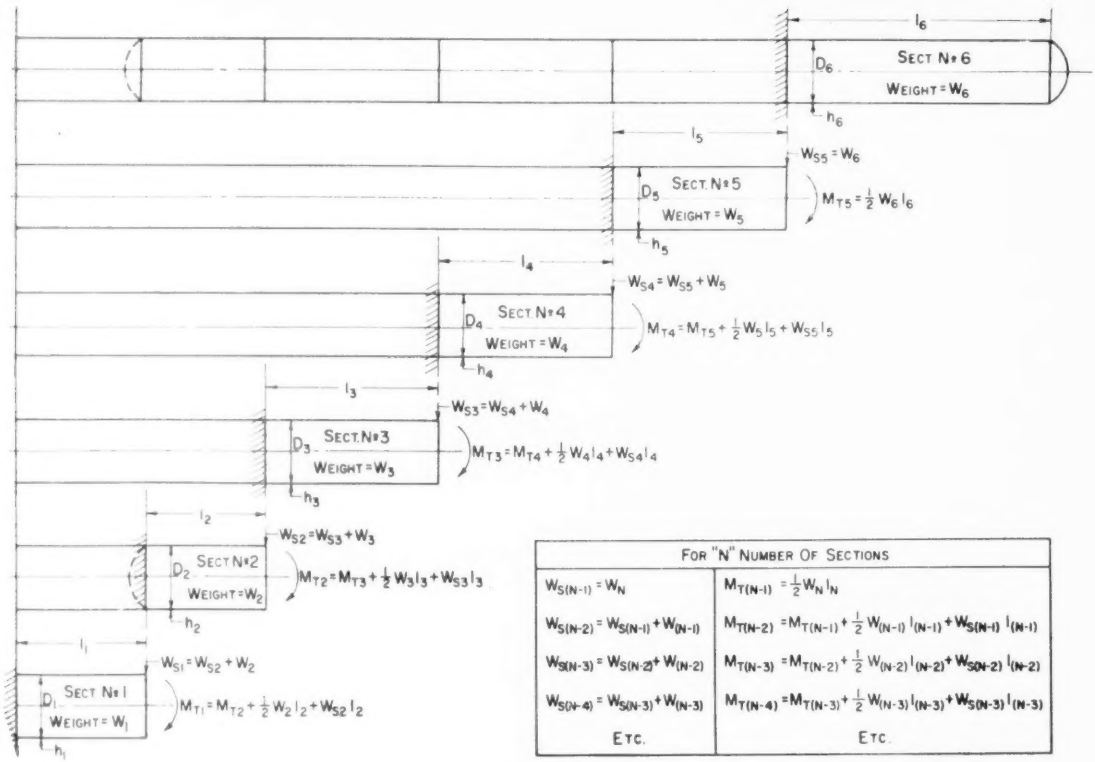
SECT. N° 6
WEIGHT = W6
SECT. N° 5
WEIGHT = W5
SECT. N° 4
WEIGHT = W4
SECT. N° 3
WEIGHT = W3
SECT. N° 2
WEIGHT = W2
SECT. N° 1
WEIGHT = W1
$W_{S5} = W_6$
$M_{T5} = \frac{1}{2} W_6 l_6$
$W_{S4} = W_{S5} + W_5$
$M_{T4} = M_{T5} + \frac{1}{2} W_5 l_5 + W_{S5} l_5$
$W_{S3} = W_{S4} + W_4$
$M_{T3} = M_{T4} + \frac{1}{2} W_4 l_4 + W_{S4} l_4$
$W_{S2} = W_{S3} + W_3$
$M_{T2} = M_{T3} + \frac{1}{2} W_3 l_3 + W_{S3} l_3$
$W_{S1} = W_{S2} + W_2$
$M_{T1} = M_{T2} + \frac{1}{2} W_2 l_2 + W_{S2} l_2$

FOR "N" NUMBER OF SECTIONS	
$W_{S(N-1)} = W_N$	$M_{T(N-1)} = \frac{1}{2} W_N l_N$
$W_{S(N-2)} = W_{S(N-1)} + W_{(N-1)}$	$M_{T(N-2)} = M_{T(N-1)} + \frac{1}{2} W_{(N-1)} l_{(N-1)} + W_{S(N-1)} l_{(N-1)}$
$W_{S(N-3)} = W_{S(N-2)} + W_{(N-2)}$	$M_{T(N-3)} = M_{T(N-2)} + \frac{1}{2} W_{(N-2)} l_{(N-2)} + W_{S(N-2)} l_{(N-2)}$
$W_{S(N-4)} = W_{S(N-3)} + W_{(N-3)}$	$M_{T(N-4)} = M_{T(N-3)} + \frac{1}{2} W_{(N-3)} l_{(N-3)} + W_{S(N-3)} l_{(N-3)}$
ETC.	ETC.

Fig. 10

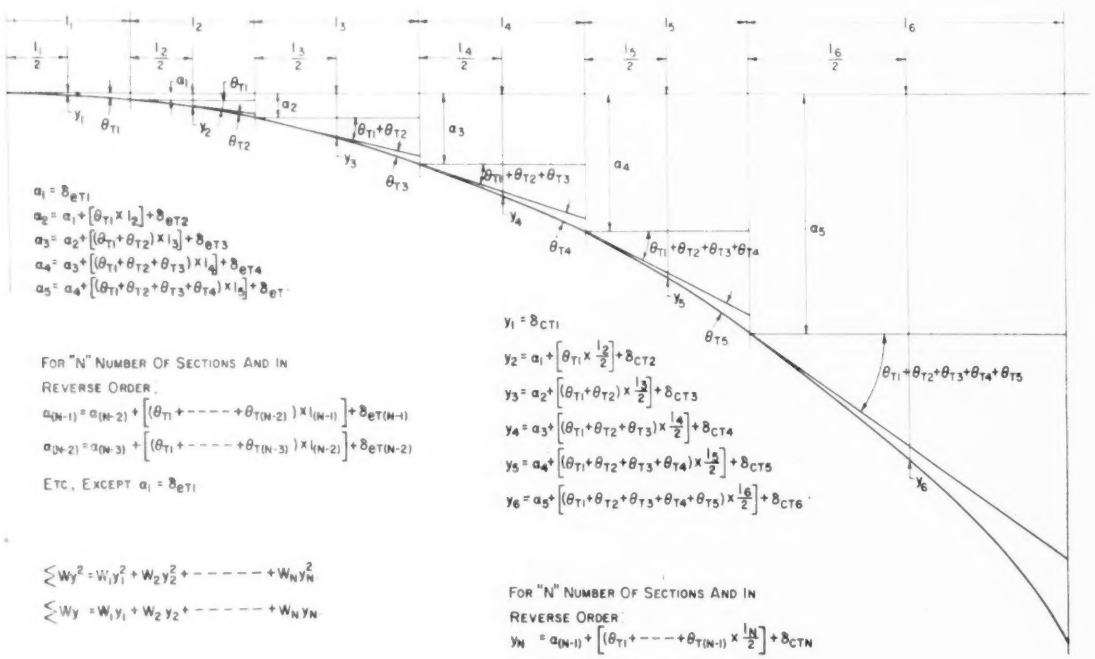
$a_1 = \delta_{eT1}$
$a_2 = a_1 + [\theta_{T1} \times l_2] + \delta_{eT2}$
$a_3 = a_2 + [(\theta_{T1} + \theta_{T2}) \times l_3] + \delta_{eT3}$
$a_4 = a_3 + [(\theta_{T1} + \theta_{T2} + \theta_{T3}) \times l_4] + \delta_{eT4}$
$a_5 = a_4 + [(\theta_{T1} + \theta_{T2} + \theta_{T3} + \theta_{T4}) \times l_5] + \delta_{eT5}$
FOR "N" NUMBER OF SECTIONS AND IN REVERSE ORDER:
$a_{(N-1)} = a_{(N-2)} + [(\theta_{T1} + \cdots + \theta_{T(N-2)}) \times l_{(N-1)}] + \delta_{eT(N-1)}$
$a_{(N-2)} = a_{(N-3)} + [(\theta_{T1} + \cdots + \theta_{T(N-3)}) \times l_{(N-2)}] + \delta_{eT(N-2)}$
ETC., EXCEPT $a_1 = \delta_{eT1}$
$y_1 = \delta_{CT1}$
$y_2 = a_1 + [\theta_{T1} \times \frac{l_2}{2}] + \delta_{CT2}$
$y_3 = a_2 + [(\theta_{T1} + \theta_{T2}) \times \frac{l_3}{2}] + \delta_{CT3}$
$y_4 = a_3 + [(\theta_{T1} + \theta_{T2} + \theta_{T3}) \times \frac{l_4}{2}] + \delta_{CT4}$
$y_5 = a_4 + [(\theta_{T1} + \theta_{T2} + \theta_{T3} + \theta_{T4}) \times \frac{l_5}{2}] + \delta_{CT5}$
$y_6 = a_5 + [(\theta_{T1} + \theta_{T2} + \theta_{T3} + \theta_{T4} + \theta_{T5}) \times \frac{l_6}{2}] + \delta_{CT6}$
$\sum Wy^2 = W_1 y_1^2 + W_2 y_2^2 + \cdots + W_N y_N^2$
$\sum Wy = W_1 y_1 + W_2 y_2 + \cdots + W_N y_N$
FOR "N" NUMBER OF SECTIONS AND IN REVERSE ORDER:
$y_N = a_{(N-1)} + [(\theta_{T1} + \cdots + \theta_{T(N-1)}) \times \frac{l_N}{2}] + \delta_{CTN}$
$y_{(N-1)} = a_{(N-2)} + [(\theta_{T1} + \cdots + \theta_{T(N-2)}) \times \frac{l_{(N-1)}}{2}] + \delta_{CT(N-1)}$
ETC., EXCEPT $y_1 = \delta_{CT1}$

Fig. 11

DISCUSSION

M. Ludwig[2]

This paper deals with a problem that has long challenged this writer and his associates. His recommended procedure for calculation of dynamic wind forces can, however, lead to much more costly designs than we have found to be necessary. The author is primarily concerned with the possibility of forced resonant vibrations stimulated by transverse cyclic wind forces associated with the Karman vortex trail and, to deal with this possibility, suggests that flexible vertical pressure vessels be designed to resist a lateral force equal to 20 per cent of the gravity force. This lateral force is, for most flexible vessels (those with shell thicknesses greater than 0.4 in. if the total mass is twice the mass in the shell) greater than our customary design for either wind or earthquake. The justification for use of this seismic force is not presented, either as factor for a seismic design or for avoiding wind-induced vibrations.

An anomalous feature of the author's "seismic analogy" method of design is that it logically leads to the conclusion that a simple vertical cylindrical shell, such as a steel smokestack up to 0.8 in. thick, requires no special consideration because of possible wind vibration, whereas a fractionating column of the same thickness and diameter must be strengthened because of the added mass due to insulation, trays and fluid thereon, ladders, piping, and other appurtenances. Such a conclusion cannot be supported by past experience; excessive vibration of steel stacks has occurred, whereas vibration of fractionating columns has seldom been a problem. The author notes one case of fractionating column vibration but this stopped when the column was put into operation; either the liquid on the trays provided adequate damping or the added mass of the liquid increased the natural period to a less critical value.

Our own experience is that fractionating columns can be safely designed for static wind loads alone. The possibility of excessive wind vibration simply appears too remote to justify any added expense to prevent such vibration. Strengthening of the steel shell, by adding thickness, merely reduces the natural period of vibration and increases the wind velocity necessary to produce forced oscillations; it is not at all safe to assume that it would eliminate or reduce the amplitude of vibrations that might otherwise occur.

Why is it that tall vertical pressure vessels, such as fractionating columns, are far less severely affected by wind vibration than are self-supporting steel smokestacks? The greater mass per unit of gross cross-sectional area cannot alone be responsible since large above-ground oil pipelines have been observed to vibrate in the wind. There will be added aerodynamic damping because of attached platforms, piping, etc., but it can be shown that the energy absorbed by this form of damping is probably not enough to limit the vibration amplitude to reasonable values. The external irregularities due to platforms, piping, etc., could, however, reduce the applied periodic wind force.

A sound theoretical analysis for forced vibration of the resonant frequency will answer the question raised in the previous paragraph. Actual numerical values for the possible vibration amplitude and resulting stress can be evaluated if the damping constant for the column can be determined or estimated. The detailed analysis, although straightforward, is too lengthy for inclusion in this brief review, but the final equations are listed. It is assumed that the vessel vibrates in a sustained wind as a uniform cantilever beam in the fundamental mode.

$$A_m = 3.30 \times 10^{-6} \frac{C}{S^2 \ln\Delta} \frac{D^2}{Bt} \tag{9}$$

[2] Standard Oil of California, San Francisco, Calif.

$$\sigma = 1.76\, E \frac{DA_m}{L^2} \tag{10}$$

or

$$\sigma = 5.81 \times 10^{-6}\, E \frac{C}{S^2 \ln\Delta} \frac{D^3}{BtL^2} \tag{11}$$

in which

A_m = maximum vibration amplitude at top of column
B = ratio of total mass per foot to mass per foot of steel shell
C = coefficient for peak periodic wind force—given as 1.71 by Steinman (reference [10] of the paper)
D = diameter of shell
E = modulus of elasticity of steel
L = height of column
S = Strouhal number
t = thickness of shell
Δ = amplitude ratio for two successive maxima for free oscillations
$\ln\Delta$ = natural logarithm of Δ. (This is the "logarithmic decrement." The "damping ratio" or ratio of actual to critical damping is equal to the logarithmic decrement divided by 2π.)
σ = peak vibratory stress at base of column

Any consistent set of units may be used in these equations. As a numerical example, let

$C = 1.71$
$S = 0.20$
$B = 2.00$
$D = 4.00$ ft
$L = 150$ ft
$t = 1$ in. or $^1/_{12}$ ft
$E = 30 \times 10^6$ psi or 4320×10^4 psf
$\ln\Delta = 0.10$ (damping ratio $= 0.10/2\pi = 0.0159$)

Then, from equation (9), $A_m = 0.135$ ft or 1.62 in.
From equation (10) or (11), $\sigma = 1270$ psi.

The possible deflection and stress calculated here are hardly large enough for concern. The assumed damping is reasonably small but could be much less without serious results. As a matter of further interest, the natural period of vibration for this column is 2.39 sec, the wind velocity for resonant vibrations is 8.4 fps, and the Reynolds number for this wind velocity is 214,000. This is within the region where C should be around 1.71 and S around 0.20, as was assumed. A value of 1.71 for C is probably the maximum obtainable. It actually determines the *peak* value of the periodic force, which probably includes higher harmonics; the coefficient for the fundamental frequency component may be substantially less. Also, the coefficient will be less if the column is not a true circular cylinder or if the Reynolds number is greater than 500,000.

Note especially, as shown by equation (11), that the bending stress is, for a given damping ratio, proportional to the cube of the diameter, inversely proportional to the square of the height, inversely proportional to the shell thickness, and inversely proportional to the mass ratio B. The greater values of the thickness and mass ratio for pressure vessels, as compared to steel smokestacks, are particularly important in minimizing the seriousness of possible wind-excited vibration. Thus, both experience and theory lead to the conclusion that vertical pressure vessels, such as fractionating columns, are not nearly as likely to vibrate excessively in the wind as are self-supporting steel smokestacks.

Earl J. Hicks[3] and J. R. Sellers[4]

The author implies that the vibration of a tall vessel is a case of forced vibration, with resonance occurring when the Karman vortex trail frequency corresponds with the natural frequency of the vessel. This is supported by Baird [14][5] in his investigation of a pipeline bridge vibration. We have had a similar experience with a pipeline bridge in which a critical wind velocity was observed. A search of the literature finds an exception to this with experimental data to support the claim that tall stacks vibrate as self-excited vibrational systems with no critical wind velocity causing forced vibrational response. Ozker and Smith [15] make the following statements in the summary and conclusions portion of their paper which are contrary to this paper: (1) "The stack structure under wind action constitutes a self-excited vibrational system"; (2) "The vibrational frequency is the natural frequency of the structure and remains constant for all wind velocities"; (3) "The stack is at resonance at all times"; (4) "There is no critical wind velocity in the sense of forced vibrational response"; and (5) "The amplitude increases with increasing wind velocities." If this were found to be true for a stack, could it not also be true for a tall vessel? The bulk of the data seems to support the theory of forced vibration excited by the Karman vortex trail, but there is this one notable exception. There may be others.

The basic assumption in calculating the natural frequency of a tall cylindrical vessel is that the base is fixed at the top of the foundation. This implies that the horizontal displacement or deflection is due to the elastic deformation of the vessel and that the horizontal displacement due to the elastic deformation of the soil is negligible. This means that the vessel would act like a true cantilever beam fixed at one end. This is one extreme assumption.

The opposite extreme assumption would be that the vessel and foundation is a rigid structure resting on an elastic subgrade. This implies that the horizontal displacements of the tower are negligible compared to the deflection due to deformation of the soil.

Assuming the latter assumption to be correct, it can be shown for a vessel on an octagonal foundation resting on an elastic subgrade that the natural frequency of vibration is equal to the following:

$$f = 0.232 \frac{B}{H} \left(\frac{d_s}{q} \right)^{1/2}$$

where

B = short diameter of the base in feet
H = distance between the base and the center of gravity of the foundation and vessel
d_s = coefficient of dynamic subgrade reaction
q = static soil pressure per unit of area

From this equation the following conclusions can be drawn. The softer the supporting soil, the lower is the natural frequency and the frequency may be raised by increasing the area of the foundation base [16].

In general, observed frequencies have been lower than the calculated frequencies. This is probably due to the vessel and foundation acting together in a manner somewhere in between the two extreme assumptions. If the supporting soil is relatively strong, the first assumption is more nearly correct. If the supporting soil is relatively soft, the actual condition tends to approach the second assumption. Past observations on various stacks have indicated reasonably close agreement between the observed frequency and the calculated frequency, the latter being based on the fixed cantilever beam assumption. If the frequency of a vessel is determined, assuming a fixed cantilever beam, and the supporting soil is soft, the error would be on the unsafe side; that is, the calculated critical wind velocity would be high.

The method of design suggested for wind induced vibration appears to be arbitrary and most likely finds justification in the number of successful towers. It would be desirable to have a more analytical approach to the problem. Apparently, any relation between the wind induced vibration and the 0.2 seismic factor is purely coincidental.

It appears a more realistic approach would be to equate the energy input in terms of amplitude to the energy dissipated in terms of amplitude and solving for the amplitude where the energy input is equal to the energy dissipated. The vibrations at this point would be an undamped steady-state free vibration and the resulting amplitude would be a maximum. Knowing the maximum deflection, the maximum stress could be readily calculated. If the resulting stresses are excessive, then other methods to dissipate the energy would have to be used.

This method would require reasonably accurate knowledge of the coefficient of lift C_L, the Strouhal number S, and damping decrement δ. Only meager information on the numerical value of these coefficients is available at this time. It appears desirable to study the loads and dynamic response in a series of wind tunnel tests. Does the author know of any such studies?

Aerodynamic paneling, liquid loading on trays, and liquid chambers are practical solutions. One other worth mentioning is that of tieing adjacent vessels and structures together. Vessels arranged in a triangle or square with common ties have a different vibrational mode and a higher resonant frequency than a single tower. In addition, more damping is introduced. A single vessel tied at an intermediate level to an adjacent structure will vibrate in a different mode and higher frequency. These can be used as safeguards for vessels classed as critical.

The liquid chamber suggested is one form of the Frahm dynamic absorber system. A word of caution should be given on this application. The Frahm dynamic absorber system has two resonant frequencies and one frequency of zero amplitude. A properly sized liquid chamber would decrease the amplitude to zero at one frequency, reduce it over a limited range of frequencies, but amplify it at two frequencies outside this range. In other words, at certain frequencies the liquid may not slosh to oppose the vibration, but instead be in phase to amplify it. Frahm antiroll tanks for ships are dealt with in Den Hartog's book [17]. A liquid chamber appears to be an energy absorber of this same type.

In Case III, no excessive movement has been reported although the critical wind velocity is in the neighborhood of 8-10 miles per hour. In Case I, the vessel has operated successfully with a calculated wind velocity to cause resonance of 10-12 miles per hour. Both of these vessels were designed to the seismic analogy method. In Case II where the seismic analogy method of design was not used, the vessel vibrated during the construction period. Does the author imply that since Cases III and I were dynamically designed and Case II was not that this was the main reason that vibration did not occur or could it be that the ladders and platforms were distributed around the former two vessels such that the formation of the Karman vortex trail does not materialize? It appears that the ladders, platforms, piping, and insulation might be the major factor in preventing vessels from vibrating. No doubt there are many vessels with a height to diameter ratio greater than 20 which are operating

[3] Engineering Department, Phillips Petroleum Company, Bartlesville, Okla. Mem. ASME.
[4] Engineering Department, Phillips Petroleum Company.
[5] Numbers in brackets designate References at end of this discussion.

satisfactorily and have not been designed as recommended by the author. The author implies that any vessel with a period which falls above the line shown in Fig. 1 should be designed dynamically. Would this be true for vessels whose heights are less than 100 or 75 or 50 ft? In general, is there some approximate height regardless of the H/D ratio where vessels below this height would not have to be investigated?

Although the author does not say specifically that the vessel should be designed such that the "critical wind velocity" is high enough to exclude the possibility of the second mode of vibration, it is mentioned. If this item is not critical, then why is it necessary to use such an accurate and time consuming method to determine the period when it could probably be estimated by other methods. Apparently, the designers were not concerned in Cases I and III about the low critical wind velocity since they were designed dynamically.

The author's paper is very timely indeed and is viewed with considerable interest since the trend in pressure vessel design is to increase their height and decrease the internal pressure. We wish to compliment him on a very excellent paper and also thank him for stimulating our interest in the subject.

References

14 R. C. Baird, "Wind-Induced Vibration of a Pipe-Line Suspension Bridge, and Its Cure," TRANS. ASME, vol. 77, 1955, pp. 797–804.

15 M. S. Ozker and J. O. Smith, "Factors Influencing the Dynamic Behavior of Tall Stacks Under the Action of Wind," TRANS. ASME, vol. 78, 1956, pp. 1381–1391.

16 Karl Terzaghi, "Theoretical Soil Mechanics," John Wiley & Sons, Inc., New York, N. Y., pp. 454–457.

17 J. P. Den Hartog, "Mechanical Vibrations," McGraw-Hill Book Company, Inc., New York, N. Y., second edition, pp. 129–135.

18 W. L. Dickey and G. B. Woodruff, "The Vibrations of Steel Stacks," *Trans. ASCE*, vol. 121, 1956, p. 1054.

19 E. A. Dockstader, W. F. Swiger, and E. Ireland, "Resonant Vibration of Steel Stacks," *Trans. ASCE*, vol. 121, 1956, p. 1088.

L. Acquaviva[6]

The proposed criteria for dynamic design of pressure vessels appear to yield more conservative results than the method we have been using for many years. It appears that the seismic coefficient of 0.20 applied on all vessels with height to diameter ratio exceeding 15 or natural period exceeding 1.0 sec may be too conservative based on our experience. For example, as an extreme case, there is a tower within the Esso interests which is 173 ft high, topmost 40 per cent of height is 6 ft 6 in. in diameter and lower 60 per cent 5 ft 0 in. in diameter. The approximate L/D ratio is 30, natural period of vibration 3.7 sec and critical wind velocity 6.5 miles per hour for the top section. The tower is on pile foundations and has given no vibration difficulties even though subjected many times to the critical wind velocity for the top section; nor has there been any tendency to vibrate at its second mode for which the critical wind velocity is about 40 miles per hour. The bottom section shell thickness for this vessel is $^7/_8$ in. The thickness required to conform with the proposed dynamic design would be $1^3/_8$ in.

Unlike steel stacks, for which there are many instances of excessive vibration reported in technical literature, Case II in the paper is the first example to our knowledge of such occurrence in vertical pressure vessels. In this case, the maximum amplitude of 0.45 ft during resonance does not appear to be of sufficient magnitude to cause excessive stresses in the vessel shell. It would be of interest to know if any remedial measures were taken in this case.

[6] Esso Research and Engineering Company, Linden, N. J.

Donald J. Bergman[7]

This paper is particularly interesting because it includes some actual field data which have been extremely difficult to get. It seems important to note that minor changes in resonant frequency have little effect on the over-all situation as this merely results in a slightly different wind velocity to reach resonance. It was much more important to note how greatly the liquid on the trays of a column increased the damping effect. This absorbs the energy of the wind forces and cuts down the magnification factor, decreasing the maximum amplitude of vibration.

We had several instances of stack vibration starting in 1938, all far removed and all solved by use of permanent guys. The first key to the causes came from Sir James Jeans' book "Science and Music." Here the comment was made that a set of eddies broke off from a cylindrical surface every 5.4 diam along the wind stream and that these eddies caused a push from side to side. The example was given of a ship with $^1/_2$ in. rigging at sea in a 40-mile gale where the frequency comes out to correspond to middle "C" on a piano.

The policy of providing light guys and spreaders was adopted for columns with high L/D ratios and springs were provided to take care of column elongation by heat. Several hundred columns were thus equipped over past years without having one case of resonant vibration. Perhaps this was just fortuitous because of presence of ladders, platforms, etc., to interfere with resonance, and absence of critical winds. Most of these columns were within the critical range as defined by the author.

Later study indicated the same conclusions that the author reached: That the guys and springs were probably not effective and, consequently, about a year ago provision of these guys was abandoned. Since then one tower was found to have a resonant period with the wind and permanent guys were added.

Perhaps it should be noted that the elasticity of fixed guys actually makes them springs with a very high spring constant. Limiting the movement of the tower is the desired result, and this the guys do by resisting the wind forces.

The lateral forces resulting from the action of the Karman eddies seem to be somewhat greater than the normal wind drag for any wind velocity. With a low decrement, or high magnification, say, 20, only a relatively small force, 1 lb/sq ft, is required to give the deflection obtained when designing for a 100-mile per hour wind at 20 lb/sq ft, on the projected area of the column.

The lateral forces generated on cylinders were actually utilized shortly after World War I by the German *Flettner* rotor ship which cruised from Germany to New York using two 10 × 60-ft cylinders mounted on the deck and rotated in order to furnish a fixed instead of an oscillating force.

Rouse's book "Engineering Hydraulics" on page 130 gives formulas for an approximation of the aerodynamic lift caused by the Karman eddies on fixed and rotating cylinders. Additional information for higher Reynolds numbers was obtained from Prof. L. Landweber of the Iowa Institute of Hydraulic Research by correspondence. For the 7.67-ft column which gave trouble with a 27-mph wind, I calculate a loading of 9.1 lb/ft or 1.18 lb/sq ft of projected area. Stiffening a column and increasing its frequency will decrease the deflection for a given load, but the wind forces increase as the square of the wind velocity.

Some comment was made regarding the second mode of vibration. This will always require a very much higher wind velocity than the first mode, but the column is so much more stiff because of the complicated second mode curve that it is probable that vibration is not noticeable if it does occur.

[7] Engineering and Development Department, Universal Oil Products Company, Des Plaines, Ill. Mem. ASME.

Patent no. 2604838, dated July 29, 1952, to W. B. Traver, of Standard Oil Company of Indiana, teaches provision of a roughened surface near the top of a stack either by small strips ranging from 1/4 to 1 in. depth, or by the use of steel grating. This increases the skin resistance on the surface of the cylinder to prevent formation of Karman eddies. However, it does not seem to be a very practical remedy because of the cost of attaching the large number of small strips to the stack.

Author's Closure

Before replying to specific questions or comments, the author wishes to thank the discussers for their review and comments pertaining to the design of vertical vessels subject to vibration.

It is hoped that sufficient interest has been stimulated in this subject to result in obtaining more field data than we presently have at our disposal. Up to the present time very little has been done to obtain information pertaining to tall, slender vessels. If no complaint was received from the operators, it has been assumed that no critical vibration would ever occur. This is a normal and expected attitude; however, it has not contributed to our knowledge of vessel behavior as heights have increased.

As pointed out in this paper and described more in detail in the paper given by Mr. Baird, we have had definite experience with one vessel which did give trouble and, after completing this paper, the author was informed that this vessel still has to have anchor bolts retightened at intervals which indicates that some excessive vibration may still be taking place.

The author does not agree with Mr. Ludwig that we can generalize regarding the relationship of total mass to the mass of the shell itself. Mr. Ludwig's use of a mass equal to twice the mass of the shell in his 4-ft 0-in. diam × 1-in. thick example would result in very heavy internals. To me, each vessel should be considered individually during the design stage. Obviously, there will be those where conditions of terrain and prevailing winds will cast doubt regarding the justification of added cost to the vessel.

The cost angle of designing to the method recommended in this paper has been overemphasized. Taking Mr. Ludwig's example and designing it to the 0.2 seismic analogy results in the following thicknesses:

Top	104 ft—1-in. plate (orig. thickness)
Next	16 ft—1 1/8-in. plate
Next	8 ft—1 1/4-in. plate
Next	8 ft—1 3/8-in. plate
Next	8 ft—1 7/16-in. plate
Skirt	6 ft—1 7/16-in. plate

This represents an increase of only 7,500 lb added to a vessel originally designed as 146,000 lb (when 16,000 lb is subtracted for insulation). This approximation is based on ASTM A-212-B Material, S.R. and x-rayed, and includes 1/8-in. corrosion allowance in the 1-in. plate, which means that this vessel would have 7/8-in. thickness for resisting pressure in the hoop direction. We then have 7/16 in. of material available to resist the bending in the longitudinal direction. Mr. Ludwig ignores the pressure stress when he reports his bending stress due to his estimate of the maximum amplitude of vibration. Costwise, this vessel would represent an investment of approximately $36,500 as originally outlined. The added material and labor would be approximately $1350 which is an increase of only 3.7 per cent. In this case, the added material accomplishes two things; first, it increases the section of the vessel where bending stresses occur and will reduce the possibility of failure from fatigue, a condition which could exist if the critical wind velocity was prevalent; second, it gives more resistance to bending if a harmonic condition occurs.

Mr. Ludwig reported a critical wind velocity of 8.4 fps or 5.7 mph, and apparently used a 4-ft 0-in. diam with his selected Strouhal number of 0.20. Adding 3 in. of insulation, and using a Strouhal number of 0.18 (based on field data for two vessels reported in the paper) gives a critical velocity of 7.1 mph for the vessel as originally outlined and 7.8 mph for the design as recommended in the paper. (The period of vibration decreased from 2.39 to 2.19 sec.) It is agreed that the recommended design does not materially affect the critical wind velocity for most vessels.

It is also agreed that stacks may cause more trouble from vibration than vessels, because they do not have liquid loading and are usually lighter in weight. However, the inference pertaining to ignoring a stack of 0.8 in. thick should be further clarified, because the L/D ratio would determine whether or not the stack should be designed for vibration. Also, there is no mention of stacks in this paper and it is *not* recommended that this design procedure should be applied to them. Since processing is not involved, stack designers usually increase the resistance to vibration by a generous conical section in the lower zone which sometimes runs from 1/4 to 1/3 the height of the stack. The pressure vessel designer can seldom resort to this because of internal construction. In order to clarify the statements concerning stacks, the following tabulation is based on Mr. Ludwig's definition of a flexible vessel; i.e., one with a shell thickness greater than 0.4 in. if the total mass is twice the mass in the shell:

Diam, in.	Shell th, in.	Vessels wt/ft,[a] lb	L/D	Max L, ft
36	7/16	360	20	60
48	7/16	480	18	72
60	7/16	600	17	85
72	7/16	720	15	90

[a] This is double the wt/ft for 7/16-in. plate.

Diam, in.	Shell th,[b] in.	Stacks wt/ft, lb	L/D	Max L, ft
36	7/16	180	24	72
48	7/16	240	21	84
60	7/16	300	19	95
72	7/16	360	18	108

[b] L/D and max L values for stacks actually are independent of shell thickness because the value of the abscissa (wD/h) of the graph shown in Fig. 1 does not change as the material thickness is changed (w and h are proportional).

A comparison will show that the 36-in-diam vessel can be considered as a static structure if not over 60 ft high, whereas the 36-in. stack could be considered as a static structure up to 72 ft high, regardless of its thickness. Similar values are shown for other diameters. As previously mentioned, it was not intended to apply the graph shown in Fig. 1 to stacks. However, there does not appear to be a great discrepancy in this respect when it is realized that all of the metal put in a stack may be used for structural strength since there is no internal pressure.

Stacks are frequently built using the thinnest calculated material thickness, and sometimes local buckling has occurred due to warpage and/or external forces. I do not believe a true comparison between stacks and vessels can be made.

The calculation of the periodic force and resulting amplitude is difficult to make with any degree of accuracy, because we lack field data on vessels. Past attempts to apply some of the data from Reference [10] in the paper have not always give results consistent with the field data taken to date. This does not mean that approximations of this nature should not be made, but we cannot place too much reliance in them.

Mr. Ludwig's bending stresses are very low because he included all of the shell material for bending, whereas in actual design work we have to combine the pressure stresses with the bend-

ing stresses. Also, Mr. Ludwig's stress is based on his estimate of the amplitude and ignores the fact that a deflection exceeding the normal amplitude might result if resonance occurs, as reported for the vessel outlined as Case II and reported by Baird.

Mr. Hicks and Mr. Sellers discuss the possibility of the foundation and soil-bearing capacity as contributing to the flexibility of the system. This possibility has not been ignored. However, there has been no observation to justify this assumption. A check into the effect of anchor bolt stretch did not affect the period of vibration estimate sufficiently to bother with it—other than to require pretightening to reduce elongation during vessel deflection. When the total mass of concrete and the surface charge of earth is considered, it is difficult to agree that they materially influence the natural frequency. If the soil bearing capacity is low, it is usually necessary to drive piles to support vessels and similar heavy equipment.

The desire for the analytical approach is appreciated. However, pressure vessels do not always lend themselves to a true scientific analysis. In this case, so many variables exist that assumptions made in order to solve equations are apt to produce misleading results. The fact that a number of successful vessels have been built using this somewhat empirical approach is reasonable justification for its consideration. If we cannot justify a design method on the basis of successful operation, then we would be forced to discard many of our practices which are based on experience, including earthquake design. It is also noted that some reviewers are equally positive that it is unnecessary to take any precautionary measures because they have not experienced any difficulty in the past. Therefore, we have one more instance where the variables are too many to draw a definite conclusion and data pertaining to location, terrain, wind currents, detail vessel design, and vibration for each case are not available. If we had at our disposal sufficient data taken from existing units, we probably could work out a more analytical approach.

To my knowledge there have been no wind-tunnel tests pertaining to vertical vessels except those mentioned in Reference [10]. Investigation of testing models for tall, slender columns will immediately reveal that, in order to obtain reliable data for L/D ratios of 30 and 40 to one, the model size will be difficult to work with, because the diameter is so small in order to avoid excessive height. Some of the larger wind tunnels could probably handle models large enough to be practical, but the cost would be very high.

Connecting critical vessels to nearby structures or to adjacent vessels is always desirable if the location of the equipment permits. This cannot be accomplished in many instances.

I do not agree that the use of a single liquid chamber is comparable to Frahm antiroll tanks. The type of motion differs and I believe that there is very little possibility of the liquid amplifying vibration. However, as pointed out in Conclusion No. 6 in the paper, any proposed remedy must be carefully analyzed to avoid additional trouble from some other source.

The paper does imply that the vessel reported under Case II might have been satisfactory if designed to the seismic analogy method, but there is no proof of this. Recognition is given to the desirability of distributing ladders, platforms, and other accessories circumferentially about the vessel to reduce the effect of periodic eddy shedding.

The heavy reference line shown in Fig. 1 is independent of height and considers L/D ratios more important than height. A vessel 30 in. in diameter and 90 ft 0 in. high can be more critical than a 200-ft 0-in-high vessel of a larger diameter. This reference line from 0.4 sec on the left to the 0.8 sec on the right of the graph is empirical. There certainly are vessels having periods of vibration above this line which were not designed as recommended that are satisfactory. This line at one time was a horizontal line at 0.4 sec, and experience indicated that it could be safely changed as shown. Future data may result in another revision for this limit.

The method outlined in the paper for numerically estimating the period of vibration for a vessel having a shell varying in thickness is intended for designers who are not experts in vibration. We are programming this work for computing machines along with our other vessel program, but computing machines are not always available, and other methods of approximation are not very reliable unless performed by experts in the field of vibration. It is not always necessary to estimate this period and frequently it can be approximated by using the graph in Fig. 1. It is up to the designer to decide the degree of accuracy he wishes to attain.

The column described by Mr. Acquaviva has considerable difference in the diameter of the top and bottom section. Our experience has been that vessels of this type are not as critical as tall, slender columns which are the same diameter for their entire length. I have some reservation regarding the accuracy of estimating critical wind velocities for this type of vessel when the diameter difference exceeds 6 to 12 in.

Here is another example of experience and each individual will have his own idea of a correct solution.

If I were compiling data pertaining to existing vessels, I would definitely attempt to include all possible information on surrounding structures, wind currents, and geological data, in addition to details of vessel construction. A successful installation in one locality may not be trouble free in another.

The vibration dampener shown in Fig. 3 in the paper was applied to the vessel which vibrated at an excessive amplitude. This had practically no effect on the behavior of the vessel, but was not removed. Liquid loading helped to prevent excessive amplitude build-up, but as previously mentioned, it was recently discovered that the anchor bolts have to be retightened at frequent intervals.

My reply regarding cost of designing to a 0.2-seismic factor was included with the reply to Mr. Ludwig's comments.

Mr. Fred Ruud's statement that the U. S. Bureau of Reclamation uses a seismic analogy method for some of their tall vessels is particularly interesting in view of the fact that seismic factors of 0.25 to 0.30 were mentioned, and the author wishes to thank Mr. Ruud for his interest and express regret that he did not have the opportunity to prepare written discussion on this paper.

Journal of ENGINEERING FOR INDUSTRY

Technical Briefs

G. A. NELSON

Staff Metallurgist
Shell Development Company
Emeryville, Calif.

Revisions to Published Chart: Metals for High-Pressure Hydrogenation Plants

In a paper published by the author in 1951[1] a chart (Fig. 4) was included to indicate safe operating limits for carbon and alloy steels in hydrogen service, being based on information available at that time.

Until recently, the information obtained showed the limits to be adequate and in certain installations to be slightly on the conservative side. However, information has now been received concerning failures of carbon steel at low pressures and very high temperatures. The data were supplied by committees of the American Petroleum Institute and the American Society for Metals. They indicate that in long-time service, welded carbon steel suffers hydrogen attack at limits below those which would be resisted by steel in the unwelded condition.

In view of these data, which show attack on welded steel under conditions below those for unwelded steel, it is considered advisable to install a curve on the chart to indicate safe operating limits for equipment fabricated in this manner. Accordingly a new chart No. VT-627, Fig. 1, has been drawn to incorporate this line. A slight adjustment has also been made to the limit for unwelded steel, reflecting data received since issuance of the paper concerning the long-time performance of ordinary steel. Aside from the changes to the carbon-steel limit, the curves for low-alloy steels remain the same as on the former chart.

[1] G. A. Nelson, "Metals for High-Pressure Hydrogenation Plants," TRANS. ASME, vol. 73, 1951, pp. 205–213.

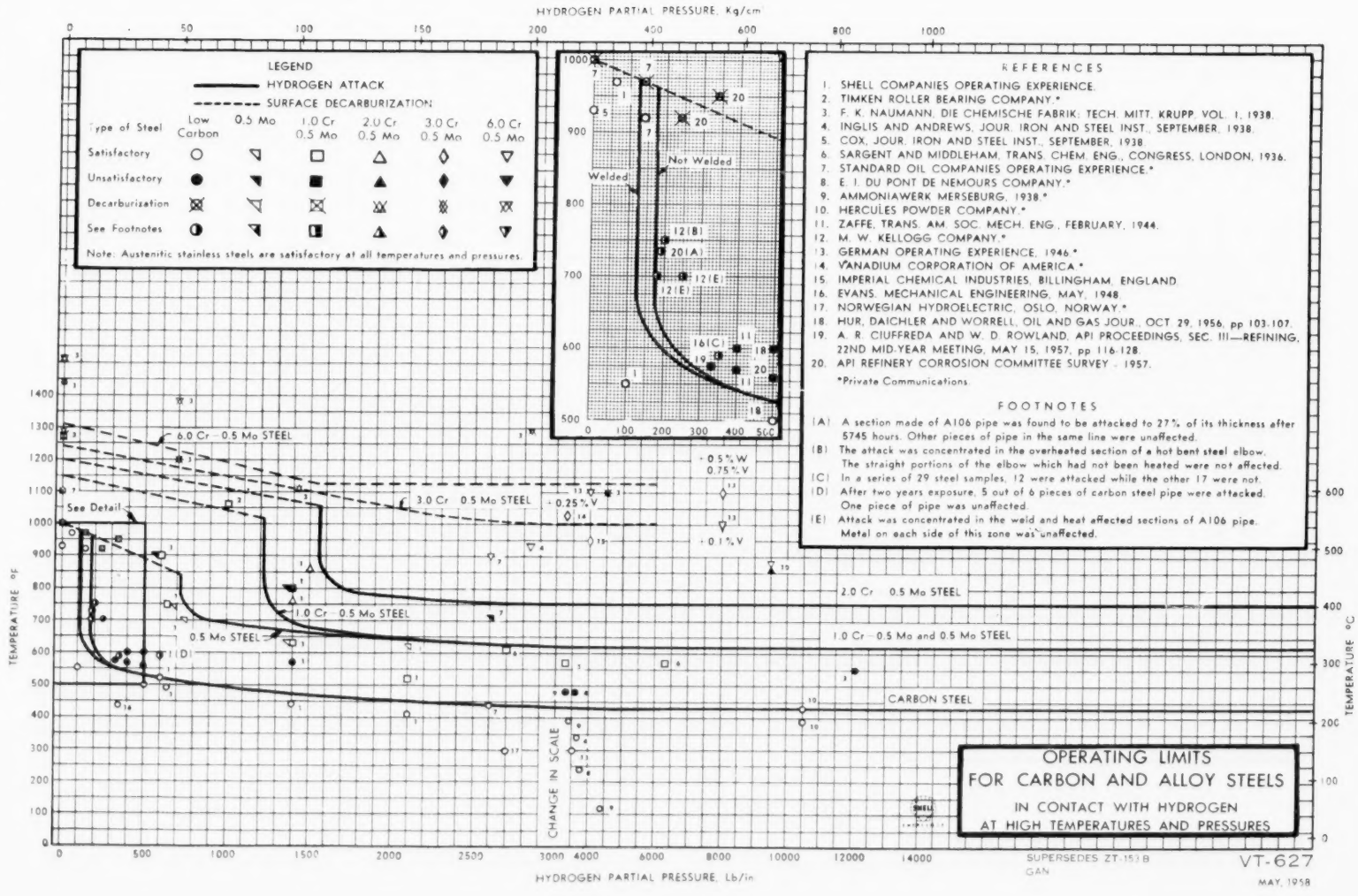
HYDROGEN PARTIAL PRESSURE, Kg/cm
HYDROGEN PARTIAL PRESSURE, Lb/in
TEMPERATURE °F
TEMPERATURE °C
LEGEND
HYDROGEN ATTACK
SURFACE DECARBURIZATION
Type of Steel
Low Carbon
0.5 Mo
1.0 Cr 0.5 Mo
2.0 Cr 0.5 Mo
3.0 Cr 0.5 Mo
6.0 Cr 0.5 Mo
Satisfactory
Unsatisfactory
Decarburization
See Footnotes
Note: Austenitic stainless steels are satisfactory at all temperatures and pressures.
Welded
Not Welded
12(B)
20(A)
12(E)
16(C)
6.0 Cr - 0.5 Mo STEEL
3.0 Cr 0.5 Mo STEEL
See Detail
1.0 Cr 0.5 Mo STEEL
0.5 Mo STEEL
11(D)
0.5 %W
0.75 %V
0.25 %V
0.1 %V
2.0 Cr 0.5 Mo STEEL
1.0 Cr - 0.5 Mo and 0.5 Mo STEEL
CARBON STEEL
CHANGE IN SCALE
REFERENCES
1. SHELL COMPANIES OPERATING EXPERIENCE.
2. TIMKEN ROLLER BEARING COMPANY.*
3. F. K. NAUMANN, DIE CHEMISCHE FABRIK; TECH. MITT. KRUPP, VOL. 1, 1938.
4. INGLIS AND ANDREWS, JOUR. IRON AND STEEL INST., SEPTEMBER, 1938.
5. COX, JOUR. IRON AND STEEL INST., SEPTEMBER, 1938.
6. SARGENT AND MIDDLEHAM, TRANS. CHEM. ENG., CONGRESS, LONDON, 1936.
7. STANDARD OIL COMPANIES OPERATING EXPERIENCE.*
8. E. I. DU PONT DE NEMOURS COMPANY.*
9. AMMONIAWERK MERSEBURG, 1938.*
10. HERCULES POWDER COMPANY.*
11. ZAFFE, TRANS. AM. SOC. MECH. ENG., FEBRUARY, 1944.
12. M. W. KELLOGG COMPANY.*
13. GERMAN OPERATING EXPERIENCE, 1946.*
14. VANADIUM CORPORATION OF AMERICA.*
15. IMPERIAL CHEMICAL INDUSTRIES, BILLINGHAM, ENGLAND.
16. EVANS, MECHANICAL ENGINEERING, MAY, 1948.
17. NORWEGIAN HYDROELECTRIC, OSLO, NORWAY.*
18. HUR, DAICHLER AND WORRELL, OIL AND GAS JOUR., OCT. 29, 1956, pp 103-107.
19. A. R. CIUFFREDA AND W. D. ROWLAND, API PROCEEDINGS, SEC. III—REFINING, 22ND MID-YEAR MEETING, MAY 15, 1957, pp 116-128.
20. API REFINERY CORROSION COMMITTEE SURVEY - 1957.
*Private Communications.
FOOTNOTES
(A) A section made of A106 pipe was found to be attacked to 27% of its thickness after 5745 hours. Other pieces of pipe in the same line were unaffected.
(B) The attack was concentrated in the overheated section of a hot bent steel elbow. The straight portions of the elbow which had not been heated were not affected.
(C) In a series of 29 steel samples, 12 were attacked while the other 17 were not.
(D) After two years exposure, 5 out of 6 pieces of carbon steel pipe were attacked. One piece of pipe was unaffected.
(E) Attack was concentrated in the weld and heat affected sections of A106 pipe. Metal on each side of this zone was unaffected.
OPERATING LIMITS
FOR CARBON AND ALLOY STEELS
IN CONTACT WITH HYDROGEN
AT HIGH TEMPERATURES AND PRESSURES
SHELL
SUPERSEDES ZT-151 B
GAN
VT-627
MAY, 1958